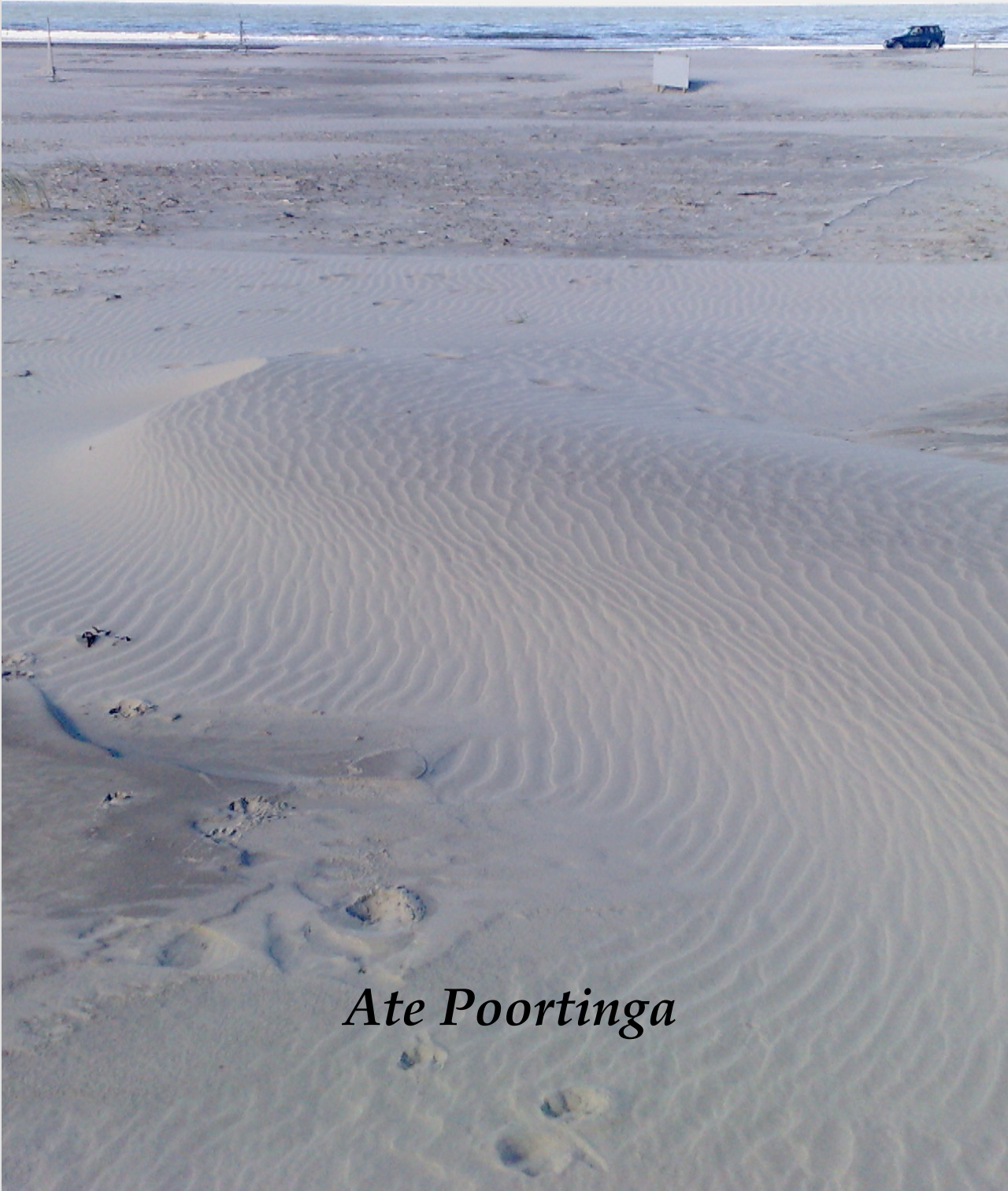


Ate Poortinga — Beach sand dynamics: measurements, models and scales

Beach sand dynamics: measurements, models and scales



Ate Poortinga

Beach sand dynamics: measurements, models and scales

Ate Poortinga

Thesis committee

Promotor

Prof. Dr C.J. Ritsema
Professor of Soil Physics and Land Management
Wageningen University

Co-Promotors

Dr S.M. Visser, Teamleader, Alterra
Wageningen UR

Dr M.J.P.M. Riksen, Assistant professor, Soil Physics and Land Management Group
Wageningen University

Other members

Prof. Dr J. Wallinga, Wageningen University
Dr D. Goossens, KU Leuven, Belgium
Dr M. Seeger, University of Trier, Germany
Prof. D.J. Sherman, University of Alabama, USA

This research was conducted under the auspices of Graduate School: C.T. de Wit Production Ecology and Resource Conservation

Beach sand dynamics: measurements, models and scales

Ate Poortinga

Thesis

submitted in fulfillment of the requirements for the degree of doctor

at Wageningen University

by the authority of the Rector Magnificus

Prof. Dr A.P.J. Mol

in the presence of the

Thesis Committee appointed by the Academic Board

to be defended in public

on Monday 30 November 2015

at 4 p.m. in the Aula

Ate Poortinga

Beach sand dynamics: measurements, models and scales

235 pages.

PhD thesis, Wageningen University, Wageningen, NL, (2015)

With references, with summaries in English and Dutch.

ISBN: 978-94-6257-585-1

Contents

Contents	iv
1 Introduction	1
1.1 Societal relevance of aeolian research	1
1.2 Current aeolian research on wind-blown sand	2
1.3 Scales in aeolian research	3
1.4 Measurements of beach-sand dynamics	6
1.4.1 Wind	6
1.4.2 Surface moisture	9
1.4.3 Saltation	10
1.4.3.1 Passive methods	11
1.4.3.2 Active Methods	12
1.4.4 Erosion and deposition patterns	14
1.5 Modelling beach sand dynamics	15
1.5.1 Models	15
1.6 The challenge	19
1.7 Aim of this study and research questions	20
1.8 Applied research approaches and thesis outline	20
2 Beneficial effects of wind erosion: Concepts, measurements and modeling	22
2.1 Introduction	23
2.2 Examples of beneficial wind erosion	25
2.2.1 Wind erosion for maintaining biodiversity	26
2.2.2 Wind erosion for coastal defense by dune formation	30
2.2.3 Wind erosion for harvesting soil fertility in the Sahel	32
2.2.4 Discussion	35
2.2.5 Conclusion	37
2.2.6 Acknowledgements	38
3 Self-emergent behaviour in particle based simulations	39

3.1	Introduction	40
3.2	Materials and Methods	42
3.2.1	Experimental setup	43
3.2.2	The model	43
3.3	Results and Discussion	47
3.4	Conclusion	53
3.5	acknowledgments	54
4	Measuring fast-temporal sediment fluxes with an analogue acoustic sensor: a wind tunnel study	55
4.1	Introduction	56
4.2	Materials and methods	58
4.2.1	Instrumental design	58
4.2.1.1	Modified Wilson and Cooke	58
4.2.1.2	Basaran Erpul Sediment Trap (BEST)	59
4.2.1.3	Saltiphone	60
4.2.2	Experimental setup	61
4.2.3	Sediment	62
4.2.4	Analysis method	63
4.2.4.1	Wind data	63
4.2.4.2	Saltiphone	64
4.2.4.3	Regression analysis	65
4.2.4.4	Sediment fluxes	67
4.2.5	Efficiency	70
4.3	Results and discussion	70
4.3.1	The efficiency of the different catchers	70
4.3.2	Calibration of the saltiphones	73
4.3.3	Sediment fluxes calculated from the saltiphone	74
4.3.3.1	Kinetic energy	74
4.3.3.2	Particle velocity profile	75
4.3.4	Sediment fluxes	75
4.3.5	Shear velocity and sediment fluxes	79
4.3.6	Comparison between the saltiphone and the BEST trap	81
4.3.7	Limitations	82
4.4	Conclusions and recommendations	84
4.5	Acknowledgements	85
5	Measuring aeolian sand transport using acoustic sensors	86
5.1	Introduction	87
5.2	Background	90
5.3	Materials and methods	92

5.3.1	Laboratory experiment	93
5.3.1.1	The saltiphone	93
5.3.1.2	Laboratory methods	96
5.3.2	Field experiment	97
5.3.2.1	The miniphone	97
5.3.2.2	Field methods	97
5.3.2.3	Data analysis methods	97
5.4	Results	98
5.4.1	Laboratory experiment	98
5.4.2	Field experiment	101
5.5	Discussion	103
5.6	Conclusions	106
5.7	Recommendations	106
5.8	Acknowledgements	106
6	Measurement uncertainties in quantifying aeolian mass flux: Evidence from wind tunnel and field site data	107
6.1	Introduction	108
6.2	Materials and Methods	111
6.2.1	Data collection	111
6.2.2	Study area	111
6.2.3	Measurement of sand size	111
6.2.3.1	Measurement of sediment flux	112
6.2.3.2	Weather data	114
6.2.4	Data analysis	115
6.2.4.1	Vertical distribution of aeolian mass flux	115
6.2.4.2	Uncertainties in estimation of aeolian mass flux	118
6.3	Results and Discussion	120
6.3.1	Wind tunnel data	120
6.3.2	Field data	125
6.4	Conclusion and recommendations	132
6.5	Acknowledgments	132
7	Temporal and spatial variability in event scale aeolian transport on Ameland, The Netherlands	134
7.1	Introduction	135
7.2	Materials and methods	137
7.2.1	Study area	137
7.2.2	Data collection	138
7.2.3	Analysis method	141
7.2.3.1	Wind speed profile and shear velocity	141

7.2.3.2	Threshold shear velocity	142
7.2.3.3	Sediment fluxes	142
7.3	Results	145
7.3.1	Beach morphology and ground water dynamics	145
7.3.2	Aeolian sediment transport events	147
7.3.3	Spatial variability in aeolian sediment transport events	154
7.4	Discussion	157
7.5	Conclusion and recommendations	161
8	Measuring and modeling the effect of surface moisture on the spectral reflectance of coastal beach sand	162
8.1	Introduction	163
8.2	Background	166
8.2.1	Spectral reflectance	166
8.2.2	Surface moisture	169
8.2.3	Surface moisture - spectral reflectance models	170
8.3	Materials and Methods	172
8.3.1	Experimental setup	172
8.3.2	Analysis method	174
8.4	Results and Discussion	174
8.4.1	Laboratory experiment	174
8.4.2	Practical applications	180
8.5	Conclusions	182
9	Synthesis: Beach sand dynamics: measurements, models and scales	184
9.1	Beach sand dynamics: measurements, models and scales	184
9.2	Discussion	189
9.3	Research challenges and future research directions	192
	Bibliography	194
	Summary	219
	Samenvatting	225

Chapter 1

Introduction

1.1 Societal relevance of aeolian research

Aeolian processes occur in a variety of environments, such as arid, semi-arid and coastal areas, but also in cold regions and along the borders of rivers and lakes. Besides the interest in the physical fundamentals of particle (sediment) and fluid (wind) interaction, these processes are considered as being societal relevant. The role of aeolian sediment transport is for example extensively studied in coastal areas, as dune morphology provides a natural defence against the destructive forces of the sea. In-depth knowledge on the system dynamics that drive the morphological development of natural coasts is important, as maintaining the natural dynamics in this system allows vegetation to flourish in different successive stages [Buckley, 1987], while preserving an appealing area for tourism and recreation, and naturally, not compromising the safety of the hinterland [Van Koningsveld and Mulder, 2004]. In agricultural areas, wind erosion is often considered a threat [Lal et al., 1994, Pimentel, 2006, Pimentel and Kounang, 1998], as the fertile soil is removed from the area, inducing food insecurity due to nutrient loss and health hazards due to inhalation of very fine dust particles [Copeland et al., 2009, de Longueville et al., 2009]. Moreover, young seedlings can be destroyed beyond redeem by the impact of saltating particles. On the other hand, the deposition of dust, transported from the source areas, is an important source of nutrients for vegetation in

the sink areas, but also, when deposited in the ocean, for algae, the primary food source for many marine species at the base of the food chain [Gao et al., 2001, Mctainsh and Strong, 2007].

1.2 Current aeolian research on wind-blown sand

In 1941 the book of Ralph Alger Bagnold "*The physics of blown sand and desert dunes*" was published [Bagnold, 1941]. This book became the standard work for the field of aeolian research, as it describes the physics of aeolian sediment transport based on empirical data and theoretical considerations. Since this early work, a large amount of studies have been conducted, resulting in numerous new theories and concepts on the physics of wind blown sand. The broad variety of different methods and approaches, ranging from windtunnel studies [e.g. Bauer et al., 2004, Burri et al., 2011, Butterfield, 1998, Goossens et al., 2000, Van Pelt et al., 2009, Youssef et al., 2012b], field measurements at a variety of scales [e.g. Delgado-Fernandez and Davidson-Arnott, 2011a, Ellis et al., 2012, Namikas, 2003, Riksen and Goossens, 2005, Visser et al., 2004b, Weaver and Wiggs, 2011], but also model approaches on grain-to-grain interactions [e.g. Durán et al., 2011, Mitha et al., 1986, Willetts and Rice, 1986] to large scale dust models [Ginoux et al., 2001, 2004, Shao et al., 1996] have resulted in a large variety of theories, concepts and ideas. Methods developed in disciplinary fields, such as fluid dynamics, environmental modelling and remote sensing have been used extensively, whereas the results of these methods have found their application in other disciplines, such as land degradation and coastal management. This makes the discipline of aeolian research inherently an inter-disciplinary playground. However, there are currently no standardized methods to obtain and process scientific data in the field of aeolian research, which makes results from different studies difficult to compare [Barchyn et al., 2011].

Most studies use the positivist doctrine, where scientific knowledge is deduced from empirical data. The positivist doctrine has very strong roots in the scientific code of conduct of today. This doctrine dictates that a theory (or mathematical) model to describe for example the natural dynamics of coastal fore-dune development in the

Netherlands, or the impact of wind erosion on food (in)security in Burkina Faso should satisfy two requirements: "(1) it must accurately describe a large class of observations on basis of a model that contains only a few arbitrary elements, and (2) it must make accurate predictions about the results of future observation" [Hawking, 1996].

Advances in the field of erosion research are, seriously hampered due to the lack of large amounts of high quality data [Stroosnijder, 2005] for a variety of spatio-temporal scales. In an era where data abundance (big data) is seen as a constraint rather than an advantage for aeolian research, there is a lack of resources to develop adequate tools to develop and (extensively) test methods to obtain large datasets.

The complex non-linear behaviour of fluid flow, combined with the irregular composition of sediment and individual grains add an extra layer of complexity. As a consequence, it is not (yet) possible to deduce a purely deterministic model to describe the processes at a range of different spatial and temporal scales.

Due to this lack of data and inherent complexities in model development, a definite answer on the nature and behaviour of aeolian sediment transport (at any scale) can not be formulated. Results of a specific study should be generally interpreted as valid for the specific space-time dimension under consideration. In fact, there is a strong analogy with current issues in the field of physics, where quantum theory (the very small) is inconsistent with the mathematical models of cosmology (the very big). However, in the field of physics, there is a considerable amount of resources available to search for the "Theory of everything", whereas resources in aeolian research are often limiting.

1.3 Scales in aeolian research

A main challenge in studying aeolian sediment transport (in coastal environments) is the interpretation of the processes that occur through a range of scales [Sherman, 1995]. Figure 1.1 shows the processes of aeolian sand transport, dune development and coast-line evolution in association with the spatial and temporal scale at which they occur. It can be seen that aeolian sediment transport occurs mainly at the micro scale, influenced by wind unsteadiness, particle properties, meteorology and surface conditions.

Dune development on the other hand, takes place over longer temporal and spatial scales, and is influenced by seasonal climate, vegetation growth, but also by wave tide and surge conditions. Coastline evolution is measured on the macro-scale and impacted by climate, sea level and geology. While these scaling problems are common in geomorphological research, it inhibits the development of clear understanding of dune and coastline evolution and overall system behaviour [Sherman, 1995].

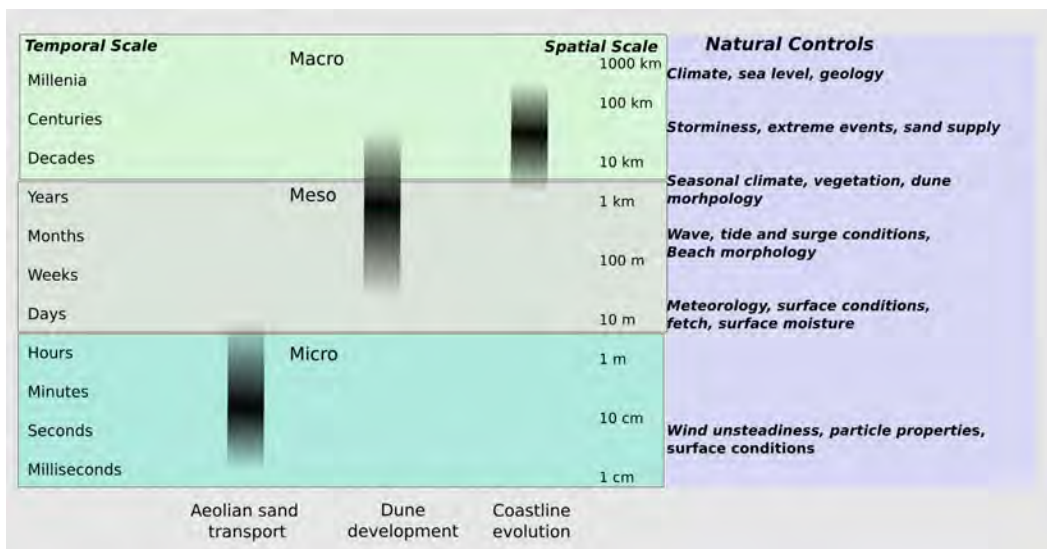


FIGURE 1.1: The processes of aeolian sand transport, dune development and coastline evolution act at different spatial and temporal scales. The natural controls associated with the different scales are shown in the blue box.

The processes associated with aeolian sediment transport in a coastal environment are shown in figure 1.2. Wind initiates the movement of sediment, resulting in erosion of sediment from the source area and deposited in the sink area. Heavy particles roll and slide over the surface (creep) and the lighter particles are entrained by the wind and jump over the surface (saltation). Whereas suspension, the process in which the smaller particles are carried large distances plays an important role in arid environments, the portion is often negligible in coastal environments [Illenberger and Rust, 1988]. Surface moisture and fetch might limit the amount of sediment transported as well.

Figure 1.3 shows the processes, controls and effects of aeolian sediment transport according to spatial and temporal scale. Creep and saltation occur at a small temporal

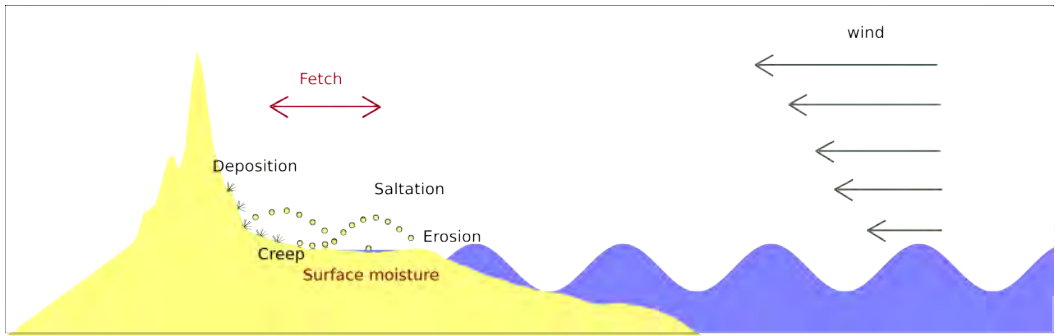


FIGURE 1.2: The processes of aeolian sediment transport in a coastal environment. Aeolian sediment processes are shown in black, the controlling factors in red.

and spatial scale, whereas meteorology, as the primary driver behind the transport has a larger range. Surface moisture varies from hours to days, but can also show a considerable variation over relatively short distances. Sea level also plays an important role, as it affects fetch distance at the short term, while an increase in sea level becomes more important over larger temporal domains. Vegetation, morphology and climate are important factors at the macro scale.

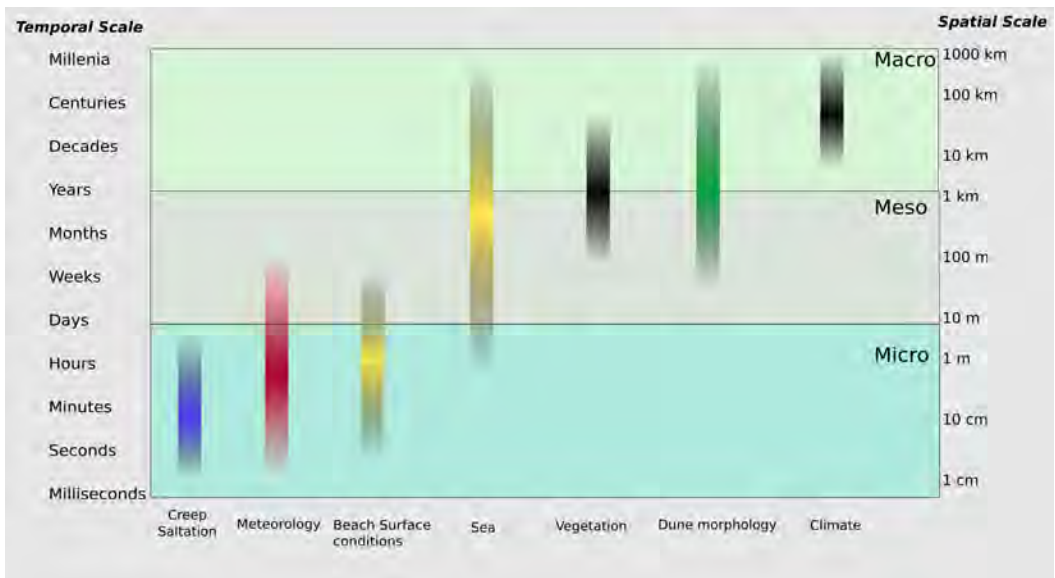


FIGURE 1.3: The processes, controls and effects of aeolian sediment transport according to the spatial and temporal scales they act on.

1.4 Measurements of beach-sand dynamics

A wide variety of instruments are available to measure the processes and controlling factors of aeolian sediment transport. An overview of the measurement technologies are shown in figure 1.4. The colors of the boxes can be linked with the colors in figure 1.3. As this thesis is mainly focused on the short-term transport processes, only these processes and controls were incorporated. The background and evolution of these measurement techniques are further described in the next sections.



FIGURE 1.4: The technologies used to measure aeolian sediment transport processes and controls. The colors are linked with the processes and controls in figure 1.3) .

1.4.1 Wind

Wind is the most important driver behind aeolian processes as aeolian sand transport is a response to fluid forces within the near boundary of the surface whenever shear velocities exceed a certain threshold shear velocity (u_{*t}). As wind is a fluid, the physical behaviour of wind flow can be described by fluid mechanics, the discipline in physics that describes fluid flows. The first mathematical descriptions of fluid dynamics were formulated by Newton et al. [1833], followed by work of Leonhard Euler who derived two non-linear partial differential equations by applying the basic formulations of Newton's second law. While the Euler equation includes conservation of mass, energy and momentum, friction was not included. The Euler Equation was independently modified by Henry Navier [Navier, 1823] and George Stokes [Stokes, 1851], in order to account for internal friction.

The resulting Navier–Stokes equations are now the standard mathematical description of (incompressible) fluid flows.

Turbulence is a typical characteristic of wind flow and has been associated with the initiation of sediment movement [Walker, 2005]. Turbulence is a chaotic eddying motion of a fluid with rapid variation in pressure and velocity in space and time. The dimensionless Reynolds number [Reynolds, 1883] (eq 1.1), which can be obtained from the Navier-Stokes equation, is often used to describe the ratio of inertial forces (UL) to viscous forces (v). The kinematic viscosity (v ; m^2s^{-1}), can be obtained from the dynamic viscosity (μ ; $Pa \cdot s$) and the density of the fluid (ρ ; kgm^{-3}) by $v = \mu\rho^{-1}$. Low Reynold numbers (< 2000 ; i.e. viscous forces are dominant) indicate a laminar flow, whereas a high Reynold value characterizes a turbulent flow. Turbulence can also be expressed in terms of Reynold stress, which is a second order closure method for the Navier-Stokes equation to determine the mean force imposed on an area on the mean flow by fluctuations in turbulence.

$$Re = \frac{\rho UL}{\eta} = \frac{UL}{v} \quad (1.1)$$

Since there is no closed-form solution for the Navier-Stokes equations, it is only possible to approximate the behaviour of flow fields. These approximations are computational very demanding. For practical application, the "boundary theory" developed by Prandtl [1932] is often used, as this reduces the Navier-Stokes equation to a much simpler one. Ludwig Prandtl recognized that a flow over a boundary can be divided into two different regions: In a friction dominant thin boundary layer near the surface and inviscid flow outside the boundary layer where friction is negligible. This concept allows a closed form solution of the Navier-Stokes equations. With this simplification, the shear stress on a surface can be obtained from the velocity gradient of the fluid.

In 1921, the "law of the wall" (Eq. 1.2) was published [Kármán, 1921], which was obtained by the integral of the boundary layer theory. This integral form has great applicability, as the shear velocity (u_* ; also referred to as friction velocity) on a plane

can directly be obtained from the wind velocity (u) at height (z), the dimensionless Von Kármán constant (k ; approximately equal to 0.4), and roughness length (z_0).

$$u_z = \frac{u_*}{\kappa} \ln \frac{z}{z_0} \quad (1.2)$$

A precise estimation of the shear forces on the surface is imperative when aeolian sediment transport dynamics are studied. These shear forces are typically determined from wind velocity, measured with time-averaged equipment such as cup or vane anemometers as well as high frequency equipment such as thermal anemometry (hot film or wire thermal probes) and acoustic Doppler technologies. Cup or vane anemometers, which consist of hemispherical cups or a propeller that rotate in proportion to the wind speed, are used most frequently. Hot-wires or hot-films, applied in numerous studies of e.g. Bauer et al. [2004, 1998], Burri et al. [2011], Butterfield [1998, 1999a], Castro and Wiggs [1994], Goossens et al. [2000], Kang et al. [2008a,b], Lee [1987], Rasmussen and Sørensen [1999], Wiggs et al. [2004a,b], detect changes in the resistance of a heated film or wire when a fluid passes. Acoustic Doppler technologies, such as sonic anemometers [Leenders et al., 2005a, Van Boxel et al., 2004, Walker, 2005], use the velocity of an ultrasonic sound signal in air to determine the wind velocity. The time between emission and reception of an ultrasonic signal is used to determine the wind velocity, as wind either supports or opposes the propagation of sound through the air, dependent of the direction.

Thermal anemometry and acoustic Doppler are fast-response technologies to study turbulence near the boundary. These techniques allow to measure in the three components of wind speed simultaneously. Data of these technologies can be used to determine the Reynold stress, defined as covariance between the horizontal and vertical wind speed [Van Boxel et al., 2004]. For aeolian research, thermal anemometers are advantageous because of their size and small volume, and, as such, minimize obstruction of wind flow. However, they are also fragile and have to be calibrated for atmospheric conditions [Kaimal and Finnigan, 1994]. Acoustic Doppler devices are more robust, do not require field calibration, but cover a larger volume, possibly obstructing the natural wind-flow.

Cup and vane anemometer come in all sizes and shapes and are often used to determine shear velocity (eq. 1.2). As shear velocity is obtained from the log-linear time-averaged wind profile, it is necessary to measure the wind velocity at different heights. A minimum of three anemometers is required to determine the log-linear velocity profile. However, a higher number is recommended for a higher accuracy and error estimation. A detailed description of sources of uncertainty can be found in [Bauer et al. \[1992\]](#). Due to the design with rotating parts, cup and vane anemometers can not be used to study turbulence and coherent flow structures. Response times in the order of 0.2 to 0.5 s have been reported [[Baas, 2008](#), [Schubauer and Adams, 1954](#)] for wind velocities between 4 and 10 ms^{-1} .

High resolution measurements have improved our understanding of turbulent wind flow upon aeolian sediment transport. The work of e.g. [Sterk et al. \[1998\]](#) and [Schonfeldt and von Lowis \[2003\]](#) shows there is no well-defined relation between instantaneous shear stress and saltation flux. They state that, to estimate aeolian saltation fluxes, it is more useful to also incorporate horizontal wind speed and its fluctuations. Furthermore, instruments that measure wind velocity obtain only data on one specific point. Natural conditions such as unsteady, multi-directional winds, flow modification, vegetation and surface roughness modify the flow field. It is even suggested that secondary lee-side flow patterns play a significant role in dune morphodynamics [[Walker and Nickling, 2002](#)]. Research on morphology induced flow modification [e.g. [Hesp et al., 2005](#), [Walker et al., 2009](#)] and the effect of vegetation on wind flow and sediment transport [e.g. [Leenders et al., 2007](#), [Youssef et al., 2012b](#)] are therefore also important.

1.4.2 Surface moisture

Surface moisture is widely recognized as an important transport limiting factor [[Cornelis et al., 2004b](#), [Davidson-Arnott et al., 2008](#), [Namikas and Sherman, 1996](#), [Wiggs et al., 2004b](#)]. However, data on the spatial variability of the surface conditions is scarce, whereas it is critical to account for quantification of aeolian sediment transport rates. Moisture probes are frequently used to estimate surface moisture conditions, but often

designed to measure the average moisture conditions over a column of sediment, whereas the top layer is the area of specific interest for aeolian research. Moreover, they are impractical for larger areas and require a proper calibration for salty or fresh water conditions [Yang and Davidson-Arnott, 2005].

A method to acquire high spatio-temporal information on moisture conditions is through a photographic methodology combined with regression analysis, developed by McKenna Neuman and Langston [2006] and Darke et al. [2009]. This method links beach surface moisture content to a corresponding normalized beach surface reflectance. The relation is then applied to obtain temporal beach surface moisture maps. The method is applicable with every common camera and provides a means to gather both temporally and spatially dense information on the surface moisture conditions. A map with surface moisture content would be ideal as an input parameter for temporal wet threshold friction velocity estimations. A number of recent studies have used the method and demonstrated the potential utility of a photographic approach to characterize spatio-temporal patterns in surface moisture conditions. Studies of Delgado-Fernandez and Davidson-Arnott [2011a] and Delgado-Fernandez et al. [2009] use the exponential relation between surface moisture and luminance from literature. Studies of Nield et al. [2011] and Nield and Wiggs [2011] use a similar approach for a terrestrial laser scanner.

1.4.3 Saltation

Aeolian sediment transport can be categorized into three different modes: creep, saltation and suspension. Finer particles (0.001 to 0.1 mm) are transported in suspension over large distances and higher elevation, whereas larger particles roll (creep; 1 to 2 mm) or jump (saltation; 0.1 - 1.0 mm) over the surface over short distances [Fryrear et al., 1991]. A variety of instruments is available to measure the volume, intensity and composition of airborne particles. These methods can be divided in active and passive measurements methods.

1.4.3.1 Passive methods

Most measurements of aeolian sediment transport have been done by use of passive sediment traps. There are a large number of passive sediment traps such as the vertically integrated Leatherman/Rosen trap [Leatherman, 1978, Rosen, 1978], or traps consisting of a number of compartments like the Modified Wilson and Cook [Sterk and Raats, 1996, Wilson and Cooke, 1980a], Big Spring Number Eight [Fryrear, 1986], WITSEG [Dong et al., 2004b], Basaran and Erpul Sediment Trap [Basaran et al., 2011], or mesh-type trap [Sherman et al., 2014]. Vertically integrated traps involve a single chamber, thus integrating the vertical flux into one measurement. Others comprise sets of different compartments so that the flux profile can be measured. Typically, static traps are deployed over periods of 1 to 30 minutes (or sometimes longer), sampling sediment transport through openings (single or cumulative through several) with areas of the order of 10^5 mm^2 or greater.

To estimate the total amount of sediment transport, the sediment caught in the traps over a known time period is dried and weighed. These results are used to calculate a transport rate in units (typically) of $\text{kgm}^{-1}\text{s}^{-1}$ or $\text{gm}^{-1}\text{s}^{-1}$. When a trap array has gaps in vertical coverage (such as the BSNE), the total transport rate can be estimated by log-linear curve fitting for the segmented data and then by integration.

The total amount of sediment transport of a vertically integrated catcher can be calculated directly, whereas log-linear curve fitting is required for compartment traps. For each trap in the vertical array the total amount of sediment caught is multiplied by the area of the inlet to get an amount in kgm^{-2} . Then, regression analysis calculates the vertical transport flux within the entire sediment transport layer. However, there is disagreement in the literature as to how to best describe the vertical profile of sediment transport [Ellis et al., 2009a, Panebianco et al., 2010]. Exponential functions (equation 1.3) as well as power functions (equation 1.4) have been used. The regression parameter q_0 is often associated with the portion of creep, whereas β represents the decay rate of the saltation layer with height (z ; m). Moreover, some software packages use these formulae in a logarithmic form McCullough and Heiser [2008].

$$q(z) = q_0 e^{\beta z} \quad (1.3)$$

$$q(z) = q_0 z^{\beta} \quad (1.4)$$

1.4.3.2 Active Methods

Field-deployable active sensors measure saltation at much greater temporal resolution compared with passive traps. However, unlike the data obtained with passive sediment traps, it is difficult to use the data acquired to quantify aeolian sediment transport without extensive signal processing and calibration. Electronic saltation sensing instruments or active methods operate from one of three bases: acoustic detection; piezoelectric detection; or optical detection. These sensors have been reviewed and discussed extensively in numerous studies [e.g. [Barchyn and Hugenholtz, 2010](#), [Davidson-Arnott et al., 2009](#), [Hugenholtz and Barchyn, 2011b](#), [Sherman et al., 2011](#), [Van Pelt et al., 2009](#)].

The use of acoustic sensors for aeolian research started with [Spaan and van den Abeele \[1991\]](#). They designed and tested a microphone-based device and called it the saltiphone. The microphone in the saltiphone responds to the impact of saltating grains that compress its diaphragm. The generated signal is then recorded digitally. A large number of studies have used this device in different environments such as beaches, deserts and windtunnels. [e.g. [Anthony et al., 2009](#), [Arens, 1996b](#), [Goossens et al., 2000](#), [Leenders et al., 2005a](#), [Riksen and Goossens, 2007](#), [Sterk et al., 2012](#), [Van Pelt et al., 2009](#), [Visser et al., 2004b](#)]. Other studies [[Ellis et al., 2009b](#), [Sherman et al., 2011](#), [Yurk et al., 2013](#)] used a modified version of the saltiphone, that they called the ‘mini-phone’ because of its small sensor area. Studies that used the output of microphone-based systems, translated the output signal to grain-impact count to represent saltation intensity, rather than total transport rates. Although acoustic sensors have been used in numerous studies, the output can not be linked to coincidental measurements of sediment transport [[Ellis et al., 2009b](#), [Goossens et al., 2000](#), [Sherman et al., 2011](#)].

Impact sensors based on the piezoelectric principle were started with the development of the piezoelectric-ring based sensit [Gillette and Stockton, 1986] the experiments of Hardisty [1993] mounting a crystal on a phonograph needle. The principle of the Sensit was also the basis for the development of the Safire [Baas, 2004]. Both sensors have been used in numerous studies [e.g. Fryrear et al., 1991, Gillette et al., 1997, 1996, Larney et al., 1995, Stout and Zobeck, 1997, Stout, 2004, Stout and Zobeck, 1996, Wiggs et al., 2004b]. However, both devices were found difficult to calibrate for a wide range of conditions, partly because of the curved sensing surface. The output signal from piezoelectric sensors also requires some degree of signal processing. However, some of the instruments have an internal circuitry for signal processing and produce impact counts directly. Innovations for the piezoelectric devices have not stopped, as a new device, the FP5 Flat Plate Movement Sensor (Sensit company, 2013, [Sensit, 2013]) has evolved.

Lasers have also been used for a number of decades to detect and measure saltation. Perhaps the first use was in a wind-tunnel experiment of Nickling and Ecclestone [1981] where the beam was used to detect the initiation of motion. Later, Butterfield [1999b] used a laser system and thermal anemometry in a wind-tunnel to study saltation profiles. The next technological advances came with the development of a laser particle counter that could also size the grains [Mikami et al., 2005]. More recent studies used a commercial fork-sensor particle counter (produced by Wenglor Sensoric GmbH) in field studies of aeolian sediment transport [e.g. Chapman et al., 2013, Davidson-Arnott et al., 2009, Hugenholtz and Barchyn, 2011b, Martin et al., 2013]. These studies use the grain count output from the circuitry without subsequent signal processing. While this output is an advantage in terms of usability, the output was found to relate poorly to actual sediment transport rates [Hugenholtz and Barchyn, 2011b]. However, the recent manuscript of Barchyn et al. [2014a] demonstrates that the Wenglor is suitable for measuring aeolian sediment transport at high temporal and spatial resolution. In order to quantify aeolian mass fluxes, they suggest to apply the wenglors in co-located pairs and collect sediment simultaneously using a sediment trap. This allows to identify the periods when one instrument ceases to operate properly and convert counts to flux.

The different studies that explore the efficiency and behaviour of electronic saltation sensing instruments found low fidelity for active sensors. This is partly caused by the often harsh operating conditions such as varying wind speed, temperature, saltation intensity, and grain size [Ridge et al., 2011]. However, particular designs and signal processing protocols also play important roles here. Radial variance in sensitivity is for example a problem for the omnidirectional Sensit and Safires [Baas, 2004, Van Pelt et al., 2009], whereas the fragility and implicit cut-off boundary, i.e. the translation from a voltage to a count, impede the use of laser particle counters. While sensor degradation might be a severe drawback for some of the acoustic sensors [Ellis et al., 2009b], they have a limited effect in terms of flow distortion.

1.4.4 Erosion and deposition patterns

Data on wind induced erosion and deposition patterns are important when evaluating the geomorphological impact of wind erosion. Several methods are available to acquire high resolution data on surface elevation or to reconstruct erosion and deposition patterns from the past. Optically stimulated luminescence (OSL) dating is for example used to study aeolian processes on the time-scale of centuries to decades [Ballarini et al., 2003, Madsen and Murray, 2009, Murray and Clemmensen, 2001, Yang et al., 2006]. Another method used to study erosion and deposition patterns on the decadal timescale is analysing the redistribution of Cesium-137, which was released into the atmosphere with the testing of nuclear weapons during 1950s and 1960s. As Cesium-137 is strongly bound onto soil particles, all redistribution occurs to soil erosion processes. Studies of e.g. Chappell [1999], Chappell et al. [1998], Ritchie and McHenry [1990] describe the method, results and uncertainties of this approach.

Erosion and deposition patterns can also be determined by comparing surface elevation models of different moments in time. Methods to measure elevations have undergone fast improvements over the last decades. For example, annual elevation profiles of the Dutch coasts were measured by levelling until 1977, by aerial photography from 1978 to 1995 and by laser altimetry thereafter [Bochev-Van der Burgh et al., 2011, van der

Wal, 2004], with continuously improved measurement accuracies [De Graaf et al., 2003, Oosterwijk and Ettema, 1987, Sallenger Jr et al., 2003]. However, these methods are either labour intensive or require a substantial amount of financial resources. Digital terrain models obtained from satellite data is freely and widely available nowadays, however, mainly suitable for large scale studies due to the rather coarse spatial resolution and limited accuracy. For studies with a smaller spatio-temporal scale, erosion pins have frequently been used to estimate erosion and deposition patterns (e.g. De Ploey and Gabriels [1980], Delgado-Fernandez and Davidson-Arnott [2011a], Riksen and Goossens [2007]). As the elevation from the top of the pin to the surface has to be measured at given time intervals for each pin, it is relatively time demanding to cover a large spatial domain or acquire data with a high spatial-temporal resolution. Moreover, erosion pins obstruct the airflow causing sedimentations at the lee-side of the pin.

1.5 Modelling beach sand dynamics

1.5.1 Models

A wide variety of model approaches are available for a range of spatio-temporal scales to estimate aeolian sediment transport rates, to simulate landscape evolution or to emulate bed-form development. Current approaches include small-scale reductionist approaches, large-scale self-organizing or statistical models and global scale empirical approaches. Reductionist models have a strong physical basis, whereas statistical models aim to describe a system or variable by means of a distribution or a range of predictions. Empirical models are the so-called black-box models, and rely on a scientific relationship between the input and output of the model. Some models aim to provide a qualitative estimation or a prediction whereas other models are used to give quantitative information on a system. Where the first generation of model operated on a point scale, more recent approaches often operate on a gridded landscape. Despite considerable progress in computational means and methods of operation, it remains challenging to obtain reliable estimations of aeolian sediment transport processes. This is mainly caused by

the inherent non-linear relation between wind forcing and sediment transport, but also other environmental factors that affect aeolian sediment transport such as vegetation, surface moisture, crop residues, wrack line materials etc.

Bagnold [1941] introduced the first point scale model to link aeolian sediment transport with a forcing agent. Until now, the model (eq. 1.5) is the most widely used to estimate aeolian sand transport rate q ($kgm^{-1}s^{-1}$), incorporating a dimensionless parameter for surface sediments (C), the mean grain diameter (d ; mm), a reference diameter (D ; mm), the shear velocity (u_* ; ms^{-1}), and air density (ρ ; kgm^{-3}).

$$q = C \sqrt{\frac{d}{D}} \frac{\rho}{g} u_*^3 \quad (1.5)$$

Numerous other studies, such as Hsu [1971], Kadib [1965], Kawamura [1951], Lettau and Lettau [1978], Owen [1964], Sørensen [2004], Zingg [1953] have developed similar empirical parametrizations, often incorporating the threshold shear velocity (eq. 1.6); where u_{*t} is the threshold shear velocity, A is a dimensionless constant (assumed to be 0.085 for the fluid threshold and 0.1 for the impact threshold), g is the gravitational acceleration (ms^{-2}), d is median (d_{50}) grain size (m), ρ_s is the density of the sediment (kgm^{-3}) and ρ is the density of air (kgm^{-3}). Unfortunately, there is not a strong correspondence between the measured and predicted rates of transport using any of these models [Sherman et al., 1998, Sherman and Li, 2012]. Sherman et al. [1998] recognized that moisture content is a critical factor in model performance and that none of the models is adequate for general applications to coastal-aeolian environments where moisture content is an important regulating factor.

$$u_{*t} = A \sqrt{gd \left(\frac{\rho_s - \rho}{\rho} \right)} \quad (1.6)$$

The more recent approaches on wind erosion modelling can be divided into different categories. The specific approach of these different schools is often connected to the objective of the study. In the studies of e.g. Durán and Herrmann [2006], Herrmann [2002], Kroy et al. [2002], Sauermann et al. [2001], Schwämmle and Herrmann [2005]

the saltation flux and feedbacks with flow forcing and local topography are considered in a continuum model of a transport layer of a developing profile, driven by an airflow model [Baas, 2012]. These studies are mainly interested in a physical derivation using wind flow, to describe aeolian bed-form development qualitatively.

Point and transect models are a different category of models. A method to estimate aeolian sediment transport rates at a point scale was developed by Fryberger and Dean [1979], and has since been used in numerous other studies (e.g. Al-Awadhi et al. [2005], Arens et al. [2004], Kalma et al. [1988]). In this method, drift potential is calculated using meteorological data based on an expression derived by Lettau and Lettau [1978]. Another method that operates on the transect scale is the Simulation of Aeolian Foredune Evolution (SAFE) model [Van Dijk et al., 1999]. This model uses the flow model developed by Van Boxel et al. [1999] and the Kawamura [Kawamura, 1951] sand transport model. Later work with this model included the effects of nourishments [van der Wal, 2000b] and the effects of vegetation. Other approaches in wind angle, beach geometry and fetch effects simulate sediment supply into the dunes [Bauer and Davidson-Arnott, 2003, Delgado-Fernandez and Davidson-Arnott, 2011b]

Studies that focus on the agro-environmental impact of wind erosion often include a quantitative evaluation of the model performances. The Revised Wind Erosion Equation (RWEQ) [Fryrear et al., 2001, 1998] was developed to estimate event based soil and nutrient loss. Similarly, the Wind Erosion Prediction System (WEPS) for wind-driven soil erosion on agricultural fields [Hagen, 1991] was developed. Both models combine empirical and process-based components obtained from windtunnel and field studies and perform calculations on a gridded landscape. The models have been applied in numerous studies [e.g. Buschiazzo and Zobeck, 2008, Funk et al., 2004, Visser et al., 2005b, Youssef et al., 2012a, Zobeck et al., 2001]. They have been developed for field scale application and require a large amount of spatial explicit input, such as crop and soil parameters, but also time-series on shear velocity. These type of models were developed to estimate soil loss quantities and do not predict qualitative indicators such as bed-form and dune development.

Cellular automata are a different branch of models. In cellular automata, physical processes are represented as a set of simple rules of interactions between neighbouring cells on a grid [Burks, 1970]. This set of simple rules result in a self-organizing process which is qualitatively linked to the behaviour of a natural system. Bak et al. [1987] introduced the concept to simulate self-emergent sand-pile formation. When grains are randomly added to a sand-pile, represented by cells on a regular finite sized grid, the slope angle increases. When the angle of repose is reached, every additional grain will cause the structure to topple, resulting in avalanches of various sizes. The Werner dune model uses a similar approach to simulate dune formation. The Werner dune model [Werner, 1995] uses a grid containing a stack of slabs that represent the height of sand in a specific cell. Aeolian bed-forms are simulated moving slaps over the grid under a specific set of rules. The Discrete ECogeomorphic Aeolian Landscape model (DECAL) for vegetated dunes [Baas and Nield, 2007, Baas, 2007, Baas and Nield, 2010, Nield and Baas, 2008] relies on the Werner dune model, but also incorporates vegetation. Current innovations of the model include quantitative dune development in an coastal environment.

Cundall and Strack [1979] were the first to propose a methodology to calculate grain interaction on a particles scale, called the Discrete Element Method (DEM). In this model approach, the forces that act on each individual particle are calculated stepwise. A contact force is calculcated using a contact model, which allows multi-body interactions defined by the relative overlap between two particles. A large number of studies of e.g Lee and Herrmann [1993], Li et al. [2005], Liffman et al. [2001], Luding [1997], Matuttis et al. [2000], Smith and Tüzün [2002], Zhou et al. [1999, 2002, 2003] used the DEM to study sandpile formation with a focus on the angle of repose, stress distribution and properties such as sliding friction and particle characteristics. However, these studies used a small number of particles due to the large computational demand. Recent advances on parallel computing techniques allow to run computational demanding algorithms on the Graphical Processing Unit (GPU) rather than the Central Processing Unit (CPU). Here, calculations are done parallel instead of serial. Despite the lower

clock-speeds, speed-ups of e.g. 80 times [Shimokawabe et al., 2010] have been reported. These more efficient implementations of the DEM on the GPU allow to realistically simulate real world systems.

There are a number of other methodological issues that should be considered when choosing a model strategy (see e.g. Malamud and Baas [2013]). It is important to keep the number of parameters (model parsimony) if any additional parameters do not add significantly to the explanatory or predictive nature of the model. Furthermore, the model should preferably be calibrated and validated using empirical data. In general, a dataset is often split into two parts, where the first part is used for calibration and the second part for validation purposes. Calibration is required to optimize the empirical parameters for the environmental conditions under consideration. In the validation stage, these parameters are kept constant to evaluate the model performance. Additionally, the sensitivity and confidence levels of the model to specific parameters or processes can be analysed in a sensitivity analysis and uncertainty assessment respectively.

1.6 The challenge

Research on aeolian transport processes has largely been done on the very small temporal scale (seconds to minutes) and spatial scale (centimetres to meters). Dune development on the other hand, is mainly studied at the larger spatio-temporal scale (years and kilometres). While there have been substantial improvements in the ability to measure near surface winds, equipment to measure aeolian sediment transport have remained disproportional unsophisticated. Moreover, there is a fundamental mismatch between empirical measurements and mathematical models that describe aeolian process [Barchyn et al., 2014b]. Improvement in measurement equipment, methodologies and models will narrow the gap between micro, meso and macro-scale studies and provide a better understanding of the processes and responses involved in aeolian sediment transport.

1.7 Aim of this study and research questions

The aim of this thesis is to explore, challenge and improve current technologies and methodologies to measure, analyse and model beach sand dynamics through a range of spatial and temporal scales. The following research questions were posed:

1. What are the current measurement techniques to measure aeolian saltation, how reliable are they and can they be improved?
2. Is it possible to measure aeolian sediment transport in a coastal environment on meso scale (weeks to months)?
3. What are the factors and processes regulating aeolian transport fluxes at different spatio-temporal scales in a coastal environment?
4. What possibilities offer the recent advances in computational techniques for the field of aeolian research?

1.8 Applied research approaches and thesis outline

Different research methodologies were used to formulate an answer to the research questions. The research consists of two field experiments, laboratory measurements, a wind tunnel study and model development. Figure 1.5 provides an overview of the thesis setup, the applied methods and the spatio-temporal scale under consideration. Three other published studies by the author (with another lead author) are included in figure 1.5 (yellow), as they are closely related to the topic of this thesis.

This thesis contains 4 different laboratory experiments (Chapter 3, 4, 5 and 8). The first laboratory experiment was done with a high-speed camera to study non-linear behaviour of avalanches in sand-pile formation. This data was used for model validation. A second experiment (Chapter 4) was performed in a wind tunnel to evaluate current measurement techniques to measure aeolian saltation and propose better alternatives. The third experiment (Chapter 5) was devised to measure the signal processing scheme

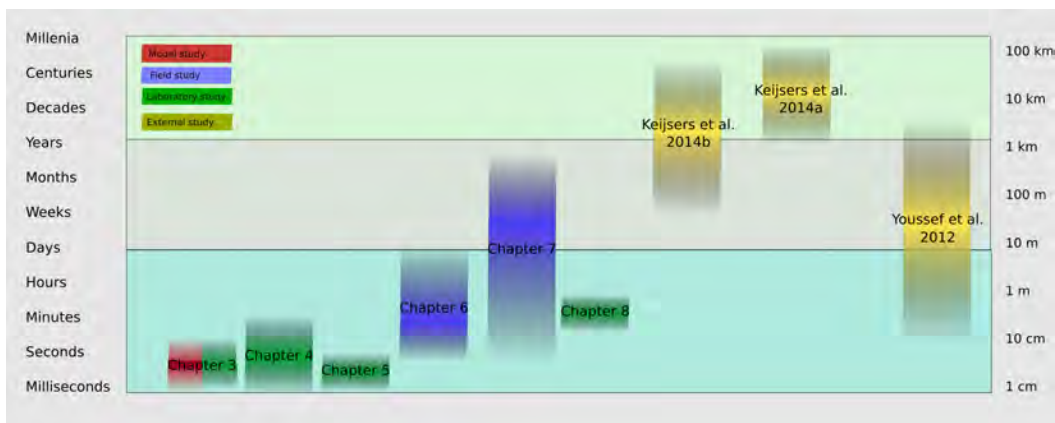


FIGURE 1.5: The setup of the different Chapters with the research methodologies used.

at the circuit board of the saltiphone acoustic sensor using an oscilloscope. In the last laboratory experiment (Chapter 8), a spectrometer (400 - 2500 nm) was used to measure spectral reflectance of beach sand upon wetting.

The field experiments were conducted at the north-western end of Ameland (Chapters 6 and 7), one of the Frisian barrier islands located in the northern part of the Netherlands. During the field campaign, a meteorological stations, a comprehensive grid of customized passive sediment traps, two acoustic sensing devices, groundwater tubes and a camera were installed on the beach to evaluate the reliability of the measurement equipment and measure aeolian sediment transport over a wide beach on an event scale.

The last chapter of this thesis is a synthesis of all work conducted in this thesis. This concluding chapter aims to integrate the findings of the different chapters and formulates an answer to the research questions.

The data presented in this thesis was made available to an open access repository. Furthermore, a conceivable amount of the Chapters was published in open access journal, so that the information is freely available to everyone.

Chapter 2

Beneficial effects of wind erosion: Concepts, measurements and modeling

Poortinga, A., Visser, S. M., Riksen, M. J., & Stroosnijder, L. (2011). Beneficial effects of wind erosion: Concepts, measurements and modeling. *Aeolian Research*, 3(2), 81-86.

Beneficial effects of wind erosion: Concepts, measurements and modeling

abstract

Aeolian research is still dominated by a technocentric worldview. With a focus on the negatives, it is believed that all separate components should be studied as detailed and possible, and combined, they explain the complete system dynamics. This paper presents a new conceptualization of the benefits of wind erosion and argues to work towards a more holocentric approach. Three examples show how aeolian processes can be beneficial for biodiversity, recreation, coastal defense and even for harvesting soil fertility. Current measurement techniques and modeling approaches are contested. As data from lacking measurement techniques can not be used for extrapolation and modeling purposes. Larger system dynamics are studied by simulating the small scale (reductionist) processes, leading to a complex model structure based on weak empirical and physical considerations. A more holistic approach suggests to monitor the greater systems dynamics and value the essential part of wind erosion in the natural system dynamics.

2.1 Introduction

Though benefits do exist, the negative effects and dangers of soil erosion attract public attention through media, research reports and from policymakers. It is widely known that soil erosion by wind or water causes the fertile top layer to be removed, the soil aggregates to break down, organic matter content to decline and the cultivable soil layer to decline. As such, soil erosion is seen as the main cause for land degradation with a focus on hill-slope water erosion processes and removal of soil particles by wind. Alarming erosion rates inevitably lead to declining agricultural production and food shortages. While requirements for food, fiber and other resources increase, soil erosion by wind and water continues unabated [Pimentel, 2006].

Beside this main focus on the role of soil erosion processes as major cause of land degradation, researchers have started to pay more attention to potential benefits of erosion processes. Potential benefits of water erosion processes are widely known and used.

Clear examples of land and water management practices that are based on this principle are Zai [Visser et al., 2003] and spate irrigation [Tesfai and Stroosnijder, 2001], in which the fertile soil lost by erosion upstream, considerably increases downstream onsite soil fertility and water holding capacity. Also in Kenya the process of erosion and sedimentation is utilized through the construction of sand dams. The coarse sediment collected behind the dams serves as an underground reservoir providing water during the dry season [Lasage et al., 2008]. More recently, research projects have been developed in which the economic benefits of water erosion are considered in benefit-cost analyses [Firew, 2010]. These examples make contextuality an important concept in water erosion research. With the statement: The perception of land degradation often lies in the conceptualization and cannot be judged independently from only one perspective, Warren [2002] made this contextual appraisal of erosion processes explicit. Using Bawden [1997] four fundamental worldview types, the shift from a technocentric attitude with respect to erosion processes towards a more holocentric attitude can be made more explicit (Fig. 1). In a technocentric worldview it is believed that complex systems can be explained by understanding the interactions between the smaller parts, with only one truth (objectivism). Contrary, in the holocentric worldview, there is no absolute truth (relativism), therefore the world cannot be explained by combining the parts alone.

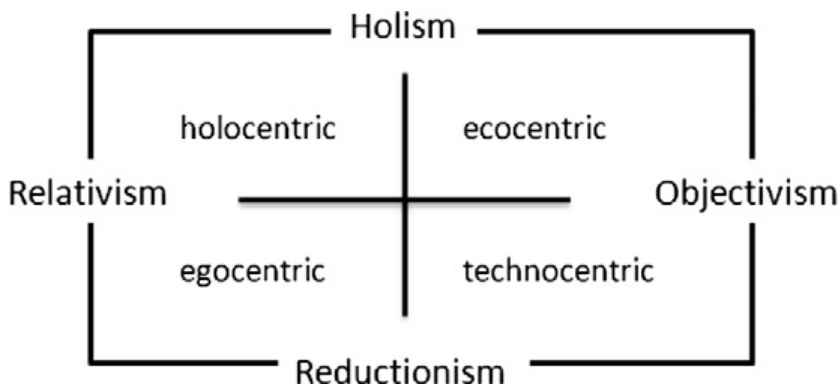
In wind erosion research, we can see a change from the common belief in the reducible wholeness of nature (reductionism) towards a more holistic approach [e.g. Ravi et al., 2010]. However, the technocentric worldview is still pronounced in measuring and modeling approaches; small components and their interactions are often studied in as much detail as possible [Best, 1993, Cornelis and Gabriels, 2003, Leenders et al., 2005a]. This information subsequently cannot be used to simulate and predict larger-scale geomorphological processes because models at the landscape scale validated with traditional point-scale measurements are arguably inadequate for testing model accuracy over broad geographic extents [Webb and McGowan, 2009]. These point-scale measurements often are not taken over a sufficiently long period, do not capture the

large spatial variability and are not calibrated for specific field situations [Stroosnijder, 2005]. Furthermore, in many projects only erosion and transport are measured and modeled [Van Donk and Skidmore, 2003, Youssef et al., 2012a]. When deposition is considered, the focus is often on the qualification and quantification of the negative effects [Huszar and Piper, 1986, Riksen and De Graaff, 2001]. However, Li et al. [2004] demonstrate that dust deposition increases soil fertility.

The beneficial effects of wind erosion is based on a new conceptualization of wind erosion processes, by moving towards a more holocentric world view. Discourses on for example, the new ecology [Scoones, 1999] and political ecology [Blaikie et al., 1985] have underlined the total complexity, broader context and dynamics of a system. More recently, there is a trend to leave the hard engineering mindset behind in order to work with nature. Warren et al. [2001] emphasize the benefits of soil erosion as part of a natural system. Measurement and modeling methodologies are erosion measurement techniques are not so accurate [Stroosnijder, 2005] and often do not cover the spatio-temporal resolution for validation of model outcomes. Therefore, it is questionable if current measurement and modeling methods are sufficient for studying soil erosion processes in the context of a natural system. In this article we contribute to the discussion on the new conceptualization of wind erosion processes by showing that erosion processes can be managed such that the impact and consequences are beneficial at a variety of spatial scales. We discuss three examples in which wind erosion can be used to maintain biodiversity, to improve coastal defense and to harvest soil fertility. In these three cases also the limitations of existing measuring techniques and models are discussed.

2.2 Examples of beneficial wind erosion

Though less well known, wind erosion processes can be managed such that the impact and consequences are beneficial. Three examples are presented hereafter.

FIGURE 2.1: Four worldviews (after [Bawden \[1997\]](#)).

2.2.1 Wind erosion for maintaining biodiversity

Kootwijkerzand is one of the largest inland drift sands in the Netherlands and is a good example of an ecosystem which strongly relies on geomorphological processes. Wind erosion is the dominant process causing high temporal and spatial variation in habitat conditions. In active inland drift-sand areas, wind erosion is an autonomous process which maintains the open-sand habitat. The ecological value of the present inland drift-sand areas in the Netherlands is in the unique combination of relatively high erosion activity causing fine sandy soils low in nutrient and water availability, along with vegetation and fauna species adapted to these poor conditions [[Riksen and Jungerius, 2010](#)]. However under present high N-deposition rates, caused by intensive livestock farming, industry and traffic, the drift-sand habitat tends to disappear due to increased vegetation succession rate.

Kootwijkerzand is one of the largest inland drift sands in the Netherlands and is a good example of an ecosystem which strongly relies on geomorphological processes. Wind erosion is the dominant process causing high temporal and spatial variation in habitat conditions. In active inland drift-sand areas, wind erosion is an autonomous process which maintains the open-sand habitat. The ecological value of the present inland drift-sand areas in the Netherlands is in the unique combination of relatively high erosion activity causing fine sandy soils low in nutrient and water availability, along with vegetation and fauna species adapted to these poor conditions [[Riksen and Jungerius,](#)

2010]. However under present high N-deposition rates, caused by intensive livestock farming, industry and traffic, the drift-sand habitat tends to disappear due to increased vegetation succession rate. where mainly transport and deposition in combination with vegetation development take place; and a regeneration zone, where vegetation succession and soil formation are the dominant processes.

With regular erosion activity in the deflation zone, the conditions remain poor or further degrade and vegetation and algae will not develop. In the transition zone the vegetation consists of pioneer species which are adapted to extreme conditions such as high mobility of sand, low water-holding capacity, extreme micro-climate (high differences in temperature between day and night) and low nutrient content of the soil. Pioneer species are adjusted to flourishing in moving sands. Soil formation in the first succession stage is limited. The organic matter content in the topsoil increases slowly, which creates favorable conditions for species that cannot bear the poor conditions and/or the high sediment deposition rates found near an active deflation/transport zone. As more sand is stabilized, plaques of green algae might develop followed by mosses (Fig. 2), and some humus forms inside the top two centimetres of sand. The vegetation cover in this zone displays strong fluctuation, which is related to the extent of sediment accumulation. Sometimes parts of this zone change back into a deflation zone as a result of an extreme erosion event, but the long-term trend for these zones is to turn into a regeneration zone. The rate at which bare sand can stabilize mainly depends on weather conditions, but research has confirmed that the complete stabilization of the deflation zone can be realized within 1.5 years [Ketner-Oostra and Riksen, 2005].

A certain level of erosion activity is needed to preserve ecosystems, which is accomplished by suppressing vegetation development in the deflation zone. This allows wind erosion to maintain the dynamic conditions in the transition zone needed for the development of the pioneer vegetation and fauna species. Riksen and Goossens [2005] tested different management approaches for their effect on wind-blown mass transport at a 4 m



FIGURE 2.2: Drift-sand nature in the Netherlands. Top: the drift-sand area of Kootwijkerzand, the Netherlands; bottom from left to right: Transition zone; Maintaining active drift sand with a rotary cultivator; Sand earwig; Pioneer moss *Polytrichum piliferum*.

wide and 30 m long plot in Kootwijkerzand in the Netherlands, in order to find the optimal vegetation suppressing technique. The impact of the management approaches was also simulated with the Wind Erosion Prediction System (WEPS) rewritten in PCRaster [Riksen and Visser, 2008], to exclude unwanted border effects causing an increase or decrease of measured sediment transport.

WEPS is a process-based, computer model that predicts wind erosion for a rectangular simulation region on a daily time-step basis [Hagen, 1991]. Visser et al. [2005b] translated the erosion sub-model of WEPS in the environmental modeling language PCRaster, for event based model simulations. Although the model output confirmed most of the field observations, limitations remain in the applicability of WEPS in PCRaster [Riksen and Visser, 2008]. Van Donk and Skidmore [2003] performed a field test of the full WEPS at a field near Burlington, CO, USA. They found that WEPS is very sensitive to small changes in standing biomass. They assumed that this sensitivity was caused by the fact that the model was developed based on measurements in wind tunnels with uniform vegetation cover. A non-uniformly distributed vegetation cover, which is generally the case with natural vegetation, cannot be described by a single, average input value because its spatial distribution also affects the erodibility and/or protection of the soil. Applying WEPS in PCRaster at the spatial scale of the complete nature reserve would

require a temporal and precise input of the vegetation characteristics. Furthermore, research by [Feng and Sharratt \[2005\]](#) concluded that soil moisture content is one of the most sensitive parameters in the standalone erosion model of WEPS. The sensitivity for soil water content is probably correct because the natural wind erosion process is also very sensitive to this parameter. To enable running the model taking into account the soil moisture content, accurate and timely measurements of soil moisture content are necessary. Given the highly dynamic nature of driftsand ecosystems it is almost impossible to obtain input parameters with the required spatial and temporal detail, which makes it difficult to apply WEPS in PCRaster at larger spatial and temporal scales.

Simulations of wind erosion are very important for the evaluation of different management scenarios. However, reductionistic models such as WEPS in PCRaster are complex because the numerous processes such as climate, soil, vegetation, crusts and wind direction have a direct impact on sediment transport. Knowledge about the processes and all the interactions between those processes are of vital important to control the model, keeping in mind that some processes rely on empirical or experiential considerations that are not site-specific and do not represent the necessary spatial and temporal variability. The optimum use of the wind erosion processes for environmental management requires knowledge of the long-term and large-scale effects of the management approaches used. Information is needed on the larger scale wind erosion processes and the impact of windblown mass transport on vegetation development. This can be realized through the long-term monitoring of a whole system after implementation of a specific management approach. This is a time and resource-consuming approach. The combination of the constraints in modeling and measuring shows the need to work toward a more holistic model that simulates the larger scale landscape dynamics based on simple physical and stochastic consideration, representing the inherent complexities.

2.2.2 Wind erosion for coastal defense by dune formation

Coastal dunes play an important role as natural defense zones against flooding of the hinterland. Dune formation is important to maintain or restore the natural defense zone after coastal erosion from severe storm events. Coastal erosion, nourishments and wind erosion (Fig. 3) determine the rate at which a system can transport and fix sediment volumes, where storm events are very important. [Houser and Hamilton \[2009\]](#) studied dune recovery after a hurricane. They found that for barrier islands the alongshore variation in recovery is not only related to island width, but also to offshore bathymetry, height of the pre-storm dunes and overwash. The level of impact during subsequent storms and the ability of the island to recover will depend on the frequency of storm events because this determines the time allowed for the return of vegetation and the recovery of the dunes.

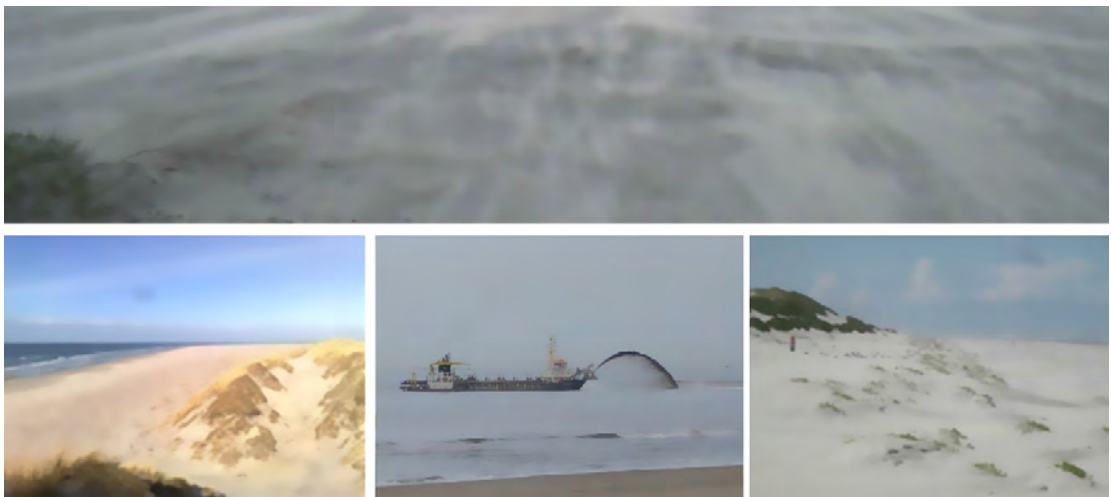


FIGURE 2.3: Wind erosion and coastal dune formation at the isle of Ameland in the Netherlands. Top: aeolian streamers. Down from left to right: dunes as coastal protection; nourishments and embryonic dunes.

New management approaches based on sand nourishments have generally resulted in a positive sediment balance and the formation of new dunes [[VanKoningsveld et al., 2008](#)]. These new dunes contribute to the role of dunes as a buffer against sea level rise

and increasing storm frequency and intensity. A constant supply of new sediment leads to landscape rejuvenation with an ecosystem at different succession stages. Wind erosion plays an essential role in this system, as wind is the driving factor, transporting large amounts of sediment from the beach to the dunes, as such wind erosion is important for coastal protection and ecology. Despite the significant work of, for example [Arens et al. \[2004\]](#), [van der Wal \[2000b\]](#), little is known about the effect of these nourishments on dune formation processes. To estimate the effect of these nourishments, it is essential to gain insight into the effects and interactions of vegetation, meteorological conditions and soil properties on sediment transport and landscape evolution.

Lack of information is still the main constraint hampering the development of a theory of spatial and temporal beach-dune interactions [[Houser, 2009](#)]. Erosion pins, GPS and aerial photographs give insight into slope development, rates of processes, and a general indication of geomorphic activity [[Arens et al., 2004](#)]. However, flux measurements are needed to develop a thorough understanding of the coastal formation mechanisms. But equipment for measuring aeolian mass fluxes are often calibrated in the wind tunnel, where some of the most important aspects of sediment transport dynamics cannot be reproduced [[Baas, 2008](#)]. To capture the spatial resolution, [Baas and Sherman \[2006\]](#) suggest that the measurements should be conducted with multiple sand traps or sensors deployed over lateral distances similar to the height of the internal boundary layer. Together with measurements of air flow, rainfall, humidity, evaporation, sea-water level (fetch) and some accurate estimations of parameters, this can be used for the evaluation of different transport equations, as suggested by [[Arens, 1996b](#)]. The effect of vegetation is also an important factor in sediment transport [[Wolfe and Nickling, 1993](#)]. [Arens et al. \[2001\]](#) discovered that different densities of vegetation lead to differences in dune morphology. However, doubts remain whether combining all the information and interactions of the different components can explain the landscape evolution. This is part of the wider geomorphologic methodological discussion whether ‘reductionist’ studies can explain dune forms and patterns [[Livingstone et al., 2007](#)]. Where it is argued that that reductionism breaks down because these are complex systems governed by nonlinear

dynamics [Kocurek and Ewing, 2005].

Werner [1995] was the first to develop an algorithm simulating the evolution of dunes based on stochastic considerations. Baas and Nield [2007] added a vegetation component to this algorithm, in order to simulate the evolution of vegetated dunes with multiple types of plant response in the environment. This approach is elegant in the sense that it realistically simulates dune development using simple local rules in a self-organizing cellular automaton algorithm. The problem with this holistic approach is that it does not allow for the simulation of different physical properties such as wind regimes, soil moisture or particle sizes, as numerical modeling results depend on parameter choice, and not on physical considerations. On the other hand, it is questionable that ‘reductionist’ complex computational models, which in detail describe flow structures, soil properties and other important parameters will lead to better scenario analysis regarding coastal defense strategies. Therefore, it is necessary to find an integration where stochastic models capture the complexities, but physical parameters determine the forms and patterns. Clearly, wind erosion supports the natural system dynamics in drift-sands and coastal dune systems.

2.2.3 Wind erosion for harvesting soil fertility in the Sahel

The African Sahel forms a transition zone from the arid Sahara in the north to the more humid savanna in the South. The Sahelian climate is characterized by a dry season and a short (3 months) wet season. Wind and water erosion processes are closely related in the early rainy season [Visser et al., 2004a]. Rainfall is often preceded by strong winds, causing severe wind erosion [Visser et al., 2003]. The events are usually short-lived but may result in intense sediment transport, which is ended by intense rainfall that often directly follows the wind erosion events. Sediment initially eroded from the fields by wind may partly be returned by the sediment transport processes aligned with water erosion. Another possibility is that the energy of the water erosion processes may further enhance the erosion started by the forces of the wind. In the dry season, strong

dry and dusty winds called Harmattan originate from the Sahara and transport large amounts of fine sediments.

Numerous studies on wind erosion processes have been executed in the sahelian zone [e.g. [Gomes et al., 2000](#), [Leenders et al., 2007](#), [Sterk et al., 2004](#), [Visser and Sterk, 2007](#)]. Most studies conclude that the sahelian zone is subject to serious degradation through nutrient and sediment losses by wind erosion. However, many studies use small datasets and have a small spatial resolution. Upscaling the field measurements toward regional statements of soil and nutrient losses has led to large overestimations of the negative effects of wind erosion processes ([Farge and Magid, 2004](#)). For example, the sahelian zone has long been characterized by a large outflow of dust [[Prospero, 1999](#)]. Other studies on dust emission estimate a large exodus of the very small and fertile particles by wind erosion [e.g. [Stoorvogel et al., 1990, 1993](#)]. However, dust is also an important long-term continual nutrient renewal vector to the soils in this area [[Drees et al., 1993](#), [Visser and Sterk, 2007](#)] show that most of the dust entrapped outside the Harmattan season originates from local sources whereas the Harmattan dust is considered a real source of nutrient input.

The effect of nutrient dynamics by wind and water erosion at village scale (about 75 ha) were investigated by [Visser and Sterk \[2007\]](#). They found that nutrient losses at the village scale were considerably smaller than losses at the plot scale. Where sediment in suspension can travel over distances up to thousands of kilometers, long-term nutrient losses due to saltation on a village scale can be assumed to be nil, indicating that nutrients are reallocated within the area. This is supported by [Buerkert and Lamers \[1999\]](#), who found that most sediment transported during a wind erosion event is transported over a small distance. Most erosion takes place on bare plots, but the sediment transported from those plots is subsequently deposited in a field, bush or mulch cover plot nearby (Fig. 4). For local farmers, this is an important dynamic, which is used in order to accommodate their food supply by capturing the sediment and mitigating the loss of their soil fertility.



FIGURE 2.4: From left to right: entrapment of sediment by vegetation in the Sahel; the parkland system in the Sahel; Seedbed preparation to test the effect of size of sowing pits.

Source: [Visser et al. \[2010\]](#)

In northern Burkina Faso, some subsistence farmers use branches of trees to capture sediment on their fields [[Leenders et al., 2005b](#)] to improve their soil's fertility. The layer of sediment often has a higher nutrient content than the underlying soil [[Visser et al., 2005b](#)], diminishes the negative effects of crust formation [[Visser et al., 2003](#)], enhances water infiltration, and increases soil faunal activity [[Mando and Stroosnijder, 1999](#)]. Farmers that harvested sediment on their fields claimed to obtain a higher yield in the consecutive year. Furthermore, the interaction between wind and water erosion has some clear benefits as well. [Visser et al. \[2010\]](#) studied the possibilities of making effective use of soil crust in northern Burkina Faso. Larger sowing pits were created on fields that were sensitive to crust formation. The crust develops under the combined processes of wind and water erosion, where wind erosion removes the particles on top of the crust developed by runoff [[Valentin and Bresson, 1992](#), [Visser et al., 2003](#)]. It was found that a larger sowing pit is positively related with a higher yield, especially on soils with a well-developed erosion crust. Larger sowing pits increase the volume of water trapped in the pit, that give higher infiltration and faster seedling development. Furthermore the seedlings are stronger and more resistant to wind erosion. The crust around the sowing pits remains intact, protects the soil against wind erosion, and reduces the chance that seedlings are abraded by saltating grains. This example shows how farmers can make use of a normally undesired effect of wind and water erosion and the soil crust to protect the soil and vegetation against wind erosion and locally increase the soil fertility.

Problems related to the large dust emissions from the Sahelian zone cannot be denied. However, the above-mentioned options of actively utilizing the wind and water erosion processes for mitigating total loss for agricultural production are promising. But these examples are based on plot-sized experiments by individual researchers and farmers. Since the application of these management approaches requires degradation at one location before the benefits can be obtained, more insight into the large scale potential of these management approaches is required. Regional-scale modeling of the dynamics of the natural resources (water, nutrients and sediment) will provide these insights. This holistic approach combines the positive view of ‘working with nature’ with a focus towards the whole system dynamics, and not only on the ‘negative’ outflow of sediment from this region.

2.2.4 Discussion

In the three examples we have looked at the wind erosion process at system level. By looking at the effects of wind erosion at system level the system and its stakeholders determine whether the effects of a process are positive or negative. The reductionist approach to study these processes can help to understand the basic principles of the process, but a more holistic approach is needed to see its function(s) in the system studied. The three different examples in this paper show the positive role of wind erosion in a driftsand nature reserve system, coastal dune system and in local farming systems in the Sahel. The main question is if the existing research methodology and approach are suitable to study these processes at system level. It has been shown that there are still many pitfalls in the research methodology and approach. One of the main pitfalls is the measurement of soil erosion. [Stroosnijder \[2005\]](#) argues that “there is a crisis in soil erosion measurements because there are insufficient empirical data of adequate quality, and a lack of funds to improve that situation”. Soil erosion is complex because of the spatial and temporal variability. Equipment is calibrated and tested in the controlled environment of a wind tunnel for a series of scenarios. Field situations account for much more variability, and conditions not accounted for during the

calibration. Another pitfall is found in the extrapolation of small-scale erosion studies, which generally results in large overestimation in sediment fluxes. [Visser and Sterk \[2007\]](#) show that detached soil is often deposited close to the source. With changing wind regimes, sediment is returned to the source area, not leading to large net export of sediment from the area, but merely to a redistribution of the sediment within the area. The beneficial effects of wind erosion also means to consider the potential benefits for sink areas, as these benefits are often left outside the discussion. Opting for a more holistic approach shed more light on the total system dynamics. This means that not only sediment fluxes should be measured, but the whole system should be monitored, where sediment budgets can be linked with erosion and deposition areas and interactions between water and wind erosion should be taken into account [[Field et al., 2009](#)]. Assumptions and errors in measurement set-up and techniques should be made more explicit, leaving room for a broader or different interpretation of the system dynamics (relativism). Furthermore, onsite calibration of the equipment is needed to test the performances under site specific conditions. The study by [Goossens et al. \[2000\]](#) is an excellent example of combined lab and field experiments.

It has been shown that modeling approaches are still characterized by a highly reductionist approach, in which the smaller components are studied, where the sum of all different components do not necessarily explain the larger system dynamics. This follows from the large complexity of the separate components combined with unknown interactions and feedback mechanisms. In modeling approaches unknown factors are parameterized, resulting in a model structure, where the output depends on the choice of parameters, rather than on simulating a real world system. [Beven \[1993, 2006\]](#) introduced the concept of equifinality in hydrological modeling, where different sets of parameters give acceptable fits for observational data. In modeling of aeolian processes, this problem is even more emergent. Partly because unlike water erosion, wind erosion is not strictly delineated by watershed boundaries. Boundaries have to be determined arbitrarily and boundary effects on model output may be large. But also because interactions and feedback mechanisms are largely influenced by great spatial and temporal

variability. As a result, interactions are often based on empirical and physical considerations that are found in a context dependent environment, and therefore not widely applicable. It is argued here that wind erosion research should not only focus on the small interacting components, but should move forward towards a more holistic world-view. Stochastic models can simulate large-scale geomorphologic processes, without using all the complex interactions. [Baas and Nield \[2007\]](#) found unexpected emergent behavior in the form of competition between vegetation in a stochastic dune evolution model. This indicates that cellular automata can capture some non-linear complexities in aeolian research. It should be studied if a minimum of well established physical considerations can drive those stochastic models, to simulate the complex non linear interactions on a larger scale.

The goal of this article is not to trivialize the problems of wind erosion, but to stimulate scientists and policy makers to adopt a different mindset. Sediment fluxes can only be measured on a small scale with a small temporal dimension, but small scale studies cannot be extrapolated to evaluate the dynamics in a larger system. Therefore, the causes and consequences of wind erosion should not always be looked at as disadvantages and problems. Wind erosion is an integrated part of natural systems.

2.2.5 Conclusion

In aeolian research, for a long time, the focus has been on problems related to soil loss and deposition. This focus is often supported by empirical data and extrapolation of small-scale studies. Modeling approaches try to comprehend the inherent complexities, but rely on empirical data combined with some physical considerations, with a large gap between (reductionist) small and (holistic) large scale aeolian processes. Three examples show that the physical energy of wind erosion can indeed have a positive contribution to food security, biodiversity, and safety. With an holistic approach, we can look at the larger system dynamics and look at wind erosion as an integrated part of the natural system dynamics. Wind erosion has both threats and opportunities, where one does not exclude the other.

2.2.6 Acknowledgements

The authors thank three anonymous reviewers for their constructive comments and suggestions, which greatly improved this manuscript. Furthermore, we would like to thank Erik Slingerland for his useful comments on an earlier version of the manuscript.

Chapter 3

Self-emergent behaviour in particle based simulations

Published as preprint: Poortinga, A., Wesseling, J. G., & Ritsema, C. J. (2014). Stratified chaos in a sand pile formation. arXiv preprint arXiv:1403.0741.

Self-emergent behaviour in particle based simulations

abstract

Non-linear self-emergent behaviour of complex systems is an important topic of investigation in geophysical research. Sand-pile formation is often used as an example to describe scale-invariant power law fluctuations in a system. Cellular automata are often applied to describe chaotic behaviour, as simulating physical interactions between individual particles is computationally demanding. However, recetechniques allow to calculate the forces acting on large numbers of particles. In this study, we apply a state-of-the-art parallel implementation of the discrete element method on a graphical processing unit to simulate sand pile formation. Interactions between individual grains were simulated using a contact model in an Euler integration scheme. Computational results show non-linear self-emergent power-law and scale-invariant behaviour, which is in good agreement with experimental results, theoretical work and self organized criticality (SOC) approaches. This study shows that the fully deterministic model, where the position and forces on every individual particle can be determined every iteration has great potential to study non-linear and self-emergent behaviour in geophysical research.

3.1 Introduction

Non-linear dynamics in complex systems are an important topic in geophysical research. Systems driven by local non-linear interactions and perpetually changing feedback mechanisms on a small scale are the basis of self-organization on the larger scale. However, the large scale self-emergent processes do not directly correspond to the forcing template [Murray and Fonstad, 2007]. While there is a fair understanding of small scale geophysical processes, it remains challenging to model and predict larger scale geomorphological phenomena considering the wide range of complex non-linear processes and feedback mechanisms. A number of studies explored the concept of using a set of simple rules (reduced complexity) to simulate geomorphological phenomena while neglecting most of the physics. These so-called cellular automata have e.g. be used in the context of aeolian bed-form evolution [Anderson and Bunas, 1993, Baas, 2002, Nield and Baas, 2008, Werner, 2003], bar morphodynamics [Nicholas, 2010] and fluvial geomorphology

[Coulthard et al., 2007, Coulthard and Van De Wiel, 2007, De Boer, 2001, Fonstad and Marcus, 2003]. These models are powerful in qualitative terms (self-organization, patterns and shapes), but often have a limited predictability in quantitative terms.

Sand-pile formation is often used to describe self-organization. When dry sand is poured on a surface, a conical pile will be formed with an angle of repose around 34° . Additional particles result in an unstable state causing the structure to topple into a state where gravitational and frictional forces are in equilibrium. The Bak-Tang-Wiesenfeld (BTW) model [Bak and Sneppen, 1993, Bak et al., 1987], also referred to as the abalian sand-pile model, laid the basis for self-organized criticality (SOC). The model consists of a regular finite sized grid, where every cell corresponds to the slope of the sand-pile. The angle of the slope increases as grains are randomly added to the pile until the maximum angle of repose (34°) is reached. Every additional grain will cause the structure to topple, resulting in avalanches of various sizes. Nowadays, the SOC concept is widely used in different scientific disciplines such as economics [Cont and Bouchaud, 2000], neural science [Buzsáki and Draguhn, 2004] and earthquake research [Bak et al., 2002, Christensen et al., 2002].

Like many physical systems, (sand or rice) pile formation exhibits scale invariant behavior driven by small scale non-linear system properties [Held et al., 1990, Liu et al., 1991, Tebaldi et al., 1999]. The system contains a critical attractor with events of various sizes that can be described by a power law. Like many natural systems, the temporal signal of sand-pile formation is characterized by a $1/f^\alpha$ spectrum [Jensen et al., 1989]. Besides experimental studies [Aegerter et al., 2004, Frette et al., 1996, Held et al., 1990], a variety of approaches, varying from cellular automata [Bak and Sneppen, 1993, Bak et al., 1987] to numerical integration models [Jensen et al., 1989] have been conducted to describe the deterministic chaos in sand pile formation. Despite the rich history on particle based modelling [Cundall and Strack, 1979, Cundall, 1971, Williams and Mustoe, 1987], simulations in a three-dimensional space with a large number of particles have just recently become within reach of the computational means.

Studies by e.g. Bell et al. [2005], Iglberger and Rüde [2010], Longmore et al. [2013],

[Stahl and Konietzky \[2011\]](#) are examples of how particle based computations are integrated in a discrete element model (DEM). As interactions between bodies ($n > 2$) can not be solved analytically, a time integration scheme and contact model are used to describe the forces between particles. The behavior of granular matter can be simulated in a realistic manner by computing all forces acting on a particle and calculating their effects in three dimensions within a time step. These models can be applied to study stratified chaos in more detail (i.e. in combination with variation in gravitational forces, particle geometry and mass, frictional forces etc.). Applications of DEM in geoscience include studies on rock and soil avalanches [[Chang and Taboada, 2009](#), [Mollon et al., 2012](#), [Taboada and Estrada, 2009](#)], boundary stresses [[Tewoldebrhan et al., 2011](#)], weathering [[Utili and Crosta, 2011](#)] and sediment deformation [[Damsgaard et al., 2013](#)]. Literature in the topic of granular flows is vast, however, as recognized by [Frey and Church \[2011\]](#), it is mainly published in the literature about physics, chemical engineering, powder and grain technology.

The aim of this paper is to demonstrate the potential use a particle based model to study non-linear self-emergent chaotic behaviour in geophysical research. We use highly efficient parallel implementation of the DEM on the Graphical Processing Unit (GPU) of the computer to simulate sand-pile formation. Results are compared with previously obtained experimental and theoretical findings.

It should be noted that we mainly focus on the applicability of particle based simulations for geophysical research, i.e. the coherence between numerical simulations and analogue experiments. Elaborate information on granular physics can be found in e.g. [Herrmann and Luding \[1998\]](#), [Jaeger et al. \[1992\]](#), [Mehta \[2007\]](#), [Wolf \[1996\]](#). More information on parallel model optimization using the GPU was presented by e.g [Buck et al. \[2004\]](#), [Kessenich et al. \[2004\]](#), [Longmore et al. \[2013\]](#).

3.2 Materials and Methods

Experiments were performed in a laboratory and their results were compared with model results. The descriptions of the experimental setup and the applied model are

given below.

3.2.1 Experimental setup

A uniform sand fraction ($d_{50} = 285 \mu\text{m}$) was filtered and painted in five different colours. Five equal fractions were weighed and added in separate layers to a small transparent funnel. A high speed camera (Casio EX-F1) was positioned in front of the funnel. High speed images of sand flowing through the funnel were acquired .

3.2.2 The model

The DEM is a well recognized method to simulate large numbers of particles. The method was introduced by [Cundall and Strack \[1979\]](#), [Cundall \[1971\]](#) to study the motion of rocks. Forces that act on each individual particle are calculated every time-step. A contact model allows multi-body interactions using the relative overlap between two particles to calculate the contact force. Similar to [Silbert et al. \[2002\]](#), we use a cohesionless and inelastic Herzian [[Hertz, 1882](#)] contact model. Newton's second law is used to calculate the motion caused by gravitational, normal and tangential (frictional) forces. The method requires quite some computational power, as all forces between particles have to be calculated individually. While the core of model (contact model) is rather simple, the framework to efficiently handle all the computations on the GPU is rather complex and extensive.

We have used the framework of [Longmore et al. \[2013\]](#), an adoption of the method as described by [Bell et al. \[2005\]](#), which is based on the original concept [Cundall and Strack \[1979\]](#). Spheropolygonal grains (a tetrahedral arrangement of four spherical particles) were used, to ensure that computations can be handled efficiently while maintaining static friction due to interlocking [[Longmore et al., 2013](#), [Pöschel and Buchholtz, 1993](#)] and preventing stick-slip behavior [[Bell et al., 2005](#)]. During each iteration (Euler integration), the individual forces working on a particle are updated and summed to a total force (for the grain). The total force F (N) for particle p in particle collection P can be calculated by the particle mass m (kg) and the gravitational acceleration g ($m.s^{-2}$) :

$$F_p = \sum_{i \in \{P-p\}} F_i + mg \quad (3.1)$$

The total force working on the grain is calculated by summing the forces acting on the connected particles. These forces are split into the total normal force (F^g) (N) and the torque (T^g)(N·m)

$$\vec{F}^g = \sum_{i=1}^{N_p} \vec{F}_i \quad (3.2)$$

$$\vec{T}^g = \sum_{i=1}^{N_p} \vec{r}_i \times \vec{F}_i \quad (3.3)$$

where N_p is the number of connected particles and r_i represents the relative vector from the center of the granule to its child particle i . With Newton's second law and the particle mass the acceleration at time t can be calculated.

The contact forces of two colliding particles p_i and p_j are separated into the normal force and the tangential component:

$$\vec{F}_{ij} = \vec{F}_{ij}^n + \vec{F}_{ij}^t \quad (3.4)$$

To simplify the contact detection and force calculation, an area of overlap ξ (m^2) between two particles is defined. In case of spherical particles, the normal vector (\vec{N}) and the overlap area can be found by

$$\vec{N}_{ij} = \frac{\vec{X}_j - \vec{X}_i}{\|\vec{X}_j - \vec{X}_i\|} \quad (3.5)$$

and

$$\xi_{ij} = \max(0, R_i + R_j - \|\vec{X}_i - \vec{X}_j\|) \quad (3.6)$$

where R_i is radius and \vec{X}_i is the center of particle i .

It should be noted that eq. 3.6 defines ξ_{ij} rather as a mutual compression or deformation than as an overlap, so the time interval of the model should be small enough

to prevent soft sphere behavior. Using the normal vector \vec{N} , the relative velocity $\dot{\xi}_{ij}$ of the compression can be calculated as

$$\dot{\xi}_{ij} = (\vec{v}_j - \vec{v}_i) \cdot \vec{N}_{ij} \quad (3.7)$$

The most basic formulations of the tangential and normal forces, incorporating the dissipative and friction terms are:

$$\vec{F}_{ij}^n = (-k_\alpha \dot{\xi}_{ij}^\alpha \xi_{ij} - k_\beta \xi_{ij}^\beta) \vec{n}_{ij} \quad (3.8)$$

$$\vec{F}_{ij}^t = -\min(\mu_s \cdot \|\vec{F}_{ij}^n\|, k_t \cdot \|\vec{V}_{ij}\|) \frac{\vec{V}_{ij}}{\|\vec{V}_{ij}\|} \quad (3.9)$$

where μ_s (N) represents friction. The viscous damping coefficient k_α is calculated from the coefficient of normal restitution (e_n), the reduced mass (m_{eff}) and the time-step (Δt) [Bell et al., 2005]. A dimensionless coefficient of 0.02 was added to produce rapid damping:

$$k_\alpha = \frac{-2 \cdot m_{eff} \cdot \log(e_n)}{0.02 \cdot \Delta t} \quad (3.10)$$

where m_{eff} is obtained as the harmonic mean of the mass of particles m_1 and m_2 :

$$\frac{1}{m_{eff}} = \frac{1}{m_1} + \frac{1}{m_2} \quad (3.11)$$

The stiffness coefficient k_β was calculated with Youngs parameter E_{eff} and particle diameter P_d :

$$k_\beta = \frac{4}{3} \cdot (E_{eff}) \cdot \sqrt{0.25 \cdot P_d} \quad (3.12)$$

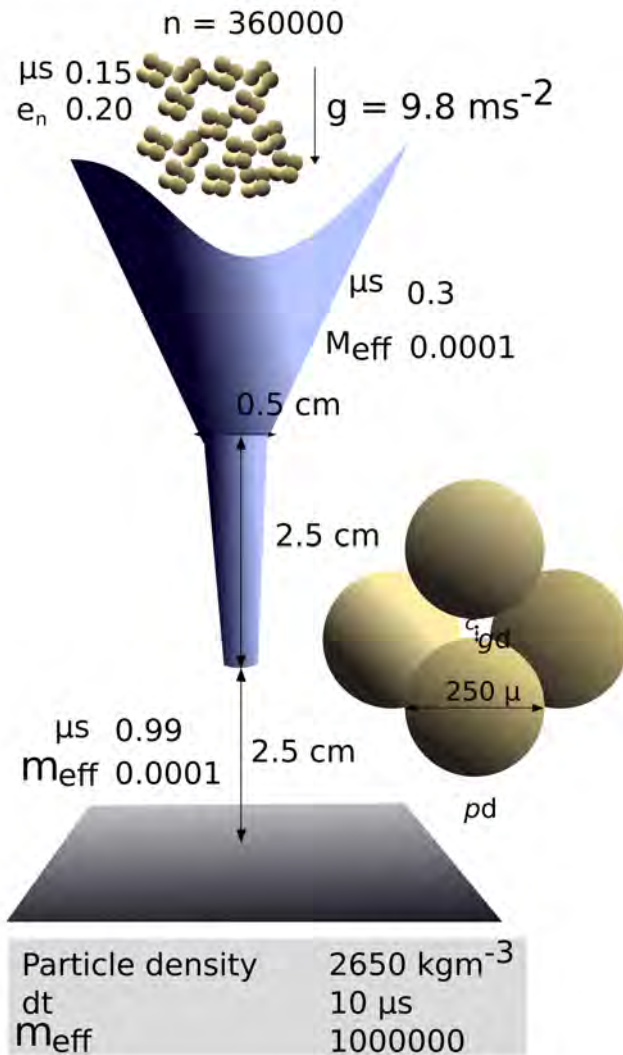


FIGURE 3.1: A schematic overview of the dimensions and parameter settings used in the model simulation and a representation of the spheropolygonal grains.

The parameters used in the simulation are shown in Fig. 3.1. Different coefficients for friction and restitution were used for the floor, funnel and particles. A small variation in distance to the center of mass of the spheropolygonal grains was included to emulate a variation in particle characteristics. Particle size and mass were kept constant for all grains, as a variation would add an extra layer of complexity to the study.

One of the problems in time integration is finding the optimal time step size, as time integration is a trade-off between computational efficiency and a physically correct

representation of the process. A time-step of $10 \mu\text{s}$ was found to give reliable results for a particle diameter of 250μ . However, in the current framework, data on the GPU can only be rendered directly to the screen (for visual interpretation) and not directly be read from the GPU memory. In order to obtain the data, a memory transfer from the GPU to the CPU is required, which is a computational very demanding task. After testing different sampling resolutions on relatively small datasets, a sampling resolution of $100 \mu\text{s}$ was found to give reliable results.

The framework was written in C++, the OpenGL shading language GLSL and was rendered in OpenGL. Calculations were performed on a Graphic processing Unit (GPU) as this allows to perform the computations in parallel, thus significantly reducing the calculation time. The model runs were done on a regular desktop PC, containing two graphical cards (gtx 560ti) in a SLI configuration.

3.3 Results and Discussion

In both laboratory and simulation experiments different layers of colored grains were added to the funnel for visual comparison of the simulated results with the experimental ones (Fig. 3.2 top and middle). The experimental results as well as the model results show a rapid mixing between the different colors. The different layers mix in the middle of the funnel, while maintaining the layered structure on near the walls of the funnel. The flow of sand contains different colors that form a cone with an angle of repose of approximately 34 degrees. The particles added to the top of the sand-pile result in a non-equilibrium situation where the angle of repose exceeds the 34 degrees, resulting in an avalanche where the sand from the top flows over the surface of the sand-pile. This is clearly visible in both the experimental and the modeled results (Fig. 3.2 middle and bottom and accompanied movie)

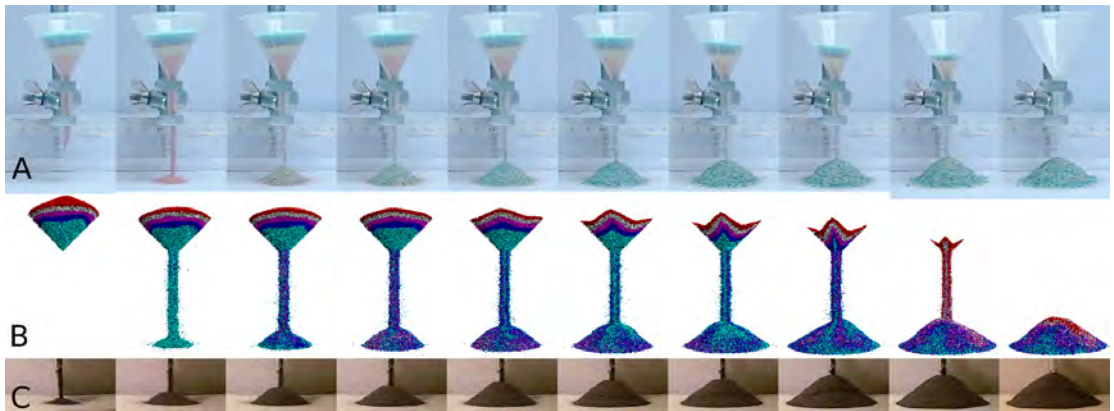


FIGURE 3.2: A visual comparison between an experiment with layers of different colours (A), the model run with a layer of different colors (B) and an experiment with black sand focused on the avalanches of the sand-pile (C).

The constant grain throughput of the funnel leads to a linear decrease in potential energy (Fig. 3.3). The entropy of the system diverges through intermittent dissipation of kinetic energy in the sand-pile (Fig. 3.3). The data show a periodic signal with an increasing amplitude. With gravitational forces exceeding the frictional ones, the sand-pile shows relaxation oscillations when kinetic energy is dissipated by avalanches. Considering the constant input of energy into the system, an increase in kinetic energy implies energy dissipation, whereas a decrease in kinetic energy represents the build up of energy. Previous studies [Frette et al., 1996, Held et al., 1990] used the fluctuation in the mass of a sand-pile to study the energy distribution in a sand-pile formation. We are able to use the kinetic energy directly to study the fluctuations in energy distribution.

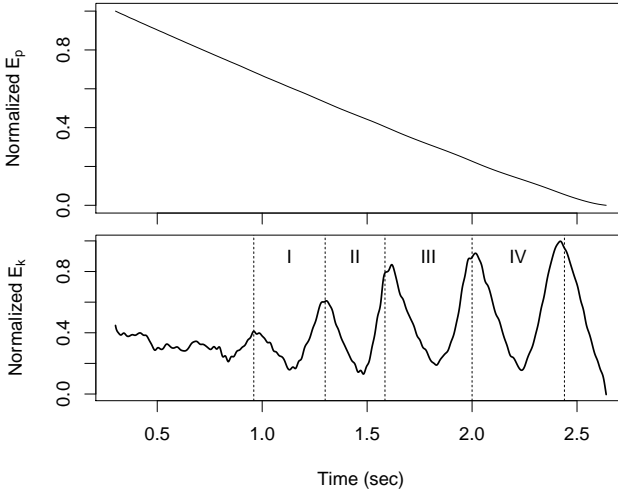


FIGURE 3.3: The normalized potential energy of the entire system (top), indicating a constant throughput of particles and the normalized kinetic energy for the sand-pile (bottom), with periods of energy dissipation and absorption. The kinetic energy release was divided into four different periods (I II, III, IV) for further analysis.

Like rock falls, earthquakes and landslides [Guzzetti et al., 2002, Hergarten, 1999], the cumulative frequency-magnitude probability of the kinetic energy obeys power law behaviour:

$$P(E_k) = E_k^\beta \quad (3.13)$$

with $\beta = -0.78$. By dividing the periodic signal into different periods (I, II, III and IV, Fig. 3.4), we find finite-size scaling behaviour for the growing sand-pile. The lines fitted through the data-points include the upper and lower cut-off values in an upper truncated Pareto distribution (equation 3.14) [Hergarten, 2002]. We have found $\beta = 0.21, 0.16, -0.29$ and -0.81 for period I, II, III and IV respectively. The cumulative frequency-magnitude probability E_k for energy dissipation for a pile with potential energy E_p can be given by equation 3.15 [Barabási and Stanley, 1995], with $f(x)$ constant up to some value and $D = 0.56$ (Fig. 3.4 bottom)

$$P(E_k) = \frac{\left(\frac{E_k}{E_{kmin}}\right)^{-\beta} - \left(\frac{E_{kmax}}{E_{kmin}}\right)^{-\beta}}{1 - \left(\frac{E_{kmax}}{E_{kmin}}\right)^{-\beta}} \text{ for } E_{kmin} < E_k < E_{kmax} \quad (3.14)$$

$$P(E_k, E_p) = E_k^{-\beta} f \frac{E_k}{E_p^D} \quad (3.15)$$

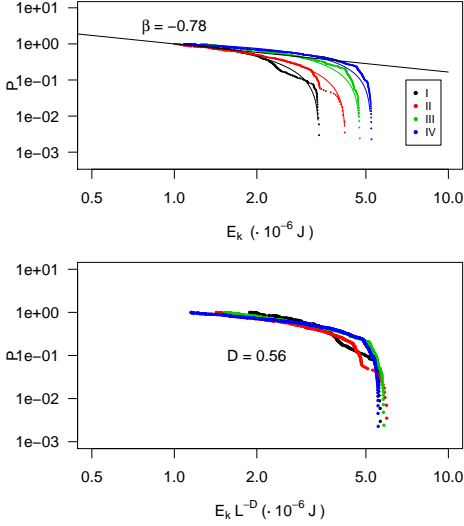


FIGURE 3.4: The cumulative probability distribution of avalanches for four different periods (see Fig. 3.3). The data show that periods of energy dissipation follow a power law and finite-size scaling for the different periods. The data scales following the parameter $D = 0.56$.

Scale invariance is governed by the build-up of energy in the sand-pile since the δE_k has the same order of magnitude for the different time periods (I,II,III and IV, Fig. 3.5). Fig. 3.5 (top) clearly shows that energy build-up (and thus dissipation) increases with the growing sand-pile due to consecutive steps of energy build-up through time. This implies that finite sized scaling is governed by consequential build-up and dissipation of δE_k and not by differences in δE_k . Due to the laws of entropy, the system is attracted towards the low energy state, which is an equilibrium situation between friction and gravity. The δE_k and it's derivative $\delta^2 E_k$ (Fig. 3.5 bottom) have no scale dependency and show a chaotic behaviour within the specific domain.

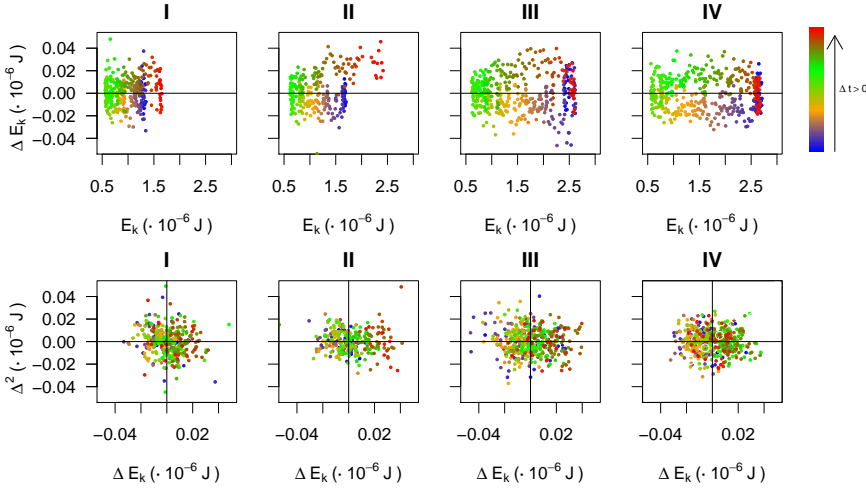


FIGURE 3.5: The energy distribution for periods I, II, III and IV with E_k versus δE_k (top) and δE_k versus $\delta^2 E_k$ bottom. Scale invariance is governed by the build-up of energy, where δE_k remains within the same range for the different periods.

Bak et al. [1987] used the BTW model to explain the ubiquitous $1/f$ noise signal, found in many natural systems, whereas an experimental study [Jaeger et al., 1989] found no $1/f$ noise signal. Later studies claimed that this was in fact a brown $1/f^2$ noise spectrum [Jensen et al., 1989, Kertész and Kiss, 1990], whereas Laurson et al. [2005] found a power spectrum $1/f^\alpha$ with $\alpha < 2$. Similar results were found in this study, the power spectrum of the kinetic energy of the particles in the sand pile moving in a x and y direction has a brown noise signal ($1/f^2$) (Fig. 3.6). However, the kinetic energy of the flow in the vertical (z) direction is closer to a white noise spectrum ($1/f$). This implies that the frequencies of the distribution in the z direction have the same amplitude, whereas there is a dominance to low frequencies in the x and y direction. When boundary conditions are included (i.e. interaction with the floor) this white noise changes to a brown noise spectrum. The stream of particles from the funnel has a white noise spectrum in the x, y and z direction. The rotational motion of the grains have a pink noise spectrum ($1/f^\beta$) in the x, y and z direction.

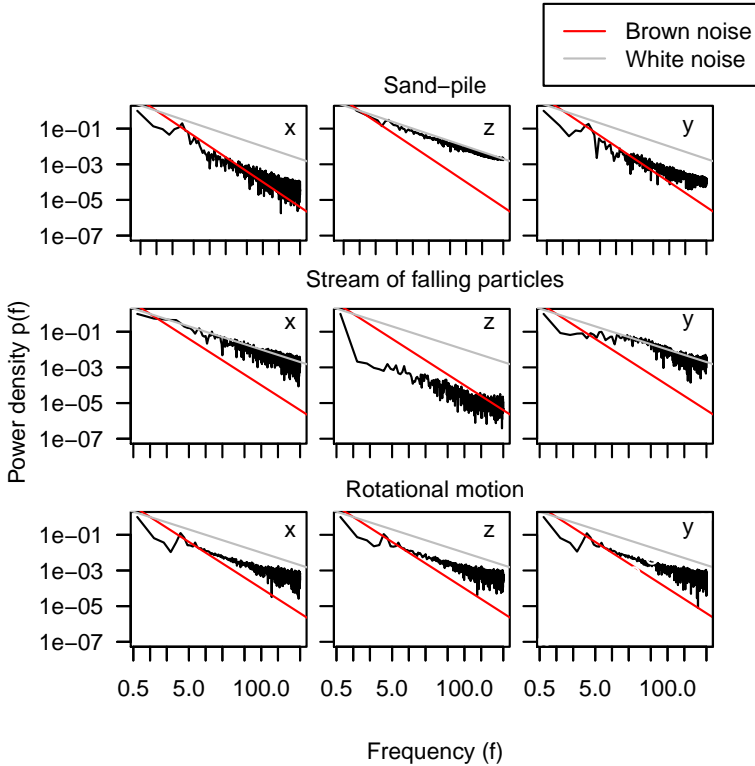


FIGURE 3.6: Power spectrum of the sand-pile (top), stream of particles from the funnel (middle) and rotational motion (bottom).

Previous experimental work used the falloff (of mass) from a sand-pile of every time-step to study the behavior of avalanches [Held et al., 1990, Jaeger et al., 1989]. In this study the frequency distribution of energy dissipation was used in the same manner. However, an avalanche is the build-up and dissipation of energy over a larger number of consecutive time-steps and was therefore not used in this study. For example, fig. 3.3 shows for example five events of large energy dissipation which can be labelled as an avalanche. Furthermore, it should be noted that whereas physical considerations form the core of the current approach, the correctness of the output is still dependent on the parameter settings in the contact model and the numerical integration scheme.

In this study we have used particles in a tetrahedral arrangement to simulate static friction by the interlocking of neighbouring grains. However, a sand fraction does not

consist of regular geometrical shapes but consists of a large variety of different shapes and sizes. Future work might replace spheres and other regular shapes by irregular shapes of various sizes, as demonstrated by [Buscombe and Rubin \[2012\]](#), [Buscombe et al. \[2010\]](#) for a more realistic representation of the granulates.

A rather elaborate and complex framework is required to efficiently handle all computations. However, the basic principle of the model is very simple compared to traditional models in geophysics, as it solely relies on gravity and contact forces. Future applications might include the physics of wind erosion processes, such as the evaluation of Bagnold [[Bagnold, 1941](#)] type sand transport models [[Sherman et al., 1998](#)], aeolian streamers [[Baas and Sherman, 2005](#)] and intermittent saltation [[Stout and Zobeck, 1997](#)]. But also non-linear dynamics in aeolian and fluvial bedform development can be studied, as well as the drivers behind superimposed bed-form development [[Kocurek et al., 2010](#)].

Self organization and chaos are important characteristics in many natural systems. Though often applied, SOC approaches are controversial in explaining non-linear dynamics in complex system because they lack any physical basis. Computational limitations remain a constraint for the current framework (in the order of days of required computing time), however, with the ever increasing computational power and more efficient implementations, these physical based approaches can find their way in a variety of scientific disciplines in the near future. Specifically. studies involving the physics of particle movement could benefit from the approach, as deployed in this study.

3.4 Conclusion

We used the discrete element method to simulate sandpile formation using particles in a tetrahedral arrangement and compared the results with experimental results and previous work. We have shown that a simple set of rules, defined here as gravity and particle interactions in a contact model, results in non-linear self-emergent behaviour which is in good agreement with experimental results, theoretical work and SOC approaches. The model is fully deterministic, i.e. the position and forces on every individual particle

can be determined every iteration, while showing complex non-linear self-organizing behaviour. With this approach, we show potential use for particle based modelling geophysical research.

3.5 acknowledgments

We are grateful to the Department of Computer Science, University of Cape Town, for sharing their source code, with specific gratitude to Juan-Pierre Longmore and Craig Leach. We thank Paul Torfs for his comments on the model simulations. We thank Remco Pieters for the high-speed camera and his assistance.

Chapter 4

Measuring fast-temporal sediment fluxes with an analogue acoustic sensor: a wind tunnel study

Poortinga, A., Van Minnen, J., Keijsers, J., Riksen, M., Goossens, D., & Seeger, M. (2013). Measuring Fast-Temporal Sediment Fluxes with an Analogue Acoustic Sensor: A Wind Tunnel Study. *PLoS One*, 8(9), 1-15.

Measuring fast-temporal sediment fluxes with an analogue acoustic sensor: a wind tunnel study

abstract

In aeolian research, field measurements are important for studying complex wind-driven processes for land management evaluation and model validation. Consequently, there have been many devices developed, tested, and applied to investigate a range of aeolian-based phenomena. However, determining the most effective application and data analysis techniques is widely debated in the literature. Here we investigate the effectiveness of two different sediment traps (the BEST trap and the MWAC catcher) in measuring vertical sediment flux. The study was performed in a wind tunnel with sediment fluxes characterized using saltiphones. Contrary to most studies, we used the analogue output of five saltiphones mounted on top of each other to determine the total kinetic energy, which was then used to calculate aeolian sediment budgets. Absolute sediment losses during the experiments were determined using a balance located beneath the test tray. Test runs were conducted with different sand sizes and at different wind speeds. The efficiency of the two traps did not vary with the wind speed or sediment size but was affected by both the experimental setup (position of the lowest trap above the surface and number of traps in the saltation layer) and the technique used to calculate the sediment flux. Despite this, good agreement was found between sediment losses calculated from the saltiphone and those measured using the balance. The results of this study provide a framework for measuring sediment fluxes at small time resolution (seconds to milliseconds) in the field.

4.1 Introduction

Quantitative evaluation of aeolian sediment fluxes is important to assess the varied roles of aeolian processes in landscape and nature development (e.g. [Poortinga et al. \[2011\]](#), [Riksen and Goossens \[2005\]](#), [Riksen et al. \[2008\]](#)), in coastal defense (e.g. [Arens \[1996b\]](#), [de Vries et al. \[2012\]](#)), and in nutrient dynamics especially in arid environments (e.g. [Sterk et al. \[1996\]](#), [Visser et al. \[2005a, 2004b\]](#)). Sediment fluxes are often measured using sediment catchers such as the Big Spring Number Eight (BSNE) [[Rajot, 2001](#), [Zobeck et al., 2003](#)], the Basaran and Erpul Sediment Trap (BEST) [[Basaran et al.,](#)

2011, Temur et al., 2012] or the Modified Wilson and Cooke sediment Catcher (MWAC) [Mendez et al., 2011, Visser et al., 2005a, Zobeck et al., 2003]. These traps are usually mounted in a vertical array to trap sediment at various heights above the surface. Sediment caught in the collection chamber is removed, dried, and weighed. By plotting the results as a function of height and fitting a curve through the data points the vertical sediment flux can be calculated. However, the data only provide information on sediment flux during the measurement interval itself. Moreover, there is no standardized method for the application of sediment traps and the data analysis method, which makes intercomparison between different studies difficult [Barchyn et al., 2011, Ellis et al., 2009a].

The efficiency and behaviour of different sediment traps was reported in numerous studies [Basaran et al., 2011, Goossens et al., 2000, Mendez et al., 2011, Sterk and Raats, 1996, Youssef et al., 2008]. Most of these studies used the controlled environment of a wind-tunnel, but some also performed a relative calibration in the field. However, due to the variety of techniques used when processing the data, the efficiencies reported were often not comparable. For example, for the MWAC sampler Sterk and Raats [Sterk and Raats, 1996] using a three-parameter power function and a five-parameter combined model found an efficiency of between 43 and 66 %, whereas Goossens et al. [2000] who directly compared the trap with an isokinetic sampler, reported efficiencies of 90 to 120 %. Mendez et al. [2011] also found that the flux characterization used has a large impact on the calculated sediment flux.

A variety of instruments are currently available to investigate aeolian sediment fluxes over time [Pelt et al., 2009], which can be grouped into four categories: (1) acoustic, (2) piezoelectric, (3) laser, and (4) pressure sensitive samplers. (1) The saltiphone [Spaan and van den Abeele, 1991] is a popular device, but other acoustic devices like loudspeakers [Barchyn et al., 2011] and small microphone systems [Ellis et al., 2009b] have also been used. Acoustic samplers register the signal generated when airborne particles strike a sensitive membrane. (2) The Sensit [Stockton and Gillette, 1990] and Safire [Baas, 2004] are examples of piezoelectric sensors. A small electric pulse

is generated when a saltating particle hits a piezoelectric element. (3) The Wrenglor sampler is a laser-based system [Davidson-Arnott et al., 2009, Hugenholtz and Barchyn, 2011b] that uses a laserbeam and photo sensor to detect sediment particles. (4) Recently, a pressure sensitive sampler was developed and tested by Ridge et al. [2011]. This instrument continuously monitors sediment accumulation by means of a water-level logger. However, it remains difficult to link the output of the instrument with the actual sediment budget.

Various studies [Spaan and van den Abeele, 1991, Sterk et al., 2012] have tried to directly link sediment fluxes measured by the saltiphone to actual sediment fluxes. However, none of these studies found an acceptable level of agreement. Reasons for this include: (1) the digital signal output used, (2) only one saltiphone was used, whereas data from different heights are required to characterize aeolian sediment fluxes for the entire sediment transport layer, and (3) the output of the saltiphone is only a representation of the amount of kinetic energy, which is difficult to directly link to sediment flux. Consequently, when using more than one saltiphone in an experimental array, all saltiphones need to be adequately calibrated as the response curve may slightly vary between instruments.

In this study, we test two passive traps (BEST sampler and MWAC sampler) and one acoustic device (saltiphone) in an aeolian sand wind tunnel to investigate how the experimental setup and the subsequent data processing affect the quantification of the aeolian sand flux.

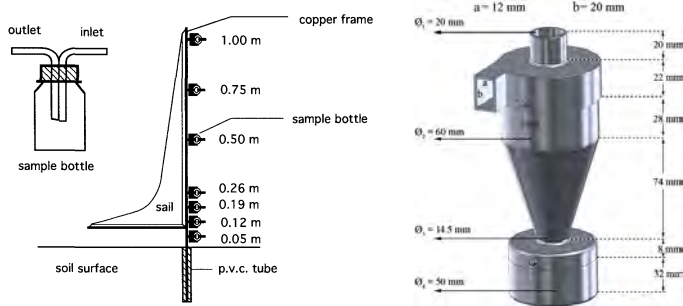
4.2 Materials and methods

4.2.1 Instrumental design

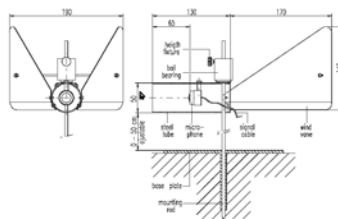
4.2.1.1 Modified Wilson and Cooke

The original Wilson and Cooke catcher (WAC) Wilson and Cooke [1980a] consists of a bottle containing an inlet and outlet, whereby the trapped sediment is deposited in the bottle. In later studies, these bottles were mounted on a pole equipped with a sail to

ensure that the inlet was always directed towards the wind (Fig 4.1(a)). This extended setup is called the Modified Wilson and Cooke (MWAC) trap. A detailed description of the conventional MWAC (referred to as MWAC-old hereafter) can be found in Sterk and Raats [Sterk and Raats \[1996\]](#). In the current study, we used a commercially available version of the MWAC, with an iron sail where the position of the bottles on the pole are adjusted (we refer to this modified setup as MWAC-new).



(a) MWAC (from [Sterk and Raats \[1996\]](#)) (b) Best (from [Basaran et al. \[2011\]](#))



(c) Saltiphone

FIGURE 4.1: Schematic overview of the (a) Modified Wilson and Cook (MWAC), (b) Basaran and Erpul Sediment Trap (Best) and (c) the Saltiphone acoustic sampler

4.2.1.2 Basaran Erpul Sediment Trap (BEST)

The BEST, developed and tested by [Basaran et al. \[2011\]](#), is a cyclone-type catcher with a conical shape (Fig 4.1(b)). Sediment enters the catcher via an inlet and follows a circular trajectory within the cone. The heaviest particles will settle due to gravitational and centrifugal forces whereas the lightest particles will be evacuated through

the outlet. The principle is comparable to the separation of soil fractions in soil remediation equipment but BEST samplers are used with lower wind speeds to collect the smaller particles. Earlier developed cyclone samplers were mostly designed to measure dust (not sand) and may have similar conic shapes but were sometimes also cylindrical or elliptical [Ogawa and Ugai, 2000]. Another difference between the BEST and the earlier developed cyclones samplers is that the BEST is composed of three parts instead of only one. The three units are: a lid including the inlet and outlet, a conical central body, and the proper collector.

4.2.1.3 Saltiphone

The saltiphone is a commercially available sampler which consists of a microphone installed in a stainless steel tube mounted on a ball bearing (Fig 4.1(c)). Two vanes at the back of the tube ensure proper alignment with the wind. The ball bearing can be connected to a stain rod, which is height-adjustable. A cable connects the microphone to the electronics, which is stored in a waterproof aluminium housing. Sand particles that hit the microphone produce a high-frequency signal. Frequencies of about 8 Khz are amplified and used to determine saltation whereas other frequencies that are caused by rain and wind are reduced using a narrow band filter. The pulse created by each particle is cut off after 1 millisecond. Two output signals are provided: a digital pulse and an analogue voltage. The digital signal gives an output that is translated into number of counts. The analogue output signal also provides this information but has the additional option of measuring the intensity of particle impacts because it measures the energy of impact on the membrane. In this mode, the output signal represents the kinetic energy of the particles, and thus particle size and speed. The analogue output option was used in this study. Data were measured with the same interval as the sampling rate of 1 millisecond.

4.2.2 Experimental setup

The study was conducted at the wind tunnel of the International Center for Eremology (ICE), Ghent University, Belgium. The wind tunnel has a length of 12 m and is 1.2 m wide and 3.2 meters high [Cornelis et al., 2004a, Gabriëls et al., 1997]. Wooden spires and roughness cubes were placed to create a boundary layer of 0.6 m at the entrance of working section of the wind tunnel [Gabriëls et al., 1997]. A test tray of 1.2 m long, 0.4 m wide and 0.012 m deep was placed at 7.4 m downwind from the entrance and filled with sand (Fig 4.2). To ensure similar roughness compared to the sand, sand paper was applied before and after the tray. Wind velocity was measured using five vane-type probes (type 0635-9540, Testo GmbH & Co, Lenzkirch, Germany). These probes have a vane diameter of 16 mm and are appropriate to measure wind velocities up to 60 ms^{-1} . The first was installed at 70 cm height near the upwind edge of the test section and the others 2.1 m in front of the tray at 5, 10, 15 and 30 cm heights, respectively. Wind velocities were measured with one-second intervals. The sediment catchers and saltiphones were installed downwind from the test tray and were separated by a distance of 10 cm (Fig 4.2).

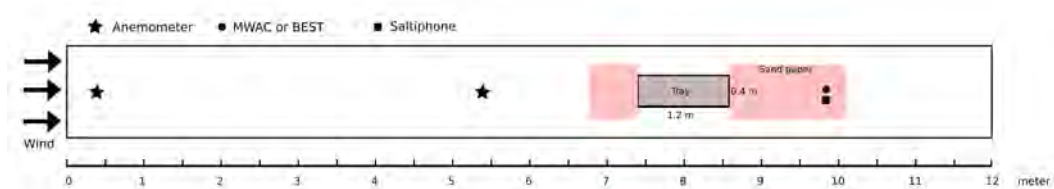


FIGURE 4.2: Schematic (top view) diagram the experimental setup. A balance was placed underneath the test tray to measure the weight of the sediment throughout the experiment.

To measure the sediment loss during an experiment, a balance was placed underneath the test tray (Fig 4.3). The balance was programmed to register the time when the weight of tray changed. However, during an experiment the air pressure can change thereby potentially affecting the measurements. Therefore, several test runs were performed with a fully covered tray. Results indicated that any potential effects were within

the measuring error of the balance. Thus, corrections for pressure differences were not required in this study.



FIGURE 4.3: Image of the experimental setup. The balance was placed underneath the test tray in order to measure the weight of the sediment throughout the experiment. The image taken during the calibration, when the five saltiphones were placed next to each other.

4.2.3 Sediment

Three industrial sands (referred to as *s50*, *s60* and *s80*) were used. All sediments consisted predominantly of quartz (99.5%) with traces of hematite, aluminium oxide and titanium dioxide. All sands were industrially washed and pre-sieved. The median diameters (d_{50}) were 285, 230, and 170 μm , respectively, with their grain size distributions shown in figure 4.4.

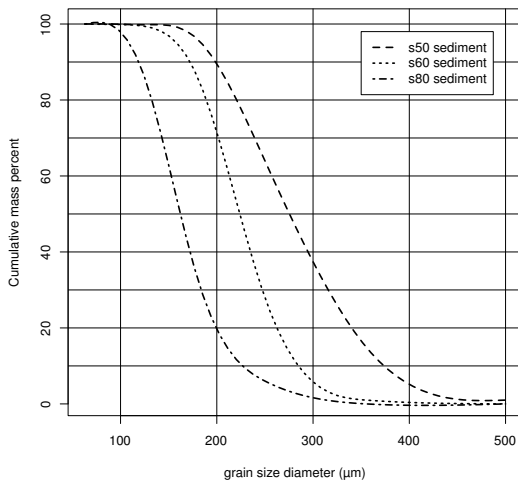


FIGURE 4.4: Grain size distribution of the three sediment types (s50, s60 and s80) used in the wind tunnel experiments

4.2.4 Analysis method

4.2.4.1 Wind data

Wind data collected from four altitudes were used to calculate the roughness length (z_0) and shear velocity (u_\star) using the law of the wall:

$$u_z = \frac{u_\star}{\kappa} \ln \frac{z}{z_0} \quad (4.1)$$

where u_z is the wind speed at elevation z above the bed, u_\star is the shear velocity, and κ von Karman's constant (0.4). Plotting the elevation on a vertical axis and the wind speed on a horizontal axis, rearranging equation 4.1 into $\ln(z) = au_z + b$, and applying a regression analysis, the values of u_\star and z_0 were calculated as $u_\star = k/a$ and $z_0 = e^b$, respectively.

The threshold shear velocity was calculated using equation 4.2 [Bagnold, 1941]:

$$u_{\star t} = A \sqrt{gd \left(\frac{\rho_s - \rho}{\rho} \right)} \quad (4.2)$$

where u_{*t} is the threshold shear velocity, A is a dimensionless constant (assumed to be 0.085 for the fluid threshold and 0.1 for the impact threshold), g is the gravitational acceleration (ms^{-2}), d is median (d_{50}) grain size (m), ρ_s is the density of the sediment (kgm^{-3}) and ρ is the density of air (kgm^{-3}).

4.2.4.2 Saltiphone

For a given impact, the analogue energy output signal may vary between saltiphones. Therefore, a calibration procedure was developed, where all five saltiphones were deployed next to each other (Fig 4.3). Figure 4.5 shows the raw output signal of the saltiphones placed horizontally next to each other under constant saltation conditions. Two observations were made. (1) During periods without saltation there is still a signal because in the analogue energy mode, the output signal is sensitive to the input signal (volts) and, (2) the amplitude of the output is different for the different saltiphones, even when sediment transport is measured under similar conditions. This problem can be resolved by using one saltiphone as a reference, because the temporal patterns of the output signals are very comparable (Fig 4.5). In this study, the saltiphone in the centre was used as the reference. Before and after the experimental runs, the output of each saltiphone was recalculated using a simple linear regression $Y = bX$ where Y is the output of a given saltiphone and X the output of the reference saltiphone. To account for horizontal variability in sediment flux, the positions of the saltiphones were regularly changed during the calibration.

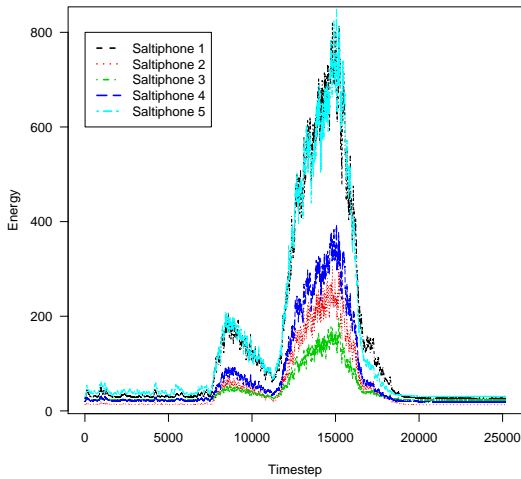


FIGURE 4.5: Output signal of the five saltiphones when placed next to each other. Output represents energy but is dimensionless.

4.2.4.3 Regression analysis

For each trap in the vertical array the total amount of sediment caught was multiplied by the area of the inlet to get an amount in kgm^{-2} . These data were used for regression analysis to calculate the vertical transport flux within the entire sediment transport layer. However, there is disagreement in the literature as to how to best describe the vertical profile of sediment transport [Ellis et al., 2009a, Panebianco et al., 2010]. Exponential functions (equation 4.3) as well as power function (equation 4.4) have been used:

$$q(z) = q_0 e^{\beta z} \tag{4.3}$$

$$q(z) = q_0 z^{\beta} \tag{4.4}$$

The regression parameter q_0 is often associated with the portion of creep, whereas β represents the decay rate with height (z). To facilitate calculating this regression, some

software packages use these formulae in a logarithmic form [McCullough and Heiser, 2008]:

$$\ln(q_z) = \ln(q_o) + \beta z \tag{4.5}$$

$$\ln(q_z) = \ln(q_o) + \beta \ln(z) \tag{4.6}$$

Note that the result for β will be different for these two approaches because of the difference in the last term on the right.

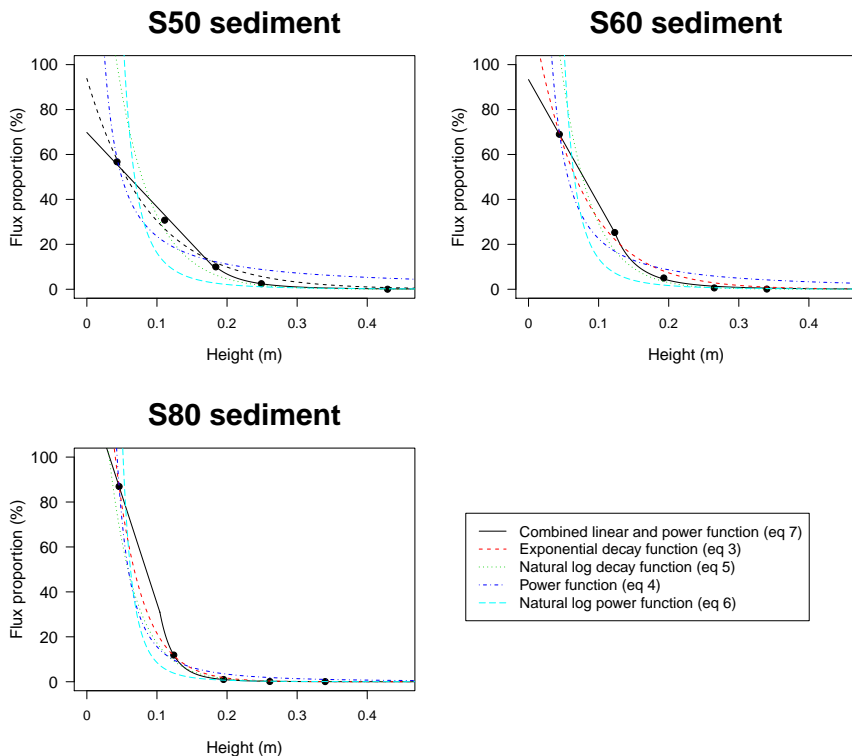


FIGURE 4.6: Five regression models plotted through the data points, for the three sediments tested (s50, s60 and s80).

Figure 4.6 shows the relative (normalized) sediment flux plotted against height for three representative runs of each test sediment. The data were taken from three measurements with the MWAC-old, where the sediment from the bottles is expressed as a

portion of the total sediment flux in order to make them comparable. The data indicate that neither the power nor the exponential function adequately describe the measured sediment profiles of the s50 and s60 sediments. Visual interpretation of the profiles suggests a linear trend in the lowermost part of the saltation layer. For the s50 sediment, a linear line can be fitted through the three measurements points closest to the bed, whereas for the s60 and s80 a linear line can be drawn to the two points closest to the bed in the upper part of the profile a power function gives the best fit. Therefore the following combination was used: a linear function in the lowermost part of the saltation layer and a power function in the upper part. Separate regressions were made for each part and the total sediment flux (kgm^{-1}) is calculated as follows:

$$Q = \int_0^{zl=p} a + \beta_1 z + \int_{zl=p}^{\infty} q_0 z^{\beta_2} \quad (4.7)$$

The two functions intersect at the point $zl = p$, where $zl = a + \beta_1 z$ and $p = q_0 z^{\beta_2}$.

4.2.4.4 Sediment fluxes

Sediment fluxes were calculated by combining the saltiphone data with wind speed data and data from the balance. Figure 4.7 presents a schematic overview of the procedure.

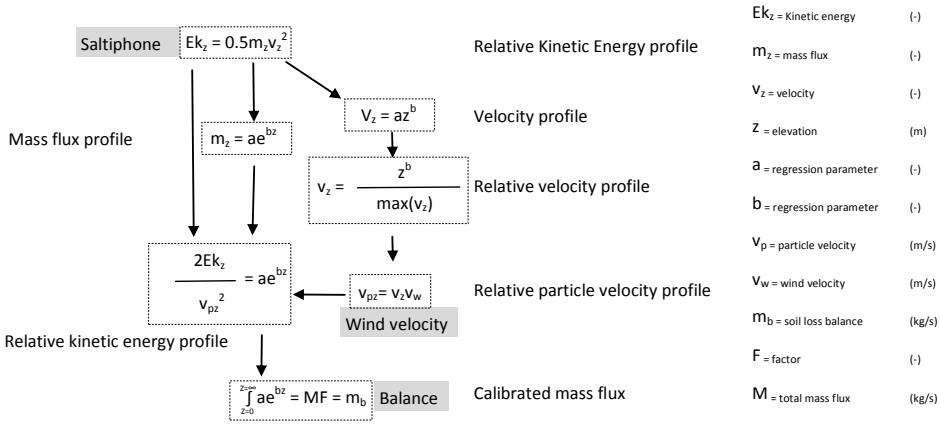


FIGURE 4.7: Sediment fluxes were calculated from the saltiphone data using wind data and data from the balance.

The amplitude of the analogue output of the saltiphone is determined by the kinetic energy of the particles hitting the membrane of the microphone. This kinetic energy depends on the mass (kg) and velocity (ms^{-1}) of the particles (equation 4.8):

$$E_k = 0.5m_z v_z^2 \tag{4.8}$$

However, the translation of vibrations of the membrane to a voltage is influenced by the characteristics of the membrane. Therefore, the analogue output cannot be directly translated to Joule (J), the unit of kinetic energy. Moreover, no data on particle velocity were collected during the experiments. Equation 4.8 can thus only be used to express the characteristics of the sediment flux in relative terms.

To estimate the variation of kinetic energy of the impacting particles with height, we used separate functions for the particles' mass and velocity. For the mass, we used an exponential function similar to equation 4.3, and for velocity, a power function similar to equation 4.4. The exponential function was chosen because experimental work has

shown that the vertical distribution of the sand transport rate of medium and fine-grained sands (such as the ones used in this study) is typically expressed by such a function [Dong et al., 2009]. The power function was selected based on the studies [Yang et al., 2007, Zou et al., 2001]. The variation in kinetic energy with height is then described by:

$$E_{kz} = 0.5a_1 \exp^{-b_1 z} (a_2 z^{b_2})^2 \quad (4.9)$$

Equations 4.8 and 4.9 were used to estimate particle velocity during the experiments using the following steps. First, the total analogue output for all five saltiphones together was calculated. Next the relative proportion of each saltiphone in the total analogue output was computed. The measured sediment fluxes of the sediment traps were treated in the same way to calculate the relative proportion of each trap in the vertical array. The saltiphone and sediment trap data were then correlated in a non-linear model, where the parameters a_2 and b_2 were optimized until a weighted least-squared optimum was found. The value derived for b_2 was used to estimate an average particle velocity at the elevation of the saltiphone. As this can only be done in relative terms, the particle velocity (v_p) profile was fitted for a 30-cm interval using $v_p = z^{b_2}$ (see equation 4.9) and normalized by dividing it through the maximum value of v_p . To estimate the real particle velocity the relative particle velocities were then multiplied by the wind velocity of the highest anemometer (30 cm), which is located close to the sediment tray.

All saltiphone data (which were measured every millisecond) were averaged to seconds to ensure the same temporal resolution as for the wind data. Particle velocity was then calculated for every second. From the v_{pz} and e_{kz} , the relative mass flux at the elevation of the saltiphone was calculated using equation 4.8. To obtain the total sediment flux an exponential function (equation 4.3) was fitted through the data points. Integration over the entire height of the sand transport layer then yielded the total sediment flux. However, because e_{kz} is dimensionless and v_{pz} is described as a function multiplied by the wind velocity, the total sediment flux measured by the saltiphones was compared with the total amount of soil loss measured by the balance. A linear

function ($y = bx$) was fitted through the data points to scale the relative output of the saltiphone (y) to the balance (x). The value of b was then used to convert the calculated sediment flux from the saltiphone into a real sediment flux. This was done by using equation 4.10, which is equation 4.8 with the inclusion of a factor F and v_p as particle velocity. The b value found in the linear regression was used as F in equation 4.10.

$$M_b = M_s F = \frac{E_k}{0.5(v_p)^2} = \frac{2E_k}{(v_p)^2} \quad (4.10)$$

M_b represents the mass flux from the balance, and M_s the flux measured by the saltiphone.

4.2.5 Efficiency

In this study efficiency is defined as the ratio of the vertically integrated (over the entire height of the sand transport layer) sediment flux as measured by the catcher, relative to the total sediment flux derived from the sediment loss from the balance. The vertical integration can be done using any of the empirical approaches displayed in the equations 4.3 to 4.7.

4.3 Results and discussion

4.3.1 The efficiency of the different catchers

Efficiencies were calculated for all five approaches (equations 4.3 to 4.7), with the results shown in Figure 4.8. The ordinate displays the calculated efficiencies (%) as well as the goodness of the statistical fit for each approach (using R^2) with the results being very dependent on the equation (approach) used. A similar conclusion was made by Panebianco et al. [2010]. For both MWACs, the combined linear-power equation gives the best results, with efficiencies around 100%. For the BEST sampler, the exponential function (equation 4.3), the power function (equation 4.4) and the combined linear-power function gave similar results, with efficiencies around 80%. The importance of the statistical software package used can also be seen: for the same experiment,

large differences in calculated efficiencies may be obtained depending on whether or not the logarithmic versions (4.5) and (4.6) of equations (4.3) and (4.4) were used. The logarithmic versions also resulted in a poorer fit (lower values for R^2).

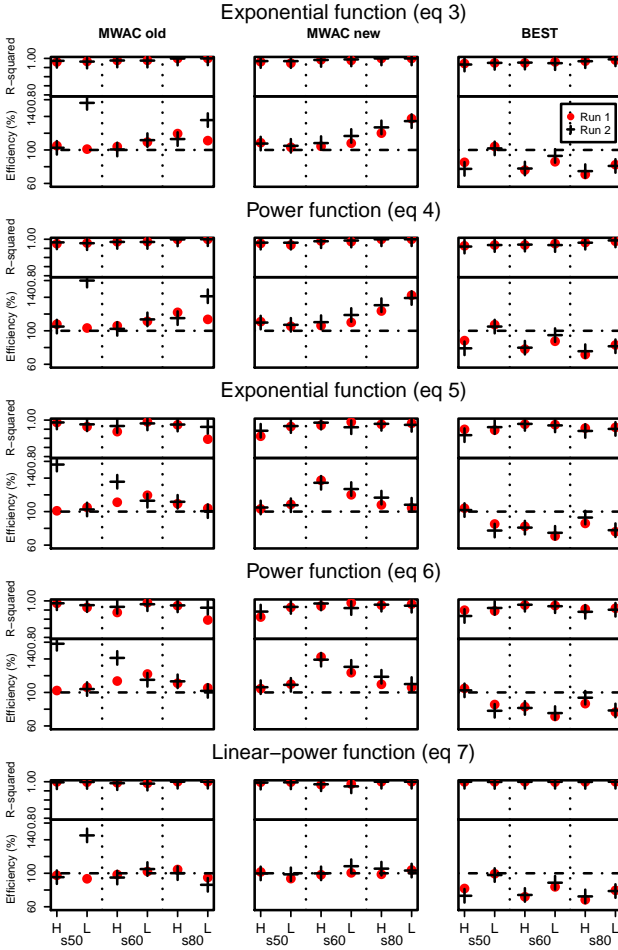


FIGURE 4.8: Efficiencies and goodness of fit (R^2) of the three catchers as calculated from five regression models. H and L are high and low wind velocity, respectively, and s50, s60 and s80 are the three sediments used in this study.

The difference in efficiency between the MWAC and the BEST when using the exponential function is most probably explained by the elevation of the lowest trap. For the BEST, the lowest trap was located directly on the surface, whereas for the MWAC, the lowest bottle was located around 4-5 cm from the surface. When an exponential curve is fitted through the data points, the β -exponent is mainly determined by the

slope between the two lowest points. The higher these points are situated above the surface, the more likely q_0 and β will become overestimated. This can also be seen when q_0 and β are calculated for the normalized sediment flux (the amount of sand captured in a bottle relative to the total amount in all the bottles). Figure 4.9 illustrates this overestimation. Literature [Dong et al., 2003] shows that a perfect linear relationship between q_0 and β can be expected under similar conditions of surface moisture and sediment. In Figure 4.8 the relationship is excellent for the BEST catcher whereas it is less pronounced (but still remains acceptable) for the MWAC catcher. The lower correlation and the different value for the slope for the MWAC are likely caused by the higher position of the lowest bottle, resulting in a larger uncertainty for the flux in the lowermost zone of the sediment transport layer and an overestimation of the values for q_0 and β . When equation 4.7 is used, efficiency is mostly around 100% (Fig. 4.8), suggesting that the exponential function overestimates q_0 and β . The results for the BEST sampler, point towards the same conclusions since equations 4.3 and 4.7 produce similar results.

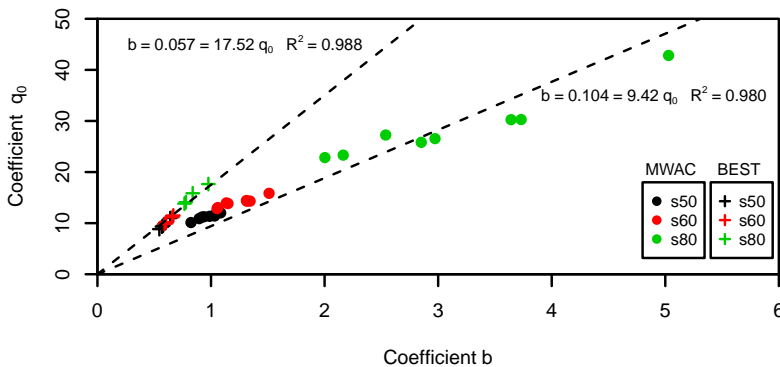


FIGURE 4.9: Dimensionless regression coefficients q_0 and β calculated for the MWAC and BEST samplers, for the three sediments used in this study.

No relationships were found between efficiency and sediment type and efficiency and wind speed. This contrasts with previous results [Youssef et al., 2008], where higher efficiencies occurred as the sediment became coarser, and where differences in

efficiencies as the wind speed increased were also noted. However, in [Youssef et al. \[2008\]](#) a large range of sediment sizes was used, varying between 50 - 500 μm . The result here are in agreement with other studies [[Goossens et al., 2000](#), [Sterk and Raats, 1996](#)], who found no relation between the efficiency of the MWAC catcher and wind velocity. MWAC efficiency is substantially determined by the experimental setup (in particular, the elevation of the lowest bottle) and the analysis method (type of regression) used. The current study suggests that efficiencies close to 100 % results when exponential curve fitting is used. For the BEST sampler, almost identical efficiencies were observed regardless of the curve fitting technique used.

4.3.2 Calibration of the saltiphones

The saltiphones were calibrated before, during and after the experiments. In total, 12 calibration experiments were performed, where the energy output of the saltiphone in the center (saltiphone 3, see [Fig. 4.5](#)) was used as the reference. The duration of a calibration run was approximately 3 - 4 minutes. To avoid results being affected by potential differences in sediment concentration across the wind tunnel's test section, we reversed the relative position of the saltiphones during several of the tests (saltiphone 1 was moved to position 5 and saltiphone 5 to position 1; and saltiphone 2 was moved to position 4 and saltiphone 4 to position 2; saltiphone 3 remained in place at all times) and averaged the result. To estimate the difference in sediment concentration between position 1 and position 5, the difference in energy output between saltiphones 1 and 5 was compared for the two setups and the average was calculated; the same procedure was followed for saltiphones 2 and 4. As expected, sediment concentration was not identical within the wind tunnel section. At position 1 ([Fig. 4.5](#), saltiphone in the back) it was 48% higher than in the center, and at position 2 it was 23% higher; at position 4 it was 22% lower than in the center, and at position 5 ([Fig. 4.5](#), saltiphone in the front) it was 37% lower. This difference in horizontal sediment flux was incorporated into the output data of the saltiphone. With this correction, the calibration factor (i.e. the difference in response between the saltiphones) was calculated ([Table 4.1](#)).

TABLE 4.1: Calibration of the Saltiphones using linear regression ($X = bY$). Parameter b expresses the multiplication factor of the representative saltiphone to saltiphone 3.

Saltiphone number	Calibration factor b
1	2.4
2	1.9
3	1.0
4	2.8
5	1.6

The variation in sediment flux over the tunnel section is rather large considering the relatively homogeneous wind field in the test area [Gabriëls et al., 1997]. Basaran et al. [2011] used a transparent sellotape to determine this variation for different sediments and wind velocities in the wind tunnel used in the current study and found that 29.7 to 55.5% of the sediment was transported within the central 35 cm of the tunnel section.

4.3.3 Sediment fluxes calculated from the saltiphone

Sediment fluxes were calculated for every second, based on the kinetic energy measured by the saltiphones. This was done in three steps: (1) fitting a function through the individual data points to establish the kinetic energy profile, (2) determine the particle velocity profile, and (3) calculate the sediment flux from the kinetic energy and particle velocity profiles.

4.3.3.1 Kinetic energy

Figure 4.10 shows the normalized kinetic energy plotted against elevation for the three sediments tested. The values for a_1 , a_2 , b_1 and b_2 are also shown.

A peak occurs in the normalized kinetic energy around 2 cm above the surface for all three sediments. This peak is more pronounced as the sediment becomes finer. Therefore, for fine sediments, a larger fraction of the kinetic energy is found close to the surface compared to coarse sediments. For the latter, the total kinetic energy carried by the airborne particles is less concentrated near the bed. These results are consistent with previous findings [Zou et al., 2001].

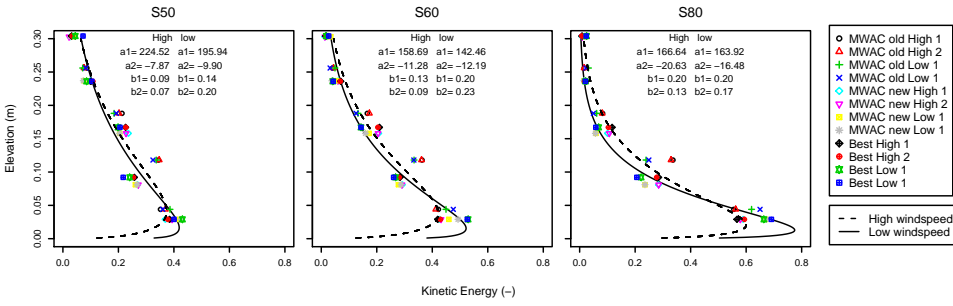


FIGURE 4.10: Normalized kinetic energy flux for the three sediments, for high and low wind velocities. a_1 , a_2 , b_1 and b_2 are the regression parameters from equation 4.9.

4.3.3.2 Particle velocity profile

The particle velocity profile can be constructed using the power function $v = a^{bz}$ [Yang et al., 2007, Zou et al., 2001]. Note that the value for a depends on the choice of the units; by normalizing the particle velocities, the exponent b fully describes the profile.

Figure 4.11 shows the normalized profiles. For high wind velocities the value for b increases from 0.07 for the coarsest sediment (s50) to 0.17 for the finest sediment (s80). For low wind velocities the b -values are 0.20 (coarse sediment s50), 0.23 (medium-sized sediment s60), and 0.17 (fine sediment s80).

The normalized velocity profiles differ for the two wind speeds investigated. Therefore, we opted for using the average of both wind speeds when calculating the particle velocity profile for the whole experiment.

4.3.4 Sediment fluxes

In Figure 4.12, we compare the calculated total sediment flux with the measured soil loss from the balance. Good relationships were found between the measured and calculated flux for all three sediment types, but the slopes of the curves differ. For the coarse (s50) and medium-sized (s60) sediment the F-value was close to unity (0.986 and 0.933, respectively), whereas for fine sediment (s80) the F-value was 0.601.

Previous studies Dong et al. [2003, 2004a] have shown that particle velocity decreases with an increase in particle size. For the current study, this would imply that the

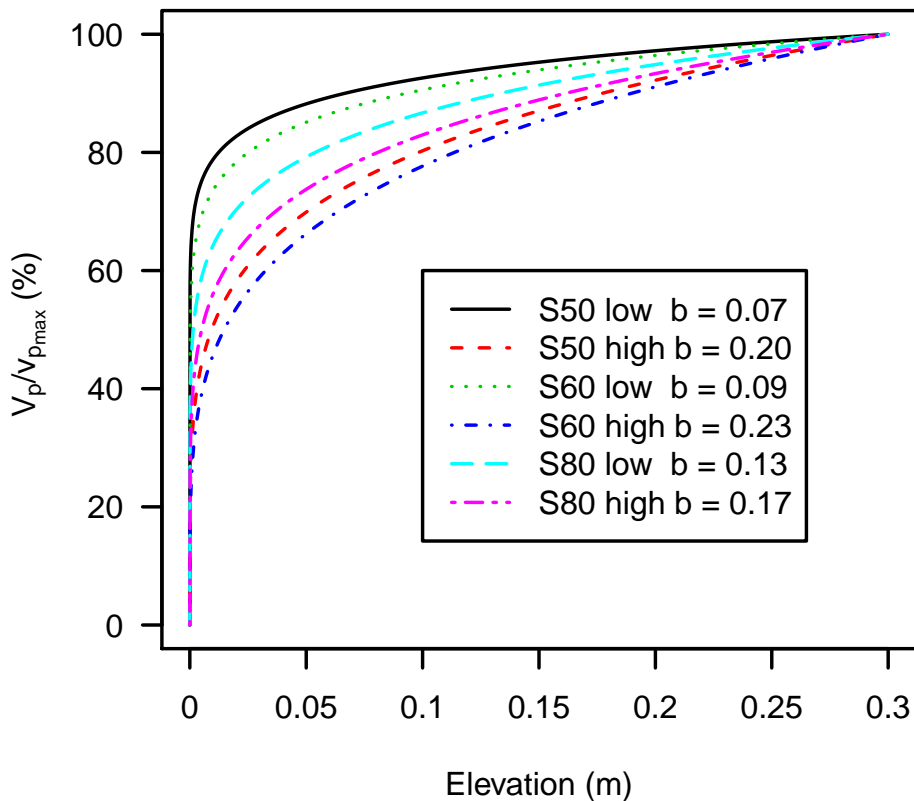


FIGURE 4.11: Particle velocity profiles for the three sediment types used, for high and low wind speed.

particles of sediment s80 should have higher velocities compared to those of sediments s60 and s50. Rearranging equation 4.10 into:

$$v_p \sqrt{F} = \frac{\sqrt{E_k}}{\sqrt{0.5m}} \quad (4.11)$$

and using the F-values derived from Figure 11, our results confirm this trend. For a given amount of kinetic energy and a specified amount of mass equation 4.11 predicts a lower particle velocity as particles become coarser. However, no direct measurements were made of the particle velocity in this study. Also, the physical characteristics of

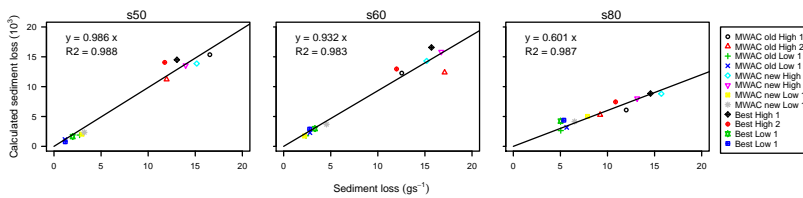


FIGURE 4.12: Sediment loss measured from the balance compared to the total sediment loss calculated from the saltiphones, for the three sediments tested in this study.

the saltating grains were not taken into consideration. In reality, the sediment source is characterized by a mix of different shapes and sizes, and every particle will have its own saltation trajectory. The angle at which the particle hits the microphone might also have a considerable impact on the total amount of energy transferred to the membrane.

Equation 4.11 was used to calculate the sediment flux with an exponential function fitted through the data points to estimate the total sediment flux for each second. Results are displayed in Figures 4.13, 4.14, 4.15 for sediments s50, s60 and s80 respectively. Each sediment type has a total of 12 experiments, for three different sediment catchers (MWAC-old, new and BEST) using high and low wind velocities in duplicates. Each figure shows the shear velocity, threshold shear velocity and normalized analogue output of the saltiphone. The normalized output was calculated by summing all calibrated outputs of the saltiphone and divide this sum by the maximum value during one experiment. Also shown in Figures 4.13, 4.14, 4.15 are the output (weight loss) recorded by the balance and the sediment flux calculated from the saltiphone data.

Results show that the analogue output of the saltiphone can indeed be used to assess sediment fluxes on a small temporal time scale. For the s50 sediment, the results for the measurements with the new MWAC at the lowest wind velocity show a small underestimation, whereas the BEST gives a small overestimation for the highest wind speed. The same is true for the s60 sediment, but for the s80 sediment, an over estimation can be seen for the second run, for both wind speeds. Accepting a small measurement error in the balance weights all results are well within acceptable boundaries.

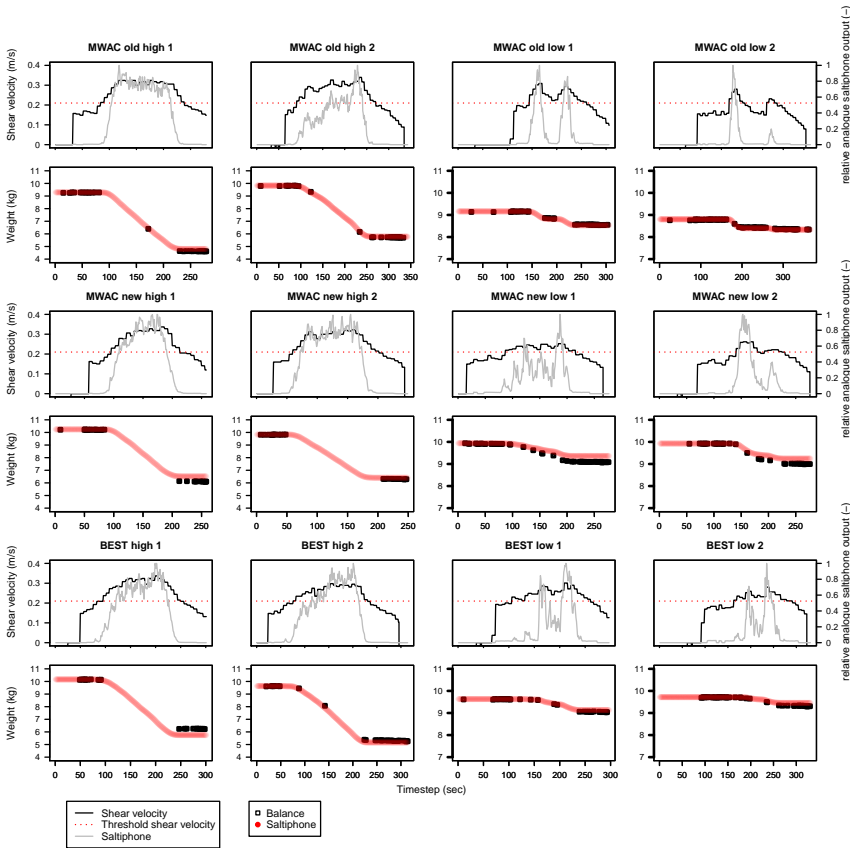


FIGURE 4.13: Sediment loss, relative analogue saltiphone output and shear velocity over time for the different experiments with sediment s50. The experiments were done using three types of catchers (MWAC-old, MWAC-new and BEST) with high and low wind velocities. Two replicates were done for each test. Sediment loss was measured from the balance (black) and calculated from the saltiphone (red)

To check whether or not the procedure to calculate the sediment flux from the analogue output of the saltiphone can be replicated by using the saltiphone’s digital pulse output, the two raw signals were compared. Figure 4.16 shows the results for the first two saltiphones. For saltiphone 1, there is a good correlation between the two outputs, but at high energy levels the relationship becomes less well expressed. The output of saltiphone 2 illustrates why the digital pulse output cannot be used to quantitatively assess wind erosion as an almost parabolic relationship was found between the digital pulse and the analogue output. Saturation might be the most plausible cause for this phenomenon.

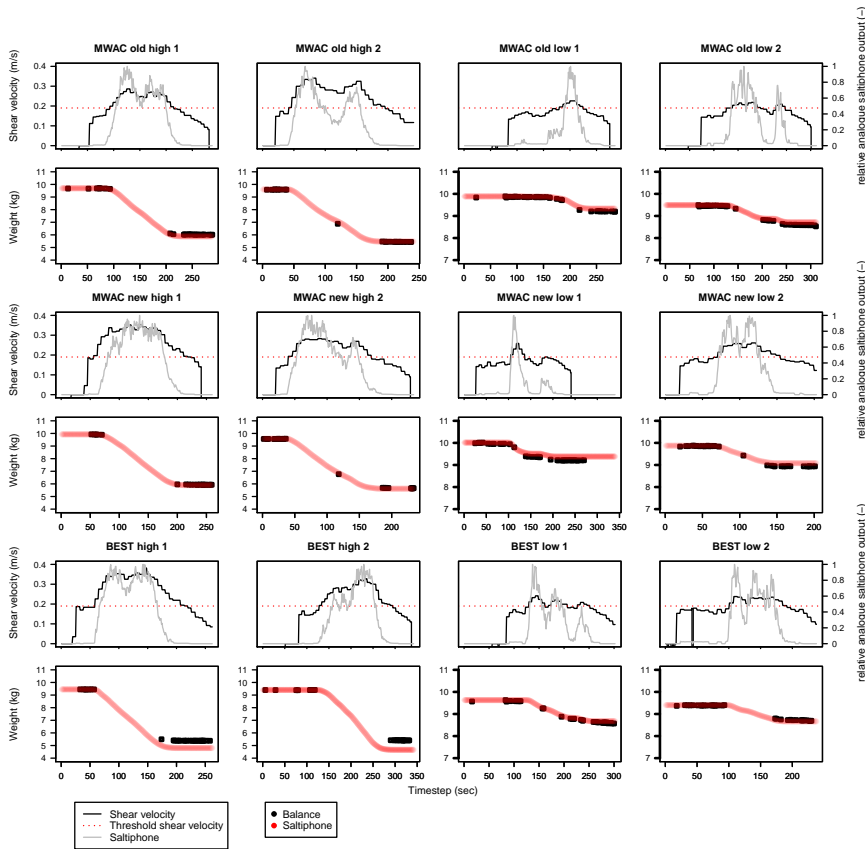


FIGURE 4.14: Sediment loss, relative analogue saltiphone output and shear velocity over time for the different experiments with sediment s60. The experiments were done using three types of catchers (MWAC-old, MWAC-new and BEST) with high and low wind velocities. Two replicates were done for each test. Sediment loss was measured from the balance (black) and calculated from the saltiphone (red)

4.3.5 Shear velocity and sediment fluxes

Apart from sediment flux, Figures 4.13, 4.14 and 4.15 also show both shear velocity and threshold shear velocity. Shear velocities and roughness lengths (z_0) were calculated from the wind velocity profiles. Data for the roughness length varied considerably, from 0.002 to 0.103 mm (a factor of 50). These values are low compared to the values measured for comparable sands (refer to Youssef et al. [2012b]), who used a value of 1 mm. Threshold shear velocities were calculated for all three test sediments by means of equation 4.1, using the median grain diameter (d_{50}) as the reference diameter and

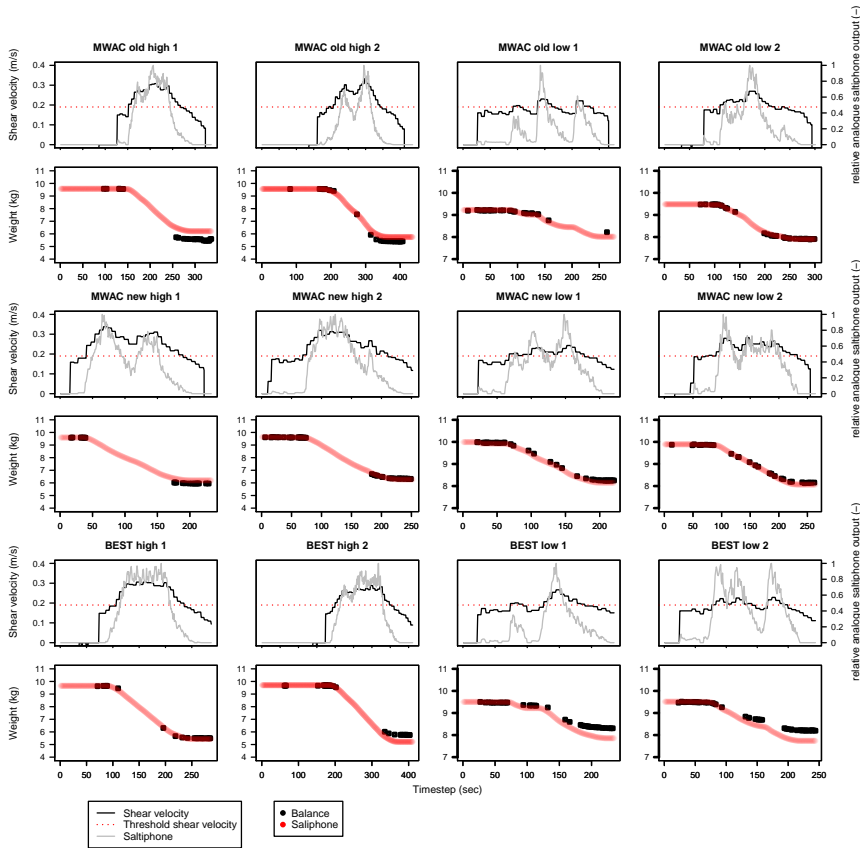


FIGURE 4.15: Sediment loss, relative analogue saltiphone output and shear velocity over time for the different experiments with sediment s80. The experiments were done using three types of catchers (MWAC-old, MWAC-new and BEST) with high and low wind velocities. Two replicates were done for each test. Sediment loss was measured from the balance (black) and calculated from the saltiphone (red)

using particle density equal to 2650 kg m^{-3} .

The calculated threshold shear velocities (table 4.2) are consistent with the data. When shear velocity exceeds the fluid threshold sediment transport is measured by the saltiphone. However, the data also show a clear difference between high energy levels and low energy levels (Fig. 4.17). When wind is still accelerating, sediment fluxes are lower than when the wind is slowing down. This phenomena is also known as hysteresis, which means sediment flux is not only dependent on the current shear velocity, but also on the previous shear velocities [Baas and Sherman, 2005].

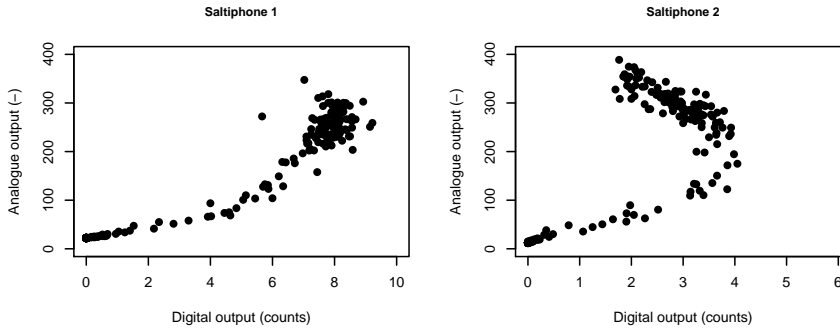


FIGURE 4.16: Raw analogue output compared to the raw digital output for the first two saltiphones.

TABLE 4.2: Threshold shear velocities calculated for the different sediments using equation 4.2

sediment	impact threshold ms^{-1}	fluid threshold u_{*t} ms^{-1}
s50	0.21	0.25
s60	0.19	0.22
s80	0.16	0.19

4.3.6 Comparison between the saltiphone and the BEST trap

To determine whether the technique developed in this study to calculate sediment fluxes from saltiphone data leads to more accurate results, the sediment flux profiles from the saltiphone and the BEST sampler were compared. For the saltiphone we first calculated the average fluxes of the individual experiments. Relative fluxes were then calculated by dividing the sediment flux obtained from each saltiphone by the total of all saltiphones. The same procedure was adopted for the BEST. Only the BEST was used in the test because this sampler provides more data points in the saltation layer than the MWAC, which guarantees a better characterization of the sediment flux profile.

Results are shown in Figure 4.18 with an exponential function used to fit the data points. Similar patterns were obtained for all wind speeds and sediments tested. In general, the results are comparable for the saltiphone and the BEST, illustrating the usefulness of the techniques. For the two coarsest sediments (s50 and s60), the agreement

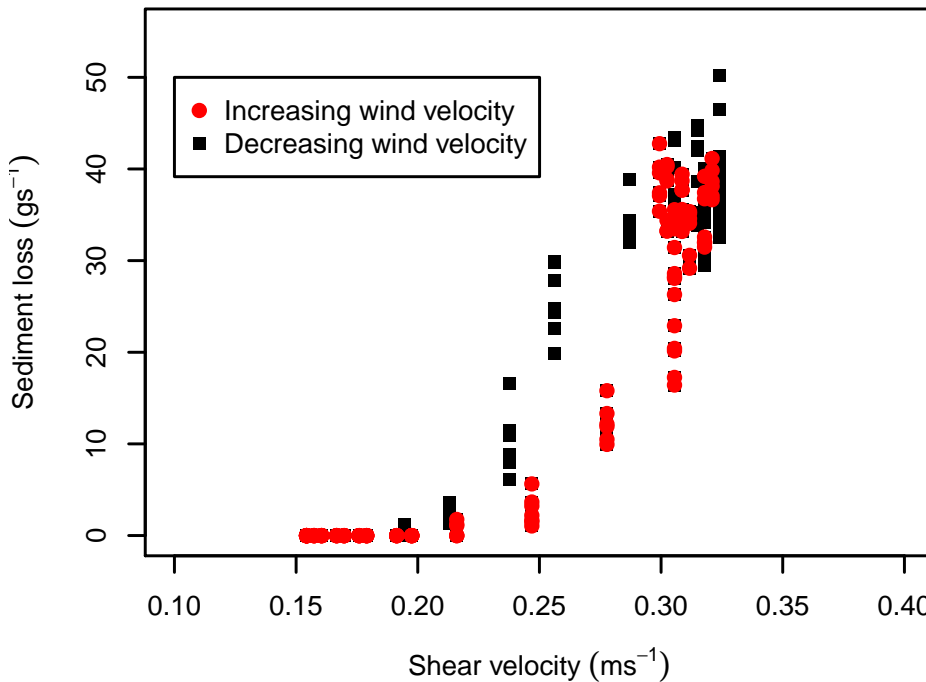


FIGURE 4.17: Sediment flux for different shear velocities, for an accelerating and a decelerating wind velocity.

is less encouraging close to the bed for the high-wind velocity case. At low elevations, the saltpHONE overestimates the sediment flux compared to the BEST.

4.3.7 Limitations

Despite a good relationship between the saltpHONE output, the loss of mass measured by the balance, and the measured sediment flux by the sediment catchers, there are several limitations for the current reported method. When calibrating saltpHONES the output of the instruments should be compared under identical conditions. This is seldom the case, either in a wind tunnel or in the field. In wind tunnels variations in the sediment flux may occur in the test section, such as during our experiments. In the field, spatial and temporal variations in soil roughness, soil moisture content, soil structure and soil

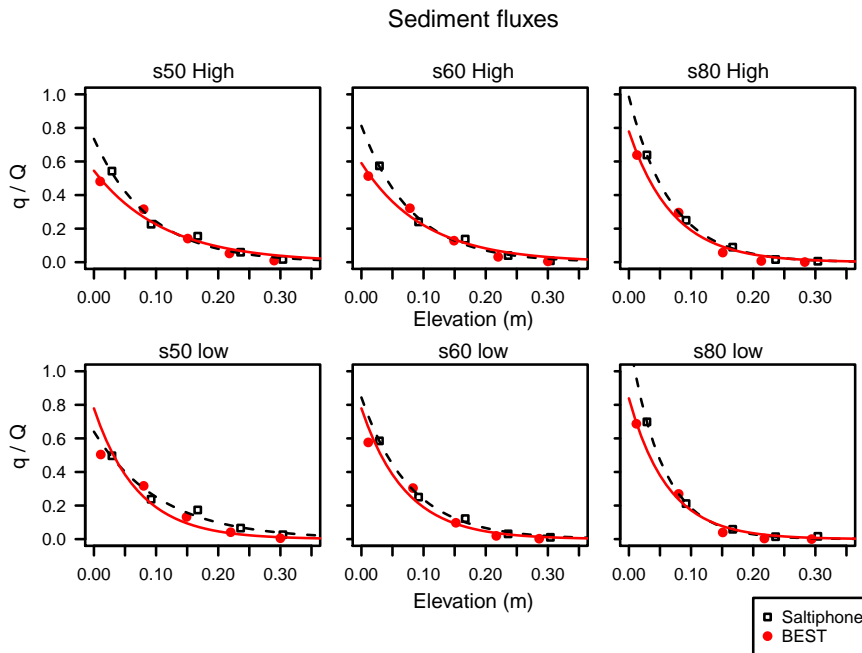


FIGURE 4.18: The total dimensionless sediment fluxes of the BEST and Saltiphone compared. s50, s60 and s80 are the three sediment types tested; High and Low refers to high and low wind velocity.

texture occur. Also, recalibration or replacement of the microphone is required after some time due to normal wear of the microphone’s membrane. This was not a problem in the current study but was reported in a previous study [Ellis et al., 2009b]. Another problem is that, when the sediment flux is calculated from saltiphone data, shear velocity information is required. This information is usually collected from a vertical tower of anemometers, and thus subject to some uncertainty [Bauer et al., 1992]. Finally, this study used only three types of (industrially washed and sieved) sediment. Although results were very comparable, more tests are recommended, especially with natural sediments characterized by a lower degree of sorting than those used in this study.

4.4 Conclusions and recommendations

Three samplers were tested in this study: the saltiphone, the MWAC and the BEST. Their efficiencies were tested by comparing the vertically integrated sediment flux measured (or calculated) with these samplers to the emission flux of the sediment source, which was directly measured with a balance. In general, the measured and calculated sediment fluxes are comparable, confirming the usefulness of the samplers and the calculation procedures.

No relationships were found between the efficiency of either sampler and sediment type or wind velocity. Efficiency mainly depends on the design of the samplers, the experimental setup (in particular, the number and elevation of the individual traps in the saltation layer), and on the choice of the regression function when fitting data into the vertical sediment flux or particle velocity profiles.

The saltiphone is a reliable tool to determine aeolian sediment fluxes at fast temporal scales. However, this study was performed in the controlled environment of a wind tunnel. Field conditions are much less stable and usually cannot be controlled, making this type of research much more complicated. However, we think the instrument can produce reliable results under field conditions provided sufficient attention is paid to the experimental setup. Issues to be considered include (but are not limited to): the number of saltiphones in the saltation layer; the vertical distance between adjacent saltiphones (especially close to the bed where sediment transport is highest and the variation of the sediment flux with height is most pronounced); the accuracy in determining the exact elevation of each saltiphone; the difference in sensitivity of each microphone, which affects the acoustic signal; the cleanliness of the output signal, which can be affected by wind or rain; and the measurement interval, which should be identical to the internal sampling rate of the instrument.

When comparing other traps to the saltiphone in the field, attention must also be paid to the distance between the instruments because of very small-scale differences in particle concentration that may occur in the transport layer (sand streamers). Finally, when using the analogue output of the saltiphone to calculate sediment fluxes the wind

profile near the bed should be accurately measured, preferably at a sufficiently high temporal resolution.

4.5 Acknowledgements

Acknowledgement. Many thanks are expressed to the Department of Soil Management, University of Ghent, for its permission to use the ICE wind tunnel and the generous support. We also thank Jerry Maroulis for the language revision.

Chapter 5

Measuring aeolian sand transport using acoustic sensors

Ate Poortinga, Hans van Rheenen, Jean T. Ellis, Douglas J. Sherman, Measuring aeolian sand transport using acoustic sensors, *Aeolian Research*, Volume 16, March 2015, Pages 143-151

Measuring aeolian sand transport using acoustic sensors

abstract

Acoustic sensors are frequently used to measure aeolian saltation. Different approaches are used to process the signals from these instruments. The goal of this paper is to describe and discuss a method to measure aeolian saltation with acoustic sensors. In a laboratory experiment, we measured the output from an advanced signal processing scheme on the circuit board of the Saltiphone. We use a software implementation of this processing scheme to re-analyse data from four miniphones obtained during a field experiment. It is shown that a set of filters remove background noise outside the frequency spectrum of aeolian saltation (at 8 kHz), whereas signals within this frequency spectrum are amplified. The resulting analogue signal is a proxy of the energy. Using an AC pulse convertor, this signal can be converted into a digital and analogue count signal or an analogue energy signal, using a rectifier and integrator. Spatio-temporal correlation between field deployed miniphones increases by using longer integration times for signal processing. To quantify aeolian grain impact, it is suggested to use the analogue energy output, as this mode is able to detect changes in frequency and amplitude. The analogue and digital count signals are able to detect an increase in frequency, but are not able to detect an increase in signal amplitude. We propose a two-stage calibration scheme consisting of (1) a factory calibration, to set the frequency spectrum of the sensor and (2) a standardized drop-test conducted before and after the experiment to evaluate the response of the sensor.

5.1 Introduction

Aeolian research aimed at understanding the processes associated with saltation has advanced rapidly over the last decade, in part as a consequence of substantial improvement in the instruments available for field experiments. The ability to measure the wind near the sand surface, especially, has improved greatly with the adoption of ultrasonic anemometry [e.g. [Van Boxel et al., 2004](#), [Walker, 2005](#)]. Until recently, however, instruments and methods to measure characteristics of sand flux have remained disproportionately unsophisticated. A number of recent articles and discussion papers have been published on the use of acoustic sensors in aeolian research. Several [[Poortinga](#)

et al., 2013a, Schönfeldt, 2012, Yurk et al., 2013] demonstrate that acoustic sensors are suitable for the measurement of aeolian mass fluxes, although the work of Ellis et al. [2009b] and Sherman et al. [2011] show some discrepancies between the output of the acoustic sensors and coincidental measurements of sand transport.

Electronic saltation sensing instruments operate from one of three physical bases: acoustic detection; piezoelectric detection; or optical detection. These types of sensors have been reviewed and discussed extensively elsewhere [e.g. Barchyn and Hugenholz, 2010, Davidson-Arnott et al., 2009, Hugenholz and Barchyn, 2011b, Sherman et al., 2011, Van Pelt et al., 2009] and we focus, therefore, mainly on acoustic sensors. The use of acoustic sensors in aeolian research dates back to Spaan and van den Abeele [1991], who designed and tested a microphone-based device called the saltiphone. The microphone responded to the impact of saltating grains that compressed its diaphragm, thereby generating an acoustic signal that could then be digitally recorded. A large number of studies have relied on saltiphone technology. These studies were conducted in a variety of aeolian settings, including coastal environments [e.g. Arens, 1996b, 1997, Poortinga et al., 2014, Schonfeldt and von Lowis, 2003, van der Wal, 2000a], (semi-) arid regions [Leenders et al., 2005a, Mei et al., 2006, Visser et al., 2005b, 2004b, Youssef et al., 2012b], nature reserves [Riksen and Goossens, 2007], as well as wind tunnels [e.g. Goossens et al., 2000, Van Pelt et al., 2009, Youssef et al., 2012b]. Similar custom built microphone systems have been developed and used in recent studies [Ellis et al., 2009b, 2012, Schönfeldt, 2012, Sherman et al., 2011], which have focused mainly on the measurements and technology.

Ellis et al. [2009b] designed a modified version of the saltiphone, that they termed the ‘miniphone’ because of its small sensor area. Acoustic sensors can sample at very fast rates, approaching 100 kHz when using sound cards, for example, and with an unprotected sensing surface that are able to detect the impacts of small sand grains moving at slow speeds. This sensitivity, however, comes at the expense of durability [Sherman et al., 2011]. The less sensitive saltiphone is substantially more durable and thus suitable for long-term deployments. Studies employing these devices used the output of

grain-impact counts to represent saltation intensity, rather than sand transport rates. [Poortinga et al. \[2013a\]](#), however, were able to correlate sand transport rates with the analogue outputs (a proxy for the kinetic energy) from a vertical array of saltiphones.

The output from a saltiphone is not directly comparable with those from other acoustic sensors, such as those used by [Ellis et al. \[2009b\]](#), [Sherman et al. \[2011\]](#), [Yurk et al. \[2013\]](#), because signals from the saltiphone sensor are processed through a range of amplifiers and filters, and those from the miniphone are just amplified. For both types of acoustic sensor, processing the signal to obtain a robust and reliable grain impact count, with the potential to be used as a sand transport rate proxy, has remained a challenge.

A second category of impact sensors is based on piezoelectric crystals and dates back to the development of the piezoelectric-ring based Sensit [[Gillette and Stockton, 1986](#)] and to the experiments of [Hardisty \[1993\]](#) with a crystal mounted on a phonograph needle. Commercialization of piezoelectric sensors began with the development of the Sensit and evolved to the Safire [[Baas, 2004](#)]. Both of these devices proved difficult to calibrate under wide ranges of conditions, in no small part because of their relatively large and curved sensing surfaces. This issue was addressed using small, sensitive buzzer disks – flat, circular piezoelectric surfaces [[Li, 2010](#)]. The buzzer disk is not quite as sensitive as an unshielded acoustic sensor, but is much more durable [[Li et al., 2011](#)]. Analogue output from piezoelectric sensors also requires some degree of signal processing, although some of the instruments include internal circuitry for signal processing and produce impact counts directly. This includes a new, more sensitive instrument from Sensit, the FP5 Flat Plate Movement Sensor [[Sensit, 2013](#)] to be used for initiation of motion studies, similar to that incorporated into the bed load trap system developed by [Swann and Sherman \[2013\]](#).

There is also a multi-decade history of the use of lasers, to detect and measure saltation. Perhaps the first use of this technology was a wind-tunnel experiment where the beam was used to detect the initiation of motion [[Nickling and Ecclestone, 1981](#)].

Butterfield [1999b] used a laser system, coupled with thermal anemometry, in his wind-tunnel study of saltation profiles. The next two technological advances came with the development, by Mikami et al. [2005] of a laser particle counter that could also size the grains, and the use of a commercial, fork-sensor particle counter (produced by Wenglor Sensoric GmbH) in field studies of aeolian sand transport [e.g. Chapman et al., 2013, Davidson-Arnott et al., 2009, Hugenholtz and Barchyn, 2011b, Martin et al., 2013]. One of the advantages of the Wenglor fork sensor is that its circuitry is able to produce grain counts with no subsequent signal processing required, and they are suitable for relatively long deployment. They are, however, directionally sensitive, and prone to signal saturation under conditions with intense saltation [e.g. Barchyn et al., 2014a, Hugenholtz and Barchyn, 2011b].

Acoustic sensors remain valuable tools in the quest to better understand the dynamics of aeolian saltation, especially given their ability to detect grain impacts at high frequencies on small sensing surfaces. One of their major drawbacks has been the issue of calibration and signal processing necessary to convert the acoustic signatures of impact into a reliable grain impact count. The purpose of this study is to provide a technical description of an advanced signal processing protocol to improve the detection and counting of grain impacts during aeolian saltation. We devised an experiment where we measured the analog signals at different locations within the electrical circuit in order to evaluate the signal processing scheme and its applicability to study aeolian saltation processes. We use this protocol to analyze field-based data obtained using a miniphone [Ellis et al., 2009b]. We discuss and compare the results of this study with previous approaches in order to assess its general applicability. The aim of this paper is to make a contribution to the discussion on the use and application of acoustic sensors in aeolian research, using the saltiphone and miniphone as examples.

5.2 Background

Aeolian sediment transport can be categorized into three different modes: creep, saltation (including reptation) and suspension. Finer particles (0.001 to 0.1 mm) are usually

transported as suspended load within the air column, whereas larger particles (1 to 2 mm) reptate (creep or move via small hops) and intermediate-sized particles (0.1 to 1 mm) saltate or reptate (path lengths long relative to grain diameter) over the surface [Fryrear et al., 1991, Lancaster and Nickling, 1994]. Most sand transport on Earth and Mars occurs in the saltation mode [e.g. Bagnold, 1941, Kok et al., 2012, Nickling and Neuman, 2009], and thus saltation load has been the focus of much of the aeolian sediment transport research in wind tunnel and field research, and in modelling efforts. Over the last several decades there have been substantial advances in our ability to measure the characteristics of the wind (see reviews by Nickling and Neuman [2009] or Sherman et al. [2013a]), especially in the time domain. For the most part, however, measurements of sand transport have relied on the use of passive sediment traps such as the Leatherman/Rosen trap [Leatherman, 1978, Rosen, 1978], the Guelph trap [Nickling and McKenna Neuman, 1997], Modified Wilson and Cook [Poortinga et al., 2015, Sterk and Raats, 1996, Wilson and Cooke, 1980b], Big Spring Number Eight [Fryrear, 1986], WITSEG [Dong et al., 2004b], Basaran and Erpul Sediment Trap [Basaran et al., 2011], or mesh-type trap [Sherman et al., 2014]. Some of these traps involve a single chamber (e.g. Leatherman [1978], Nickling and McKenna Neuman [1997]), thus integrating the vertical flux into one measurement. Others comprise sets of different compartments so that the flux profile can be measured (e.g. Dong et al. [2004b], Wilson and Cooke [1980b]). The sediment caught in the traps over a known time period is dried and weighed, and the results used to calculate a transport rate in units (typically) of $\text{kgm}^{-1}\text{s}^{-1}$ or $\text{gm}^{-1}\text{s}^{-1}$. When a trap array has gaps in vertical coverage (such as the BSNE), the total transport rate can be estimated by log-linear curve fitting for the segmented data and then by integration. The use of passive-style traps typically involves sampling transport over periods of 1 to 30 minutes through openings (single or cumulative through several) with areas of the order of 10^5 mm^2 or greater.

The work of Sterk et al. [1998] shows a good linear correlation between measured mass fluxes with a modified Wilson and Cooke sediment trap and the count output of a saltpHONE measured at the same height in a windtunnel. However, as they argue, the

range of fluxes measured in the experiments was rather narrow. It is therefore uncertain whether this relationship is still valid for higher and lower fluxes. Other studies that explored the efficiencies of different active sensors generally found low fidelity when comparing measurements from several devices. This is partly due to the often variable environmental conditions, e.g., varying wind speed, temperature, saltation intensity, and grain size [Ridge et al., 2011], but particular designs and signal processing protocols also play an important role. For example, radial variance in sensitivity is a problem for the omnidirectional Sensit and Safires [Baas, 2004, Van Pelt et al., 2009], whereas the fragility and implicit cut-off boundary, i.e. the translation from a voltage to a count, impede the use of laser particle counters. While sensor degradation might be a severe drawback for some acoustic sensors [Ellis et al., 2009b], they have a limited effect in terms of flow distortion and can be used to quantify the kinetic impact of a sediment laden airflow, when the correct signal processing is applied. With assumptions or measurements concerning particle size distribution and velocity, impact counts or kinetic energy can be used to estimate total flux characterization.

The advent of field-deployable, active sensors, such as those highlighted above, allows sampling of saltation at much greater spatial and temporal resolutions than those associated with passive traps. Active sensors can have sensor areas of less than 100 mm^2 and their sampling frequency can approach 10^5 Hz . These scales allow for intensive examination of saltation systems at scales that are now much finer than those sampled by typical wind instruments. However, unlike the data obtained with passive sediment traps, it is difficult to use the data acquired with active sensors to quantify grain impact counts without complicated signal processing.

5.3 Materials and methods

Data from a laboratory and field experiment were used in this study. Laboratory experiments used a modified saltiphone acoustic sensor where we tested the impact signals at different locations in the electrical wiring scheme to develop an improved protocol for estimating particle flux. In the field experiment, four miniphones were deployed on a

sandy beach. We provide a detailed description of the saltiphone and signal processing scheme and the experimental setup.

5.3.1 Laboratory experiment

5.3.1.1 The saltiphone

The saltiphone [Spaan and van den Abeele, 1991], consists of a microphone (SA-18) positioned in the centre of a stainless steel tube mounted on a ball bearing (Fig. 5.1). The two vanes at the back of the steel tube ensure that the saltiphone is aligned with the wind when the ball bearing is connected to a steel rod. A screw in the ball bearing makes the device height adjustable. In the first version of the saltiphone, a ball bearing was connected to the bottom of the tube. In the newer versions, this ball bearing is positioned on top of the tube, so that it can rotate freely while the tube is located in closer proximity to the surface. The ball bearing is simultaneously the centre of mass, to ensure the tube will only rotate horizontally. Although never scientifically tested, the wings were specifically designed to create a low pressure field behind the tube to accelerate flow inside the tube. The acceleration was intended to steer particles within the tube toward more direct (perpendicular) impacts on the microphone and prevent clogging. This microphone has a frequency range of 0.1-10 kHz and is connected to the electrical circuit via a cable.

To measure aeolian saltation, the signal of the microphone is processed into a digital or analogue signal (Fig 2). First, the signal is amplified and filtered by a two-stage active bandwidth filter. The typical frequency of aeolian saltation (8 kHz, Spaan and van den Abeele [1991]) is used to identify the sound of colliding sand particles. The low and high frequency signals are attenuated and the band frequency signals of interest are amplified. Figure 2 in Spaan and van den Abeele [1991] (shown in the bottom of Fig 2 here) shows the frequency curve of the microphone amplifier. The resulting signal is a proxy for energy.

The analogue energy signal is a collection of pulses with varying frequency and amplitude. This signal is processed into three different signals: (1) analogue energy, (2)

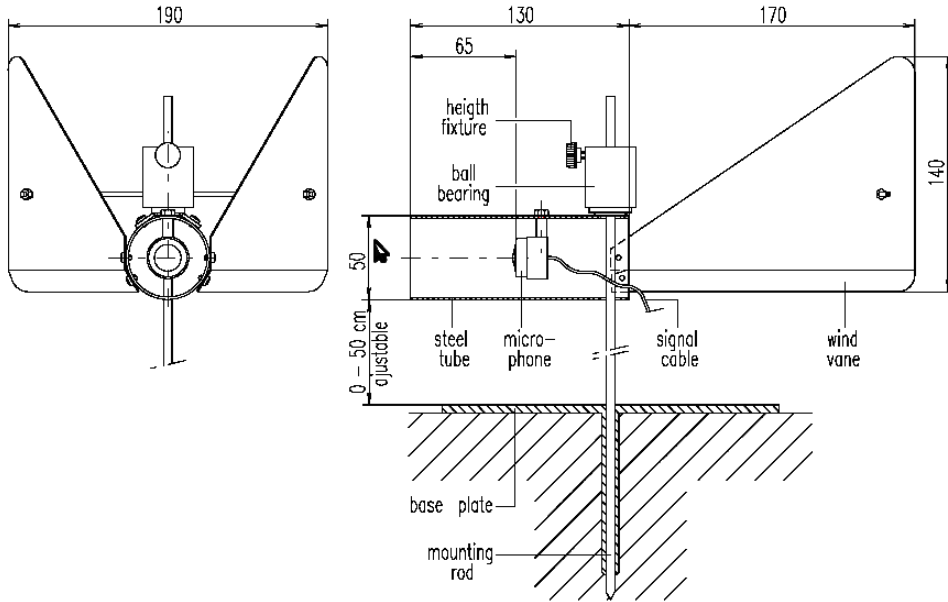


FIGURE 5.1: A schematic overview of the Saltiphone acoustic sensor.

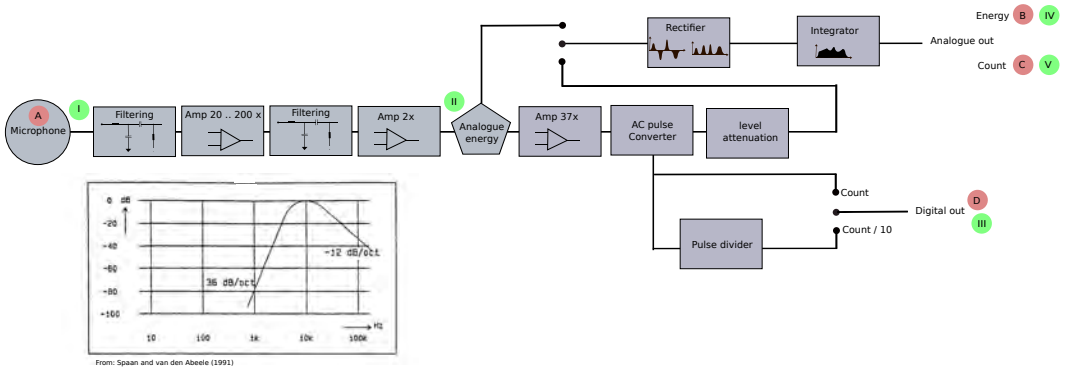


FIGURE 5.2: A flow diagram of the electrical wiring of the saltiphone. Image top: the frequency curve of the microphone amplifier. The input (A) and output (B,C,D) signals are shown, as well as the measurement locations (I-V).

analogue count and (3) digital count. Output signals of the analogue energy, analogue count and digital count are shown in Fig. 5.2, B, C, and D, respectively. The analogue energy (B) is determined by rectifying the signal, where all negative pulses are converted into positive pulses. A combination of an active and passive integrator is used to determine the total amount of energy in the signal.

The analogue energy signal is also used to determine a total number of counts (analogue and digital). Here, the signal is amplified and wired through an AC pulse converter where signals above a certain threshold are converted into pulses (0 or 1). For the digital output, a pulse divider (divided by factor 10) was included to prevent saturation. For the analogue output, the signal is attenuated and converted into an analogue signal in an integrator, so that the signal can be read as a voltage from the analogue count output.

A calibration of the microphone is required as the specific characteristics of a microphone might differ from one to another. Different characteristics might result in differences in sensitivity and/or the frequency spectrum. A calibration device (Fig. 5.3) was used to apply a constant signal of 8 kHz. to the microphone, while the bandwidth filter was set.

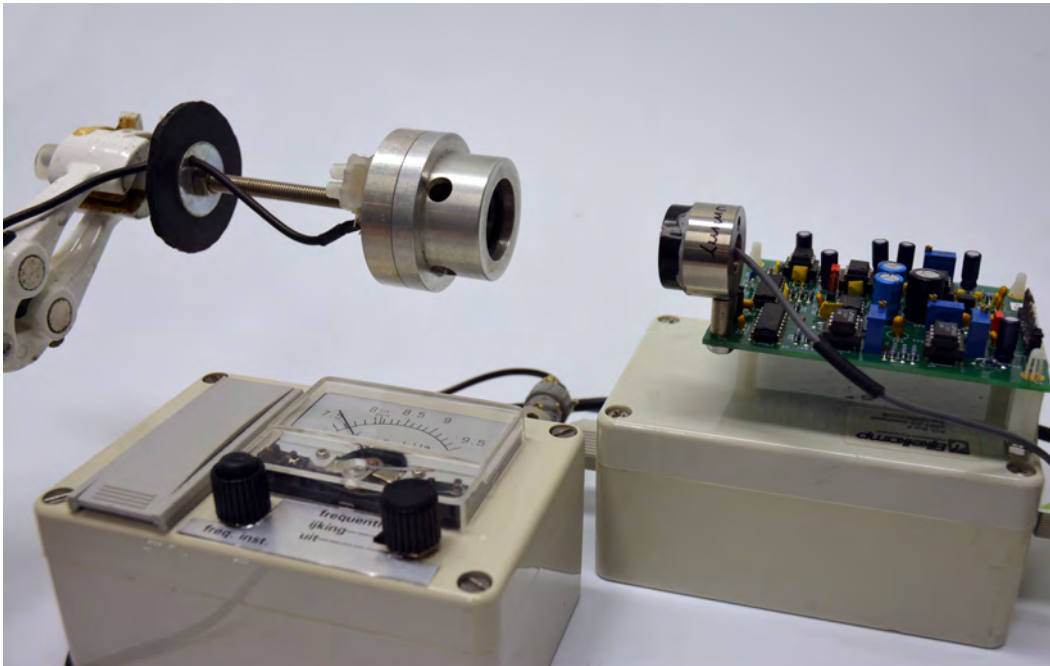


FIGURE 5.3: Factory calibration of the saltiphone. The frequency spectrum of the microphone amplifier is adjusted while applying a constant signal of 8 kHz to the microphone.

5.3.1.2 Laboratory methods

At different locations in the electrical circuit (Fig 5.2: locations I – V) the electrical signal was measured by connecting different channels of the oscilloscope (Fig 5.4: left) to the circuit board of the saltiphone. The impact of a small number of grains was measured by manually dropping round ($400\ \mu\text{m}$) glass beads on the microphone. To simulate the signal of an aeolian saltation cloud, the microphone was located in the centre of a cylinder (Fig 5.4: right). Inside the cylinder, a funnel with a diameter of 2 mm was filled with glass beads, approximately 0.15 m above the microphone. Variations in sediment flux were simulated by manually re-directing part of the flow. Due to internal memory limitations in the oscilloscope, there is a trade-off between measurement frequency and durations. The sampling interval was varied in order to obtain datasets of different durations.

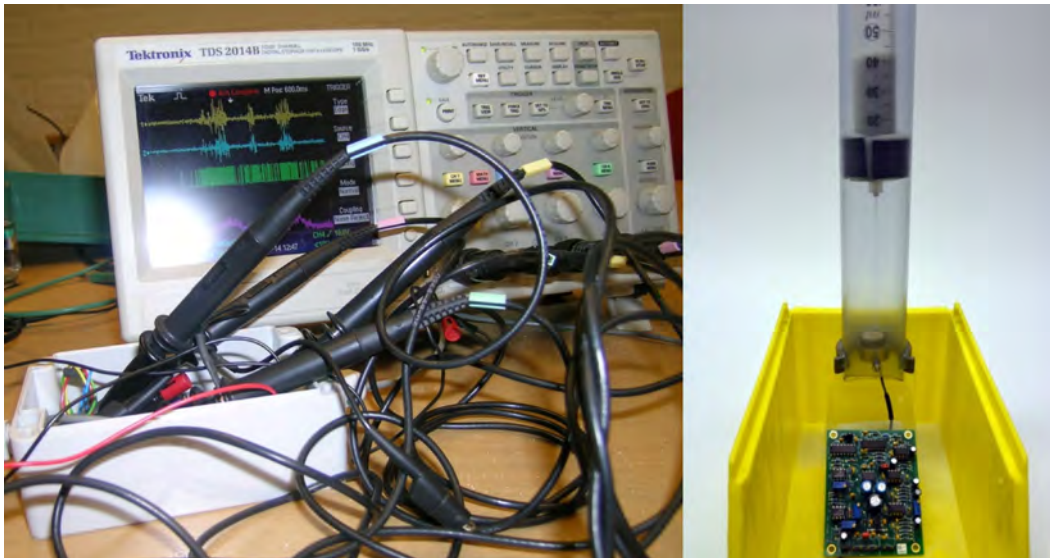


FIGURE 5.4: The experiments were conducted by connecting a Tektronix (TDS 2014B) digital storage oscilloscope to different locations in the electrical circuit (left). The image right shows the equipment used for the drop-tests. Glass beads located in a funnel in the cylinder were dropped from a fixed height on the microphone, which was located in the centre of the cylinder.

5.3.2 Field experiment

5.3.2.1 The miniphone

The miniphone, as introduced by [Ellis et al. \[2009b\]](#), consists of a modified JLI Electronics electret microphone mounted in a brass tube. The microphone modification process includes removal of the felt and metal cover protecting the diaphragm. The frontal diameters of the ‘big’ and ‘small’ microphones are 6 mm and 4 mm, respectively. The microphones are placed inside a 0.4 m brass tube that has a diameter equivalent to the microphones. The brass tube serves as a housing for the microphone for easier mounting in field-based environments. [Ellis et al. \[2009b\]](#) wired the modified microphone to circuitry that amplified the signal before reaching the analogue to digital data acquisition system sampling with a rate of 4 kHz. In later studies [[Ellis et al., 2012](#)], the miniphone was wired to a sound card, thus allowing sampling rates up to 44.1 kHz.

5.3.2.2 Field methods

The field experiment was conducted in November 2011 in Ceará, Brazil, in the vicinity of Jericoacoara. Four miniphones were installed in a flow-perpendicular, 3 m long array, at an elevation of 0.09 m above the surface. The miniphones were connected to a data acquisition system with a sampling rate of 44.1 kHz, and were aligned perpendicular to the prevailing wind direction. Miniphone records were obtained for a period of 35 minutes. The field site is the same as that described by [Ellis et al. \[2012\]](#) and [Sherman et al. \[2013b\]](#).

5.3.2.3 Data analysis methods

A software implementation consistent with the flow diagram described in figure 5.2 was used to analyse the data from the miniphone. Similar to [Yurk et al. \[2013\]](#), the signal from the miniphone was filtered using a high-pass Butterworth filter (fifth order). Whereas [Yurk et al. \[2013\]](#) used a cutoff frequency of 1 kHz, we use a lower and upper boundary of 7 and 9 kHz respectively. The signal was rectified and integrated using

varying time intervals. Linear regression was applied to compare the correlation of the different microphones.

5.4 Results

5.4.1 Laboratory experiment

Four experiments were selected to illustrate the signal processing of aeolian saltation. Table 5.1 provides an overview of the measurement location in the electrical circuit for the different experiments. For experiment 1, we made measurements at three locations along the signal (Fig. 5.2) when manually dropping glass beads on the microphone. The funnel was used for experiment 2, 3 and 4, and the electrical signal was measured at four locations. The sampling interval varied from 100-10000 Hz.

TABLE 5.1: The measurement locations (see Fig. 5.2) in the electrical circuit, droptest and sampling frequency for the different experiments.

Experiment	Measurement Locations	Droptest	Sampling frequency (Hz)
1	I, II ,III	Manual	10000
2	I, II,III V	Funnel	250
3	I, II, IV	Funnel	500
4	I, II, IV	Funnel	100

Figure 5.5 shows the measured signals of the first experiment signal directly behind the microphone (top Fig 5.5: I in Fig. 5.2), behind the filtering and amplification (middle Fig 5.2: II in Fig. 5.2) and the digital pulse output (bottom Fig 5.5: III in Fig. 5.2). The left figures represent a period of 0.0025 second, whereas the right images provide a detailed description of two pulses within 0.005 seconds, indicated with dotted lines in the left images. The signal from the microphone contains a considerable amount of noise that is removed by the filter. The resulting signal varies in frequency and amplitude. Values above a threshold result in a digital pulse. Every pulse lasts 0.000875 sec, or seven samples when measuring with 8 kHz.

In experiment 2, we added the analogue count signal to the signals measured in the first experiment. For a period of 10 sec, the signals were measured with a sampling

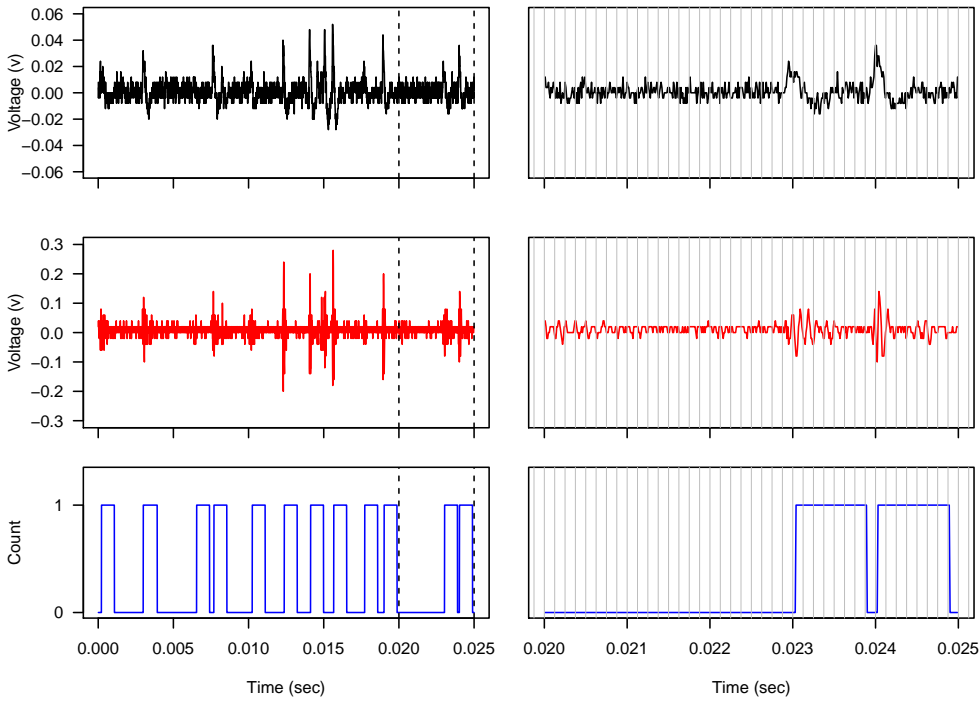


FIGURE 5.5: The signal of the saltiphone measured during experiment 1. The signal of the microphone (top), the filtered and amplified signal (middle) and the pulse output (bottom), locations I, II and III in Fig. 5.2 respectively. Figures on the right are a more detailed image of the area between the dotted lines in the left images. The vertical gray lines in the right image represent the 8 kHz.

frequency of 250 Hz. Fig. 5.6 shows the electrical signals for the microphone (top), the amplified signal (middle top), the digital count (middle bottom) and analogue count (bottom), at locations I, II, III and V in figure 5.2 respectively. For the digital count output, a variation in frequency can be observed, whereas the analogue count output shows a variation in amplitude. An increase in frequency results in an increase in amplitude for the analogue count output. In fact, the analogue count signal is constructed from the same signal as the digital count. However, the signal from the analogue count output is wired through an integrator, which integrates the pulses with respect to time, resulting in a higher voltage for a higher frequency in counts.

The signal of the microphone (I Fig 5.2), the amplified and filtered signal (II Fig 5.2) and the analogue energy output signal (IV Fig. 5.2) were measured in experiments 3 and

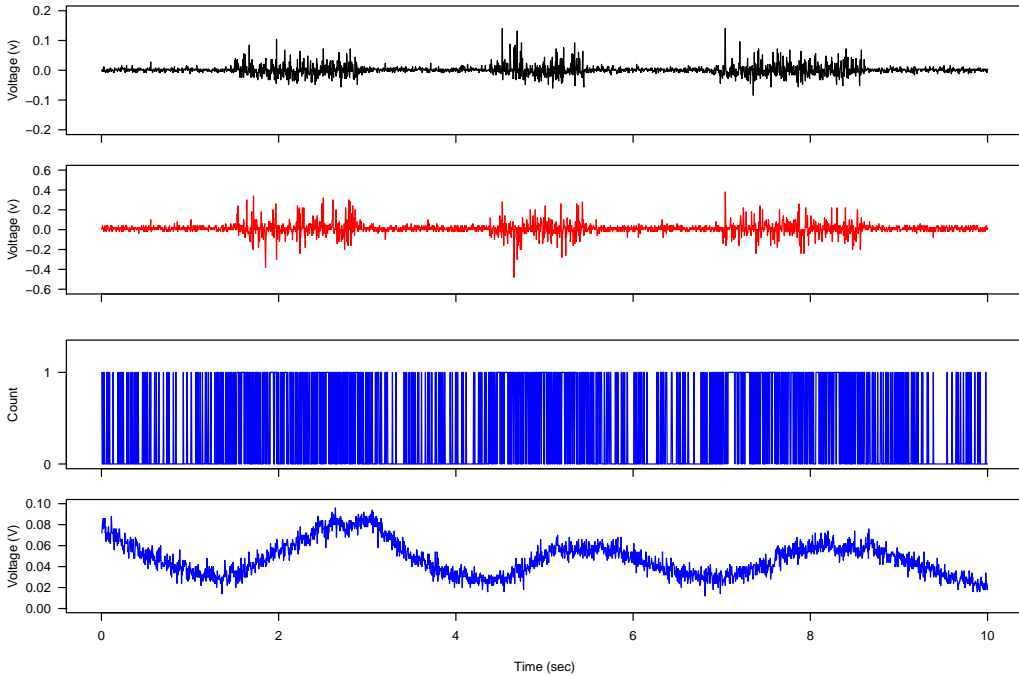


FIGURE 5.6: The signal of the saltiphone measured during experiment 2. Signals were measured for the microphone (top), the filtered and amplified signal (middle top) and the pulse output (middle bottom) and analogue count output (bottom), locations I, II and III and V in Fig. 5.2, respectively.

4. Figure 5.7 Shows the results of experiment 3 (left) and experiment 4 (right). During experiment 3, a small number of grains were dropped through the funnel for a period of 5 sec. While the filtered signal is rather constant (Fig. 5.7: middle left), the voltage from the analogue energy (Fig. 5.7: bottom left) increases towards a maximum, followed by a decrease in voltage. This can be explained by the integrator, which outputs an voltage in respect to time. In experiment 4 (Fig. 5.7: right), the duration was extended to 25 seconds. The analogue energy output also shows the time-lag here, but increases to a stable value around 2 volts. This was expected, considering the constant throughput of glass beads in the funnel.

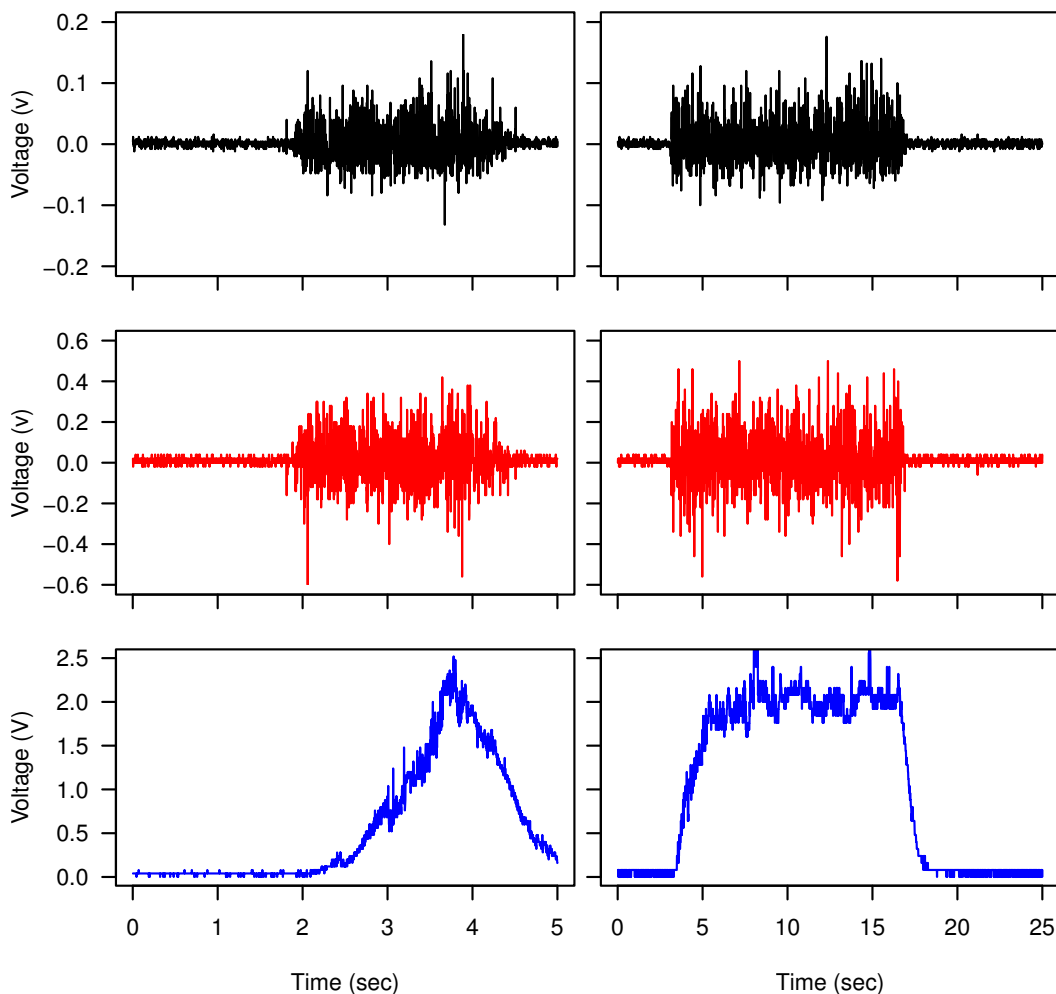


FIGURE 5.7: The electrical signals measured for experiment 3 (left) and 4 (right). Experiment 3 lasted 5 seconds, whereas experiment 4 took 25 seconds. The different figures represent the signal from the microphone (top), the signal after filtering and amplification (middle) and the analogue energy (bottom).

5.4.2 Field experiment

The miniphone records were re-analysed using the signal processing scheme. To ensure sensor integrity, only the first 10 minutes of the records were included in the regression analysis. Figure 5.8 shows the correlation between the four miniphones according to distance and time integration. This analysis was done to identify an appropriate temporal basis, especially, for sensor comparison, Thus providing a platform for assessment of the performance of the protocol. The distance between two correlated miniphones is

presented as dots. It can be seen that the outputs of the sensors are poorly correlated for small integration times (< 1 sec). This correlation improves with longer integration times up to approximately 5 seconds. Integration times longer than 5 seconds does not further improve the correlation between the miniphone outputs.

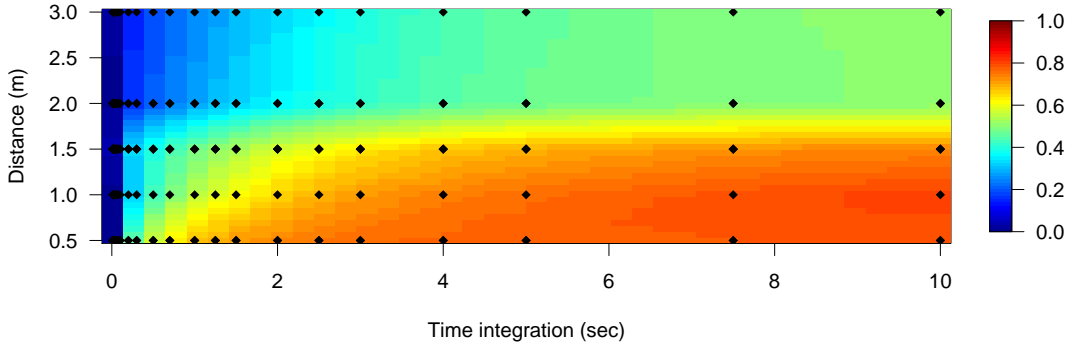
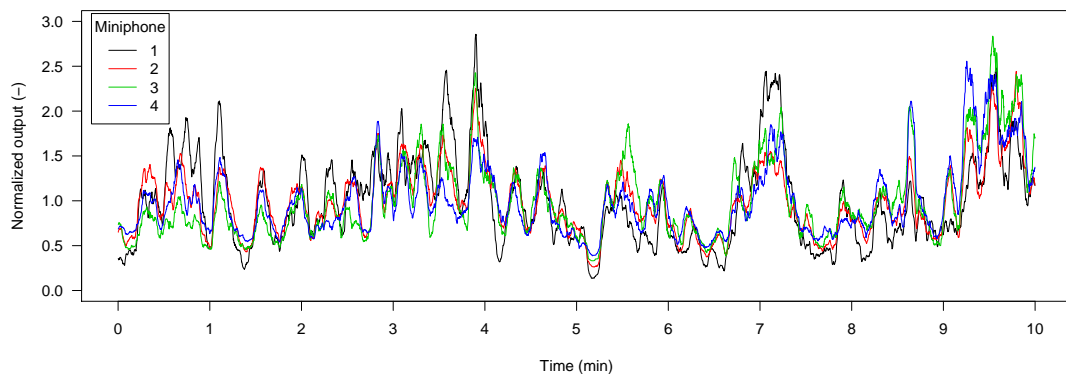
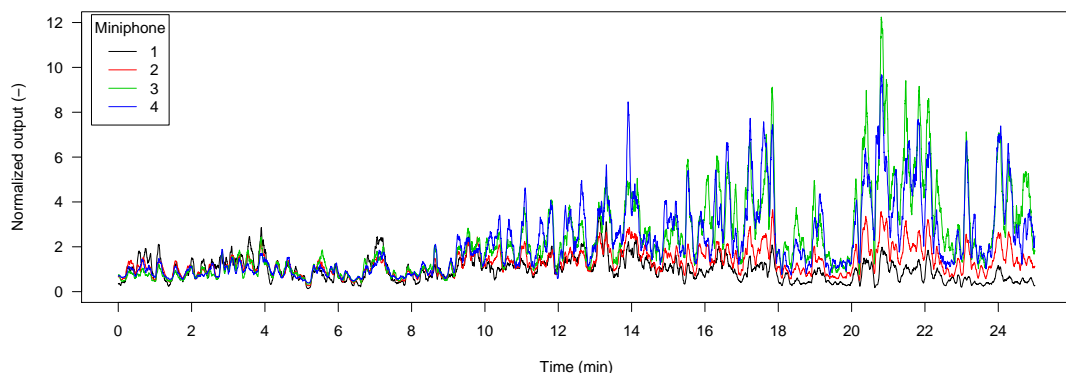


FIGURE 5.8: The correlation between the processed miniphone output located at four different locations using different time integration. The colors indicate a difference in R^2 . The dots represent the distance between two correlated miniphones.

The processed signals of the miniphones were compared using an integration time of 5 seconds. The signals were normalized using the mean of the first 10 minutes of the measurements. The results are shown in figure 5.9(a) and 5.9(b). The first figure (Fig. 5.9(a)) shows the normalized output for the first 10 minutes of the record. Despite some variance, there is a clear similarity in the processed output between the different miniphones. After 10 minutes (Fig. 5.9(b)), the variance between the different sensors becomes larger, with a notable increase in signal for miniphone 3 and 4. However, the trends in the signal (i.e. an increase or decrease in signal) remain rather similar between the miniphones. The increase in variance between the different sensors is attributed to sensor degradation.



(a) a: The first 10 minutes of the normalized output of the four miniphones. An integration time of 5 seconds was used in the signal processing scheme.



(b) b: The first 25 minutes of the normalized output of the four miniphones. An integration time of 5 seconds was used in the signal processing scheme.

FIGURE 5.9

5.5 Discussion

Acoustic sensors have a specific range of frequencies over which they are capable of detecting a signal. As aeolian saltation has a typical frequency of 8 kHz [Spaan and van den Abeele, 1991], it is important that the sensor has a high sensitivity in this frequency. Saltiphones typically use a SA-18 Microphone Cartridge which has a frequency range of 0.1-10 kHz. The JLI Electronics microphone (model F9445AL), used by Ellis

et al. [2009b] and Yurk et al. [2013], is sensitive between 0.2-16 kHz. Schönfeldt [2012] used a micro speaker (Kingstate, type KDMG15008P-025A1), sensitive in 0.9 - 20 kHz range. Each of these models should be suitable to detect aeolian saltation.

The signal processing from the acoustic sensor varies between the different studies. Studies from Ellis et al. [2009b] and Sherman et al. [2011] used an analogue to digital converter and a soundcard, whereas Schönfeldt [2012] used the microphone in conjunction with a transistor and amplifier. In the electronic circuit of Schönfeldt [2012], signals from the microphone were amplified without filtering. Positive pulses above a threshold of 0.5 volt were counted by a data logger. Their approach might be improved by applying rectification and filtering of the signal. Moreover, their setup might not be able to detect small sharp pulses in the signal.

In this study, we measured three different output signals from the saltiphone. It was found that the analogue energy output is able to detect changes in frequency as well as amplitude. The analogue and digital count output use pulses from the AC pulse converter to construct the output signal. Both signals represent an increase in frequency, but are not able to detect a higher amplitude in signal. The pulse converter applies a certain threshold of the incoming signal in order to convert it to a binary signal (0 or 1). An arbitrary cut-off value results in no count output for grains without sufficient momentum to exceed the threshold, whereas analogue energy would give a low output signal as a physical evidence for sediment transport. When a quantitative representation of the sediment flux is the primary interest, it is suggested to use the analogue energy output.

Once the signal processing protocol had been established through the laboratory trials, it was used with field data obtained in miniphone experiments. We would expect similar success with this application because the saltiphone and the miniphone are designed around similar acoustic technologies. This comparison represents an objective test for the signal processing method because the miniphone data were collected independent of any consideration of this protocol. The results are entirely consistent with those obtained through the application of much more complicated signal processing

methods [e.g. [Li, 2010](#)]. The correspondence of the processed signals from one miniphone to the next also supports the broader applicability of the protocol, requiring only calibration to convert the normalized signal to grain counts or transport rates.

In a recent discussion on the work of [Sherman et al. \[2011\]](#), [Hugenholtz and Barchyn \[2011b\]](#) raised their concerns of noise in the signal and non-linearity in the microphone response. In a reply, [Li et al. \[2011\]](#) described extensive "drop tests" to remove background noise and compare the sensor response. Sensor response was found to be consistent between sensors, especially compared to commonly used sensors with a curved surface (Sensit and Safire). In this study, it is shown that the recordings using miniphones are very consistent when compared with each other, as long as the correct processing scheme is applied.

It is suggested to apply a two stage calibration procedure for acoustic sensors. The first step involves a factory calibration (Fig. 5.3). Here, the frequency spectrum of the sensor is adjusted to the frequency spectrum of aeolian sediment transport, so that other noise will be removed from the signals. The second calibration should be performed before and after an experiment, to accommodate for potential instrument degradation. During this calibration, the sensitivity and performance should be evaluated using a standardized drop-test. In this study, we used glass beads because of their round shape and homogeneous composition. Future studies might extend this approach with sand from the field site or e.g. using different flow rates in a sand fall flume, as demonstrated by [Baas \[2004\]](#), [Hugenholtz and Barchyn \[2011b\]](#). The configuration and deployment of acoustic sensors in the field or wind tunnel is also important. Improperly attaching them to a pole or rod might alter the airflow and therefore not give an accurate representation of the impacting saltation. The sensor should be able to freely rotate, in order to align with changing wind direction.

The sources of uncertainty for acoustic sensors raised by [Hugenholtz and Barchyn \[2011b\]](#) are important considerations for the scientific application of these sensors. For future work, it is suggested to include and test all the different aspects of filtering, amplification, setup and calibration. Degradation of the sensor is known to be a problem

[Ellis et al., 2009b] and durability should be tested for different types of sensors. These tests should lead to a standardized method for using acoustic sensors in aeolian research, so that future studies that apply this technique are comparable [Barchyn et al., 2011].

5.6 Conclusions

The results from this research identify important considerations for the application of acoustic sensors for measuring saltation:

- The frequency spectrum of the microphone should include the range of aeolian saltation, which is approximately 8 kHz.
- Quantification of aeolian mass fluxes can be done by integration of the filtered and amplified analogue signal.
- Acoustic sensors should be calibrated in a two-step procedure: (1) a factory calibration where the frequency spectrum is adjusted in conjunction with that of aeolian saltation and (2) a field-test where the sensitivity and response of the sensor is evaluated.

5.7 Recommendations

For future applications, we recommend a protocol of filtering, amplification and integration as described in this study.

5.8 Acknowledgements

We thank Eijkelkamp for supplying us with information on the inner working of the saltiphone. Two anonymous reviewers are also thanked for their invaluable comments. Furthermore, we thank Rinze Poortinga for his support in the interpretation of the electrical circuits.

Chapter 6

Measurement uncertainties in quantifying aeolian mass flux: Evidence from wind tunnel and field site data

Poortinga A, Keijsers JG, Maroulis J, Visser SM (2014) Measurement uncertainties in quantifying aeolian mass flux: evidence from wind tunnel and field site data. *PeerJ* 2: e454.

Measurement uncertainties in quantifying aeolian mass flux: Evidence from wind tunnel and field site data

abstract

Aeolian sediment traps are widely used to estimate the total volume of wind-driven sediment transport, but also to study the vertical mass distribution of a saltating sand cloud. The reliability of sediment flux estimations from this data are dependent upon the specific configuration of the measurement compartments and the analysis approach used. In this study, we analyse the uncertainty of these measurements by investigating the vertical cumulative distribution and relative sediment flux derived from both wind tunnel and field studies. Vertical flux data was examined using existing data in combination with a newly acquired dataset; comprising meteorological data and sediment fluxes from six different events, using three customized catchers at Ameland beaches in northern Netherlands. Fast-temporal data collected in a wind tunnel shows that the median transport height has a scattered pattern between impact and fluid threshold, that increases linearly with shear velocities above the fluid threshold. For finer sediment, a larger proportion was transported closer to the surface compared to coarser sediment fractions. It was also shown that errors originating from the distribution of sampling compartments, specifically the location of the lowest sediment trap relative to the surface, can be identified using the relative sediment flux. In the field, surface conditions such as surface moisture, surface crusts or frozen surfaces have a more pronounced but localized effect than shear velocity. Uncertainty in aeolian mass flux estimates can be reduced by placing multiple compartments in closer proximity to the surface.

6.1 Introduction

Aeolian sediment transport is an important geomorphological process that shapes a number of landscapes including coastal [e.g. [Arens, 1996b](#), [Jackson and Nordstrom, 2011](#), [van der Wal, 2000a](#)], drift sand [e.g. [Riksen et al., 2006](#), [Riksen and Goossens, 2007](#)], deserts [e.g. [Bagnold, 1941](#), [Wiggs, 2001](#)], and also agricultural areas [e.g. [Chepil and Woodruff, 1963](#), [Visser and Sterk, 2007](#), [Visser et al., 2004b](#)]. Along sandy coasts, aeolian processes drive the morphological development of coastal dunes that protects the hinterland against flooding. Maintaining the natural aeolian dynamics allows vegetation

to flourish in different successive stages, creating an appealing area for tourism and recreation [Poortinga et al., 2011]. In agricultural areas, however, aeolian processes are often erosive, as fertile top soil is highly susceptible to wind erosion [Nanney et al., 1993]. Therefore, an in-depth understanding of the physical processes of wind-driven sediment transport is critically important.

It is widely recognized that aeolian sediment transport is highly variable in space and time [Baas and Sherman, 2005, Ellis et al., 2012]. Despite our detailed understanding of the physics of wind blown sand [e.g. Bagnold, 1941, Kok et al., 2012, Pähtz et al., 2013], accurately quantifying aeolian sediment patterns remains a challenge. Measurements of aeolian sediment budgets might improve our understanding, but often have limited spatial and temporal resolution. Approaches used to measure aeolian sediment transport include passive sediment traps [Basaran et al., 2011, Dong et al., 2004b, Mendez et al., 2011, Rasmussen and Mikkelsen, 1998, Sterk and Raats, 1996], active samplers such as acoustic samplers [Ellis et al., 2009b, Schönfeldt, 2012, Spaan and van den Abeele, 1991, Yurk et al., 2013], laser particle counters [Hugenholtz and Barchyn, 2011a,b, Li et al., 2011, Sherman et al., 2011], piezoelectric samplers [Baas, 2004, Stout, 1998], pressure sensitive samplers [Ridge et al., 2011] and terrestrial laser scanners [Nield and Wiggs, 2011]. The physics of wind blown sand are often studied in the controlled environment of a wind tunnel [e.g. Butterfield, 1999b, Goossens et al., 2000, Pelt et al., 2009, Youssef et al., 2008] but also directly in the field [e.g. Ellis et al., 2012, Namikas, 2003]. However, results from wind tunnel studies cannot be directly translated into field situations, due to differences in turbulence spectrum, wind profile above the bed and variability in environmental factors such as surface moisture, wind direction and velocity, bed elevation, vegetation, sediment composition, lag deposits, surface crusts and fetch. Despite recent progress in rapid data acquisition, where aeolian sediment flux data are collected at high temporal resolution, passive sediment catchers are still frequently used to study aeolian sediment flux.

Passive sediment traps consist of various compartments located at different elevations. Sediment captured within these compartments, provides valuable information

about the vertical sediment flux distribution [Butterfield, 1999b, Dong et al., 2003, Ni et al., 2003], which is frequently used to estimate total sediment transport [Sterk et al., 1996, 2012, Sterk and Spaan, 1997, Visser et al., 2004a]. Aeolian mass fluxes are quantified by applying non-linear curve fitting through the sediment measurements within the different compartments. However, passive sediment traps have some inherent uncertainties (average of 10%) depending on the specific distribution of sediment within the compartments and their elevation above the surface; whereas sediment mass, inlet diameter, vertical position of the catchers, trapping efficiency, horizontal spacing between catcher arrays and wind direction were also identified as potential sources of error [Tidjani et al., 2011]. Moreover, variations in elevation from the lowest compartment to the ground (referred to as base elevation hereafter) may also change during the experimental measurement. The vertical distribution of the aeolian mass flux is also important here. When the largest fraction of sediment is transported close to the surface, uncertainties related to the lowest compartment become more important for estimation of total flux; even though vertical flux distribution might also vary through time.

The aim of this study was to characterize aeolian mass flux from wind tunnel and field data by comparing passive trap and high-frequency saltiphone data. Uncertainties caused by the distribution of the different trapping compartments and the influence of the base elevation were analysed for both wind tunnel and field situations. This paper will firstly examine uncertainties resulting from the distribution of different sediment trapping compartments and the influence of base elevation on fast-temporal data acquisition from saltiphones applied in a wind tunnel study. Whereas passive sediment traps collect sediment transport data for each experiment, fast-temporal data is provided continuously throughout the experiment. The latter providing a more detailed analysis of sediment flux. Secondly, the paper will explore the implications of our findings to field studies by testing data gathered from two published studies and a newly acquired dataset. The newer dataset, obtained used three customized sediment catchers, was also used to investigate the variability in vertical sediment flux and total sediment transport.

6.2 Materials and Methods

6.2.1 Data collection

Specific details about the locations and data collection methods used in the two published field studies can be found in [Farrell et al. \[2012\]](#) and [Visser et al. \[2004b\]](#). Results and data from the wind tunnel study can be found in [Poortinga et al. \[2013a,b\]](#) respectively. The data collection procedure used for the new dataset is presented below, while the data of the present study and [\[Visser et al., 2004b\]](#) can be obtained from <http://dx.doi.org/10.1016/j.envsoft.2003.12.010>.

6.2.2 Study area

The research took place from November to December 2010 on a beach at the north-western end of Ameland, one of the West Frisian barrier islands located in the northern extremity of The Netherlands (Fig [6.1\(a\)](#)). The site is characterized by strong wind and wave dynamics in constructing bedforms and embryonic dune development. Human influence on this part of the beach is minimal compared to the middle section of the island. The study area is located east of a sand bar, which attached to the island in the mid 1980s, causing a progressive, attenuating sand wave to the East [\[Cheung et al., 2007\]](#), resulting in relatively wide beaches (> 150 m). Figure [6.1\(c\)](#) was taken from the top of the foredune and shows the experimental site at low tide.

6.2.3 Measurement of sand size

Data was obtained on sediment characteristics, sediment transport and a number of significant meteorological parameters. Surface sands are largely composed of unconsolidated quartz grains with some feldspar and a small fraction of heavy minerals [\[van der Wal, 2000a\]](#). To determine sediment size, samples were taken from the beach surface at a number of representative locations across the beach and mixed into one large sample. This sample was dried and sieved in fractions of 50, 100, 250, 500, 1000 and 2000 μm . The median diameter was found to be 180 μm .

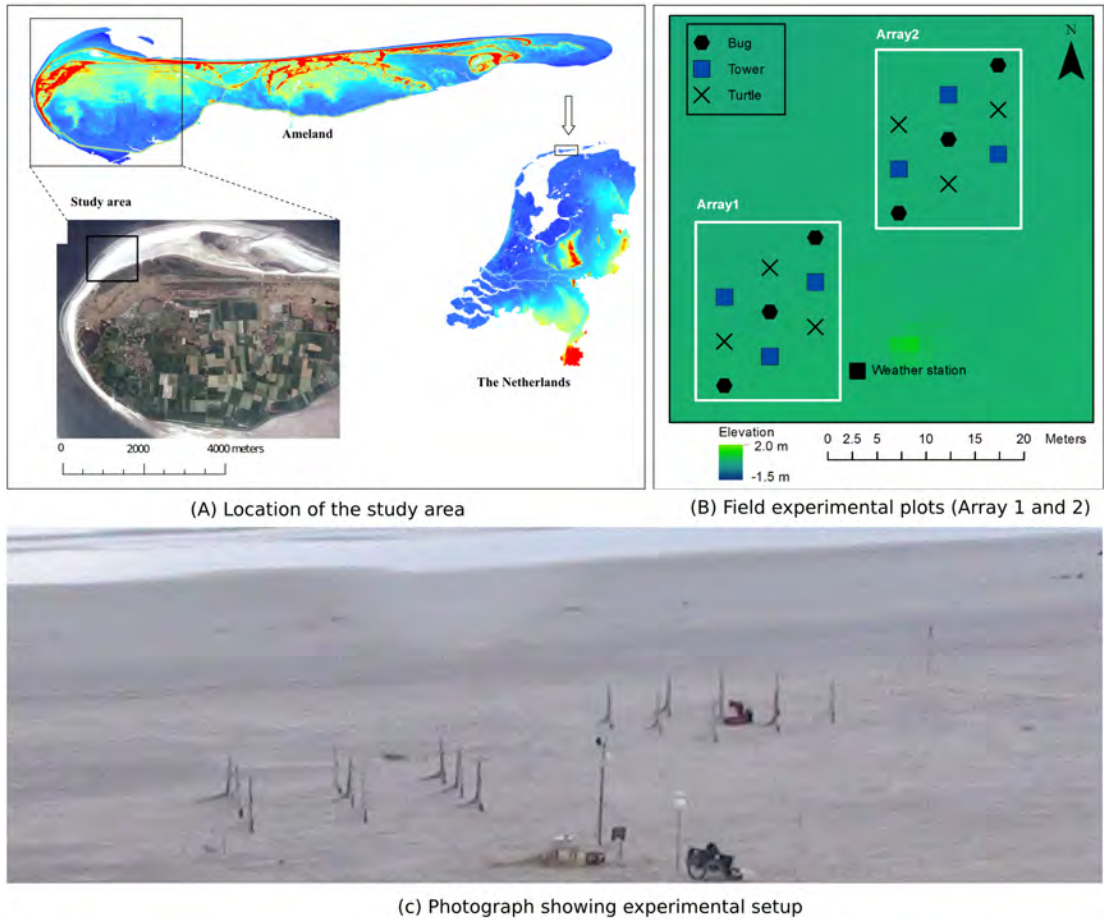


FIGURE 6.1: (a): Location of study area in northern Netherlands, on the island of Ameland and in the aerial photo of the western portion of Ameland. (b): Field experimental setup with specific equipment configuration. (c): Experimental plot at a location along the beach

6.2.3.1 Measurement of sediment flux

Sediment flux was measured using the Modified Wilson and Cook sediment catchers (MWAC). These catchers are designed and used for capturing sediment ranging from dust to sand. This instrument has been extensively tested in numerous studies [e.g. Goossens et al., 2000, Poortinga et al., 2013a, Sterk and Raats, 1996, Van Pelt et al., 2009, Youssef et al., 2008], where efficiencies between 42% and 120% were reported. The original design [Wilson and Cooke, 1980a] contained six plastic bottles with glass inlets and outlets, placed horizontally at six heights between 0.15 and 1.52 m. These bottles were mounted on a rotating pole with a wind vane. Later studies [e.g. Sterk and Raats,

1996] used the same principle, but placed the bottles vertically instead of horizontally (Fig. 6.2(a)). Under beach conditions, aeolian sediment transport is governed by saltation, which seldom reaches heights above 15-20 cm. A traditional MWAC sediment catcher would therefore only capture sediment in the lower two or three bottles. This generates significant uncertainty in the analysis, as sediment flux is calculated based solely upon the fitting of an exponential curve through only two or three data points. Therefore, three different designs based upon the traditional MWAC were introduced (Fig. 6.2(b-d)), but with all bottles mounted below 25 cm. The first design, nicknamed the "Bug" (Fig. 6.2(b)), consists of two stacks of three bottles opposite each other, with their inlets at the same height. The bottles are fixed to a wooden plate with an iron thread to ensure the vertical distance between the two inlets is 5 cm. This design allows for the collection of more measurement points in case of any small horizontal variations in sediment flux, thereby reducing any uncertainty in flux calculations. The second design "Turtle" (Fig. 6.2(c)) consists of two bottles on each side, located at various heights. In this design, the bottles are fixed in the original clips, resulting in a larger vertical spacing of 8 cm. In both designs, the horizontal distance between the inlets is 22 cm. The "Tower" design (Fig. 6.2(d)) represents the more traditional setup with three or four bottles stacked above each other. The vertical spacing between the bottles is 5 cm, as the bottles are fixed to a wooden plate with iron thread instead of the conventional clips.

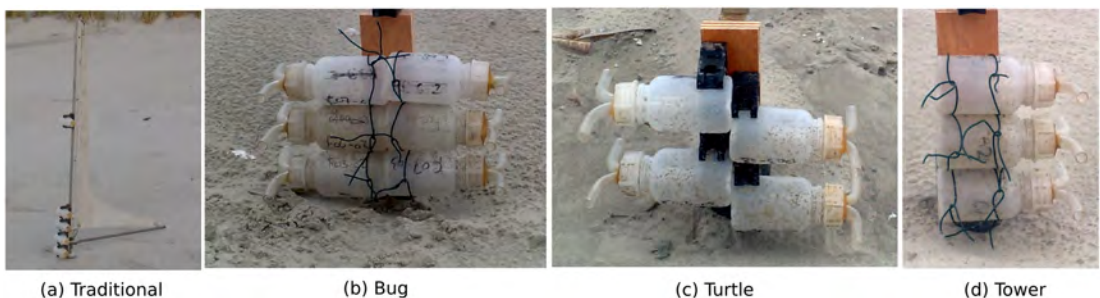


FIGURE 6.2: The traditional MWAC design with the 3 new modified designs. The traditional design (a) consists of 5 bottles distributed over 1 m. The "Bug" design (b) consists of a total of 6 bottles (3 on each side), the "Turtle" design (c) consists of 4 bottles (2 on each side) in the original clips, while the "Tower" design (d) consists of 3 bottles mounted above each other. Each bottle measures 10 cm high with a diameter of 4.5 cm.

To evaluate the differences between the three new designs, they were placed in a 3 x 3 grid and separated by a distance of 3 m. After the first event, an additional array of MWAC's was installed 8 m from the first array in order to obtain more measurements (Fig. 6.1(b)). To ensure careful monitoring of the experiment, this second array was only installed when environmental conditions were favourable. Each array contained three catchers of each type. They were placed in a relatively flat and homogeneous part of the beach to ensure that the measured sediment flux was uniformly distributed. The elevation of the bottles relative to ground level was measured to an accuracy of 1 mm. In order to account for changes in base elevation due to ripples, this was done after installation and before removal of the bottles.

6.2.3.2 Weather data

A meteorological station with four anemometers was arranged as a vertical array on a tower, which included a wind vane, tipping bucket and two saltiphones [Span and van den Abeele, 1991], installed on the beach in the middle of the study area (Fig. 6.1(b)), recording every minute to a CR10 Campbell datalogger (Table 6.1) throughout the period of investigation. The on-site meteorological station contained 3 anemometers, measuring wind speed (ms^{-1}) at elevations of 0.54, 1.15 and 1.76 m. Pulses from the anemometer were averaged over the recording period and registered as average wind velocities per minute. Wind direction was measured using the wind vane at a height of 2.5 m, while the tipping bucket recorded rainfall to an accuracy of 0.2 mm.

TABLE 6.1: Type, number and temporal resolution of instruments used during the field experiment on Ameland. The spatial distribution is shown in Figure 6.1(b).

Instrument	Number	Use	Temporal resolution
Anemometers	3	wind velocity profile	1 minute
Windvane	1	wind direction	1 minute
Tipping bucket	1	amount of rainfall	1 minute
Saltiphones	2	transport intensity	1 minute
MWAC's	18	sediment flux	event

In order to capture the temporal variability in transport intensity, two saltiphones were placed close to the surface at different locations in the experimental area (Fig. 6.1(b)). The saltiphones were also connected to a CR10 datalogger with a digital pulse output signal. For every second, the cumulative number of hits for that second were recorded.

6.2.4 Data analysis

6.2.4.1 Vertical distribution of aeolian mass flux

When using passive sediment traps, sediment is trapped in different compartments that are located at different elevations above the surface. Sediment from each compartment was weighed and then plotted against elevation from which a non-linear regression was calculated to estimate total sediment transport. Despite various thoughts on whether to use an exponential, power of five parameter regression curve, the recent literature [Ellis et al., 2009a] suggests that an exponential decay function (equation 6.1) is most appropriate to describe aeolian sediment transport.

$$q_z = q_0 e^{-\beta z} \quad (6.1)$$

Curve fitting using equation 6.1 enables us to determine the coefficients q_0 and β , also referred to as the portion of creep (q_0) and decay (β), where z (m) represents the elevation and q_z (kgm^{-2}) the amount of sediment at elevation z . Regression coefficients q_0 and β can subsequently be used to calculate the total amount of sediment transport Q (kgm^{-1}). This is done by the integral of equation 6.1 over the height of the saltation layer (taken as 1 m). Sediment fluxes were expressed in kgm^{-1} rather than $kgm^{-1}s^{-1}$, as transport was highly intermittent during some events.

The cumulative transport function (CTF) of an aeolian mass flux (q_c) can be described by equation 6.2, using coefficient β from equation 6.1. Figure 6.3 illustrates the relative sediment flux (black line) and the CTF (green line). When studying the characteristics of aeolian sediment flux, the CTF is preferred to the relative sediment

flux, as this function is independent of the number of measurement points. Moreover, only coefficient β is used in the calculation, and therefore, the shape of the CTF is determined by the specific mass distribution between the different compartments and not by their elevation above the ground.

$$q_c = 1 - e^{-\beta z} \tag{6.2}$$

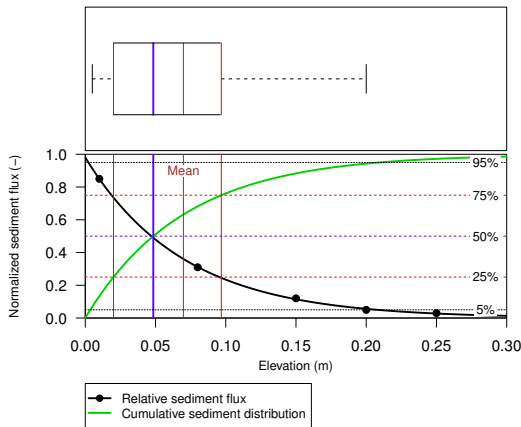


FIGURE 6.3: The vertical distribution of relative aeolian sediment flux (points), the non-linear regression (equation 6.1) fitted through the data-points and the cumulative sediment distribution calculated from regression coefficient β . The median (blue, equation 6.4), mean (brown, equation 6.3), upper and lower quartile (red, equation 6.5 and 6.6) are also shown as a boxplot.

Coefficient β (equation 6.1) can also be used to determine the mean (equation 6.3), median (equation 6.4), and lower (equation 6.5) and upper quartile (equation 6.6). Figure 6.3 shows the distribution function as a box-plot (top) and also for the relative sediment flux and CTF (bottom). The difference between the mean (brown line) and median (blue line) is the mean is calculated by the integral and the median by the point where the integral is 0.5. The median splits the CTF into two equal parts, whereas the mean describes the point where the CTF would balance. As the median is less sensitive to outliers compared to the mean, we make use of the median.

$$\bar{q}_z = \frac{1}{\beta} \tag{6.3}$$

$$q_{z_{50}} = \frac{\ln(2)}{\beta} \tag{6.4}$$

$$q_{z_{25}} = \frac{\ln(\frac{4}{3})}{\beta} \tag{6.5}$$

$$q_{z_{75}} = \frac{\ln(4)}{\beta} \tag{6.6}$$

Dong et al. [2003] performed a series of wind tunnel experiments to investigate the flux profile of wind-blown sand. They determined the cumulative mass distribution from the measured data. Moreover, they used the equation $q_z = q_0 e^{-b/z}$, where the regression coefficient β (here given as b) is divided by elevation (equation 6.1). Regression parameter β (as in equation 6.1) can be calculated by $\beta = 1/b$. The $q_{z_{50}}$ for the different sediment size fractions and wind velocities, using β , is shown in Figure 6.4.

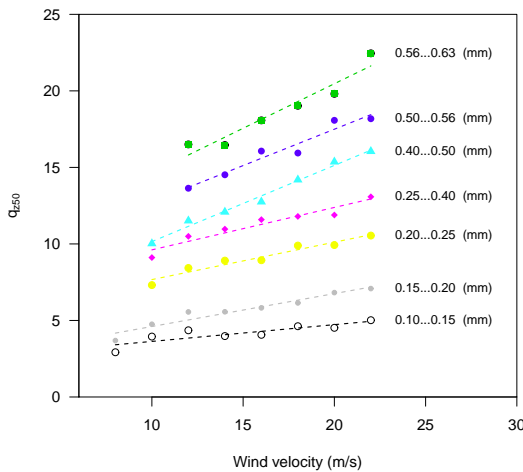


FIGURE 6.4: The $q_{z_{50}}$ for different sediment fractions and wind velocities. Data were recalculated from Dong et al. [2003].

Figure 6.4 shows the variation in $q_{z_{50}}$ for the various sediment size fractions over a range of wind speeds, especially where coarser sediments are transported at higher elevations, with $q_{z_{50}}$ increasing with wind velocity.

6.2.4.2 Uncertainties in estimation of aeolian mass flux

Ellis et al. [2009a] identified three common methodological inconsistencies and thus sources of uncertainty in measuring aeolian sediment transport using passive traps. These include: (1) inconsistent representation of sediment trap elevations; (2) erroneous or sub-optimal regression analysis; and (3) inadequate or ambiguous bed elevation measurements.

In addition, the number of trapping compartments and location of the lowest sediment trap are also important considerations. Results from Dong and Qian [2007] (Table 1) were used to illustrate how base elevation and number of traps affects sediment flux estimation. They made use of a WITSEG sampler [Dong et al., 2004b], which is a vertically integrated wedge-shaped trap with 60 different compartments, where the lowest orifice can be aligned with the surface. The high data density of the WITSEG is advantageous when interested in a detailed description of the vertical mass distribution,

Dong and Qian [2007] determined the relative sediment flux (using equation 6.7), where the relative sediment flux (qr_z) at height (z) is calculated by dividing the measured sediment flux (qz) by the total amount of sediment (Q) collected within all compartments. The dimensionless relative height (Zr) was calculated by dividing the actual height (z) by the maximum height (Z ; 0.6 m in their study). After fitting a non-linear regression (equation 6.1) through the relative sediment flux data, they found a linear correlation between the regression coefficients q_0 (portion of creep) and β (decay function).

$$qr_z = \frac{qz}{Q}, Zr = \frac{z}{Z} \quad (6.7)$$

Figure 6.5 displays the dimensionless regression coefficients q_0 and β . Using elevation data of the different compartments, we calculated the relative regression coefficient q_0 for a sequence of β 's, while changing the elevation from the base (lines with different colors), but using the same distribution of compartments. Measurements using the WITSEG were taken between 0-1 cm, which is in agreement with the experiments.

Here, it is important to note the difference in shape between the different base elevation lines. When measurements are taken close to the surface, the correlation between q_0 and β is almost linear, for the domain under consideration. However, when moving further away from the surface, the relationship becomes log-linear (Fig. 6.5), which has major implications in terms of generating uncertainty in the estimation of q_0 . Where measurements are taken further away from the surface, a small error in the calculation of β has even greater impacts upon estimating q_0 compared to measurements taken closer to the surface. An under- or overestimation in the q_0 regression parameter can have a significant effect on determining the total mass flux.

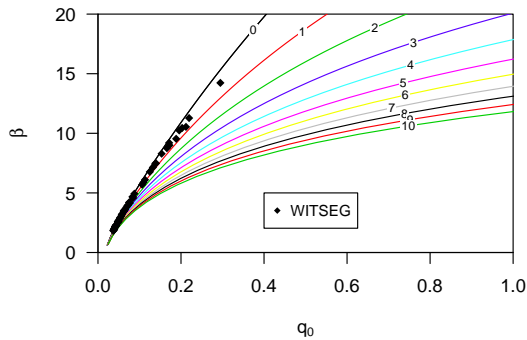


FIGURE 6.5: The regression coefficients q_0 and β calculated from the relative sediment flux (equation 6.7) for the WITSEG (data from Dong and Qian [2007]; Table 1). The coloured lines represent the relation between the q_0 and β for different base elevations (shown on the plotted line in cm).

The vertical cumulative mass distribution of the aeolian mass flux was investigated for each of the previous studies as well as for the newly collected dataset. The spatial variability for $q_{z_{50}}$ and Q was also investigated for this newly acquired dataset. Due to the relative limited number of datapoints and the desire to maintain the original values in the interpolated maps, we used a simple inverse-distance weighting algorithm, with a minimum of three and a maximum of eight neighbours for spatial interpolation.

6.3 Results and Discussion

6.3.1 Wind tunnel data

The wind tunnel study of [Poortinga et al. \[2013a\]](#) was used to investigate the CTF of an aeolian saltation cloud (data available in [Poortinga et al. \[2013b\]](#)). Sediment loss was measured in three different ways using passive sediment catchers, saltiphones and a balance. The normalized sediment flux and CTF, calculated from four saltiphones at various heights above the surface (the highest at 25 cm), are presented in [Figure 6.6](#). The BEST, MWAC new and MWAC old represent the three different types of catchers used in the experimental runs. The fit between the non-linear regression line and calculated sediment flux had an average $r^2 = 0.99$, with a minimum $r^2 = 0.96$. The data was divided into high wind velocities ([Fig. 6.6\(a,c,e\)](#)) and low wind velocities ([Fig. 6.6\(b,d,f\)](#)), where the s50, s60 and s80 represent different sediment sizes with a d_{50} of 285, 230 and 170 μm , respectively. At higher wind velocities, more sediment is transported closer to the surface for the s50 and s60 sediment with a $q_{z_{50}^-}$ of 6.71 and 7.94 cm (s50) and 5.17 and 5.61 (s60) for the high and low wind velocities, respectively. In contrast, the s80 (fine) sediment, $q_{z_{50}^-}$ of 3.68 and 2.84 cm was measured for high and low wind speeds, respectively. The s80 (finer) sediment is transported more readily closer to the surface than coarser sediment fractions (s50 and s60), which is in agreement with the literature [[Dong et al., 2003](#), [Dong and Qian, 2007](#), [Farrell et al., 2012](#)].

Saltiphones were also used to rapidly acquire aeolian sediment flux data to enable a detailed investigation of the vertical sediment dynamics. Non-linear regression (equation [6.1](#)) was applied to the data points, and for all fluxes and data with $R^2 > 0.98$, the β was used to calculate $q_{z_{50}}$ (equation [6.4](#)). In [Figure 6.7](#), $q_{z_{50}}$ is plotted against shear velocity for experiments under high ([Fig. 6.7\(a,c,e\)](#)) and low wind velocities ([Fig. 6.7\(b,d,f\)](#)). As shown in [Figure 6.6](#), finer sediment has a lower $q_{z_{50}}$ compared to coarser sediment. Despite considerable scatter, the median $q_{z_{50}}$ values increase with increasing shear velocities. In the region between the impact (vertical black dotted line: [Fig. 6.7](#))

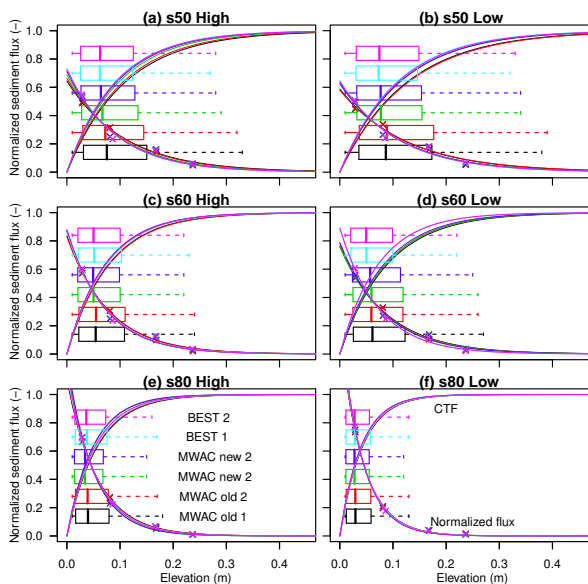


FIGURE 6.6: The relative sediment flux (equation 6.7) and CTF (equation 6.2) for three different types of sediment (s50, s60 and s80, with d_{50} 285, 230 and 170 μm , respectively), three different sediment catchers (MWAC old, MWAC new and BEST) and exposed to high (a, c, e) and low (b, d, f) wind velocities. The box plots indicate the median, upper and lower quantile.

and fluid thresholds (green dotted line), the scatter is considerable. This scatter (indicated with an alpha color), represents measurements with low sediment flux which is more pronounced in low wind velocities. A linear regression curve was calculated for the high and low wind shear velocities (straight line). While there is some correlation between shear velocity and $q_{z_{50}}$ under high shear velocities (see R^2 of the linear regression in 6.7, the R^2 under low wind velocities is rather low. All plots show a positive correlation between shear velocity and median $q_{z_{50}}$.

In the wind tunnel experiment, use was made of three different type of sand catchers: the MWAC old, MWAC new and BEST (cf. Poortinga et al. [2013a]). The findings in Figure 6.7 were used to validate the results of these sediment catchers: $q_{z_{50}}$ of the measured sediment flux was calculated for each experiment; and, $q_{z_{50}}$ based on the mean shear velocity during the experiment, was calculated using data from Figure 6.7. Figure 6.8(a-c) shows $q_{z_{50}}$ based on the values of the sediment catchers (before) and the

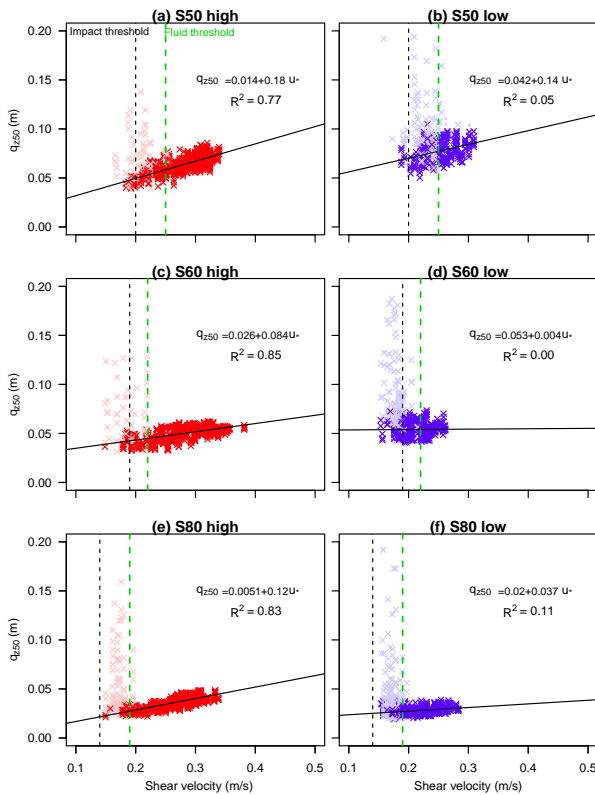


FIGURE 6.7: The shear velocity versus the q_{z50} for three different types of sediment sizes (s50, s60 and s80) under high (a, c, e) and low wind velocities (b, d, e).

values calculated from the saltiphones data (after). Differences between the two values increase from coarse to finer sediment. For measurements using BEST, the differences are generally larger than the other catchers (Fig. 6.8).

To test whether q_{z50} calculated from the saltiphones (Fig. 6.8: a-c) provides a better approximation of total sediment flux, q_{z50} was used as a reference point to reposition the base elevation; with the difference between the sediment catcher guiding the repositioning of the traps. The sediment flux was recalculated using this new base elevation. New sediment fluxes were then compared with sediment loss measured by a balance. Figure 6.8 (d-f) shows the efficiency of the initial sediment flux estimation (red) and the newly calculated sediment flux (green), where 100% is an exact match with the balance.

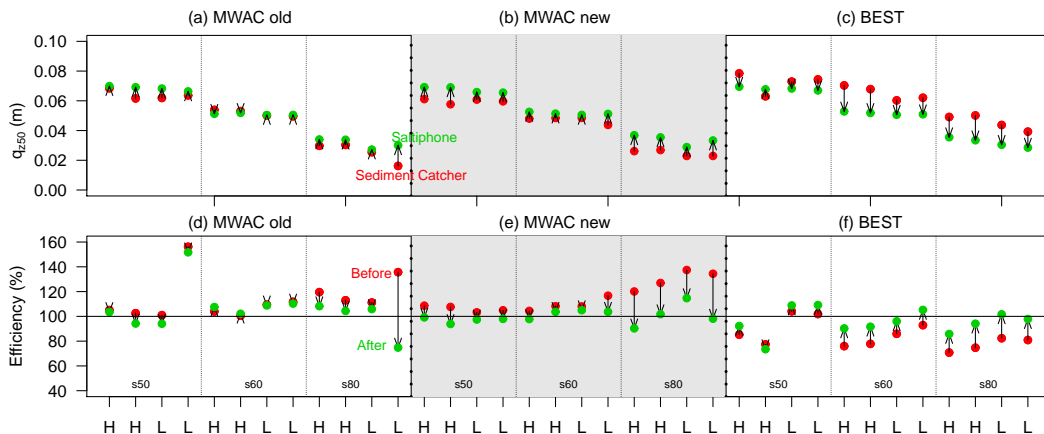


FIGURE 6.8: The q_{z50} from saltiphones (green) compared with q_{z50} from the sediment catchers (red) (a-c) and the recalculated efficiency (d-f) using the q_{z50} as a reference. Data is shown for three different sediment catchers (MWAC old, MWAC new and BEST), three different types of sediment (s50, s60 and s80) under high (H) and low (L) wind velocities. During the experiment, the sediment catcher and saltiphones were located next to each other. The arrows (a-c) indicate the shift in q_{z50} used to calculate the new base elevation. The arrows (d-f) indicate the change in efficiency.

Some 29 of the 36 measurements were shown to indicate an improvement (Fig. 6.8). In general, improvements are considerable, and a decrease in efficiency is minimal. For finer sediment, improvements were even higher when compared to coarser sediment.

The relative sediment flux of the saltiphones and sediment catchers were used to determine q_0 and β (Fig. 6.9). When the lowest saltiphones were located at 3 cm, we found a strong linear relationship between q_0 and β . Finer sediment had a larger range of regression coefficients, with higher values for β given that a higher proportion of sediment is transported closer to the surface. The intercept of the linear regression increases with coarser sediment, whereas the slope of the regression decreases. The difference between the intercept and slope of the s50 and s60 sediment is small. For passive sediment catchers, there is good agreement between the calculated base elevation and the experimental results (Fig. 6.9). The BEST catcher was located 1.5 cm from the surface, whereas the lowest trap of the MWAC catchers was located between 4 and 5 cm. Mean measurement error was 1.3 mm with a maximum of 2.4 mm.

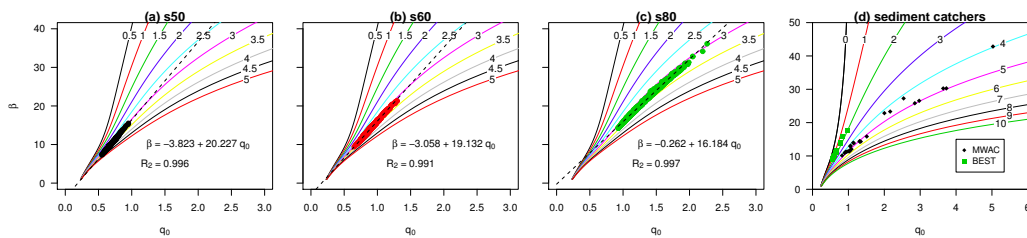


FIGURE 6.9: The q_0 and β , calculated from the relative sediment flux (equation 6.7) for different sediment sizes (s50, s60, s80) using saltiphones data (graph a-c), and for all measurements using passive sediment traps (graph d). The lines represent different base elevations.

The disagreement in vertical flux distribution between the saltiphones and sediment catchers, and also between sediment loss measured by the balance and the calculated flux from the sediment catchers, is mainly caused by the specific configuration of the sediment catcher. For instance, when applying an exponential regression function, the elevation, orientation and measurement accuracy of the lowest bottle largely determines the result as finer sediment is more susceptible to errors compared to coarser sediment. Figure 6.10 presents the experimental outputs when using the MWAC and BEST catchers with s80 (fine) sediment, highlighting the measured relative sediment fluxes (black dots), including the exponential regression (equation 6.1) and a linear regression. The BEST catcher contains one data-point below the $q_{z_{50}}$ while the MWAC has none. The influence of the lowest data-point is significant, as it determines the intersection with the y-axis and thus the total sediment flux. As for fine sediment, errors will be more pronounced as a larger portion of the mass is transported close to the surface, there are small inconsistencies in the orientation of the catcher, and thus measurement issues occur with the elevation or difference in efficiency under different mass flux density. Applying a linear function to the points close to the surface, and a power function for the higher located points (cf. Poortinga et al. [2013a]), will therefore give more coherent results, as the effect of the lowest point on the total mass flux is reduced. Moreover, Ni et al. [2003] showed that saltating grains follow an exponential decay function, whereas creeping and reptating grains deviate from it. The mathematical description might therefore also be

a source of uncertainty.

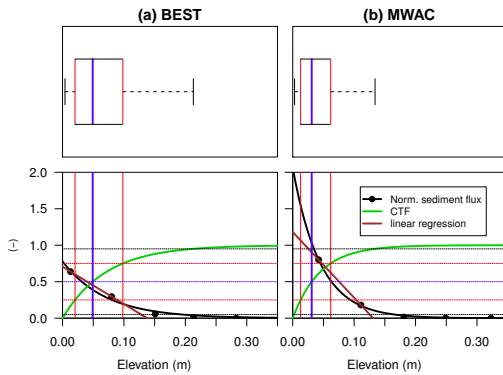


FIGURE 6.10: The vertical distribution of the relative aeolian sediment flux for the BEST and MWAC sediment catchers. The dots identify individual measurements for the s80 sediment size, while the non-linear regression curve is shown in black and the CTF in green. Furthermore, a linear function was plotted through the two points located closest to the surface (brown). The $q_{z_{50}}$ (blue: equation 6.4), \bar{q} (brown: equation 6.3), upper and lower quantile (red: equation 6.5 and 6.6) are also shown as a boxplot.

6.3.2 Field data

Where wind tunnel studies are limited in the replication of complex turbulent wind structures as seen in the field, field studies do not have the advantage of a controlled environment where specific parameters can be fixed. Surface moisture and bedform development, for instance, are known as important limiting factors in sediment transport, and can negatively affect measurements. Data from Farrell et al. [2012] were used in a re-analysis because their short-lived experiments contained several data points close to the surface. For the sub-environment Cow Splat Flat Fine (CSFF), $q_{z_{50}}$ were arranged according to date (Fig. 6.11(a)) and q_0 and β were calculated for the relative flux (Fig. 6.11(b)). For this sub-environment, the calculated elevation from the surface strongly agreed with the measured values. The variation in $q_{z_{50}}$ was best explained when arranging them according to measurement date; where no relation was found with shear velocity (ranging from 0.45 - 0.54 ms^{-1}) or grain size. A logical explanation would be the effects of surface characteristics such as surface moisture and incipient bedform

development. However, this is far from conclusive, as it was also found that $q_{z_{50}}$ increased with decreasing R^2 (ranging from 0.968 - 0.999). The same study also took three measurements at the beach sub-environment over two consecutive days. These measurements received specific attention, as they were taken at a wet and immobile foreshore without visible bedform deformation. We found $q_{z_{50}}$ values of 3,7, 4.5 and 3.1 cm with R^2 of 0.966, 0.890 and 0.997, respectively. As this dataset only contains three data-points with varying R^2 , it is difficult to draw conclusions based on $q_{z_{50}}$ or measured base elevation.

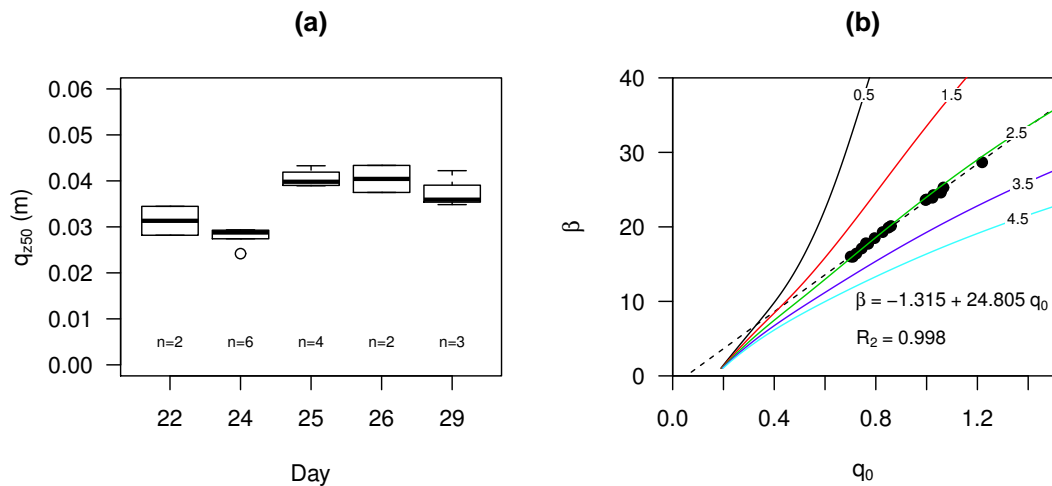


FIGURE 6.11: The $q_{z_{50}}$ for experiments performed (at the sub-environment Cow Splat Flat Fine (CSFF)) on different days (a) and the q_0 and β for all events combined (b). Coloured lines represent different base elevation. Data was obtained from [Farrell et al. \[2012\]](#).

[Visser et al. \[2004b\]](#) conducted experiments on three different geomorphic units: degraded, valley and dune. Besides sand, the soils in this area also contained considerable quantities of silt: 19.4, 15.9 and 13.0% and clay 21.6, 5.1 and 3% for the degraded, valley and dune site, respectively. The study obtained results for 11 different events in the year 2001, with 17 MWAC catchers installed at each site. In order to remove uncertainty from the data while maintaining an acceptable number of data points, measurements with $R^2 < 0.95$ were removed from the dataset. This differs from previous studies, where an $R^2 < 0.98$ was used as measurements were taken over longer periods.

Furthermore, when comparing the different units (Fig. 6.12(a,c,e)), it was found that $q_{z_{50}}$ is highest for the degraded site, followed by the valley and dune site. The degraded and valley site have higher fractions of silt and clay, which are transported over higher elevations. However, surface crusts might also cause saltating particles to reach higher elevations. The variation in $q_{z_{50}}$ within an event is generally low for the degraded and valley site, but slightly higher for the degraded site. The variation between events is also small, except for the events on 10 and 13 July (Fig. 6.12). Here the values for $q_{z_{50}}$ are high and have a large variation. During these events, large amounts of dust were transported through the study area. No clear relation was found between $q_{z_{50}}$ and wind velocity.

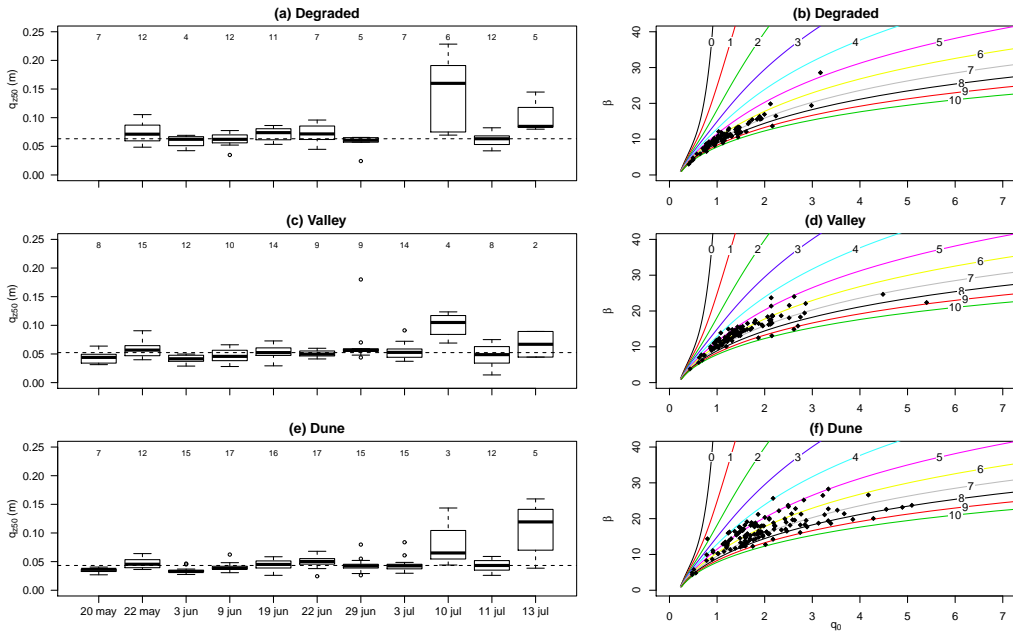


FIGURE 6.12: The $q_{z_{50}}$ for 12 events in three different geomorphic units (a,c,e) and the relation between q_0 and β (b,d,f), where the lines represent different base elevations. Data was obtained from Visser et al. [2004b]. Numbers indicate the number of measurements included.

Figure 6.12(b,d,f) shows q_0 and β , calculated from the relative sediment flux. As

surface elevation varied for the different measurements, the points are plotted on different curves. Due to a lower decay rate (coefficient β) at the degraded site, points are still closely related. However, at the dune site, sediment is transported closer to the surface, resulting in higher decay rates. As the lines spread with higher decay rates, there is higher spread in points. Compared to the degraded site, there is larger uncertainty in q_0 for the dune site, as small errors in β will result in larger errors in q_0 (Fig. 6.12).

Figure 6.13 displays the uncertainty in q_0 for one event (May 22) at the dune site. Here, the measured elevation is shown in red; where elevation is based on the relative q_0 and β , shown in green. For this event, all calculated elevations are lower compared to the measured. This indicates that there is a likely error in the measured base elevation, leading to an overestimation of q_0 . As expected, errors in q_0 are largest for the dune site, followed by the valley and degraded site. However, the larger error in q_0 does not directly correspond to a larger error in base elevation. Elevation here was estimated using $z = \ln(q_z/q_0)/\beta$ (equation 6.1), with the higher decay rates at the dune site having a more pronounced effect on equation 1 than the larger range of q_0 . For flux estimation, on the other hand, small changes in elevation have a much larger impact, as a greater portion of transport takes place close to the surface.

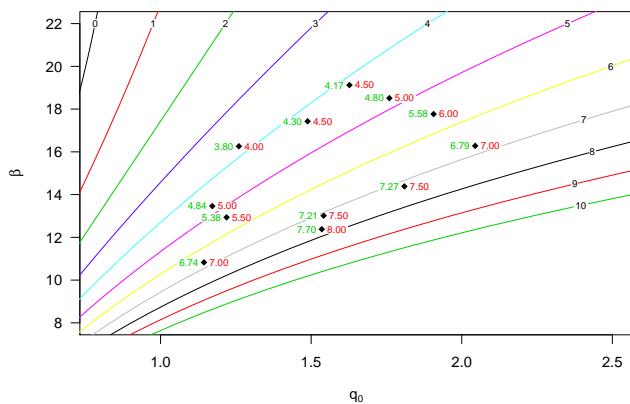


FIGURE 6.13: The q_0 and β calculated from the relative sediment flux for the Dune (May 22) site. The lines represent different base elevations. The red numbers are the measured elevations whereas green values are the calculated elevations based on relative q_0 and β .

The field experiment

New data were collected for six different events (Fig. 6.14). The duration of the experiments varied from a few hours to two days, whereas saltation was measured for several hours. The averaged shear velocity during these saltation periods varied between 0.30 ms^{-1} for event 1 and 0.41 ms^{-1} for event 3. Wind directions predominantly came from the E-NE while only event 3 had variable wind conditions (Fig. 6.14). During events 2, 3 and 4, rainfall was recorded. Saltiphone data were also included as an indication of the degree of saltation activity.

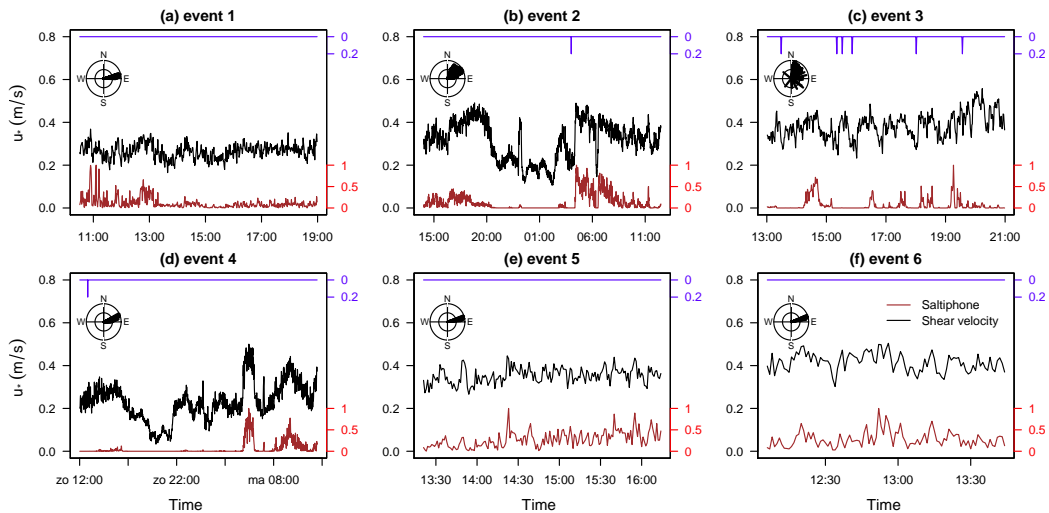


FIGURE 6.14: Shear velocity, wind direction, rainfall and normalized saltation activity for six events. The normalized saltation activity was determined using the total count of the saltiphones, divided by the maximum count during the event.

Of the three catchers (Turtle, Bug and Tower) used in the experiments, two of them contained compartments on both sides of the catchers. The impact of this horizontal variation on sediment flux was investigated by evaluating R^2 as a non-linear regression (equation 6.1) was applied to all measurements with at least four data-points. For the bug sampler, a non-linear regression which was applied to both sides of the catcher, where the middle bottle of the opposite side was included. The results (Fig. 6.15(a)) show that the Tower has the best correlation, followed by the Turtle. The Bug has

the poorest performance but contains more measurements. Disturbance of the airflow might have caused the decrease in performance. In general, most measurements have a very high correlation, indicating only minor impacts of horizontal variability. However, to exclude the effect of horizontal variability and other sources of uncertainty, only measurements with an $R^2 > 0.98$ were included for further analysis.

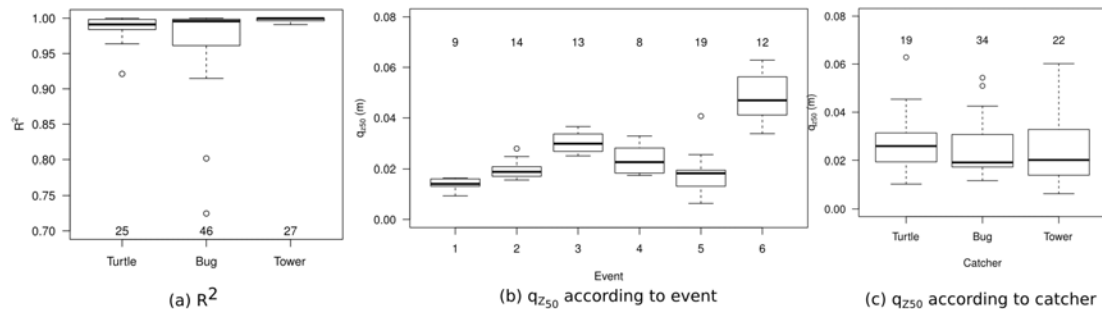


FIGURE 6.15: (a) The R^2 for the three sediment catchers, (b) the q_{z50} for every event (middle) and (c) the q_{z50} according to catcher. Numbers indicate the number of measurements included.

The q_{z50} values are shown in Figure 6.15(b). Values for event 6 are higher compared to other events, which is most likely caused by the frozen surface. During events experiencing rainfall, sediment was generally transported over higher elevations. However, the configuration of the traps on the catcher were also found to have an impact. Figure 6.15(c) shows that the the Turtle design gives generally higher values for q_{z50} compared to the other two designs. This is caused by point density being close to the surface. For the Bug and Tower designs, regression coefficient β is based on one point close to the surface, whereas the Turtle has two data points. The range in q_{z50} is larger for the Tower compared to the Bug, as the Bug has two data points at approximately the same elevation, with the measurement being refuted when these points do not match. Measured base elevation was in good agreement with the calculated base elevation, with an average difference of 0.7 mm and a maximum of 5 mm; with the Turtle displaying the largest variation, followed by the Bug and the Tower.

An Inverse Distance Weighting (IDW) algorithm was used to investigate the spatial variability of q_{z50} and Q (Fig. 6.16). We selected events 2, 3, 5 and 6, as during these

experiments, two arrays of catchers were used. For all events, the lower-located array has lower values for $q_{z_{50}}$ compared to the higher array. Based on our observations, we can confirm that the surface of the upper array was generally wetter than the lower array. This is in line with other findings by [Nield and Wiggs \[2011\]](#). [Farrell et al. \[2012\]](#) also found that sediment is transported over higher elevations on wet surfaces. The spatial variability in saltation height (and thus surface characteristics) shows no alignment with the total transported sediment. Furthermore, the large variability in sediment flux between the different events, suggests there is also large variability in total sediment transport within individual events. Peak values are eight times higher than the lowest values within measurement plots. In general, there is good agreement in measured sediment flux between points located close to each other. However, within meters of these measurements we can see major differences in total sediment flux. Besides the limiting effect of surface moisture on aeolian sediment transport [[Cornelis and Gabriels, 2003](#), [Namikas and Sherman, 1996](#), [Neuman, 2003](#)], the variability in sediment flux can be attributed to the presence of aeolian streamers [[Baas, 2008](#), [Baas and Sherman, 2005](#)] and/or fetch length [[Bauer et al., 2009](#), [Davidson-Arnott et al., 2005](#), [Delgado-Fernandez, 2010](#)].

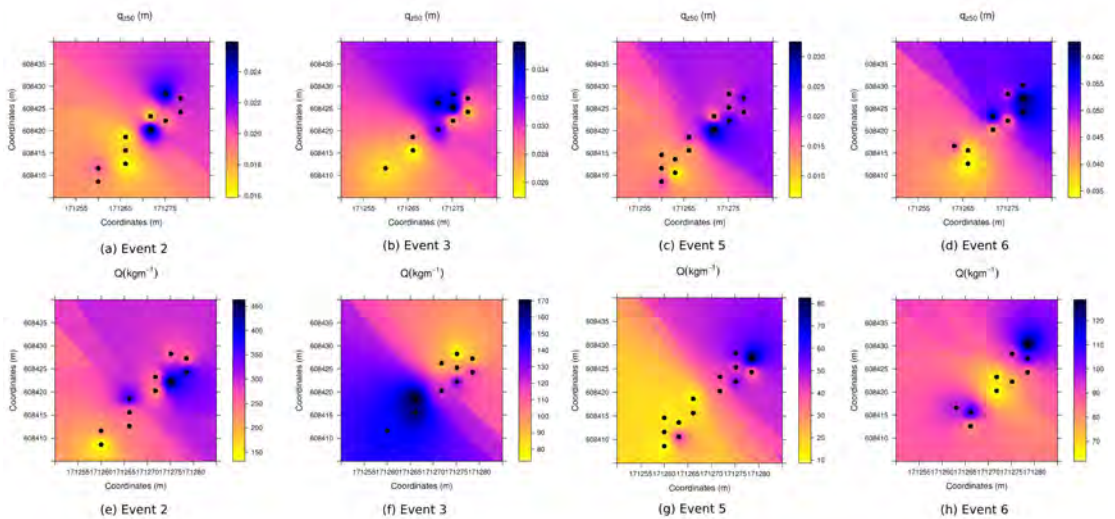


FIGURE 6.16: The spatial distribution of $q_{z_{50}}$ (a-d) and Q (e-h)

Differences in the vertical sediment flux as found in the wind tunnel studies have limited validity for field studies, as surface conditions were found to have an important impact on saltation. Wet, frozen or crusted surfaces increase saltation height, as particles retain a higher proportion of their impact energy [Farrell et al., 2012]. This effect was regarded as localized due to the spatial variability of the surface. Moreover, saltation trajectories were found to have a scattered pattern between impact and fluid threshold. This may impact results from the field, as during some events, transport was highly intermittent due to fluctuations in wind speed [Davidson-Arnott and Bauer, 2009, Stout and Zobeck, 1997]. However, additional rapidly-acquired field data are necessary to study this phenomena in more detail.

6.4 Conclusion and recommendations

Using fast-temporal data on aeolian sediment transport in a wind tunnel, we found that $q_{z_{50}}$ displays a scattered pattern between the impact and fluid threshold, but shows a linear increase with shear velocities above the fluid threshold. Furthermore, it was shown that errors that originate from the distribution of compartments and the location of the lowest sediment trap can be identified using relative sediment flux. In field situations, shear velocity was not found to be the most important controlling factor in vertical sediment flux characterization. Instead, surface moisture was an important control, although particle characteristics of the source area should also be considered. Errors have a more pronounced effect on sediment flux estimation for fine compared to coarse sediment, as fine sediment fractions have a larger portion transported closer to the surface. In order to reduce uncertainty, it is recommended to locate multiple traps closer to the surface.

6.5 Acknowledgments

We would like to acknowledge the following people who have made the completion of this manuscript possible. Pierre Jongerius and Corjan Nolet, thank you for all your

hard work in assisting us with the field data collection. Three anonymous reviewers are also thanked for their invaluable comments.

Chapter 7

Temporal and spatial variability in event scale aeolian transport on Ameland, The Netherlands

A. Poortinga, J.G.S. Keijsers, S.M. Visser, M.J.P.M. Riksen and A.C.W. Baas. (2015)
Temporal and spatial variability in event scale aeolian transport on Ameland, The
Netherlands. *GeoResJ* 5, 23-35.

Temporal and spatial variability in aeolian transport magnitudes on a wide beach

abstract

Coastal dunes are the primary defence protecting the coastline from the destructive forces of the sea in The Netherlands. Aeolian processes are important in this context as they contribute to dune accretion and thus the safety of the coastal hinterland. In this study, we analyse horizontal and vertical variability of event scale aeolian sand transport on a wide beach on the island of Ameland, The Netherlands. Data was obtained from a meteorological station, groundwater monitoring wells and a camera installed on the beach. Fifteen aeolian transport events (two involving onshore winds, seven longshore and six offshore) were measured using a comprehensive grid of 37 customized MWAC traps. The highest sand transport rates and largest variability was found for alongshore events. Surface moisture, governed by groundwater, was found to be an important controlling parameter for aeolian transport rates and vertical flux profiles. Groundwater levels were largely dominated by beach inundation, influencing the groundwater table for a two week period. Variations in vertical flux profiles between traps were larger for wet sand transport events than dry ones. In general, sand transport rates were highest at the foreshore and lowest at the dune toe. Sand transport dynamics are dependent on local conditions such as beach dimensions, beach orientation and also meteorological and surface characteristics. Moderate (high frequency, low magnitude) events are also capable of transporting large amounts of sand. Future studies should include spatially explicit measurements of elevation and surface moisture to obtain a more complete understanding of the complex sand transport dynamics.

7.1 Introduction

Sand dunes are of paramount importance in the Dutch coastal defence system. Besides coastal defence, dunes deliver goods and services such as recreational opportunities, drinking water and nature development. This makes management of the coastal zone complex, as it directly affects the functions of the dune system [Jackson and Nordstrom, 2011, Poortinga et al., 2011]. In The Netherlands, increased levels of coastal erosion due to sea level rise [Keijsers et al., 2014a, Stive, 2004, Zhang et al., 2004] form a direct

threat to the coastal zone and hinterlands, a large part of which is located below sea level.

Since 1990, the Dutch coastline is maintained by sand nourishments [De Jong et al., 2014, Hillen and Roelse, 1995, Van Koningsveld and Mulder, 2004, van der Wal, 2004]. Recently, to mitigate against the effects of coastal recession near Ter Heijde, a large nourishment involving 21.5 Mm^3 was applied to the coast [Mulder and Tonnon, 2010, Stive et al., 2013]. As marine and aeolian forces are expected to redistribute sediment northwards along the 10-20 km stretch of coastline, a single nourishment is thought to be more efficient, economical, and environmentally friendly compared to multiple small-scaled nourishment practices. In order to evaluate and predict the impact of management strategies on coastal dunes, it is important to understand sediment transport dynamics in the sandy beach zone.

However, the dynamics of aeolian sediment transport on beaches are not fully understood because of their complex non-linear character and large variability in space and time [Baas and Sherman, 2006]. Aeolian processes involve temporal scale resolutions ranging from seconds [Anthony et al., 2006, Bauer et al., 1998] to minutes, hours, days [Craig, 2000, Namikas, 2003, Weaver and Wiggs, 2011], months, even years [De Vries et al. [2012], Delgado-Fernandez [2010], Delgado-Fernandez and Davidson-Arnott [2011b], Keijsers et al. [2014b], Kroon and Hoekstra [1990], McLean and Shen [2006]. However, it is difficult to extrapolate event scale measurements to meso-scale dune development, due to the inherent scale problems between small scale process-based studies and larger scale landform development processes [Sherman, 1995].

Aeolian sediment transport has largely been investigated over broad spatial and temporal domains in arid and semi-arid dryland, non-coastal environments, using passive sand traps [Chappell et al., 2003, Visser et al., 2004b]. However, there exists very few studies of aeolian sediment transport within coastal environments [Delgado-Fernandez and Davidson-Arnott, 2011b, Lynch et al., 2013]. Lynch et al. [2013] assessed spatio-temporal patterns of sediment transport and secondary airflow under offshore winds, while Delgado-Fernandez and Davidson-Arnott [2011b] provided the first long-term

record of aeolian sediment transport, based on a combination of qualitative observations from hourly photographs, saltation probes and ED pins. Additional data on the dynamics of aeolian sediment transport over a larger spatial and temporal domains would enhance our understanding of micro and macro scale interactions in two ways. Firstly, continuous records of wind, sediment transport, and supply-limiting factors in beach-dune systems over medium time scales (periods of weeks to months) are lacking, especially in assisting in our understanding of sand transport dynamics. Secondly, there is limited high spatial resolution measurements of beach sand transport.

In this study, we measured aeolian sediment transport events at one of the beaches on the barrier island of Ameland, The Netherlands. In order to acquire high resolution measurements, we deployed a comprehensive grid of sediment traps. The objective of this study was to gain insight into event scale aeolian transport patterns and magnitude over a wide beach. In this study, we monitored, measured and analysed surface moisture, meteorological conditions, wind fetch and aeolian sediment transport for 15 different aeolian events. Variations in the horizontal and vertical distribution of sediment transport were analysed with respect to meteorological and surface moisture data.

7.2 Materials and methods

7.2.1 Study area

Fieldwork was conducted from September to December 2010, on a beach on the barrier island of Ameland, in the northwest of The Netherlands (Fig. 7.1). A sandbar, which was called the Bornrif, migrated towards Ameland and attached to the Western part of the island in the mid 1980s and continues to migrate eastward [Cheung et al., 2007]. This sandbar developed into a curved sand spit (hook) at the coast of west Ameland, with a small tidal lagoon in the middle. The remnants of this hook are still visible in the digital elevation map of Ameland (Fig. 7.1). Longshore drift from west to east has helped shape the sand bar and its shoreline position. Since 1990, the area to the west of the study site has been nourished with approximately $2000 \text{ m}^3\text{m}^{-1}$. The median

grain diameter in the study area was determined as $180\ \mu\text{m}$ [Poortinga et al., 2014]. The semi-diurnal tide has a mean tidal range of about 2.0 m at Ameland [van der Wal, 2000b]. The Ameland beaches are characterized as dissipative, due to the mildly sloping surfzone around $1^\circ\text{-}2^\circ$ [Wright and Short, 1984], with the dominant wind direction from the southwest.

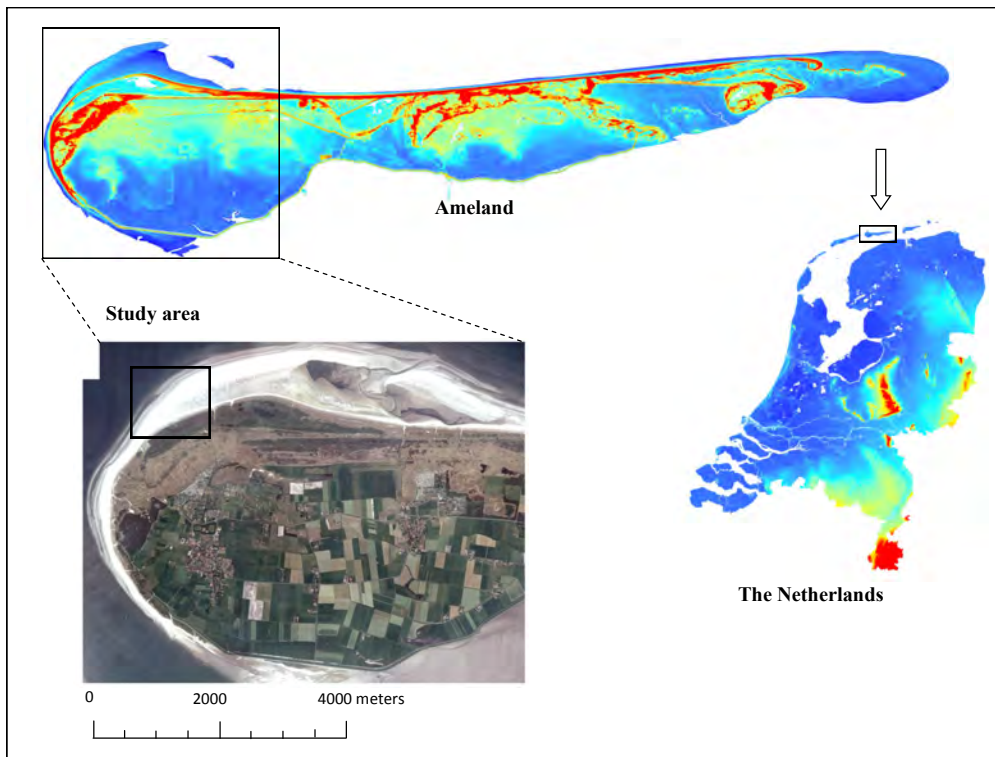


FIGURE 7.1: Aerial photo of the western portion of the island of Ameland with the inset indicating the location of the study area. At the top, the island of Ameland is shown relative to The Netherlands (right image). Image from [Poortinga et al., 2014].

7.2.2 Data collection

In the study area, 37 Modified Wilson And Cook (MWAC) sand traps, six groundwater monitoring wells, a camera and meteorological station were installed (Fig. 7.2). The meteorological station was installed in the middle of the experimental site and consisted of four anemometers, a windvane, tipping bucket and two saltiphones. A CR10 Campbell datalogger was used to record the average data values every minute, except

from the tipping bucket, as this data was summed. Four anemometers measured wind velocity at heights of 0.2, 0.5, 0.8 and 2 m. The windvane was installed on top of the meteorological station at an elevation of 2 m. The tipping bucket measured with an accuracy of 0.2 mm.

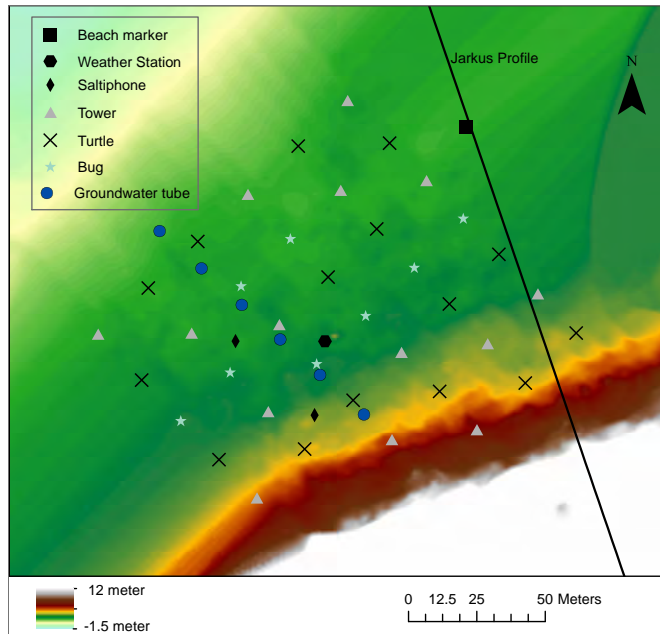


FIGURE 7.2: The spatial distribution of the various instruments used in the field experiment, displayed on a digital elevation map. The Bug, Turtle and Tower represent different new designs of the MWAC (Fig. 7.3).

The sand traps (MWAC) consist of bottles mounted on a pole equipped with a sail to ensure that the inlet was always orientated towards the wind. These MWAC's were installed in a regular grid with six rows (Fig. 7.2). The distance between traps within a row was approximately 20 meters. The distance between the rows was roughly 25 meters. Three different types of configurations were used: 'the Bug', 'the Turtle' and 'the Tower' (Fig. 7.3). Contrary to traditional layouts [Wilson and Cooke, 1980b], a newly customized design was deployed with a higher number of bottles in the lower 25 cm and no bottles above 25 cm. The customized traps were part of a comprehensive set of experiments which included the comparison of trap designs [Poortinga et al., 2014]. The different types of traps were randomly assigned to the sampling locations

in the experimental site. For every bottle, the elevation of its inlet was measured. Every day, the bottles were checked for trapped sediment; an indication of aeolian sediment transport. If sediment was captured in the bottles, the elevation of the inlet was remeasured. Afterwards, bottles were removed and new bottles connected to the trap, with elevation measured once again. The content of the bottles was weighed.

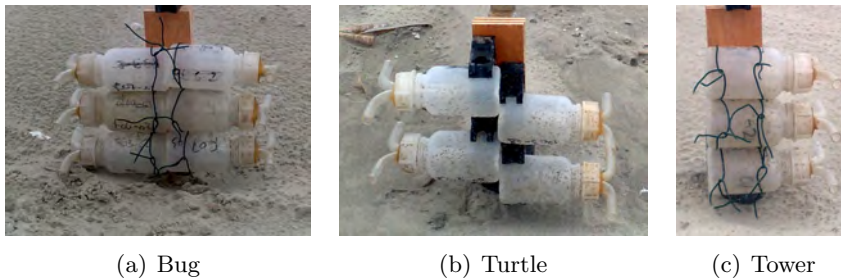


FIGURE 7.3: The three different types of sand trap used in the study. The Bug design (a) has a total of six bottles (three on each side), the Turtle design (b) contains 4 bottles (two on each side) in the original clips, and the Tower design (c) consists of three bottles mounted above each other.

The 5-megapixel time-lapse camera was installed on a pole on top of the foredune. The camera was programmed to acquire an image every five minutes during day light to monitor the study area continuously. For one image, the positions of the MWAC traps were used to create a georeferenced image (Fig. 7.4), and illustrate the coverage of the camera over the study area. Because of the oblique angle of the camera and a slight change in tilt caused by the wind, it was not possible to apply this procedure to all images.

Six groundwater tubes were installed in a perpendicular transect from sea to dune to measure ground water level. The distance between the tubes was approximately 20 meters with groundwater levels recorded daily relative to the Normaal Amsterdams Peil (NAP).

Two saltiphones were used to record saltation intensity [Poortinga et al., 2013a, Spaan and van den Abeele, 1991, Sterk and Spaan, 1997, Youssef et al., 2008] at different locations in the study area (Fig. 7.2). Surface elevation varied due to bedform development, but was generally around 5 cm. The saltiphones were connected to a

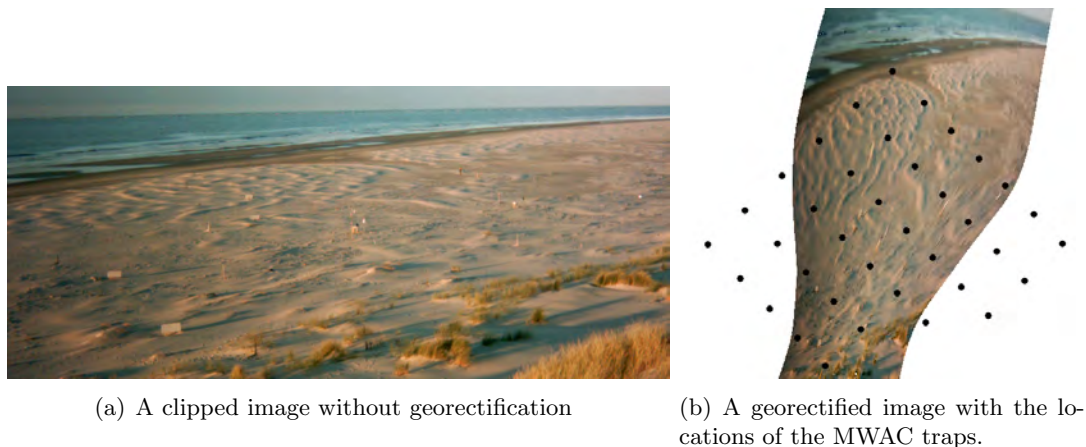


FIGURE 7.4: Image of study area taken by the time-lapse camera which was installed on the foredune.

CR10 datalogger with a digital pulse output signal. Every second, the cumulative number of hits per second were recorded by the datalogger, summed and registered over a one minute period.

Two data repositories were consulted to obtain cross-shore beach elevation profiles and data on sea level, wave height and period. Cross-shore beach profiles were obtained from the JARKUS dataset [Rijkswaterstaat, 2014a]. This dataset contains annual cross-shore elevation profiles of the Dutch coast over the period 1965 to 2012. The 2010 profile of transect 3.8 was used in this study. More information on this dataset can be found in various other studies [e.g. Bochev-Van der Burgh et al., 2011, De Vries et al., 2012, Guillén et al., 1999, Keijsers et al., 2014b, van der Wal, 2004]. Data with a resolution of 10 minutes of sea levels were obtained from Wierumergronden (53.516° , 5.958°), while wave period and wave height data were from Eierlandse Gat (53.276° , 4.661°). Both datasets were obtained from the waterbase [Rijkswaterstaat, 2014b].

7.2.3 Analysis method

7.2.3.1 Wind speed profile and shear velocity

Wind data was used to estimate roughness length and shear velocity using the law of the wall (equation 7.1). Where u_z represents the wind speed at elevation z (m) above

the bed, u_* the shear velocity (ms^{-1}), and k the von Karman's constant (0.4). The roughness length (z_0) (m) is the height at which the time averaged velocity approaches zero.

$$u_z = \frac{u_*}{\kappa} \ln \frac{z}{z_0} \quad (7.1)$$

7.2.3.2 Threshold shear velocity

An empirical approach was used to estimate the threshold shear velocity. Equation 7.2 was used to calculate the threshold for particle movement [Bagnold, 1941]:

$$u_{*t} = A \sqrt{gd \left(\frac{\rho_s - \rho}{\rho} \right)} \quad (7.2)$$

The threshold shear velocity is represented by u_{*t} (ms^{-1}), parameters A , a dimensionless constant assumed to be 0.085 for the fluid threshold and 0.1 for the impact threshold. Gravity is represented by g (ms^{-2}), d is the common grain size (m), ρ_s the density of the sediment (2600 kgm^{-3}) and ρ the density of the air (1.3 kgm^{-3}).

7.2.3.3 Sediment fluxes

The amount of sediment (kg) captured in one bottle was multiplied by the area of the inlet in order to obtain a unit per area (kgm^{-2}). An exponential decay function (equation 7.3) was fitted through the data, where q_z represents the sediment flux (kgm^{-2}), z the elevation (m) and q_0 and β are regression parameters. As the curve rapidly approaches 0 kgm^{-2} , the formula was integrated from 0 to infinity (Eq. 7.4), in order to obtain the total mass flux (Q) per crosswind area (kgm^{-1}). A total of 50 counts from the two saltiphones was used to distinguish between periods with and without saltation.

$$q_z = q_0 e^{-\beta z} \quad (7.3)$$

$$Q_z = \int_0^{\infty} q_z \partial z \quad (7.4)$$

The Turtle and Bug design contain bottles on both sides of the pole (Fig. 7.3), which might lead to uncertainties in the mass flux estimation due to variability in horizontal sediment flux. In order to account for these and other uncertainties, while maintaining an acceptable number of measurement points, only vertical fitting profiles with $R^2 > 0.95$ and three or more bottles, were included in the analysis. For the Bug, the middle bottle from the opposite side was included for equation 7.3, in order to have a total of our measurement points. In situations where the exponential fit for both sides of the Bug were found to be acceptable ($R^2 > 0.95$), the average of the two measurements, which were closely related for most measurements, was taken. A more detailed analysis of the different designs can be found in Poortinga et al. [2014].

Coefficient β (equation 7.3) can also be used to determine the median transport height (q_{z50}). Equation 7.5 was used to calculate q_{z50} (m) for every measurement [Poortinga et al., 2014]. The spatial distribution of q_{z50} and Q was investigated using an inverse-distance weighting algorithm. Sediment fluxes were calculated in unit per time using the actual duration of the measurement. This data was used in the inverse-distance weighting algorithm with a minimum of three and a maximum of eight neighbors.

$$q_{z50} = \frac{\ln(2)}{\beta} \quad (7.5)$$

The total amount of potential transport q (kg^1m^{-1}) [Bagnold, 1941] was computed whenever u_* exceeded u_{*t} using equation 7.6, where C is a dimensionless empirical constant (1.8), D the diameter of a standard sand (0.25 mm), d the mean grain diameter and g (ms^{-2}) the gravitational acceleration.

$$q = C \sqrt{\frac{d}{D}} \frac{\rho}{g} u_*^3 \quad (7.6)$$

The fetch effect is considered to be an important concept in aeolian geomorphology and is defined as the increase in sediment transport rate with distance downwind from a

boundary between an erodible and non-erodible surface to a certain maximum [Delgado-Fernandez and Davidson-Arnott, 2011b]. Together with the angle of wind approach, beach width constrains the maximum fetch length. In turn, beach width is governed by sea level, tide and wave-runup. As such, the effective beach width is dependent on sea level, wave run-up and wind direction. Figure 7.5 shows a cross-shore representation of the study area with the width of the beach strip (w_f), the still water level (swl), the deep water wave height (H_0) and wave period (T_0).

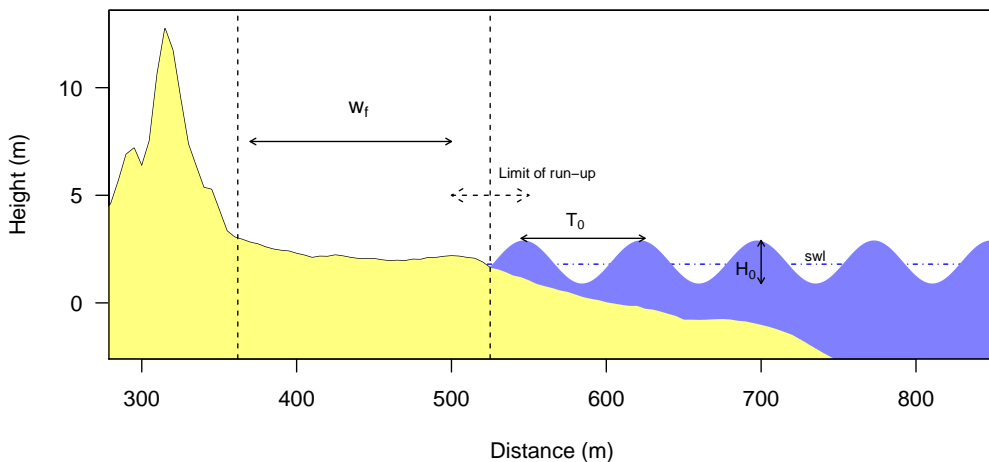


FIGURE 7.5: Cross-shore representation of the study area displaying the width of the beach strip (w_f), still water level (swl), deep water wave-height (H_0) and wave period (T_0). The wave-runup (R_2), derived from equation 7.7 and used to calculate w_f , is indicated by a vertical dotted line with two horizontal arrows.

The relation between runup height and offshore wave conditions for low-slope, dissipative beaches Holman [1986], Stockdon et al. [2006] was used to determine w_f . The runup (R_2), calculated by equation 7.7 was added to the swl . The deep-water wavelength (L_0), defined by equation 7.8, was calculated from T_0 and the acceleration due to gravity (g ; ms^{-2}). The total water level determined the effective beach width, is indicated with a vertical dashed line with two arrows in Fig. 7.9. As an inland border, the 3 m +NAP was taken as the point where the profile slope changes significantly [Bochev-Van der Burgh et al., 2011, van der Wal, 2004]. Given that the angle of wind

approach increases the maximum fetch (F_m ; m) [Bauer and Davidson-Arnott, 2003], the total beach width in the direction of wind approach was then calculated (equation 7.9) from w_f and wind direction perpendicular to the shore (α) [Chepil et al., 1964].

$$R_2 = 0.043(H_0 L_0)^{0.5} \quad (7.7)$$

$$L_0 = \frac{gT_0^2}{2\pi} \quad (7.8)$$

$$F_m = \frac{w_f}{\cos(\alpha)} \quad (7.9)$$

Delgado-Fernandez and Davidson-Arnott [2011b] distinguished transport events from wind events. They defined a wind event as a period of time when wind speeds exceed a pre-defined threshold, whereas a transport event was defined as a wind event in which sand transport on the beach was measured or observed. In this study, we define a transport event as the period between the installation and removal of the bottle, as the trap data represents the aggregated data collected during this period. Thus an event, as defined in this study, can include multiple wind and transport events as per Delgado-Fernandez and Davidson-Arnott [2011b].

7.3 Results

7.3.1 Beach morphology and ground water dynamics

During the field campaign, the study area was inundated by the sea on three occasions. Figure 7.6(a) shows the swl , R_2 , groundwater level and pictures for such an event. Figure 7.6(b) (left) shows the image taken during this high water event. It can be seen that high sea-levels in combination with high wave run-up led to inundation of the beach (Fig. 7.6(b)). Inundation of the beach was short-lived (<1 hour), but had important impacts on beach surface characteristics and groundwater levels.

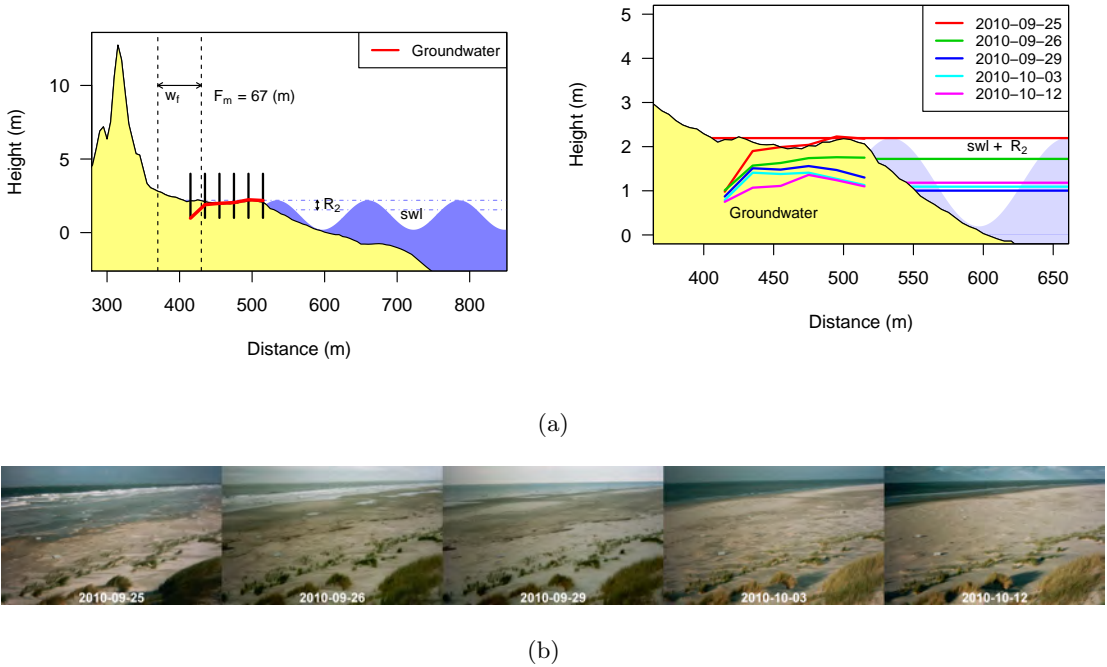


FIGURE 7.6: The effect of beach inundation on the surface characteristics. (a) The swl , R_2 and groundwater level for September 25 (left), when the beach was inundated (see image below). The right image shows the ground water levels for different days in the following days. The combined swl and R_2 is also shown for these days. (b) Images taken with the time-lapse camera (from left to right) for the inundated beach followed by succeeding days where the beach surface dried.

The prolonged effect of beach inundation on the surface characteristics of the beach is shown in Fig. 7.6(b). The wave impact removed all bedform morphology, leaving a stagnant layer of water on the lower areas of the beach. Groundwater levels remained elevated for a period of two weeks (Fig. 7.6(a): right). A visual analysis of the images (Fig. 7.6(b)) indicates that, while the higher berm dries relatively quickly, the lower zone between the berm and dune-foot remained moist for a period of two weeks.

7.3.2 Aeolian sediment transport events

From September 29 to November 10, 16 different aeolian transport events were measured. However, due to a malfunction of the equipment, only 15 events were included in the analysis. The events were grouped based on wind direction (onshore, longshore and offshore) and ranked based on median shear velocity. Onshore winds represent a mean wind direction between 295 and 25 degrees, whereas offshore winds were measured between 115 and 205 degrees. Table 7.1 presents the data measured for these 15 events (first two events occurred under onshore winds, next seven under longshore and last six under offshore winds). The duration of the events varied between 2 and 70 hours. Saltation activity during the events varied between 18 minutes for event aI to 775 minutes for event offIII. During 9 events, maximum rainfall of 6 mm was measured during event offV. The R^2 for the wind profile regressions were high for all events with a minimum of 0.97 for events longII and longIII. The z_0 varied between 0.01 mm for offIV and 3.76 mm for longIII. For events with a period of onshore wind (onI, onII, aIV, aVII and offVI), F_m was calculated. The minimum F_m during an event varied between 150 and 170 m.

To analyse the effects of spatial variability in moisture content on transport magnitude, a representative picture of the surface conditions during the events was selected (Fig. 7.7) for visual interpretation and categorization (wet, moist, dry). Categorization was done based on color, rainfall and groundwater elevation, as no quantitative data on surface moisture were available. Figure 7.7 (top) shows the surface conditions for events with onshore winds. During event onI, the surface is clearly dry, whereas onII was characterized by rainfall and categorized as moist. For the longshore events, one moist, three dry and three wet periods were measured (Fig. 7.7 middle). Under offshore winds, three moist, a dry and two wet periods were measured. Visual interpretation reveals that the low-lying middle part of the beach is relatively wet compared to the berm and dune-foot (events longI, longII, offII, offIII and offV).

The distribution of shear velocities were plotted against the distribution of mass fluxes. Figure 7.8 shows the distributions for onshore, longshore and offshore winds,



FIGURE 7.7: For every event, a representative image was selected from the 5 minute series obtained by the time-lapse camera. Onshore events are shown at the top (a), longshore events in the middle (b) and offshore events at the bottom (c). The events were categorized into three categories: wet, moist and dry.

TABLE 7.1: Characteristics of the sixteen aeolian transport events recorded during the field measurements on Ameland.

Event	Date	Duration (hour)	Saltation (min)	Rainfall (mm)	F_m^1 (m)	Z_0 (mm)	R^2
onI	12 Oct	43	435	0.0	170	1.08	0.99
onII	14 Oct	22	412	0.8	170	1.12	0.99
longI	29 Sep	22	18	0.6		1.29	0.98
longII	9 Nov	24	359	3.2		3.19	0.97
longIII	9 Oct	5	291	0.4		3.76	0.97
longIV	19 Oct	2	56	1.2	155	0.60	0.99
longV	10 Oct	4	214	0.0		1.44	0.99
longVI	8 Oct	5	288	0.0		2.03	0.99
longVII	21 Oct	2	103	0.0	150	1.63	1.00
offI	2 Oct	22	287	1.4		0.44	0.98
offII	3 Oct	70	485	0.6		0.61	0.98
offIII	29 Oct	23	775	0.0		0.56	1.00
offIV	7 Oct	22	331	0.0		0.01	1.00
offV	25 Oct	21	360	6.0		0.29	0.99
offVI	10 Nov	21	229	1.8	165	2.35	0.98

(1) The minimum F_m during the event

with surface moisture categories of dry (orange), moist (black) and wet (blue). It is evident that the highest sediment transport rates were measured under longshore winds. For the two events measured under onshore winds, there is a clear increase in sediment transport rates with shear velocities. However, for offshore and longshore winds, there is no clear relation between shear velocities, surface conditions and sediment flux. Under longshore winds, event aI shows the highest sediment fluxes while shear velocities were lower compared to other longshore events. For event longVI, higher sediment fluxes were measured compared to events longII, longIII and longIV, while shear velocities were similar and the surface was dry at the latter events. This is inconsistent with literature, as wet sand is expected to have a higher threshold shear velocity compared to dry sand [Cornelis et al., 2004c]. However, during event longVI, a layer of dry sand was transported over a wet but relatively smooth surface; whereas events longII-IV were characterized by appreciable bedform development (see Fig. 7.7). Event longVII was characterized by the highest shear velocities, however, sediment fluxes were lower on average compared to event longIV. Three events with moist conditions and relatively

low shear velocities were measured under offshore winds. For event offV and offVI, relatively high shear velocities were measured, with sediment fluxes in the same order of magnitude compared to event offIV, with a dry surface and lower shear velocities. Thus, during events longI and offI-IV, aeolian sediment transport was measured at shear velocities below the threshold shear velocity, as the meteorological station was located in the wind shadow of the dune, while the saltiphone was situated towards the foreshore. During these offshore winds, sand transported at the foreshore, was registered by the saltiphone.

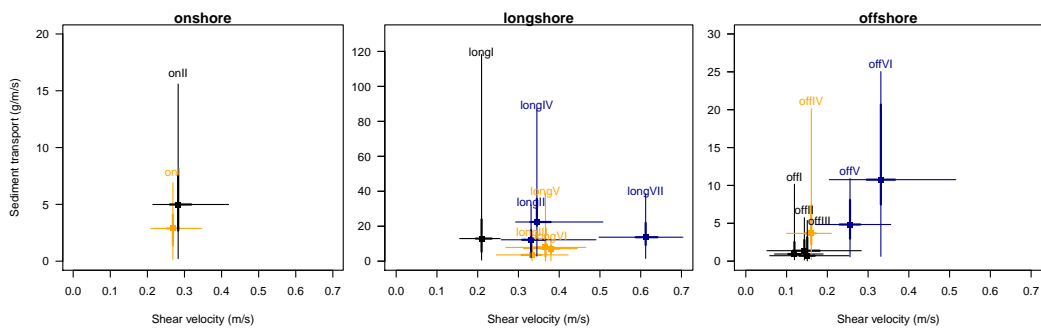


FIGURE 7.8: Distribution of shear velocities and measured sediment fluxes for the different events categorized according to wind direction onshore (left), longshore (middle) and offshore (right). The square represents the median, the thick line includes 50% of the measurements, the thin line all the measurements. The colors represent the categories dry (orange), moist (black) and wet (blue).

The total amount of potential sand transport was calculated using equation 7.6. Only periods with shear velocities higher than the threshold shear velocity ($u_* > 0.21$; eq. 7.2) were included. Figure 7.9(a) shows potential transport according to wind direction for the whole measurement period (Sept 29-Nov 10; see Table 7.1). Figure 7.9(b) however, only includes the periods where sediment traps were deployed. The different colors indicate the contribution of different categories of shear velocities. Thus, during the measurement period, longshore winds had the greatest potential to transport sediment. Winds from the south southwest had most potential to transport sediment under offshore winds. For onshore winds, most of the potential transport was controlled by strong winds ($u_* > 0.25$), whereas for longshore and offshore events, a large portion of the total potential transport was controlled by relatively mild winds ($u_* < 0.25$

). When we compare Figure 7.9(a) and 7.9(b), the measured events mainly include relatively low shear velocities. The difference in scale also reveals that only a portion of the total potential sand transport was measured. However, equation 7.6 only includes shear velocity and not any other environmental conditions such as rainfall.

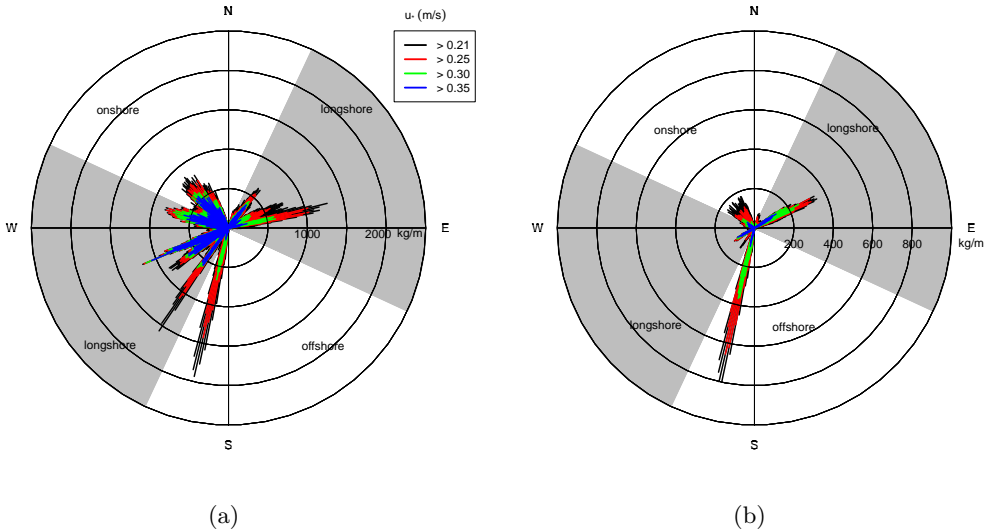


FIGURE 7.9: Total amount of potential sand transport according to wind direction. (a) includes the potential transport for the whole period (Sept 29–Nov 10; see Table 7.1); (b) includes only the events. Colors indicate the different categories of shear velocities. Note that the two figures have different scales.

Potential sand transport rates were compared with the measured data. Figure 7.10 presents the measured sediment transport rates as a percentage of calculated potential sediment transport. Median transport rates were shown to be below potential transport rates for all events. For events longI and longIV, some of the traps collected more sediment than the potential transport rates. This underestimation is caused by the spatial variability in wind strength during periods of offshore winds. For all other events, the percentage of actual transport as a function of potential transport is in the same order of magnitude. No clear trends were found in terms of wind direction, shear velocity and surface conditions.

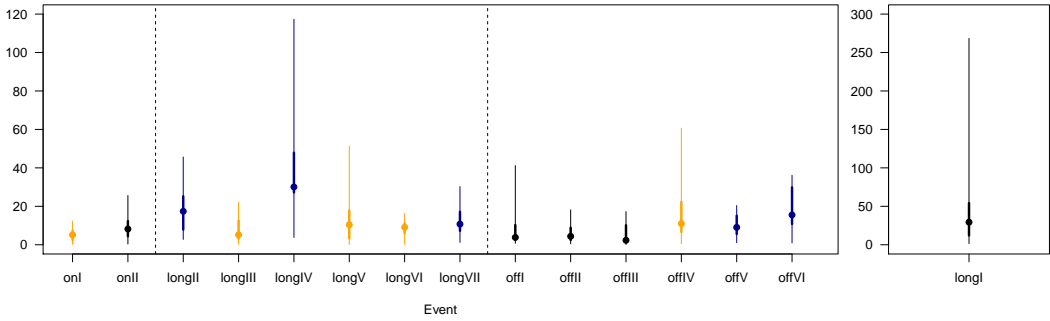


FIGURE 7.10: The distribution of actual sediment transport as a percentage of the potential transport calculated using equation 7.6 for the different events. The square indicates the median, the thick line includes 50% of observations and the thin line includes all observations.

Maximum sea and groundwater levels were analysed for all events. Groundwater and maximum sea levels ($swl + R_2$) are shown in Figure 7.11. As differences in groundwater were relatively small compared to a large increase in groundwater before event longVII, we combined the maximum sea levels of most events to an average. In Figure 7.11, sea level reached a maximum during a storm between events longIV and longVII. During this storm, the beach was inundated which led to an increase in groundwater elevation. Also, in event offV, groundwater is still relatively close to the surface, as shown in Figure 7.7. By comparing the amount of sediment transport between the events after the storm (longVII and offIII) with the event before the storm (longIV) (see Fig. 7.8), transport rates were found to be significantly lower after the storm, while surface conditions were categorized wet for all events. This indicates that surface moisture caused by high groundwater levels have a more limiting effect on sediment transport rates compared higher surface moisture levels caused by rainfall, as evident during event longIV.

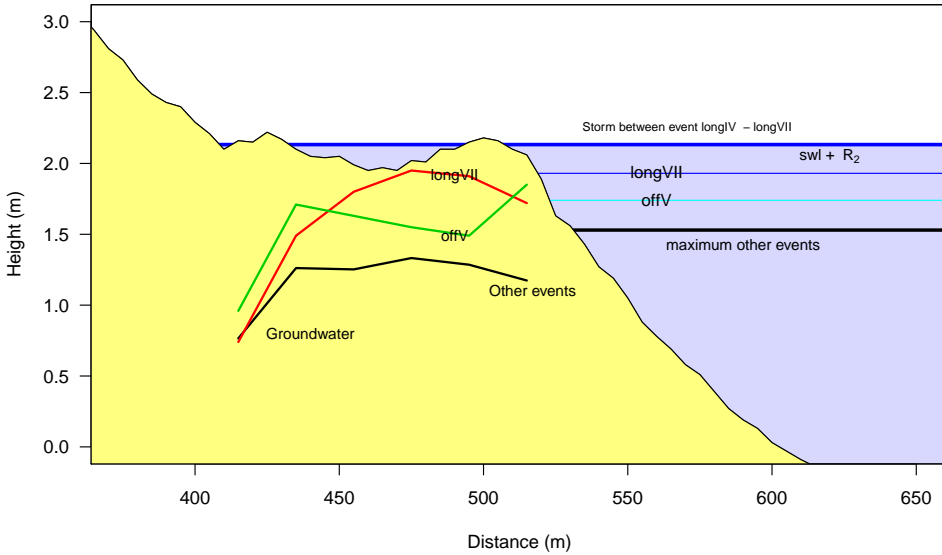


FIGURE 7.11: Average groundwater and sea level for the 15 events. Between events 11 and 12, the beach was inundated by the sea. Groundwater was elevated during events 12 and 13. Average groundwater level for the other events is also shown.

The height over which sediment is transported was studied using the q_{z50} (equation 7.5). Figure 7.12 shows the distribution of q_{z50} (the bars indicate the standard deviation) according to u_x . The wetness categorization of the events (wet, moist, dry) is indicated with different colors. From Figure 7.12, it is clear that sand is transported over higher elevations when wet. The median q_{z50} is lowest for dry events, followed by moist and wet events, respectively. The standard deviation (i.e. the differences in q_{z50} between the traps), are generally larger for the measurements under wet conditions, compared to those that were collected under moist or dry conditions. Furthermore, saltation height does not increase with u_x .

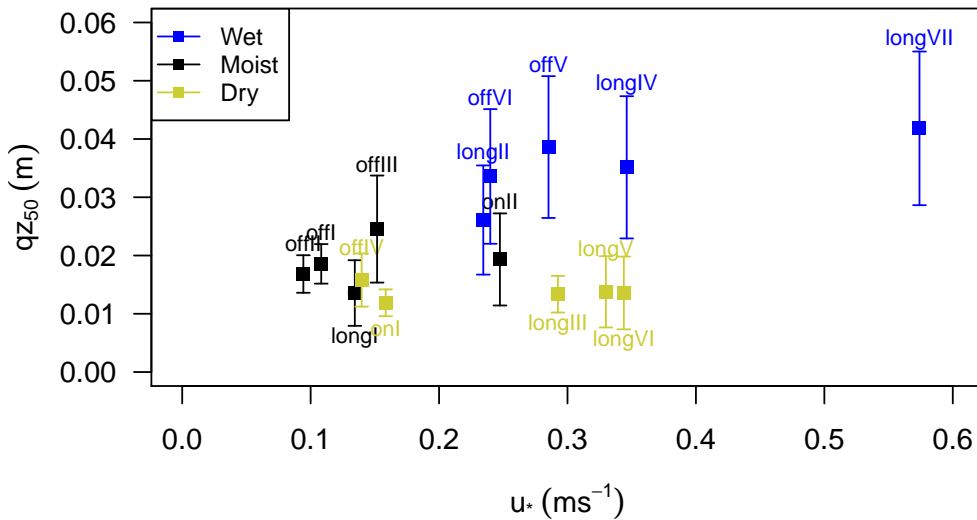
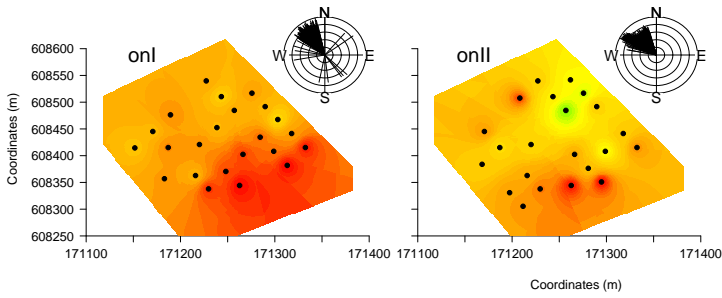


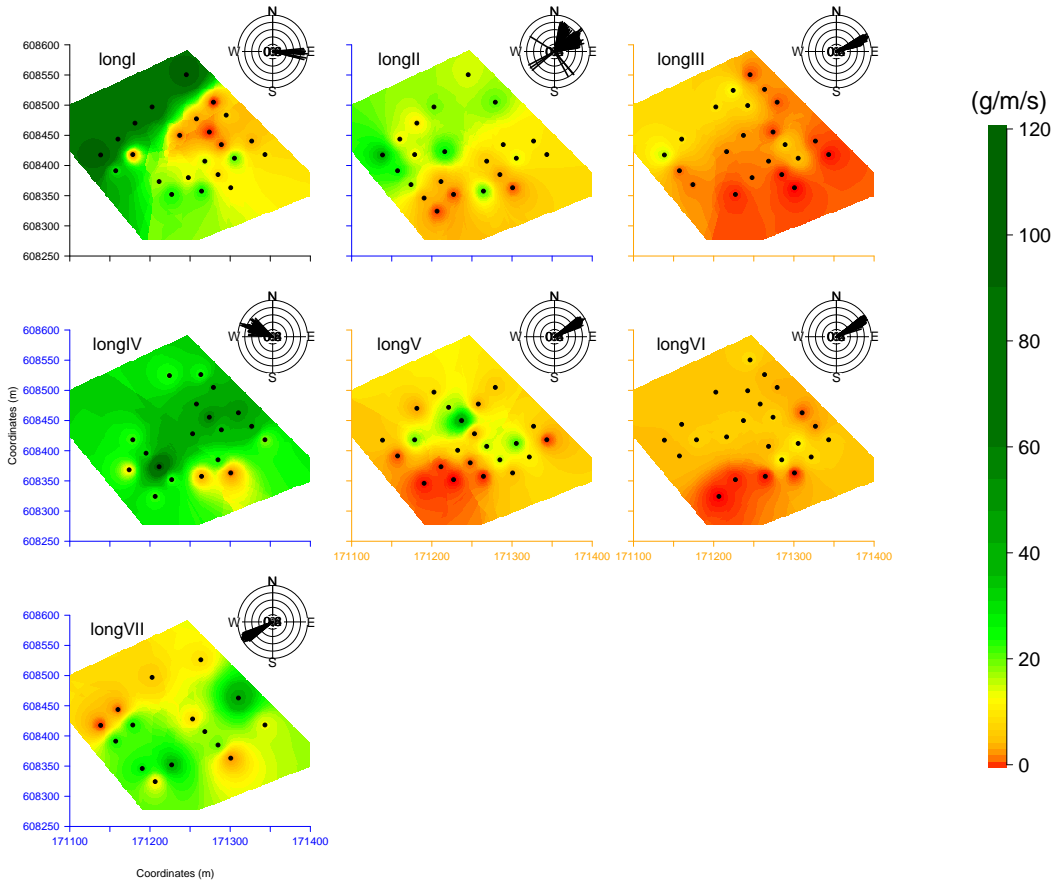
FIGURE 7.12: The q_{z50} and average shear velocities for different events. Error bars indicate the standard deviation from the mean. The number of measurement points are not equal for the different events, as measurements with a high degree of uncertainty were not included in the analysis.

7.3.3 Spatial variability in aeolian sediment transport events

The spatial distribution for different events is shown in Figs. 7.13 (for onshore and alongshore events) and 7.14 (for offshore events). A windrose with the normalized wind velocity according to wind direction was also included with colors of the axes indicating whether the events were categorized as dry (orange), moist (black) or wet (blue). Black dots indicate measurement points that were included in the interpolation. The number and position of measurements are not equal for all events, as measurements with a higher degree of uncertainty ($R^2 < 0.95$) were not included in the analysis.



(a) Onshore



(b) Alongshore

FIGURE 7.13: The Q (g/m/s) for onshore (a) and longshore (b) events. A wind-rose is included with normalized wind velocities according to wind direction during saltation (≥ 50 saltiphone counts). Colors of the axes represent the categorization as shown in Figure 7.7, where orange, black and blue represent dry, moist and wet, respectively. The number of measurement points are not equal for the different events, as measurements with a high degree of uncertainty were not included in the analysis.

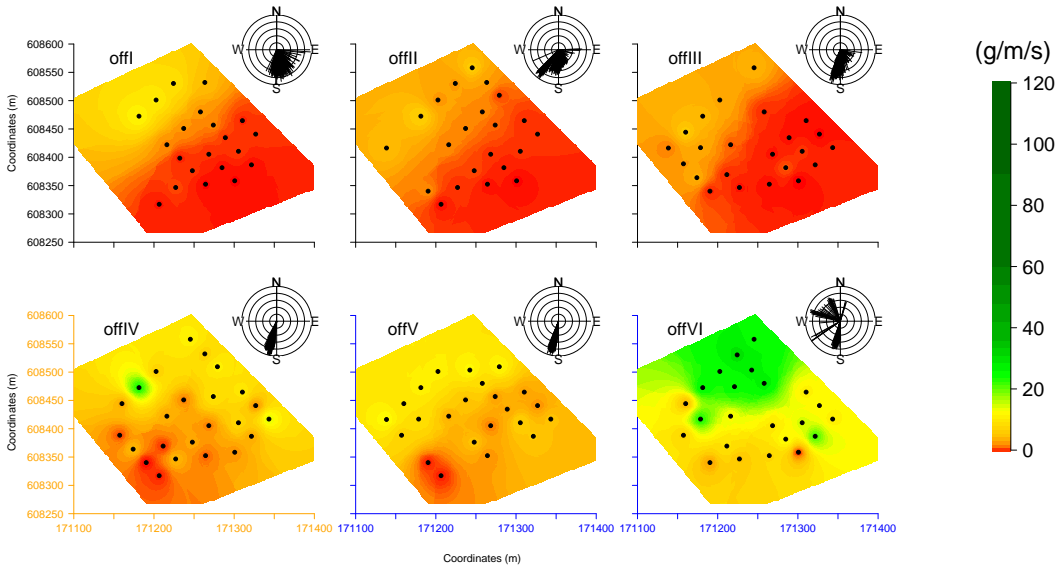


FIGURE 7.14: The Q (g/m/s) for offshore events. A wind-rose is included with normalized wind velocities according to wind direction during saltation (≥ 50 saltiphone counts). Colors of the axes represent the categorization as shown in Figure 7.7, where orange, black and blue represent dry, moist and wet, respectively. The number of measurement points are not equal for the different events, as measurements with a high degree of uncertainty were not included in the analysis.

For the onshore and offshore events, some general patterns can be distinguished. The two onshore events (Fig. 7.13) are characterized by lower sand fluxes at the dune foot, compared to sand fluxes on the beach. For offshore winds (Fig. 7.14), the transport patterns are quite similar, with higher fluxes at the foreshore compared to the backshore. This is mainly caused by the wind shadow of the dune. However, the middle zone of the beach, which was relatively wet during offII, offIII and offV (see Fig. 7.7) might also play a role here. During event offVI, the wind direction varied between onshore and offshore, which led to high transport rates at the berm.

Most variability in aeolian transport patterns can be found for longshore events (Fig. 7.13). Again, the lowest transport rates are found at the dune foot. For event longI, high sediment transport is evident at the berm. This is consistent with the surface characteristics (see Fig. 7.7), where a band of dry sand is located at the berm, whereas

the middle zone of the beach was classified as wet, limiting the supply of sediment in the upwind direction. Surface characteristics were similar during event longII, with a wet zone in the middle and a dryer zone at the berm. Transport patterns are highest at the two foremost rows of sand traps, and decrease in the direction of the dune-foot. While measured shear velocities were highest during event longI, transport rates were lower in event longII. This is most probably caused by the shadowing effect of the dune for event longI, but also the prevailing wet surface conditions.

In terms of surface characteristics, wind directions and shear velocity, events longIII, longV and longVI were similar. Transport rates during these events are in the same order of magnitude (see Fig. 7.8). The patterns that were measured during these events appear quite similar, with higher transport rates on the beach and lower amounts at the dune-foot. Event longIV was measured before the storm event and longVII after the storm event (see Fig. 7.11). These are different from other longshore events as winds come from the West, whereas winds were directed from the east for the other events. Transport rates were highest in the middle zone for event longIV, but were also quite high at the foreshore. After the beach was inundated by the sea (event longVII), sediment transport rates were lower compared to event longIV, while shear velocities were considerably higher. Most sediment transport took place in the middle zone. Figure 7.7 shows that a layer of dry sand was transported over a wet surface in the middle while the foreshore was still wet.

7.4 Discussion

Beach inundation due to high sea-levels and wave runup was found to be an important factor in horizontal and vertical transport patterns, as groundwater levels were impacted for a prolonged period. In The Netherlands, high waves and surge levels are caused by a combination of low-atmospheric pressure and strong winds but also wind direction [Winter et al., 2013]. The geographic setting is important, as winds from the northwest have the largest fetch, which, in combination with the funnel-shape of the North Sea, results in higher sea-levels and wave runup. Besides the consequent impacts on the

hydrodynamics of the coast, this affects aeolian processes due to elevated groundwater levels. Our results are consistent with the findings of [Raubenheimer et al. \[1998\]](#). They measured water table levels on a sandy beach for a period of two months. They found that over-topping increased the water table for several days, while semi-diurnal water table fluctuation were damped almost completely 100 m inland of the mean shoreline.

Our results indicate that higher surface moisture content leads to transport over higher heights compared to dry surfaces, as reported in the literature [[Farrell et al., 2012](#), [McKenna Neuman and Maljaars Scott, 1998](#), [Nield and Wiggs, 2011](#)]. Furthermore, the data shows that mean saltation height does remain essentially constant with an increase of u_* for dry, moist or wet surfaces. This is in agreement with the finding of [Namikas et al. \[2009\]](#), [Namikas \[2003\]](#), [Rotnicka \[2013\]](#) and the model proposed by [Namikas \[2006\]](#), that increasing saltation impact energy levels that occur with large u_* are dissipated by bed deformation and increased impact entrainment rather than contributing to larger saltation hops. The cohesive forces imparted by water allow wet grains to resist entrainment considerably more than dry grains, so that more impact energy is retained on wet surfaces and thus higher saltation paths are generated. Specific interaction between rainfall and wind, also referred to as splash–saltation or splash drift was not taken into account [[Riksen et al., 2008](#), [Riksen and Goossens, 2007](#), [Van Dijk et al., 1996](#)].

In this study, we used sand transport in unit per time to analyse variability in the magnitude of aeolian sand transport at an event scale. However, sand fluxes in unit per time (Table 7.1) should be considered as estimates rather than absolute values. Saltation activity was defined by an arbitrary value of 50 counts per minute. During some events, aeolian sand transport was highly intermittent [[Davidson-Arnott and Bauer, 2009](#), [Stout and Zobeck, 1997](#)], characterized by saltating streamers [[Baas, 2008](#), [Baas and Sherman, 2005](#), [Baas, 2007](#)]. For these events, the threshold of 50 counts per minute does not give an accurate representation of the duration. Wetting and drying of the top layer of the surface was observed to be an important dynamic. On a wet surface, the top layer might dry rapidly due to a combination of direct exposure to solar radiation and wind. As dry

sand has a lower threshold for transport compared to wet sand [Cornelis et al. \[2004c\]](#), [Davidson-Arnott et al. \[2008\]](#), when these particles interact with wet particles on the surfaces, they add extra momentum, causing detachment of these particles. This effect of intermittent transport on a wet surface was also reported by [Davidson-Arnott et al. \[2008\]](#), [Wiggs et al. \[2004b\]](#). Events longI, longIV and longVII, which accounted for the highest amounts of sand transport in unit per time, contain measurements in the same order of magnitude as found by [Namikas \[2003\]](#), [Nordstrom et al. \[2011\]](#), [Sherman et al. \[1998\]](#).

For all events, there is a decrease in aeolian sand transport rates towards the dune foot. For offshore events, this is clearly caused by the wind shadow of the dune. However, for onshore and longshore events, the decrease could be linked with the vegetation boundary. [Arens \[1996a\]](#) also reported a rapid decrease in sand transport landward of the vegetation boundary. However, differences in deposition patterns caused by differences in vegetation density [[Arens et al., 2001](#)] and patterns [[Youssef et al., 2012b](#)] were not measured. Furthermore, moderate events can make a significant contribution to total actual and potential transport rates, dependent on local conditions as found by [Delgado-Fernandez and Davidson-Arnott \[2011b\]](#). They found that moderate events can make a significant contribution to total sand transport rates. However, transport events that were directed towards the dune and thus enabling coastal foredune development were generally high ($u_* > 0.25$) during the measurement period. However, measurements with high shear velocities only covered a fraction of the total duration of the storm, as bottles on the sand traps were quickly saturated.

Previous small scale studies have shown that spatio-temporal variability decreases with an increase in sampling duration [[Baas and Sherman, 2006](#), [Ellis et al., 2012](#)]. In this event-scale study, we found that despite considerable variability between two closely located samplers, patterns emerge that were consistent with wind direction and surface conditions. Transport was generally highest at the berm and lowest in the middle zone; while rates were higher for longshore compared to onshore events. However, with only two onshore events recorded, it is difficult to determine if this was caused by

the availability of upwind sand, the fetch effect or other environmental factors. Fetch was included in this study, as many studies also report an increase in sand transport from the downwind distance of a border between an erodible and non-erodible surface [Anthony et al., 2006, Bauer et al., 2009, Chepil, 1957, Davidson-Arnott et al., 2005, Delgado-Fernandez, 2010, Jackson and Cooper, 1999, Lynch et al., 2006, van der Wal, 1998]. However, the data in this study was collected over hours, during which wind speed and direction varied. Due to the coarse resolution of our trap data, it is difficult to distinguish the fetch effect from meteorological factors, but also other factors such as slope, changes in topography and surface moisture.

The reduction in variability with increase sampling times is also reflected in the work of [De Vries et al., 2012, Keijsers et al., 2014b]. They found that similar amounts of sand reach the foredune annually with little correlation between meteorological conditions and coastal foredune development. Simple empirical formulations such as potential sand transport [Bagnold, 1941] or drift potential Fryberger and Dean [1979] will generally not yield adequate estimations in coastal environments. At least, estimations of sand input to dunes need to include spatial variations in sand availability that are largely controlled by topography and moisture. For better estimations of sand input to dunes, spatial variations in sand availability need to be included. These are largely controlled by topography and moisture, as shown here. By matching regional transport potential with local sand availability, event-scale predictions of sand input to the dunes can be improved, as demonstrated by Delgado-Fernandez and Davidson-Arnott [2011b].

Due to data limitations, parts of the analysis in this study have a qualitative rather than a quantitative character. Factors such as specific wind flow patterns over the foredune and beach [Hesp et al., 2005, Walker, 1999, Walker and Nickling, 2002], spatial variability in surface moisture and bed morphology were not taken into account quantitatively. Furthermore, transport rates were measured, whereas erosion and deposition patterns were not. For future event scale studies, it is suggested that quantitative surface moisture measurements [Edwards et al., 2013, 2012, Nolet et al., In Press], and

erosion and deposition patterns be included. State-of-the-art technologies such as unmanned aerial vehicles [Mancini et al., 2013], or terrestrial laser scanners [Nield et al., 2011] can be used to acquire very detailed spatially explicit information. More insight into the drivers and transport patterns of aeolian sand transport is especially important for the sustainability of a heavily managed coast such as that of the Netherlands [Arens et al., 2013, Giardino et al., 2011, VanKoningsveld et al., 2008]. In addition, this data will allow us to further improve model approaches [Bauer and Davidson-Arnott, 2003, Davidson-Arnott, 2005, De Vries et al., 2014], and better simulate the impact of future management strategies such as mega-nourishments on the coastal system.

7.5 Conclusion and recommendations

The horizontal and vertical distribution in aeolian sand transport over a beach strip in relation to sea level, groundwater dynamics and meteorological conditions was investigated at a beach on the barrier island of Ameland in The Netherlands. High sea level tides in combination with high wave runup, cause beach inundation and leads to elevated groundwater levels for a period of two weeks. Most sand transport took place during longshore events. For onshore and offshore events, some general patterns could be distinguished. However, for longshore events, more variability was found. High groundwater levels were shown to be more supply limiting compared to rainfall events. It was confirmed that higher surface moisture levels lead to higher median saltation elevations, where wet events have a higher range of median saltation elevations compared to dry ones. Transport patterns show low transport rates at the dune toe and high transport rates at the foreshore, but also large variations over small distances. Sand transport dynamics are mainly driven by local conditions, and moderate events can make a significant contribution to the total amount of sand transport. For future studies, it is suggested that spatially explicit measurements of elevation and surface moisture be included.

Chapter 8

Measuring and modeling the effect of surface moisture on the spectral reflectance of coastal beach sand

Nolet C, Poortinga A, Roosjen P, Bartholomeus H, Ruessink G (2014) Measuring and Modeling the Effect of Surface Moisture on the Spectral Reflectance of Coastal Beach Sand. PLoS ONE 9(11): e112151

Measuring and modeling the effect of surface moisture on the spectral reflectance of coastal beach sand

abstract

Surface moisture is an important supply limiting factor for aeolian sand transport, which is the primary driver of coastal dune development. As such, it is critical to account for the control of surface moisture on available sand for dune building. Optical remote sensing has the potential to measure surface moisture at a high spatio-temporal resolution. It is based on the principle that wet sand appears darker than dry sand: it is less reflective. The goals of this study are (1) to measure and model reflectance under controlled laboratory conditions as function of wavelength (λ) and surface moisture (θ) over the optical domain of 350-2500 nm, and (2) to explore the implications of our laboratory findings for accurately mapping the distribution of surface moisture under natural conditions. A laboratory spectroscopy experiment was conducted to measure spectral reflectance (1 nm interval) under different surface moisture conditions using beach sand. A non-linear increase of reflectance upon drying was observed over the full range of wavelengths. Two models were developed and tested. The first model is grounded in optics and describes the proportional contribution of scattering and absorption of light by pore water in an unsaturated sand matrix. The second model is grounded in soil physics and links the hydraulic behaviour of pore water in an unsaturated sand matrix to its optical properties. The optical model performed well for volumetric moisture content $\theta < 24\%$ ($R^2 > 0.97$), but underestimated reflectance for θ between 24-30% ($R^2 > 0.92$), most notable around the 1940 nm water absorption peak. The soil-physical model performed very well ($R^2 > 0.99$) but is limited to $4\% > \theta < 24\%$. Results from a field experiment show that a short-wave infrared terrestrial laser scanner ($\lambda=1550$ nm) can accurately relate surface moisture to reflectance (standard error 2.6%), demonstrating its potential to derive spatially extensive surface moisture maps of a natural coastal beach.

8.1 Introduction

Every decade sea water level of the North Sea rises by 2-3 cm [Solomon \[2007\]](#). This is alarming for a country as the Netherlands considering large parts are already below sea level. It puts urgency on finding coastal defense strategies that are able to adapt to climate change [Bochev-Van der Burgh et al. \[2011\]](#), [De Jong et al. \[2014\]](#), [Keijsers et al.](#)

[2014a]. In this context an unprecedented large nourishment of sand ('Sand Motor', www.zandmotor.nl) was laid down along a stretch of the Dutch coast in 2011. Its aim is to mimic the onshore migration of an intertidal sandbar, supplying the adjacent coast with a surplus of sand for years to come [Stive et al. \[2013\]](#), [Van Slobbe et al. \[2013\]](#). An important expected result is the throughput of sand by wind over the beach towards the dunes, enabling the dunes to naturally grow in volume [Keijsers et al. \[2014b\]](#), [Poortinga et al. \[2011\]](#).

Surface moisture is an important supply limiting factor for aeolian sand transport [Bauer et al. \[2009\]](#), [Davidson-Arnott et al. \[2005\]](#), [De Vries et al. \[2014\]](#), [Ellis et al. \[2012\]](#), [Namikas and Sherman \[1996\]](#), [Poortinga et al. \[2014\]](#). By binding sand grains together, through cohesive and adhesive forces, water significantly increases the resistance of the uppermost sand layer against wind erosion [Chepil \[1956\]](#), [Cornelis and Gabriels \[2003\]](#), [McKenna-Neuman and Nickling \[1989\]](#). It has been suggested by [Belly \[1962\]](#) that the required wind force to initiate saltation grows exponentially by a linear increase of moisture content. Above a certain moisture content beach sand becomes inherently resistant to entrainment by most natural winds.

To accurately predict aeolian sand availability for dune building it is thus critical to account for the control of surface moisture. However, wetting and drying processes are governed by complex hydraulics of tidal and wave action, groundwater and capillary flow, and evaporation and precipitation [Atherton et al. \[2001\]](#), [Davidson-Arnott and Bauer \[2009\]](#), [Hugenholtz et al. \[2009\]](#), [Huisman et al. \[2011\]](#), [Namikas et al. \[2010\]](#). As a result, the distribution of surface moisture on a beach can vary greatly in space and time. Therefore, to estimate the control surface moisture exerts on aeolian sand transport, data at a high spatio-temporal resolution is required [Poortinga et al. \[2013a\]](#), [Wiggs et al. \[2004b\]](#), [Yang and Davidson-Arnott \[2005\]](#).

Optical remote sensing can be a viable solution for measuring surface moisture at a high spatio-temporal resolution. It is based on the principle that wet sand appears darker than dry sand: it is less reflective. This familiar reduction in reflectance is attributed to pore water surrounding the sand grains, causing a change in scattering

and absorption of light. Scattering and absorption of sunlight occur at the same time, but their proportional contribution to reduction in reflectance depends on wavelength (λ) and moisture content (θ) [Bowers and Hanks \[1965\]](#), [Lobell and Asner \[2002\]](#), [Weidong et al. \[2002\]](#). This holds true when other parameters affecting beach surface reflectance (e.g. mineral composition, grain size distribution, packing density, surface roughness [Leu \[1977\]](#), [Shuchman and Rea \[1981\]](#)) remain unchanged.

The potential of optical remote sensing of surface moisture, for aeolian research in the coastal environment, was first demonstrated by [Darke and McKenna Neuman \[2008\]](#), [Darke et al. \[2009\]](#), [Mckenna Neuman and Langston \[2003\]](#), [McKenna Neuman and Langston \[2006\]](#) and [Delgado-Fernandez et al. \[2009\]](#). Through a photographic methodology ($\lambda = 400 - 700$ nm), beach surface moisture content was related to a corresponding normalized surface reflectance. This relationship was applied to photographs of a beach, resulting in a time-series of surface moisture maps. The same principle was later tested by [Nield and Wiggs \[2011\]](#), [Nield et al. \[2011\]](#) and [Nield et al. \[2014\]](#), where the reflective signal of a terrestrial laser scanner ($\lambda = 539$ nm) was related to beach surface moisture. It is a more convenient application since the reflected signal does not require a correction for changes in illumination. Another application of the principle was tested by [Edwards et al. \[2012\]](#) and [Edwards et al. \[2013\]](#), where point data on beach surface moisture was collected using a portable narrow band radiometer ($\lambda = 1940$ nm) and spectroradiometer ($\lambda = 970$ nm). At these wavelengths the correlation between surface reflectance and moisture content was shown to be higher than at visible wavelengths, due to stronger absorption of light in water.

In soil science, optical remote sensing is widely used to determine soil moisture content [Bowers and Hanks \[1965\]](#), [Idso et al. \[1975\]](#), [Knadel et al. \[2014\]](#), [Lobell and Asner \[2002\]](#), [Skidmore et al. \[1975\]](#). However, the recent studies that relate reflectance to surface moisture in a coastal environment, show ambiguous results, as was also recognized by [Edwards et al. \[2012\]](#) and [Edwards et al. \[2013\]](#). It is in part due to the focus on a limited range of wavelengths in which measurements were taken (see overview in [Figure 8.1-bottom](#)). The goals of this study are (1) to measure and model reflectance under

controlled laboratory conditions as function of wavelength (λ) and surface moisture content (θ) over the full optical domain of 350-2500 nm, and (2) to explore the implications of our laboratory findings for accurately mapping the distribution of surface moisture under natural conditions. A laboratory spectroscopy experiment is conducted to measure spectral reflectance (1 nm interval) under different surface moisture conditions using beach sand. Two models are developed and tested. The first model is grounded in optics and describes the proportional contribution of scattering and absorption of light by pore water in an unsaturated sand matrix. The second model is grounded in soil physics and links the hydraulic behaviour of pore water in an unsaturated sand matrix to its optical properties. A field experiment is conducted to test the potential of a short-wave infrared terrestrial laser scanner ($\lambda=1550$ nm) to derive spatially extensive surface moisture maps with a high accuracy. As such, this study aims to support practical applications for optical remote sensing of surface moisture on a sandy coastal beach.

8.2 Background

8.2.1 Spectral reflectance

Elastic scattering of light is the re-directing of light without alteration of the wavelength. It encompasses the optical phenomena of transmission, reflection, and refraction [Bohren and Huffman \[2008\]](#), [Hecht \[2002\]](#), determined by the angle of incidence and the wavelength dependent refractive index $n(\lambda)$. The refractive index is a ratio, describing how fast light propagates through a medium compared to a vacuum, and changes in direction (is refracted) as result. Transmission of sunlight into opaque beach sand is in the order of a few sand grains thick [Ciani et al. \[2005\]](#), [Leu \[1977\]](#), [Shuchman and Rea \[1981\]](#), [Tester and Morris \[1987\]](#). Optical reflectance is thus strictly a surface phenomenon

With optics [Ångström \[1925\]](#) proposed an explanation for the familiar visual darkening of sand upon wetting, ascribing it to total internal reflection within water films surrounding the sand grains. In effect, sunlight at or exceeding the critical

angle is reflected back to the surface at the liquid-air interface, increasing the likelihood of being absorbed by the sand grains. Assuming ideal diffuse reflection [Ångström \[1925\]](#) described the relation between wet (R_w) and dry (R_d) reflectance by:

$$R_w = \frac{R_d}{n^2(1 - R_d) + R_d} \quad (8.1)$$

with n the wavelength dependent refractive index of water. [Lekner and Dorf \[1988\]](#) later modified this model to account for the fraction of sunlight that is not transmitted into the water film but reflects specularly (R_s) at the air-liquid interface:

$$R_w = \frac{(1 - R_s)R_d}{n^2(1 - R_d) + R_d} \quad (8.2)$$

$$R_s \approx \left(\frac{n_w - n_a}{n_w + n_a} \right)^2 \quad (8.3)$$

Specular reflectance R_s is approximated by Fresnel reflection of normal incident sunlight [Hecht \[2002\]](#), with n_w the refractive index of water and n_a the refractive index of air, taken as 1. How specular reflectance changes with wavelength is shown in [Figure 8.1](#).

The process of absorption is also important to spectral reflectance. Absorption of sunlight is the uptake of light by conversion of its energy into thermal energy. It is strongly correlated to wavelength. Spectral absorption of sunlight is described by the Beer-Lambert law [Bohren and Huffman \[2008\]](#), stating an exponential decrease of reflectance as a function of the absorption coefficient $\alpha(\lambda)$ (cm^{-1}) and optical path length d (cm):

$$R = R_d e^{-\alpha d} \quad (8.4)$$

The spectral absorption coefficient describes the extent to which sunlight is absorbed as it passes through a medium. [Figure 8.1](#) shows the absorption coefficients for pure water in the optical domain 350-2500 nm (data: [Segelstein \[1981\]](#)). It becomes clear from

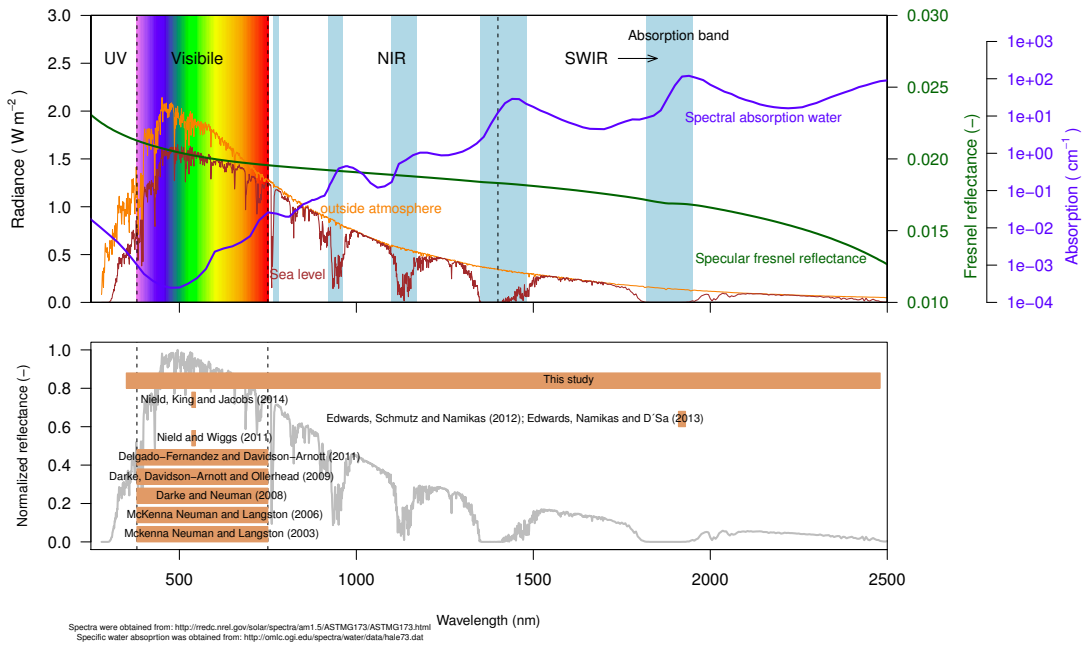


FIGURE 8.1: Top: The spectral power distribution of sunlight (in Wm^{-2}) outside the atmosphere (yellow line) and at sea level (brown line). The spectral Fresnel reflectance for a water surface and absorption coefficients for pure water are shown as the green and blue line respectively. Bottom: an overview of the studies (including this study) that demonstrate the potential of relating reflectance to surface moisture. The orange bars indicate the spectral range in which the measurements were taken.

Figure 8.1 that water is a strong absorber of sunlight at specific wavelengths. Notable absorption peaks all occur at near- and shortwave-infrared wavelengths, around 760, 970, 1200, 1470 and 1940 nm Pope and Fry [1997], Segelstein [1981]. At visible wavelengths the absorption coefficient is close to zero. Here, the penetration depth (i.e. inverse of absorption) of sunlight in water is high, which is why water appears transparent.

The effect of absorption of sunlight by water is illustrated by comparing the spectral power distribution of sunlight (Wm^{-2}) outside the atmosphere to that at sea level (Figure 8.1). Since water (vapour) is abundant in the atmosphere, certain wavelengths of sunlight are absorbed to such an extent that it may not reach the earth’s surface. This

is of consequence for collecting remotely sensed data. Passive methods, that depend on sunlight for acquiring information about an object, are 'short-sighted' or in fact blind in wavelengths strongly absorbed by water. This is true for wavelengths around the 1470 and 1940 nm absorption peaks. Here an active method must be employed, where data is collected using a light source other than the sun [Elachi and Van Zyl \[2006\]](#).

8.2.2 Surface moisture

The decrease of spectral reflectance upon wetting is non-linear, as is the hydraulic behaviour of water in an unsaturated sand matrix. Both processes can be linked conceptually, as is shown in Figure 8.2. At (and below) wilting point (fig. 8.2.1) pore water is held tightly in the sand matrix as adsorbed water films around the sand grains. Here the optical path length in water (d) is close to zero, and the decrease of spectral reflectance is almost solely due to scattering. Approaching field capacity (Fig. 8.2.2) pore water proceeds to fill micro pores and form water wedges between sand grains. This increases the optical path length in water (d), with increasing absorption as result. When the sand matrix gets fully saturated (Fig. 8.2.3) all remaining air in the sand matrix is replaced with water and free water may appear at the surface. Now the optical path length in water (d) is at its maximum and certain wavelengths may be completely absorbed [Hillel \[1998\]](#), [Lobell and Asner \[2002\]](#).

The hydraulic behaviour of water in an unsaturated sand matrix is described by the water retention curve (Fig. 8.3), relating volumetric water content θ to the water pressure head h in cm. Under unsaturated conditions the water pressure head is always negative, for cohesive and adhesive forces in the sand matrix reduce pore water potential relative to free water. A well-established empirical model to describe the water retention curve is the Van Genuchten equation (Eq. 8.5) of [Van Genuchten \[1980\]](#):

$$\theta_h = \theta_r + \frac{\theta_s - \theta_r}{[1 + (a|h|)^n]^{1-1/n}} \quad (8.5)$$

With θ_r the residual water content and θ_s the saturated water content. At these water contents the gradient $d\theta/dh$ of the water retention curve becomes zero. Parameter

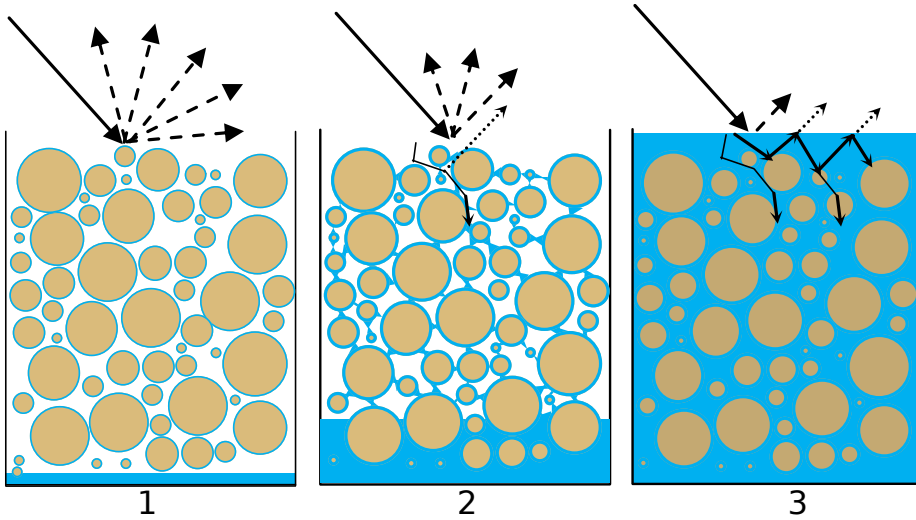


FIGURE 8.2: A conceptual representation of the non-linear decrease of spectral reflectance as moisture content in the sand matrix increases. At wilting point (1) there is almost no absorption of light in water as the optical path length (d) is close to zero. At field capacity (2) the optical path length in water (d) increases with increasing absorption as result. At saturation (3) the optical path length in water (d) is at its maximum and certain wavelengths may be completely absorbed.

a (cm^{-1}) approximately equals the inverse of the pressure head at the inflection point, where $d\theta/dh$ has its maximum value. It is interpreted as the air entry value. The dimensionless parameter n relates to the slope at the inflection point, thus reflecting steepness of the water retention curve. It is interpreted as an indicator of pore-size distribution Van Genuchten [1980], Wosten and Van Genuchten [1988]. Note that moisture levels of $\theta < \theta_r$ and $\theta > \theta_s$ are beyond the range of Eq. 8.5.

8.2.3 Surface moisture - spectral reflectance models

Two simple models are proposed to obtain a description of spectral reflectance under different moisture conditions. The first model (Eq. 8.6) is grounded in optics. Spectral reflectance R_θ as a function of volumetric surface moisture is described by:

$$R_\theta = f_s R_d e^{-\alpha d} \quad (8.6)$$

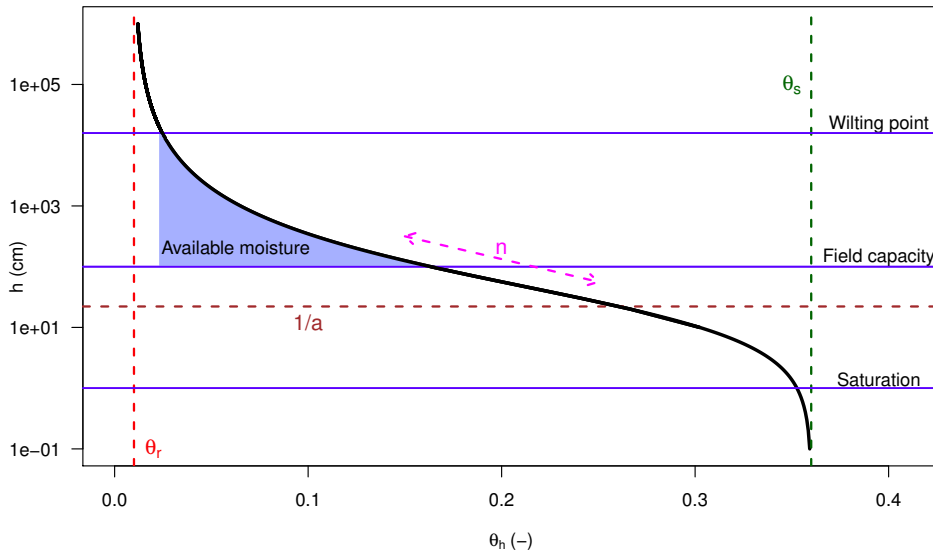


FIGURE 8.3: The water retention curve for a coarse grained sand matrix ($M_{50} = 350\text{--}500\ \mu\text{m}$), created using Eq. 8.5. Shown in the graph are the residual water content (θ_r), saturated water content (θ_s), air entry value ($1/a$) at the inflection point, and (n) which is related to the slope at inflection point and indicates pore-size distribution. Data taken from Wösten et al. [2001].

Where parameters f_s (fraction) and d (cm) at a certain wavelength and moisture content, are obtained by curve fitting. Parameter f_s describes the contribution of elastic scattering to reduction of spectral reflectance upon wetting, while parameter d (optical path length in water) describes the contribution of absorption to reduction of spectral reflectance upon wetting. Further, α denotes the wavelength dependent absorption coefficient for pure water, and R_d the dry spectral reflectance. The model is based on the approach of Philpot [2010], with omission of the fraction R_s as the contribution of specular reflectance to darkening upon wetting was shown by Philpot [2010] to be minimal. The model of Philpot [2010] is similar to the model of Lobell and Asner [2002], although the latter model takes the absorption coefficient α as a regression parameter.

The second model (Eq. 8.7) is grounded in soil physics. The Van Genuchten equation (Eq. 8.5) is modified by replacing pressure head h (cm) with spectral reflectance R_θ . Parameters a and n , at a certain wavelength, are obtained by curve fitting and become

dimensionless as spectral reflectance is a fraction. Volumetric moisture content θ_R as a function of spectral reflectance is described by:

$$\theta_R = \theta_r + \frac{\theta_s - \theta_r}{[1 + (aR_\theta)^n]^{1-1/n}} \quad (8.7)$$

Where residual water content θ_r and the saturated water content θ_s are sand matrix constants. Note that the soil-physical model is fitted at a certain wavelength, whereas the optical model is fitted over all wavelengths in the optical domain.

8.3 Materials and Methods

8.3.1 Experimental setup

A laboratory spectroscopy experiment was conducted in duplo to observe spectral reflectance in the optical domain (350-2500 nm) under different moisture conditions. A representative sample of beach sand was collected from the 'Sand Motor' (GPS location: 52.052°N 4.184°E). A field permit was not required and sample collection did not involve endangered or protected species of flora or fauna. Before the experiment the sample was coarsely sieved (2 mm) to remove shells and constituents other than sand. The sand, composed of quartz with some feldspar, had a dry bulk density ρ_b of 1.655 gcm⁻³ with mean and median grain size of 324 and 288 μm respectively.

For each experiment, a sub-sample of the collected beach sand was placed in a matte black petridish (5 cm radius, 1.5 cm height), filling it up to the rim, and oven dried for 24h at 105 °C. The sample was, after measuring its initial weight, slowly saturated with distilled water. The water was let to distribute itself uniformly in the sample and excess free water was drained from the surface. The sample was placed on a data-logging weighing scale with milligram precision.

During the drying process the reflectance (correct terminology: biconical reflectance factors or BCRF's) of the sample were acquired using the spectroscopy facility of Wageningen University [Roosjen et al. \[2012\]](#). The spectral reflectance was measured at 1 nm intervals using an ASD Fieldspec Pro spectrometer (Analytical Spectral Devices,

Boulder, CO). A 40 x 40 cm white Spectralon panel (LabSphere, Inc., North Sutton, NH) was used to calibrate the spectrometer.

The spectrometer was fitted with a 1° FOV foreoptic which was directed at nadir at 40 cm distance from the sample. As an artificial light source, a 900 watt Quartz Tungsten Halogen (QTH) lamp was placed 70 cm from the sample at a 30° zenith angle (see Figure 8.4). At the time of the measurements the room temperature was kept stable at 23°C and the humidity was kept constant at 50%. The spectrometer was programmed to take a measurement every 5 minutes. At the same time the weight of the sample was measured and stored. Data are publicly accessible at doi:10.4121/uuid:866135c2-2be3-4b74-8f9c-922505285a7b.

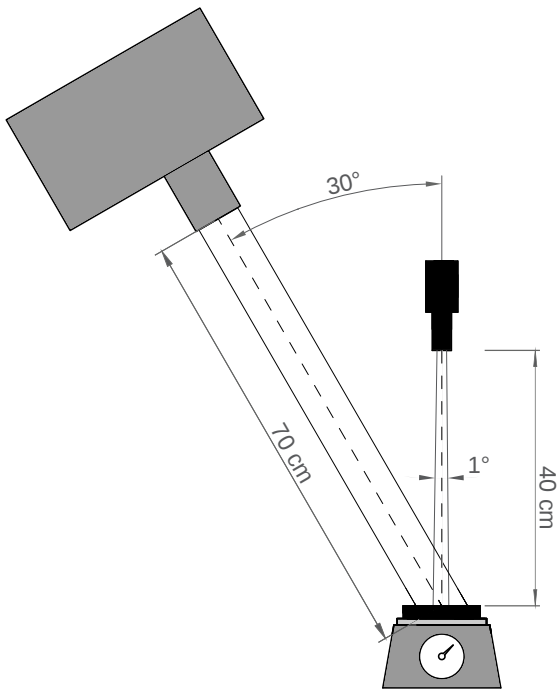


FIGURE 8.4: schematic overview of the measurement setup. The ASD Fieldspec Pro spectrometer (Analytical Spectral Devices, Boulder, CO), fitted with a 1° FOV foreoptic, was directed at nadir at 40 cm distance from the sample. A 900 watt Quartz Tungsten Halogen (QTH) lamp was placed 70 cm from the sample at a 30° zenith angle. The spectral reflectance was measured over a range of 350-2500 nm, at 1 nm intervals.

8.3.2 Analysis method

For each sub-sample the laboratory spectroscopy experiment obtained five-minute interval measurements of spectral reflectance at a certain volumetric moisture content. Only wavelengths between 350 - 2100 nm were included in the analysis, as wavelengths > 2100 nm were found to have a lower signal-to-noise ratio. Volumetric moisture content was calculated by:

$$\theta = \frac{m_w \rho_s}{m_s \rho_w} \quad (8.8)$$

With m_w and ρ_w the (decreasing) mass and density (0.997 gcm^{-3}) of water, and m_s and ρ_s the mass and dry bulk density (1.655 gcm^{-3}) of the sand sample.

Equation 8.6 and 8.7 were fitted to the spectral reflectance measurements. Parameters f_s and d (Eq. 8.6) and a and n (Eq. 8.7) were optimized using a non-linear (weighted) least-squares regression algorithm R Core Team [2012]. The spectrum of the air-dry sample was used for R_d and the spectrum for R_θ corresponded to a certain volumetric moisture content. The sand matrix constants θ_r and θ_s were determined manually, using the graphical relationship between spectral reflectance and volumetric moisture content.

8.4 Results and Discussion

8.4.1 Laboratory experiment

The laboratory spectroscopy experiment was conducted in duplo to assess the variation in spectral reflectance of the beach sand as function of surface moisture content. The spectral reflectance curves of both experiments (interpolated to regular moisture intervals) showed minimal variation between 400-2100 nm ($R^2 > 0.997$). Therefore the dataset with most data points was selected for further analysis. A total of 300 spectral reflectance measurements were taken over a period of 25 hours. Volumetric surface moisture content varied between 32% (saturation) and $< 0.01\%$ (air-dry).

Figure 8.5 shows measured spectral reflectance plotted at 4% moisture intervals. A non-linear decrease of reflectance, as moisture content increases, is observed over the full range of wavelengths. The shape of the air-dry spectral reflectance curve (top line Fig. 8.5) reflects the optical properties of the beach sand itself. Overall, at longer wavelengths, dry beach sand becomes more reflective but wet beach becomes less reflective. This is due to stronger absorption of light in water at near- and short-wave infrared wavelengths (see Fig. 8.1). Notable dips in reflectance are observed at the absorption peaks of 1470 and 1940 nm. The overall shape of the curve at visible wavelengths (400–700 nm) does not change greatly with increasing moisture content. This corresponds to the notion that soils darken when wet but with little apparent color change.

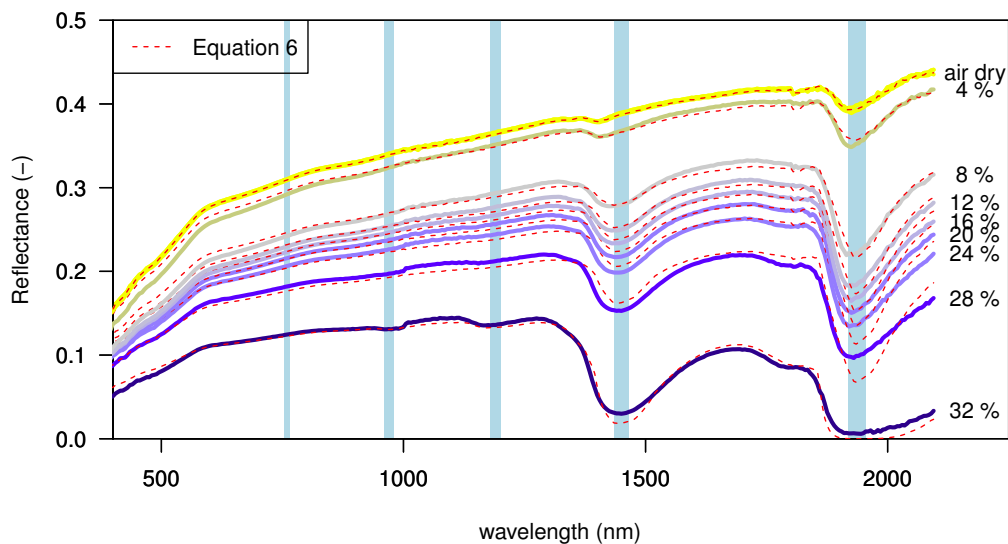


FIGURE 8.5: The measured spectral reflectance over a range of 350–2100 nm, at 4% volumetric moisture content interval between 32% (saturation) and < 0.01% (air-dry). A non-linear decrease in reflectance upon wetting is observed over the full range of wavelengths. Notable dips in reflectance occur at water absorption peaks at 1470 and 1940 nm (blue bands). The dashed red lines show the spectral reflectance R_θ as calculated by fitting the optical model (Eq. 8.6) to measured spectral reflectance.

The optical model (Eq. 8.6) was fitted to the spectral reflectance measurements and shown as dashed red lines in Figure 8.5. As can be seen in Figure 8.6 (top) the optical

model performs well for surface moisture contents $\theta < 24\%$ ($R^2 > 0.97$), but gives an underestimation in reflectance for θ between 24-30% ($R^2 > 0.92$). This is most notable around the 1940 nm water absorption peak (see Fig. 8.5). A plausible explanation is that the absorption of light is not as effective in pore water since it is partially bound to the sand matrix. This notion is supported by the fact that at saturation ($\theta \geq 32\%$), where free water is present, model performance improves ($R^2 > 0.97$).

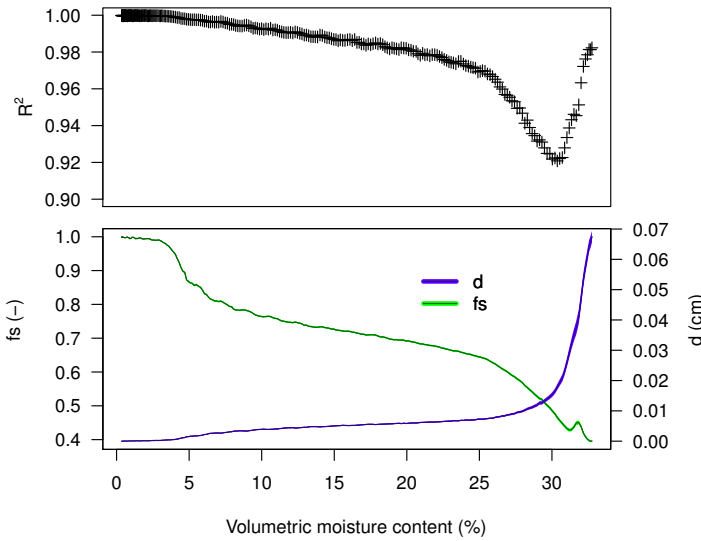


FIGURE 8.6: Top: the goodness of fit R^2 (top) for the optical model (Eq. 8.6) as function of volumetric moisture content. Bottom: the contribution of scattering (fraction f_s) and absorption (optical path length in water d) as moisture levels increase. R^2 , f_s and d are obtained by fitting Eq. 8.6 to measured spectral reflectance. The shaded areas indicate 95 % confidence intervals

Figure 8.6 (bottom) shows the values of f_s (fraction) and d (cm) at corresponding moisture content. The trajectories of the regression parameters of the optical model describe the proportional contribution of elastic scattering (f_s) and water absorption (d) to spectral reflectance upon wetting. These trajectories are in agreement with the principle outlined in Figure 8.2. At air-dry conditions (Fig. 8.2.1) pore water is held tightly in the sand matrix. The optical path length in water (d) is close to zero as there is negligible absorption of light in water. Reflectance is thus almost solely due to

scattering, and fraction f_s is close to 1. When pore water proceeds to fill micro pores and form water wedges between sand grains (Fig. 8.2.2), the contribution of absorption increases, while the contribution of scattering decreases. When the sand matrix gets fully saturated (Fig. 8.2.3) the optical path length in water (d) is at its maximum, between 0.06 - 0.07 cm. This corresponds to a thickness of a few sand grains (median 288 μm). It is encouraging that the order of magnitude is within physical expectation.

Figure 8.7 (black lines) shows measured reflectance as a function of volumetric moisture content plotted for the five water absorption peaks at 760, 970, 1200, 1470, and 1940 nm. It can be seen that at longer wavelengths the air-dry reflectance increases and reflectance upon wetting decreases, resulting in greater contrast between wet and dry reflectance. Wavelengths at 1470 and 1940 nm are absorbed by water to such an extent that saturated reflectance approaches zero. Further, it becomes clear from Figure 8.7 that the shape of the spectral reflectance curves are very similar to the shape of the water retention curve calculated by Eq. 8.5 of Van Genuchten [1980] (Fig. 8.3). This suggests that spectral reflectance influenced by surface moisture content is linked to the hydraulic behaviour of water in an unsaturated sand matrix. This link is conceivable, as both processes share common drivers such as mineral composition and texture of the soil. The spectral reflectance upon wetting and water retention characteristics of beach sand can thus be described by the same empirical formulation.

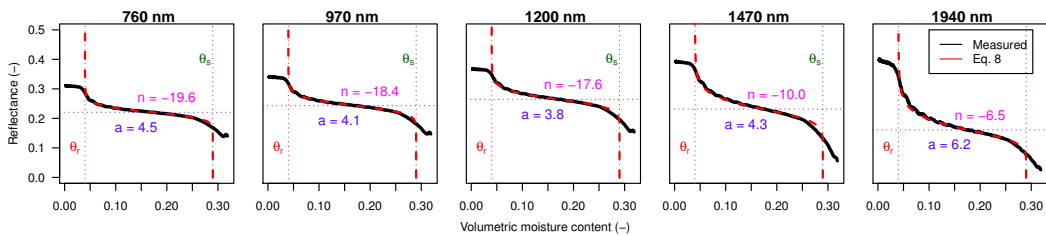


FIGURE 8.7: Black lines: measured spectral reflectance upon wetting at the water absorption peaks of 760, 970, 1200, 1470, and 1940 nm. Dashed red lines: volumetric moisture content θ_R as calculated by fitting the soil-physical model (Eq. 8.7). With sand matrix parameters $\theta_r = 0.04$ and $\theta_s = 0.29$. Non-linear regression parameters a and n are shown in the plot at corresponding wavelength.

The soil-physical model (Eq. 8.7) was fitted to the reflectance curves of Figure 8.7. Non-linear regression parameters a and n are shown in the plots at corresponding wavelength. The sand matrix parameters θ_r and θ_s were determined at 0.04 and 0.29 respectively. As a consequence, moisture levels of $\theta < 4\%$ and $\theta > 29\%$ are beyond the range of the soil-physical model. While knowledge of $\theta > \theta_s$ is not very relevant for aeolian coastal research, knowledge of $\theta < \theta_r$ is relevant. Even at low levels, surface moisture exerts a significant control on the aeolian entrainment of sand. As can be seen in Figure 8.7, the reflectance for $\theta < \theta_r$ at shorter wavelengths remain almost level and a differentiation between moisture levels $< \theta_r$ is not possible. At near- and short-wave infrared wavelengths, however, the reflectance does increase as moisture content decreases towards air-dry conditions. Here the approach of [Wesseling et al. \[2008\]](#) offers an alternative to the soil physical model, as it can describe the reflectance curve over the full moisture range using cubical spline approximations.

The soil-physical model (Eq. 8.7) was also fitted to measured spectral reflectance upon wetting over the full range of 350-2100 nm, at 1 nm interval. By obtaining the values for a and n for all optical wavelengths for the unsaturated sand matrix between θ_r and θ_s , it was possible to calculate the spectral reflectance as a function of volumetric moisture content (R_θ). Figure 8.8 shows the calculated (red dashed lines) and measured (continuous lines) spectral reflectance upon wetting between 4.5-24% volumetric moisture content plotted at 4% moisture content interval. Between these moisture levels the reconstructed spectral reflectance has an overall goodness of fit of $R^2 > 0.99$. A slight underestimation in spectral reflectance was found for higher surface moisture contents, most notable around the absorption peaks of 1470 and 1940 nm.

It becomes clear from Figure 8.9 that, at visible wavelengths averaged over 400-700 nm, there is a limited contrast between dry and wet reflectance of beach sand composed of quartz sand. The slope of the reflectance curve is, after an initial steep decline, close to zero for intermediate moisture levels (~ 5 -25%). This suggests that, for quartz sand beaches at visible wavelengths, only a distinction between a dry and a wet surface is practical. Differentiation of intermediate moisture levels would require

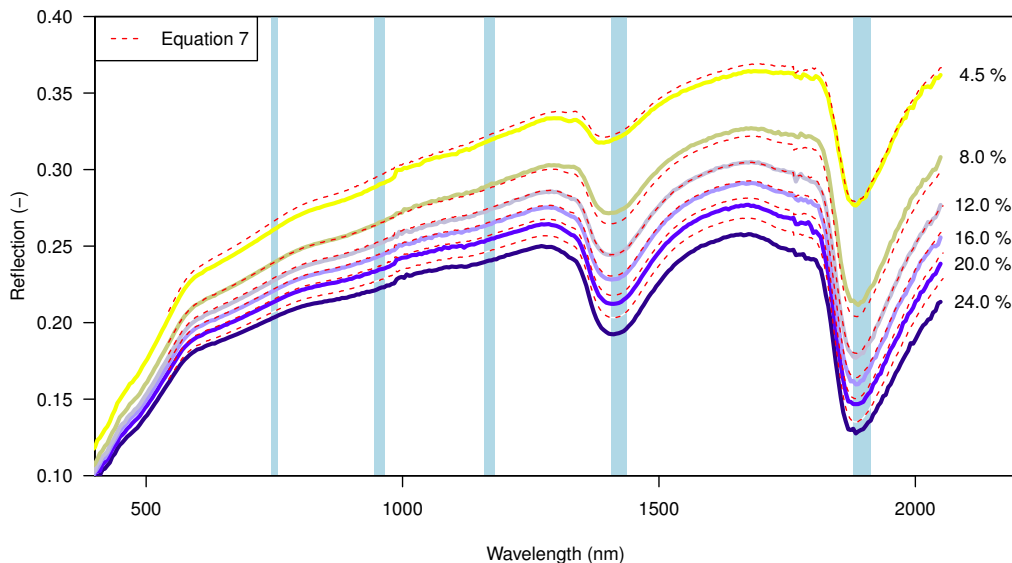


FIGURE 8.8: Spectral reflectance upon wetting (red dashed lines) obtained by fitting the soil-physical model (Eq.8.7) to measured spectral reflectance (continuous lines) at 1 nm interval. The blue bands indicate spectral absorption peaks for water. Between 4.5-24% volumetric moisture content the spectral reflectance reconstructed with Eq. 8.7 has a goodness of fit of $R^2 > 0.99$.

very accurate radiometric calibration, also considering that other parameters affecting surface reflectance (e.g. mineral composition, grain size distribution, packing density, surface roughness) may vary under field conditions. This limited contrast is a plausible explanation for the weak correlation between beach surface moisture and reflectance found in the studies of Darke and McKenna Neuman [2008], Darke et al. [2009], Delgado-Fernandez et al. [2009], Mckenna Neuman and Langston [2003], McKenna Neuman and Langston [2006] and Nield et al. [2014], Nield and Wiggs [2011], Nield et al. [2011]. A standard error of $\sim 10\%$ moisture content is reported by Edwards et al. [2012] and Edwards et al. [2013] for the photographic method, while with the terrestrial laser scanner ($\lambda = 539$ nm) the standard error increases after 7-8% moisture to such an extent that the method becomes impractical.

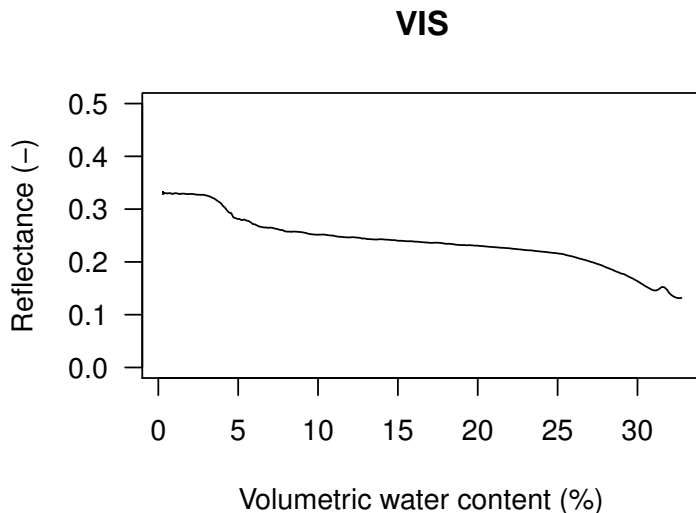


FIGURE 8.9: Averaged measured spectral reflectance upon wetting at visible wavelengths (400-700 nm), to illustrate the limited contrast in reflectance between a dry and a wet beach composed of quartz sand.

8.4.2 Practical applications

The findings of our laboratory spectroscopy experiment imply that optical remote sensing of surface moisture is most effective when measuring in the near- and short-wave infrared. These wavelengths are strongly absorbed by water and provide sufficient contrast in the signal to differentiate intermediate moisture levels (~ 5 -25%). The water absorption peaks of 1470 and 1940 nm are effective in particular. At these wavelengths there is enough contrast in the signal to also differentiate low moisture levels (~ 0 -5%). Because of strong absorption by the atmosphere an active remote sensing technique is required, for example such as employed by [Ruessink et al. \[2014\]](#) in a subsequent field experiment.

Ruessink et al. [Ruessink et al. \[2014\]](#) tested the applicability of a RIEGL VZ-400 3D terrestrial laser scanner to derive spatially extensive moisture maps of a natural beach. The wavelength of this TLS is in the short-wave infrared at $\lambda = 1550$ nm, hence close to the water absorption peak of 1470 nm. Ruessink et al. [Ruessink et al. \[2014\]](#) deployed their scanner from a tripod at Egmond Beach in The Netherlands and collected

9 panorama scans (360° in the horizontal, 100° in the vertical, with 0.002° resolution in the horizontal and vertical). Each scan took about 10 minutes to complete and resulted in a cloud of $\sim 35,000,000$ points. Simultaneously, 69 surface scrapings (thickness of a few millimetres) were taken, which were later on processed into gravimetric moisture estimates using standard laboratory techniques. The RIEGL VZ-400 outputs reflectance in decibels, with a $1/r^2$ correction to account for the reduction of returned intensity with range r . For $r = 15 - 60$ m Ruessink et al. [2014] found a linear dependence between gravimetric surface moisture content and reflectance for the full range from dry to saturated sand. This confirms that the use of TLS with a wavelength near an absorption band is inherently more suitable to detect surface moisture over its full range than a TLS with a wavelength in the visible range (for example, Nield et al. [2014]). The linear dependence is qualitatively consistent with Eq. (8.6), as decibel is a logarithmic unit. The standard error of their best-fit line amounted to about 2.6%, which is considerably lower than reported for the photographic method of Darke and McKenna Neuman [2008], Darke et al. [2009], Delgado-Fernandez et al. [2009], Mckenna Neuman and Langston [2003], McKenna Neuman and Langston [2006].

An example of a derived moisture map is provided in Figure 8.10. It illustrates the overall increase in moisture content from the dunefoot to the waterline, with superimposed variability related to secondary morphological highs and lows, consistent with Namikas et al. [2010]. The map also shows two narrow, approximately alongshore bands of apparent lower moisture content, which correspond to car tracks. While the sand in the car tracks may actually contain less pore water e.g. due to compaction, the collected reflectance could depend on surface roughness too. The rougher car tracks may increase the reflectance relative to a flat beach surface with the same moisture content. Nonetheless, Ruessink et al. [2014]’s results illustrate the potential power of active remote sensing near a water absorption band to derive accurate surface moisture maps at a spatial and temporal resolution infeasible with other techniques. A future publication will describe and analyze Ruessink et al.’s Ruessink et al. [2014] TLS data more extensively.

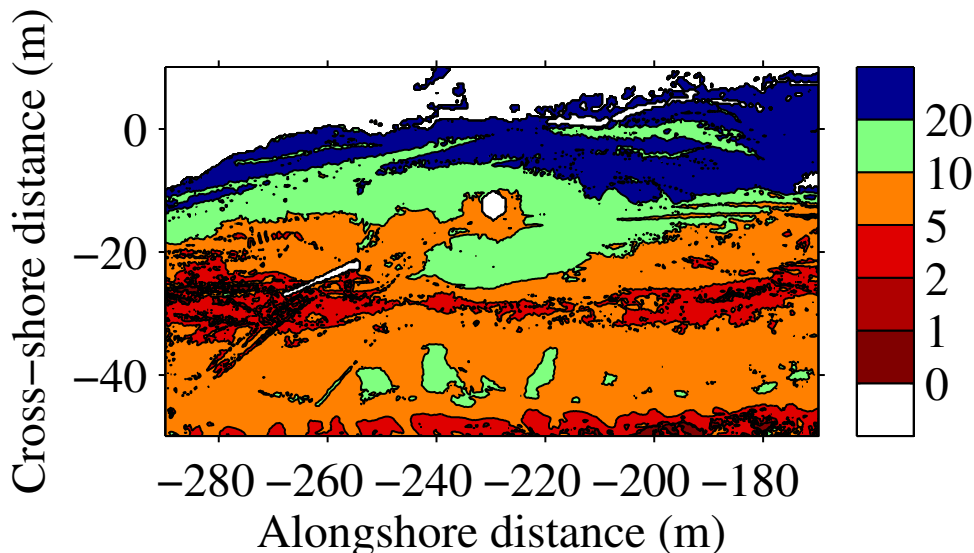


FIGURE 8.10: Example gravimetric moisture content (in %) map, estimated from the reflectance collected with a RIEGL VZ-400 3D terrestrial laser scanner at Egmond aan Zee, The Netherlands, from the upper dry beach (cross-shore distance $x \approx -50$ m) to the water line ($x \approx -10$ to 10 m) Ruessink et al. [2014]. The local co-ordinates are positive in the seaward direction and to the south. The scanner was located at $(x, y) \approx (-15, -230)$ m. The slightly drier sand immediately around the scanner position is an artifact of the conversion from intensity to reflectance; close to the scanner, as also noted by Nield et al. [2014], the imposed $1/r^2$ correction does not apply. The narrow bands with apparent lower moisture content (e.g. at alongshore y distances -200 to -180 m and $x \approx -15$ m) correspond to car tracks.

8.5 Conclusions

In this study the effect of surface moisture content on spectral reflectance of coastal beach sand is measured and modeled for the the full optical domain of 350-2100 nm, to support practical applications for optical remote sensing of surface moisture. It is shown that:

- The effect of surface moisture on spectral reflectance of coastal beach sand can be described by an optical as well as a soil physical model.
- Near- and short-wave infrared wavelengths are most effective for relating surface moisture content to reflectance due to strong absorption of light in water.

- A terrestrial laser scanner operating at $\lambda = 1550$ nm can derive accurate surface moisture maps at a high spatio-temporal resolution.

Acknowledgments

CN was funded by NatureCoast, a project of technology foundation STW, applied science division of the Netherlands Organisation for Scientific Research (NWO). GR acknowledges additional funding by NWO through Vici project 13709. The authors thank Professor W.D. Philpot for his constructive review.

Chapter 9

Synthesis: Beach sand dynamics: measurements, models and scales

9.1 Beach sand dynamics: measurements, models and scales

With the recent attention of the impact of climate-change and sea-level rise on beach and dune dynamics, aeolian research is in the center of attention in the Netherlands [e.g. [De Vries et al., 2012](#), [Keijsers et al., 2014a,b](#), [Stive et al., 2013](#)], as aeolian processes are the driver behind dune development. Historically, the beach-dune system would migrate inland in times of sea-level rise. However, nowadays, this inland migration is perceived as undesirable and therefore prevented to preserve housing and infrastructure in densely populated areas such as the Netherlands. In order to maintain the coastal zone as a buffer against the destructive forces of the sea, beach nourishments have become a common method to replenish negative sediment budgets. For example, in a recent (2011) mega-nourishment, 21.5 Mm^3 was applied to part of the Dutch coast in order to mitigate coastal recession. A single nourishment is expected to be more efficient, economic, and environmentally friendly compared to regular low-scale nourishments, as it should stabilize the coastline and feed adjacent coastal sections over an extended length of time [[Mulder and Tonnon, 2010](#), [Stive et al., 2013](#)]. In this so-called 'sand engine' project aeolian sediment transport is an integral part of a large scale research project, next to

studies on e.g. hydrodynamic, flora and fauna related aspects. Scientific research on aeolian transport processes is important to understand the impact and contribution of these processes on coastal fore-dune development and dune ecology. However, accurate and reliable measurement and analysis methods are required to collect empirical data and falsify or validate hypothesis and theories. The aim of this thesis is to explore, challenge and improve current technologies and methodologies to measure, analyse and model beach sand dynamics through a range of spatial and temporal scales. The following section formulates an answer to the research questions that were posed in Chapter 1 of this thesis.

I. What are the current measurement techniques to measure aeolian saltation, how reliable are they and can they be improved?

Aeolian saltation is measured using passive traps and active electronic sensors. Passive traps come in different shapes and sizes, but can be categorized into traps that involve a single chamber and traps that consist of different compartments, so that the flux profile can be measured, thus providing a more data rich solution compared to single chamber traps. Traps that consists of different compartments were used and studied in detail in Chapters 4, 6 and 7 of this thesis. It is shown that the reliability of these traps depends on the specific configuration of the compartments, i.e. the distance from the surface, but also the spacing between the compartments. Moreover, the reliability is also dependent on how the vertical flux profile is described. In Chapter 4, five different often applied regressions curves were fitted through measurements obtained in a windtunnel. The analysis shows that the regression method determines the final flux estimation to a large extent. In Chapter 6, it is shown that errors that originate from the specific setup are larger for fine sediment compared to coarse sediment, as for fine sediment, a larger portion of the sediment is transported close to the surface. Furthermore, it is shown that these errors can be identified using the relative sediment flux (chapter 6). This thesis reveals that it is recommendable to use multiple traps, especially near the surface

to obtain better and more reliable observational data. Preferably, an exponential decay function should be used to describe the mass fluxes obtained by such measurements.

Active sensing devices either use acoustic, piezoelectric or optical detection methods. While all these techniques are able to detect saltation and give an approximation of saltation intensity, they are not reliable in quantification of sediment fluxes. The first elaborate methodology to quantify aeolian saltation using acoustic sensors was presented in Chapters 4 and 5 of this thesis. It is shown that acoustic measurement techniques can be improved by filtering, rectification and integration of the analogue signal of acoustic sensors. This methodology allows future high frequency measurements that will create valuable data for aeolian research, especially with regard to assess aeolian saltation.

A reliable method to measure surface moisture content was described in Chapter 8. A remote sensing approach was used, as conventional moisture probes do not acquire reliable data on a sandy coast due to varying salinity levels. Moreover, they do not cover the spatio-temporal resolution relevant for aeolian processes. The method provides a reliable method to quantify surface moisture levels using specific water absorption wavelengths. The presented method is a significant improvement compared to previous studies, which measured in the visible part of the spectrum not using specific water absorption bands. Whereas previous studies reported a standard error of about 10%, the method present in this thesis can accurately relate surface moisture to reflectance with a standard error of 2.6%.

II. Is it possible to measure aeolian sediment transport in a coastal environment on meso scale (weeks to months)?

There only exist few studies that examine aeolian sediment transport on a field-scale on temporal scales from weeks to months for coastal environments [[Delgado-Fernandez and Davidson-Arnott, 2011a](#), [Lynch et al., 2013](#)]. Chapter 5 of this thesis is the first

study to apply a comprehensive grid of sediment traps on a wide beach to study sediment transport dynamics. It was found that current measurement techniques for aeolian sediment transport provide data with relatively coarse spatial and temporal resolutions. Whereas these techniques allow to identify qualitative relations between the processes in the field, they are not suitable to quantify these processes in detail. Chapter 5 shows that, to understand and quantify the drivers of the system, it is necessary to acquire high spatial and temporal resolution data on sediment transport rates, topography, surface moisture, fetch, meteorological conditions and erosion and deposition patterns. So far, field-scale studies have seriously been hampered by the lack of high quality data of sufficient resolution. More sophisticated and robust equipment are required to quantitatively assess wind erosion at the field scale. As technology improves fast, Chapter 5 recommends also to include state-of-the-art techniques to obtain high resolution elevation data using drones. Spatial explicit surface moisture measurements should be obtained as well for instance using optical remote sensing in specific water absorption bands, as described in Chapter 8. Fast-temporal data on aeolian sediment transport can be obtained using a vertical stack of instruments that rely on acoustic technology, as suggested in Chapters 4 and 5. Active samplers are preferred above passive samplers as they acquire data on a higher temporal resolution and are less labour intensive. Wind profiles should be measured at several locations at sandy coasts, as dune morphology influences the wind flow patterns.

III. What are the regulating factors and processes on aeolian transport fluxes in coastal environments at different scales?

Chapters 4 and 5 contain data from several field experiments where aeolian transport fluxes were measured on an event scale. In a beach environment, on the small scale (point and second), aeolian sediment transport is dominated by aeolian streamers which are highly variable in space and time and generated by instantaneous wind gusts. With averaging in time, the variability in space and time decreases. Chapter 5 shows that, on the event scale, variability in aeolian sediment transport rates are linked to meteorology

and local conditions such as beach surface moisture, groundwater, topology and the presence vegetation. The data show that there is a considerable amount of variability between events. Moderate events are capable of transporting a large portion of the total observed sediment transport during a certain period of time. Another publication [Keijsers et al., 2014b] of the author of this thesis shows that annual dune growth, the net effect of aeolian sediment transport, is rather stable throughout the years and, contrary to most theories, weakly correlated with meteorological conditions. However, due to the limited amount of long-term quantitative data on dune development and aeolian transport rates, it is not possible to link these processes and quantify the effect of all factors and processes on net transport rates. Spatially explicit data on all regulating factors and processes are required to quantify their contribution to net dune growth volumes. Techniques presented in Chapter 4 and 5 to quantify aeolian transport fluxes with a high temporal resolution and the remote sensing techniques presented in Chapter 8 to obtain spatial explicit surface moisture estimations should provide new insights into the processes. These techniques combined with new assessment approaches such as automated stereo-photogrammetry to obtain high resolution maps of the surface elevation offers exciting opportunities to quantify regulating factors and processes across a range of spatio-temporal scales.

IV. What possibilities offer the recent advances in computational techniques for the field of aeolian research?

There is a wide variety of model approaches available to describe sediment transport processes in different geographical settings and conditions. While a lot of work has been done with physically based models, cellular automata or simple empirical formulations, the potential of particle based models has not been fully explored so far. For this purpose, a state-of-the art computational technique on the Graphical Processing Unit (GPU) was investigated and applied in Chapter 3 of this thesis. GPU model implementation allows for substantial reductions in computation time, as a large number of calculations can be performed in parallel. In Chapter 3, sand grain interactions were

simulated on a particle scale using a simple contact model and gravity processes. Model results showed non-linear scale-invariant behaviour, which was in agreement with previous studies and analogue experiments. Despite reduction in computation times with a highly efficient implementation on the Graphical Processing Unit (GPU), it is not yet possible to use this visually appealing approach to simulate aeolian processes on the larger scale. However, with the ever increasing computational power, it is expected that this method offers great potential in the future to model aeolian processes in far more detail across a range of spatial and temporal scales than possible at the present.

9.2 Discussion

The collection of Chapters presented in this thesis show that the field of aeolian research in a coastal environment is in a relatively early stage. Chapters 4, 5, 6 and 8 are specifically focussed on measurement methodologies and protocols to acquire process related data. Chapter 7 aims to gain insight into event scale aeolian transport patterns and magnitudes, although a lot of attention was paid to measurement approaches also. At present, there are no reliable standardized methodologies to measure and analyse aeolian transport processes in sufficient detail [Barchyn et al., 2011]. Specific tailor-made equipment is required in this field of research. By quantifying uncertainties and enhancing measurement protocols, it is possible to acquire data that can be used for the development and evaluation of theories and models, leading to better understanding of beach sand dynamics and impacts as indicated in Chapter 1. The Chapters presented in this thesis make an important contribution to recent research on sandy coasts worldwide and builds further upon work presented by e.g Barchyn and Hugenholtz [2010], Barchyn et al. [2011, 2014a], Delgado-Fernandez and Davidson-Arnott [2011a], Ellis et al. [2009a], Ridge et al. [2011], Schönfeldt [2012], Sherman et al. [2011], Van Pelt et al. [2009], Yurk et al. [2013]. This thesis provides an overview of the understanding of beach sand dynamics, especially with regard to measurements, model and scale issues.

Aeolian transport processes are often mentioned in a negative context, for instance in relation to occurrence of dust storms and land degradation. In Chapter 1, it is demonstrated that there are also a large number of beneficial effects related to aeolian transport processes, such as offside fertilization, dune development and creating potential for ecological succession. Large scale nutrient dynamics play an important societal role, as e.g. African dust fertilizes the ocean and even parts of the Amazon which stimulates plant growth [Swap et al., 1992]. In coastal environments, safety of people and their living environment is of utmost importance. Regulating aeolian processes are often studied on a relatively small scale (meters and minutes), and such studies provide relevant information on the fundamental processes that govern aeolian sediment transport but do not necessary address coastal safety or ecological succession aspects as these need to be studied on a wider spatial and temporal scale. This thesis presents methods and qualitative evidence to measure aeolian processes from the point to the beach scale, which is of relevance for coastal management as a whole. However, measuring processes across scales require an integrated dense network of observation points, which is time and resource consuming. Moreover, within this context, erosional hydrodynamic processes are often felt to be more important than dune building wind driven processes [De Vries et al., 2012, Keijsers et al., 2014b] and are therefore generally felt more relevant to society.

The Chapters in this thesis are closely linked to current themes and debates in the field of aeolian research on e.g. instrument development and testing, meso-scale sediment transport processes and modelling approaches. Where Chapter 2 explores current concepts in aeolian research, Chapter 3 focusses on using an advanced particle based model to simulate sediment transport processes and interactions between individual sand particles. Chapters 4 and 5 make an important contribution to the use of acoustic technology in aeolian research to quantify aeolian saltation. The work is complementary to, and building further upon the work of Ellis et al. [2009b], Schönfeldt [2012], Sherman et al. [2011], Spaan and van den Abeele [1991], Yurk et al. [2013], and a discussion of

Hugenholtz and Barchyn [2011b], Li et al. [2011] on noise filtering and signal processing. In Chapter 5, an elaborated processing scheme was described to filter and process receiving signals in order to quantitatively measure fast-temporal aeolian sediment fluxes. Chapters 4 and 6 confirm earlier work of Ellis et al. [2009a], demonstrating that there are several methodological ambiguities in current aeolian measurement and analysis methods. The Chapters identify the need for a standardized measurement methods, as noted by Barchyn et al. [2011]. Chapter 7 deals with determining sediment transport across an entire beach during multiple events using a dense network of sediment traps. Only two other studies [Delgado-Fernandez and Davidson-Arnott, 2011a, Lynch et al., 2013] used a similar scale, but a less comprehensive setup. Lynch et al. [2013] measured alongshore variability in aeolian transport under offshore winds. The work of Delgado-Fernandez and Davidson-Arnott [2011a] provided the first long-term record of aeolian sediment transport, using a combination of qualitative observations from hourly photographs, saltation probes and ED pins. In Chapter 8, the potential of optical remote sensing to assess surface moisture was fully explored. Results obtained indicate methodological inconsistencies of the method used by Darke and McKenna Neuman [2008], Darke et al. [2009], Delgado-Fernandez et al. [2009], McKenna Neuman and Langston [2003], McKenna Neuman and Langston [2006], Nield et al. [2014], Nield and Wiggs [2011], Nield et al. [2011], who estimated surface moisture using spectral reflectance in the visible part of the radio magnetic spectrum. The approach presented in this thesis confirms findings of Edwards et al. [2013, 2012], who applied a similar method to measure surface moisture using specific water absorption bands of the radio magnetic spectrum, although their approach was less elaborate.

Chapter 3 illustrates that it is not possible at present to derive a fully deterministic model to simulate beach sand dynamics in all its details across spatial and temporal scales. Different types of model approaches can be applied for different purposes and scales, ranging from deterministic, empirical to statistical ones. In general, variability decreases from small to the larger scales, as shown in this thesis. In Chapter 5 it

is shown that the correlation between the output of two miniphones, while measuring salation, significantly increases by averaging over larger temporal domains. Chapters 6 and 7 and the work of [Keijsers et al. \[2014b\]](#) also show that the variability in aeolian transport rates decreases when moving to larger spatio-temporal domains. At the scale of fore-dune formation, the process is mainly steered by storm frequency and intensity, which exhibits power law behaviour, a mathematical formulation similar to frequency and magnitude distribution of avalanches, as shown in Chapter 3. Mathematical formulations that describe the system response using such simple empirical formulations are very useful to describe system response and e.g. identify whether a system is moving towards a point of criticality. Investigating system behaviour of aeolian processes at any scale connects it to current themes in scientific research. However, process oriented research to better understand particle interactions and responses and related deterministic modelling approaches are essential also to unravel regulating mechanisms and key properties and variables.

9.3 Research challenges and future research directions

This thesis advanced the state of knowledge on the field of aeolian beach sand dynamics. Specifically, the different Chapters provide a comprehensive analysis of a range of measurement, model and analysis methodologies, give guidelines on how to measure aeolian sediment transport processes and presents enhancements in existing measurement and modelling technologies. In the field of aeolian research, a lot of work has been done the last decades, which has significantly improved the understanding of the processes involved. Important remaining questions in the field of aeolian sediment transport, as also recognized by e.g. [Barchyn et al. \[2014b\]](#), [Kok et al. \[2012\]](#) are on the effect of saltation intermittency on time-averaged saltation properties and the mismatch between empirical data and models. The fundamental mismatch between field measurements and mathematical models impedes predictions on aeolian transport rates at a variety of scales [[Delgado-Fernandez and Davidson-Arnott, 2011a](#), [Sherman, 1995](#)]. Advances in

our understanding on both the small and the large scale is largely dependent on adequate equipment, longitudinal studies and sufficient resources to support such projects. The rapid advances in domains such as photogrammetry, hyperspectral imaging, computational science and environmental monitoring offer exciting new opportunities to obtain high resolution (both in space and time) datasets on important processes and controls such as morphology, surface moisture and wind flow. These new insight are interesting from a scientific point of view, as they enhance our understanding of the fundamental processes, but also provide societal relevant information for e.g. policy makers and environmental management.

Bibliography

- Aegerter, C.M., Lörincz, K.A., Welling, M.S., Wijngaarden, R.J., 2004. Extremal dynamics and the approach to the critical state: Experiments on a three dimensional pile of rice. *Phys. Rev. Lett.* 92, 058702.
- Al-Awadhi, J., Al-Helal, A., Al-Enezi, A., 2005. Sand drift potential in the desert of kuwait. *Journal of arid environments* 63, 425–438.
- Anderson, R.S., Bunas, K.L., 1993. Grain size segregation and stratigraphy in aeolian ripples modelled with a cellular automaton .
- Ångström, A., 1925. The albedo of various surfaces of ground. *Geografiska Annaler* 7, 323–342.
- Anthony, E., Vanhee, S., Ruz, M.H., 2006. Short-term beach-dune sand budgets on the north sea coast of france: Sand supply from shoreface to dunes, and the role of wind and fetch. *Geomorphology* 81, 316–329.
- Anthony, E.J., Ruz, M.H., Vanhée, S., 2009. Aeolian sand transport over complex intertidal bar-trough beach topography. *Geomorphology* 105, 95–105.
- Arens, S., 1996a. Patterns of sand transport on vegetated foredunes. *Geomorphology* 17, 339–350.
- Arens, S., 1996b. Rates of aeolian transport on a beach in a temperate humid climate. *Geomorphology* 17, 3–18.
- Arens, S., 1997. Transport rates and volume changes in a coastal foredune on a dutch wadden island. *Journal of Coastal Conservation* 3, 49–56.
- Arens, S., Baas, A., Van Boxel, J., Kalkman, C., 2001. Influence of reed stem density on foredune development. *Earth Surface Processes and Landforms* 26, 1161–1176.
- Arens, S., Slings, Q., De Vries, C., 2004. Mobility of a remobilised parabolic dune in kennemerland, the netherlands. *Geomorphology* 59, 175–188.
- Arens, S.M., Mulder, J.P., Slings, Q.L., Geelen, L.H., Damsma, P., 2013. Dynamic dune management, integrating objectives of nature development and coastal safety: Examples from the netherlands. *Geomorphology* 199, 205–213.
- Atherton, R., Baird, A., Wiggs, G., 2001. Inter-tidal dynamics of surface moisture content on a meso-tidal beach. *Journal of Coastal Research* 17, 482–489.

- Baas, A., 2008. Challenges in aeolian geomorphology: investigating aeolian streamers. *Geomorphology* 93, 3–16.
- Baas, A., 2012. Modelling landscape dynamics resulting from interactions between vegetation and sediment transport by wind over a range of spatio-temporal scales. *Agro Environ* 2012 .
- Baas, A., Nield, J., 2007. Modelling vegetated dune landscapes. *Geophysical Research Letters* 34.
- Baas, A., Sherman, D., 2005. Formation and behavior of aeolian streamers. *Journal of Geophysical Research F: Earth Surface* 110.
- Baas, A.C., 2002. Chaos, fractals and self-organization in coastal geomorphology: simulating dune landscapes in vegetated environments. *Geomorphology* 48, 309–328.
- Baas, A.C., 2004. Evaluation of saltation flux impact responders (safires) for measuring instantaneous aeolian sand transport intensity. *Geomorphology* 59, 99 – 118.
- Baas, A.C., 2007. Complex systems in aeolian geomorphology. *Geomorphology* 91, 311–331.
- Baas, A.C., Nield, J.M., 2010. Ecogeomorphic state variables and phase-space construction for quantifying the evolution of vegetated aeolian landscapes. *Earth Surface Processes and Landforms* 35, 717–731.
- Baas, A.C., Sherman, D.J., 2006. Spatiotemporal variability of aeolian sand transport in a coastal dune environment. *Journal of Coastal Research* , 1198–1205.
- Bagnold, R.A., 1941. *The physics of blown sand and desert dunes*. Methuen, London.
- Bak, P., Christensen, K., Danon, L., Scanlon, T., 2002. Unified scaling law for earthquakes. *Physical Review Letters* 88, 1785011–1785014.
- Bak, P., Sneppen, K., 1993. Punctuated equilibrium and criticality in a simple model of evolution. *Physical review letters* 71, 4083–4086.
- Bak, P., Tang, C., Wiesenfeld, K., 1987. Self-organized criticality: An explanation of the 1/f noise. *Physical Review Letters* 59, 381–384.
- Ballarini, M., Wallinga, J., Murray, A., Van Heteren, S., Oost, A., Bos, A., Van Eijk, C., 2003. Optical dating of young coastal dunes on a decadal time scale. *Quaternary Science Reviews* 22, 1011–1017.
- Barabási, A., Stanley, H., 1995. *Fractal Concepts in Surface Growth*. Cambridge University Press.
- Barchyn, T.E., Hugenholtz, C.H., 2010. Field comparison of four piezoelectric sensors for detecting aeolian sediment transport. *Geomorphology* 120, 368–371.
- Barchyn, T.E., Hugenholtz, C.H., Ellis, J.T., 2011. A call for standardization of aeolian process measurements: moving beyond relative case studies. *Earth Surface Processes and Landforms* 36, 702–705.
- Barchyn, T.E., Hugenholtz, C.H., Li, B., Neuman, C.M., Steven Sanderson, R., 2014a. From particle counts to flux: wind tunnel testing and calibration of the ‘wenglor’ aeolian sediment transport sensor. *Aeolian Research* .
- Barchyn, T.E., Martin, R.L., Kok, J.F., Hugenholtz, C.H., 2014b. Fundamental mismatches between measurements and models in aeolian sediment transport prediction: The role of small-scale variability.

- Aeolian Research* 15, 245–251.
- Basaran, M., Erpul, G., Uzun, O., Gabriels, D., 2011. Comparative efficiency testing for a newly designed cyclone type sediment trap for wind erosion measurements. *Geomorphology* 130, 343–351.
- Bauer, B., Davidson-Arnott, R., Hesp, P., Namikas, S., Ollerhead, J., Walker, I., 2009. Aeolian sediment transport on a beach: Surface moisture, wind fetch, and mean transport. *Geomorphology* 105, 106–116.
- Bauer, B., Houser, C., Nickling, W., 2004. Analysis of velocity profile measurements from wind-tunnel experiments with saltation. *Geomorphology* 59, 81–98.
- Bauer, B., Yi, J., Namikas, S., Sherman, D., 1998. Event detection and conditional averaging in unsteady aeolian systems. *Journal of Arid Environments* 39, 345–375.
- Bauer, B.O., Davidson-Arnott, R.G., 2003. A general framework for modeling sediment supply to coastal dunes including wind angle, beach geometry, and fetch effects. *Geomorphology* 49, 89–108.
- Bauer, B.O., Sherman, D.J., Wolcott, J.F., 1992. Sources of uncertainty in shear stress and roughness length estimates derived from velocity profiles*. *The Professional Geographer* 44, 453–464.
- Bawden, R., 1997. The community challenge: the learning response, in: invited plenary paper, 29th Annual International Meeting of the Community Development Society, Athens, Georgia, pp. 27–30.
- Bell, N., Yu, Y., Mucha, P., 2005. Particle-based simulation of granular materials, pp. 77–86.
- Belly, P.Y., 1962. Sand movement by wind. Technical Report. DTIC Document.
- Best, J., 1993. On the interactions between turbulent flow structure, sediment transport and bedform development: some considerations from recent experimental research. *Turbulence: Perspectives on Flow and sediment transport* , 61–92.
- Beven, K., 1993. Prophecy, reality and uncertainty in distributed hydrological modelling. *Advances in water resources* 16, 41–51.
- Beven, K., 2006. A manifesto for the equifinality thesis. *Journal of hydrology* 320, 18–36.
- Blaikie, P., et al., 1985. *The political economy of soil erosion in developing countries*. Longman.
- Bohren, C.F., Huffman, D.R., 2008. *Absorption and scattering of light by small particles*. John Wiley & Sons.
- Bowers, S., Hanks, R., 1965. Reflection of radiant energy from soils. *Soil Science* 100, 130–138.
- Buck, I., Foley, T., Horn, D., Sugerman, J., Fatahalian, K., Houston, M., Hanrahan, P., 2004. Brook for gpus: stream computing on graphics hardware, in: *ACM Transactions on Graphics (TOG)*, ACM. pp. 777–786.
- Buckley, R., 1987. The effect of sparse vegetation on the transport of dune sand by wind. *Nature* , 426–428.
- Buerkert, A., Lamers, J., 1999. Soil erosion and deposition effects on surface characteristics and pearl millet growth in the west african sahel†. *Plant and soil* 215, 239–253.

- Bochev-Van der Burgh, L., Wijnberg, K., Hulscher, S., 2011. Decadal-scale morphologic variability of managed coastal dunes. *Coastal engineering* 58, 927–936.
- Burks, A.W., 1970. *Essays on cellular automata*. University of Illinois Press.
- Burri, K., Gromke, C., Lehning, M., Graf, F., 2011. Aeolian sediment transport over vegetation canopies: a wind tunnel study with live plants. *Aeolian Research* 3, 205–213.
- Buschiazzo, D.E., Zobeck, T.M., 2008. Validation of weq, rweq and weps wind erosion for different arable land management systems in the argentinean pampas. *Earth surface processes and landforms* 33, 1839–1850.
- Buscombe, D., Rubin, D., 2012. Advances in the simulation and automated measurement of well-sorted granular material: 1. simulation. *Journal of Geophysical Research: Earth Surface* 117.
- Buscombe, D., Rubin, D., Warrick, J., 2010. A universal approximation of grain size from images of noncohesive sediment. *Journal of Geophysical Research: Earth Surface* 115.
- Butterfield, G.R., 1998. Transitional behaviour of saltation: wind tunnel observations of unsteady winds. *Journal of Arid Environments* 39, 377–394.
- Butterfield, G.R., 1999a. Application of thermal anemometry and high-frequency measurement of mass flux to aeolian sediment transport research. *Geomorphology* 29, 31–58.
- Butterfield, G.R., 1999b. Near-bed mass flux profiles in aeolian sand transport: high-resolution measurements in a wind tunnel. *Earth Surface Processes and Landforms* 24, 393–412.
- Buzsáki, G., Draguhn, A., 2004. Neuronal oscillations in cortical networks. *Science* 304, 1926–1929.
- Castro, I.P., Wiggs, G.F., 1994. Pulsed-wire anemometry on rough surfaces, with application to desert sand dunes. *Journal of Wind Engineering and Industrial Aerodynamics* 52, 53–71.
- Chang, K.J., Taboada, A., 2009. Discrete element simulation of the jiufengershan rock-and-soil avalanche triggered by the 1999 chi-chi earthquake, taiwan. *Journal of Geophysical Research: Earth Surface* 114.
- Chapman, C., Walker, I.J., Hesp, P.A., Bauer, B.O., Davidson-Arnott, R.G., Ollerhead, J., 2013. Reynolds stress and sand transport over a foredune. *Earth Surface Processes and Landforms* 38, 1735–1747.
- Chappell, A., 1999. The limitations of using $\int_{sup} \int_{sup}$ cs for estimating soil redistribution in semi-arid environments. *Geomorphology* 29, 135–152.
- Chappell, A., McTainsh, G., Leys, J., Strong, C., 2003. Simulations to optimize sampling of aeolian sediment transport in space and time for mapping. *Earth Surface Processes and Landforms* 28, 1223–1241.
- Chappell, A., Warren, A., Oliver, M., Charlton, M., 1998. The utility of \int_{sup} cs for measuring soil redistribution rates in southwest niger. *Geoderma* 81, 313–337.
- Chepil, W., 1956. Influence of moisture on erodibility of soil by wind. *Soil Science Society of America Journal* 20, 288–292.

- Chepil, W., 1957. Width of field strips to control wind erosion. Technical bulletin (Kansas Agricultural Experiment Station), Agricultural Experiment Station, Kansas State College of Agriculture and Applied Science.
- Chepil, W., Siddoway, F., Armbrust, D., 1964. Prevailing wind erosion direction. *Journal of soil and water conservation* 19, 67–71.
- Chepil, W., Woodruff, N., 1963. The physics of wind erosion and its control. *Advances in agronomy* 15, 211–302.
- Cheung, K.F., Gerritsen, F., Cleveringa, J., 2007. Morphodynamics and sand bypassing at ameland inlet, the netherlands. *Journal of Coastal Research* , 106–118.
- Christensen, K., Danon, L., Scanlon, T., Bak, P., 2002. Unified scaling law for earthquakes. *Proceedings of the National Academy of Sciences* 99, 2509–2513.
- Ciani, A., Goss, K.U., Schwarzenbach, R., 2005. Light penetration in soil and particulate minerals. *European journal of soil science* 56, 561–574.
- Cont, R., Bouchaud, J.P., 2000. Herd behavior and aggregate fluctuations in financial markets. *Macroeconomic Dynamics* 4, 170–196.
- Copeland, N., Sharratt, B., Wu, J., Foltz, R., Dooley, J., 2009. A wood-strand material for wind erosion control: Effects on total sediment loss, pm vertical flux, and pm loss. *Journal of environmental quality* 38, 139–148.
- Cornelis, W., Erpul, G., Gabriëls, D., 2004a. The I.C.E. wind tunnel for wind and water interaction research. Wageningen University and Research Centre. Wind and rain interaction in erosion, pp. 195–224.
- Cornelis, W., Gabriëls, D., 2003. The effect of surface moisture on the entrainment of dune sand by wind: an evaluation of selected models. *Sedimentology* 50, 771–790.
- Cornelis, W.M., Gabriëls, D., Hartmann, R., 2004b. A parameterisation for the threshold shear velocity to initiate deflation of dry and wet sediment. *Geomorphology* 59, 43–51.
- Cornelis, W.M., Gabriëls, D., Hartmann, R., 2004c. A parameterisation for the threshold shear velocity to initiate deflation of dry and wet sediment. *Geomorphology* 59, 43 – 51. *Aeolian Research: processes, instrumentation, landforms and palaeoenvironments*.
- Coulthard, T., Hicks, D., Van De Wiel, M.J., 2007. Cellular modelling of river catchments and reaches: Advantages, limitations and prospects. *Geomorphology* 90, 192–207.
- Coulthard, T.J., Van De Wiel, M.J., 2007. Quantifying fluvial non linearity and finding self organized criticality? insights from simulations of river basin evolution. *Geomorphology* 91, 216–235.
- Craig, M.S., 2000. Aeolian sand transport at the lanphere dunes, northern california. *Earth Surface Processes and Landforms* 25, 239–253.
- Cundall, P., Strack, O., 1979. Discrete numerical model for granular assemblies. *Geotechnique* 29, 47–65.

- Cundall, P.A., 1971. A computer model for simulating progressive, large-scale movements in blocky rock systems, in: Proc. Symp. Int. Rock Mech., Nancy.
- Damsgaard, A., Egholm, D.L., Piotrowski, J.A., Tulaczyk, S., Larsen, N.K., Tylmann, K., 2013. Discrete element modeling of subglacial sediment deformation. *Journal of Geophysical Research: Earth Surface* 118, 2230–2242.
- Darke, I., McKenna Neuman, C., 2008. Field study of beach water content as a guide to wind erosion potential. *Journal of Coastal Research* 24, 1200–1208.
- Darke, I., Robin, D.A., Ollerhead, J., 2009. Measurement of beach surface moisture using surface brightness. *Journal of Coastal Research* 25, 248–256.
- Davidson-Arnott, R., Bauer, B., 2009. Aeolian sediment transport on a beach: Thresholds, intermittency, and high frequency variability. *Geomorphology* 105, 117 – 126.
- Davidson-Arnott, R., Bauer, B., Walker, I., Hesp, P., Ollerhead, J., Delgado-Fernandez, I., 2009. Instantaneous and mean aeolian sediment transport rate on beaches: an intercomparison of measurements from two sensor types. *Journal of Coastal Research* , 297–301.
- Davidson-Arnott, R.G., 2005. Conceptual model of the effects of sea level rise on sandy coasts. *Journal of Coastal Research* , 1166–1172.
- Davidson-Arnott, R.G., MacQuarrie, K., Aagaard, T., 2005. The effect of wind gusts, moisture content and fetch length on sand transport on a beach. *Geomorphology* 68, 115–129.
- Davidson-Arnott, R.G., Yang, Y., Ollerhead, J., Hesp, P.A., Walker, I.J., 2008. The effects of surface moisture on aeolian sediment transport threshold and mass flux on a beach. *Earth Surface Processes and Landforms* 33, 55–74.
- De Boer, D.H., 2001. Self-organization in fluvial landscapes: sediment dynamics as an emergent property. *Computers & Geosciences* 27, 995–1003.
- De Graaf, H., Oude Elberink, S., Bollweg, A., Brögelmann, R., Richardson, L., 2003. Inwinning droge jarkus profielen langs nederlandse kust. Delft, The Netherlands: Rijkswaterstaat , 43.
- De Jong, B., Keijsers, J.G., Riksen, M.J., Krol, J., Slim, P.A., 2014. Soft engineering vs. a dynamic approach in coastal dune management: A case study on the north sea barrier island of ameland, the netherlands. *Journal of Coastal Research* .
- De Ploey, J., Gabriels, D., 1980. Measuring soil loss and experimental studies. status: published .
- De Vries, S., Southgate, H., Kanning, W., Ranasinghe, R., 2012. Dune behavior and aeolian transport on decadal timescales. *Coastal Engineering* 67, 41–53.
- De Vries, S., van Thiel de Vries, J., van Rijn, L., Arens, S., Ranasinghe, R., 2014. Aeolian sediment transport in supply limited situations. *Aeolian Research* 12, 75–85.
- Delgado-Fernandez, I., 2010. A review of the application of the fetch effect to modelling sand supply to coastal foredunes. *Aeolian Research* 2, 61–70.

- Delgado-Fernandez, I., Davidson-Arnott, R., 2011a. Meso-scale aeolian sediment input to coastal dunes: The nature of aeolian transport events. *Geomorphology* 126, 217–232.
- Delgado-Fernandez, I., Davidson-Arnott, R., 2011b. Meso-scale aeolian sediment input to coastal dunes: The nature of aeolian transport events. *Geomorphology* 126, 217 – 232.
- Delgado-Fernandez, I., Davidson-Arnott, R., Ollerhead, J., 2009. Application of a remote sensing technique to the study of coastal dunes. *Journal of Coastal Research* 25.
- Dong, Y., Namikas, S., Hesp, P., 2009. Vertical distribution models of sand transport rate of different grain size groups in coastal aeolian mass flux. *Geographical Research* 28, 1179 – 1187.
- Dong, Z., Liu, X., Wang, H., Zhao, A., Wang, X., 2003. The flux profile of a blowing sand cloud: a wind tunnel investigation. *Geomorphology* 49, 219–230.
- Dong, Z., Liu, X., Wang, X., Li, F., Zhao, A., 2004a. Experimental investigation of the velocity of a sand cloud blowing over a sandy surface. *Earth Surface Processes and Landforms* 29, 343–358.
- Dong, Z., Qian, G., 2007. Characterizing the height profile of the flux of wind-eroded sediment. *Environmental Geology* 51, 835–845.
- Dong, Z., Sun, H., Zhao, A., 2004b. Witseg sampler: a segmented sand sampler for wind tunnel test. *Geomorphology* 59, 119 – 129.
- Drees, L., Manu, A., Wilding, L., 1993. Characteristics of aeolian dusts in niger, west africa. *Geoderma* 59, 213–233.
- Durán, O., Claudin, P., Andreotti, B., 2011. On aeolian transport: Grain-scale interactions, dynamical mechanisms and scaling laws. *Aeolian Research* 3, 243–270.
- Durán, O., Herrmann, H.J., 2006. Vegetation against dune mobility. *Physical Review Letters* 97, 188001.
- Edwards, B.L., Namikas, S.L., D'Sa, E.J., 2013. Simple infrared techniques for measuring beach surface moisture. *Earth Surface Processes and Landforms* 38, 192–197.
- Edwards, B.L., Schmutz, P.P., Namikas, S.L., 2012. Comparison of surface moisture measurements with depth-integrated moisture measurements on a fine-grained beach. *Journal of Coastal Research* 29, 1284–1291.
- Elachi, C., Van Zyl, J.J., 2006. Introduction to the physics and techniques of remote sensing. volume 28. Wiley. com.
- Ellis, J., Li, B., Farrell, E., Sherman, D., 2009a. Protocols for characterizing aeolian mass-flux profiles. *Aeolian Research* 1, 19 – 26.
- Ellis, J., Morrison, R., Priest, B., 2009b. Detecting impacts of sand grains with a microphone system in field conditions. *Geomorphology* 105, 87–94.
- Ellis, J.T., Sherman, D.J., Farrell, E.J., Li, B., 2012. Temporal and spatial variability of aeolian sand transport: Implications for field measurements. *Aeolian Research* 3, 379 – 387.
- Farrell, E., Sherman, D., Ellis, J., Li, B., 2012. Vertical distribution of grain size for wind blown sand. *Aeolian Research* 7, 51–61.

- Feng, G., Sharratt, B., 2005. Sensitivity analysis of soil and pm10 loss in weps using the lhs-oat method. *TRANSACTIONS-AMERICAN SOCIETY OF AGRICULTURAL ENGINEERS* 48, 1409.
- Field, J.P., Breshears, D.D., Whicker, J.J., 2009. Toward a more holistic perspective of soil erosion: why aeolian research needs to explicitly consider fluvial processes and interactions. *Aeolian Research* 1, 9–17.
- Firew, A., 2010. Impact of institutional and socio-economic factors on sustainable land management investments in north western ethiopia. Wageningen, University, Wageningen .
- Fonstad, M., Marcus, W.A., 2003. Self-organized criticality in riverbank systems. *Annals of the Association of American Geographers* 93, 281–296.
- Frette, V., Christensen, K., Malthé-Sørensen, A., Feder, J., Jøssang, T., Meakin, P., 1996. Avalanche dynamics in a pile of rice. *Nature* 379, 49–52.
- Frey, P., Church, M., 2011. Bedload: A granular phenomenon. *Earth Surface Processes and Landforms* 36, 58–69.
- Fryberger, S.G., Dean, G., 1979. Dune forms and wind regime. A study of global sand seas 1052, 137–169.
- Fryrear, D., 1986. A field dust sampler. *Journal of Soil and Water Conservation* 41, 117–120.
- Fryrear, D., Chen, W., Lester, C., 2001. Revised wind erosion equation. *ANNALS OF ARID ZONE* 40, 265–279.
- Fryrear, D., Saleh, A., Bilbro, J., Schomberg, H., Stout, J., Zobeck, T., 1998. Revised wind erosion equation (rweq). wind erosion and water conservation research unit, usda-ars, southern plains area cropping systems research laboratory. Technical Bulletin 1.
- Fryrear, D., Stout, J., Hagen, L., Vories, E., 1991. Wind erosion: field measurement and analysis. *Trans. ASAE* 34, 155–160.
- Funk, R., Skidmore, E.L., Hagen, L.J., 2004. Comparison of wind erosion measurements in germany with simulated soil losses by weps. *Environmental Modelling & Software* 19, 177–183.
- Gabriëls, D., Cornelis, W., Pollet, I., VanCoillie, T., Ouassar, M., 1997. The ice wind tunnel for wind and water erosion studies. *SOIL TECHNOLOGY* 10, 1–8.
- Gao, Y., Kaufman, Y., Tanre, D., Kolber, D., Falkowski, P., 2001. Seasonal distributions of aeolian iron fluxes to the global ocean. *Geophysical Research Letters* 28, 29–32.
- Giardino, A., Mulder, J., Ronde, J.d., Stronkhorst, J., 2011. Sustainable development of the dutch coast: Present and future. *Journal of Coastal Research* , 166–172.
- Gillette, D., Stockton, P., 1986. Mass, momentum, and kinetic energy fluxes of saltating particles .
- Gillette, D.A., Fryrear, D., Xiao, J.B., Stockton, P., Ono, D., Helm, P.J., Gill, T.E., Ley, T., 1997. Large-scale variability of wind erosion mass flux rates at owens lake: 1. vertical profiles of horizontal mass fluxes of wind-eroded particles with diameter greater than 50 μm . *Journal of Geophysical Research: Atmospheres* (1984–2012) 102, 25977–25987.

- Gillette, D.A., Herbert, G., Stockton, P.H., Owen, P., 1996. Causes of the fetch effect in wind erosion. *Earth Surface Processes and Landforms* 21, 641–659.
- Ginoux, P., Chin, M., Tegen, I., Prospero, J.M., Holben, B., Dubovik, O., Lin, S.J., 2001. Sources and distributions of dust aerosols simulated with the gocart model. *Journal of Geophysical Research: Atmospheres (1984–2012)* 106, 20255–20273.
- Ginoux, P., Prospero, J.M., Torres, O., Chin, M., 2004. Long-term simulation of global dust distribution with the gocart model: correlation with north atlantic oscillation. *Environmental Modelling & Software* 19, 113–128.
- Gomes, L., Rajot, J., Gaudichet, A., 2000. Vertical profile of desert aerosol in a source area of the sahelian region. *Journal of aerosol science* 31, 285–286.
- Goossens, D., Offer, Z., London, G., 2000. Wind tunnel and field calibration of five aeolian sand traps. *Geomorphology* 35, 233–252.
- Guillén, J., Stive, M., Capobianco, M., 1999. Shoreline evolution of the holland coast on a decadal scale. *Earth Surface Processes and Landforms* 24, 517–536.
- Guzzetti, F., Malamud, B.D., Turcotte, D.L., Reichenbach, P., 2002. Power-law correlations of landslide areas in central italy. *Earth and Planetary Science Letters* 195, 169–183.
- Hagen, L., 1991. A wind erosion prediction system to meet user needs. *Journal of Soil and Water Conservation* 46, 106–111.
- Hardisty, J., 1993. Monitoring and modelling sediment transport at turbulent frequencies. *Turbulence: Perspectives on Flow and Sediment Transport: New York, John Wiley and Sons* , 35–59.
- Hawking, S.W., 1996. *The illustrated a brief history of time*. Random House LLC.
- Hecht, E., 2002. *Optics*. Addison-Wesley, San Francisco, CA.
- Held, G.A., Solina, D.H., Solina, H., Keane, D.T., Haag, W.J., Horn, P.M., Grinstein, G., 1990. Experimental study of critical-mass fluctuations in an evolving sandpile. *Phys. Rev. Lett.* 65, 1120–1123.
- Hergarten, S., 1999. Landslides, sandpiles, and self-organized criticality. *Natural Hazards and Earth System Science* 3, 505–514.
- Hergarten, S., 2002. *Self-Organized Criticality in Earth Systems*. Springer.
- Herrmann, H., Luding, S., 1998. Modeling granular media on the computer. *Continuum Mechanics and Thermodynamics* 10, 189–231.
- Herrmann, H.J., 2002. Evolution and shapes of dunes. *Comptes Rendus Physique* 3, 197–206.
- Hertz, H., 1882. Über die berührung fester elastischer körper. *Journal für die reine und angewandte Mathematik* 92, 156–171.
- Hesp, P.A., Davidson-Arnott, R., Walker, I.J., Ollerhead, J., 2005. Flow dynamics over a foredune at prince edward island, canada. *Geomorphology* 65, 71–84.
- Hillel, D., 1998. *Environmental soil physics: Fundamentals, applications, and environmental considerations*. Academic press.

- Hillen, R., Roelse, P., 1995. Dynamic preservation of the coastline in the netherlands. *Journal of Coastal Conservation* 1, 17–28.
- Holman, R., 1986. Extreme value statistics for wave run-up on a natural beach. *Coastal Engineering* 9, 527–544.
- Houser, C., 2009. Synchronization of transport and supply in beach-dune interaction. *Progress in Physical Geography* 33, 733–746.
- Houser, C., Hamilton, S., 2009. Sensitivity of post-hurricane beach and dune recovery to event frequency. *Earth Surface Processes and Landforms* 34, 613–628.
- Hsu, S.A., 1971. Wind stress criteria in eolian sand transport. *Journal of Geophysical Research* 76, 8684–8686.
- Hughenoltz, C., Wolfe, S., Walker, I., Moorman, B., 2009. Spatial and temporal patterns of aeolian sediment transport on an inland parabolic dune, bigstick sand hills, saskatchewan, canada. *Geomorphology* 105, 158–170.
- Hughenoltz, C.H., Barchyn, T.E., 2011a. Discussion of: Sherman, dj; li, b.; farrell, ej; ellis, jt; cox, wd; maia, lp, and sousa, phgo, 2011. measuring aeolian saltation: A comparison of sensors. in: Roberts, tm; rosati, jd, and wang, p.(eds.), proceedings, symposium to honor dr. nicholas kraus, journal of coastal research, special issue no. 59, pp. 280-290. *Journal of Coastal Research* 27, 1202–1205.
- Hughenoltz, C.H., Barchyn, T.E., 2011b. Laboratory and field performance of a laser particle counter for measuring aeolian sand transport. *Journal of Geophysical Research: Earth Surface* (2003–2012) 116.
- Huisman, C.E., Bryan, K.R., Coco, G., Ruessink, B., 2011. The use of video imagery to analyse groundwater and shoreline dynamics on a dissipative beach. *Continental Shelf Research* 31, 1728–1738.
- Huszar, P.C., Piper, S.L., 1986. Estimating the off-site costs of wind erosion in new mexico. *Journal of soil and water conservation* 41, 414–416.
- Idso, S., Jackson, R., Reginato, R., Kimball, B., Nakayama, F., 1975. The dependence of bare soil albedo on soil water content. *Journal of Applied Meteorology* 14, 109–113.
- Iglberger, K., Rde, U., 2010. Massively parallel granular flow simulations with non-spherical particles. *Computer Science - Research and Development* 25, 105–113.
- Illenberger, W.K., Rust, I.C., 1988. A sand budget for the alexandria coastal dunefield, south africa. *Sedimentology* 35, 513–521.
- Jackson, D., Cooper, J., 1999. Beach fetch distance and aeolian sediment transport. *Sedimentology* 46, 517–522.
- Jackson, N.L., Nordstrom, K.F., 2011. Aeolian sediment transport and landforms in managed coastal systems: A review. *Aeolian Research* 3, 181 – 196.

- Jaeger, H., Liu, C.h., Nagel, S.R., 1989. Relaxation at the angle of repose. *Physical Review Letters* 62, 40.
- Jaeger, H.M., Nagel, S.R., et al., 1992. Physics of the granular state. *Science* 255, 1523–1531.
- Jensen, H.J., Christensen, K., Fogedby, H.C., 1989. $1/f$ noise, distribution of lifetimes, and a pile of sand. *Physical Review B* 40, 7425.
- Kadib, A., 1965. A function for sand movement by wind. Technical Report. DTIC Document.
- Kaimal, J.C., Finnigan, J.J., 1994. Atmospheric boundary layer flows: their structure and measurement .
- Kalma, J., Speight, J., Wasson, R., 1988. Potential wind erosion in australia: A continental perspective. *Journal of Climatology* 8, 411–428.
- Kang, L., Guo, L., Gu, Z., Liu, D., 2008a. Wind tunnel experimental investigation of sand velocity in aeolian sand transport. *Geomorphology* 97, 438–450.
- Kang, L., Guo, L., Liu, D., 2008b. Reconstructing the vertical distribution of the aeolian saltation mass flux based on the probability distribution of lift-off velocity. *Geomorphology* 96, 1–15.
- Kármán, T.v., 1921. Über laminare und turbulente reibung. *ZAMM-Journal of Applied Mathematics and Mechanics/Zeitschrift für Angewandte Mathematik und Mechanik* 1, 233–252.
- Kawamura, R., 1951. Study on sand movement by wind (relationship between sand flow and wind friction, and vertical density distribution of sand). *Tokyo Daigaku Rikogaku Kenkyusho Hokoku*, (Tokyo) 5, 95–112.
- Keijsers, J.G., Giardino, A., Poortinga, A., Mulder, J.P., Riksen, M.J., Santinelli, G., 2014a. Adaptation strategies to maintain dunes as flexible coastal flood defense in the netherlands. *Mitigation and Adaptation Strategies for Global Change* , 1–16.
- Keijsers, J.G.S., Poortinga, A., Riksen, M.J.P.M., Maroulis, J., 2014b. Spatio-temporal variability in accretion and erosion of coastal foredunes in the netherlands: Regional climate and local topography. *PLoS ONE* 9, e91115.
- Kertész, J., Kiss, L., 1990. The noise spectrum in the model of self-organised criticality. *Journal of Physics A: Mathematical and General* 23, L433.
- Kessenich, J., Baldwin, D., Rost, R., 2004. The opengl shading language. Language version 1.
- Ketner-Oostra, R., Riksen, M., 2005. Active management for the preservation of living drift sand. Final report effect of measures at Kootwijkerzand drift sand. Final report effect of measures at Kootwijkerzand, Part 1.
- Knadel, M., Deng, F., Alinejadian, A., Wollesen de Jonge, L., Moldrup, P., Greve, M.H., 2014. The effects of moisture conditions – from wet to hyper dry – on visible near-infrared spectra of danish reference soils. *Soil Science Society of America Journal* 78, 422–433.
- Kocurek, G., Ewing, R.C., 2005. Aeolian dune field self-organization–implications for the formation of simple versus complex dune-field patterns. *Geomorphology* 72, 94–105.

- Kocurek, G., Ewing, R.C., Mohrig, D., 2010. How do bedform patterns arise? new views on the role of bedform interactions within a set of boundary conditions. *Earth Surface Processes and Landforms* 35, 51–63.
- Kok, J.F., Parteli, E.J., Michaels, T.I., Karam, D.B., 2012. The physics of wind-blown sand and dust. *Reports on Progress in Physics* 75, 106901.
- Kroon, A., Hoekstra, P., 1990. Eolian sediment transport on a natural beach. *Journal of Coastal Research* 6, pp. 367–379.
- Kroy, K., Sauermann, G., Herrmann, H.J., 2002. Minimal model for aeolian sand dunes. *Physical Review E* 66, 031302.
- Lal, R., et al., 1994. Soil erosion by wind and water: problems and prospects. *Soil erosion research methods* 2, 1–9.
- Lancaster, N., Nickling, W.G., 1994. Aeolian sediment transport, in: *Geomorphology of desert environments*. Springer, pp. 447–473.
- Larney, F., Bullock, M., McGinn, S., Fryrear, D., 1995. Quantifying wind erosion on summer fallow in southern alberta. *Journal of soil and water conservation* 50, 91–95.
- Lasage, R., Aerts, J., Mutiso, G., De Vries, A., 2008. Potential for community based adaptation to droughts: Sand dams in kitui, kenya. *Physics and Chemistry of the Earth, Parts A/B/C* 33, 67–73.
- Laurson, L., Alava, M.J., Zapperi, S., 2005. Power spectra of self-organized critical sandpiles. *Journal of Statistical Mechanics: Theory and Experiment* 2005, L11001.
- Leatherman, S., 1978. A new aeolian sand trap design. *Sedimentology* 25, 303–306.
- Lee, J., Herrmann, H.J., 1993. Angle of repose and angle of marginal stability: molecular dynamics of granular particles. *Journal of Physics A: Mathematical and General* 26, 373.
- Lee, J.A., 1987. A field experiment on the role of small scale wind gustiness in aeolian sand transport. *Earth Surface Processes and Landforms* 12, 331–335.
- Leenders, J., Van Boxel, J., Sterk, G., 2005a. Wind forces and related saltation transport. *Geomorphology* 71, 357–372.
- Leenders, J., Van Boxel, J., Sterk, G., 2007. The effect of single vegetation elements on wind speed and sediment transport in the sahelian zone of burkina faso. *Earth Surface Processes and Landforms* 32, 1454–1474.
- Leenders, J., Visser, S., Stroosnijder, L., 2005b. Farmers' perceptions of the role of scattered vegetation in wind erosion control on arable land in burkina faso. *Land Degradation & Development* 16, 327–337.
- Lekner, J., Dorf, M.C., 1988. Why some things are darker when wet. *Applied Optics* 27, 1278–1280.
- Lettau, K., Lettau, H., 1978. Experimental and micrometeorological field studies of dune migration. .
- Leu, D.J., 1977. Visible and near-infrared reflectance of beach sands: A study on the spectral reflectance/grain size relationship. *Remote Sensing of Environment* 6, 169–182.

- Li, B., 2010. Evaluating the von Kármán constant in sediment-laden air flow. Ph.D. thesis. Texas A&M University.
- Li, B., Sherman, D.J., Ellis, J.T., 2011. Reply to: Hugenholtz, ch and barchyn, te, discussion of: Sherman, dj; li, b.; farrell, ej; ellis, jt; cox, wd; maia, lp, and sousa, phgo, 2011. measuring aeolian saltation: A comparison of sensors. in: Roberts, tm; rosati, jd, and wang, p.(eds.), proceedings, symposium to honor dr. nicholas kraus, journal of coastal research, special issue no. 59, pp. 280-290. *Journal of Coastal Research* 27, 1206–1208.
- Li, F.R., Zhao, L.Y., Zhang, H., Zhang, T.H., Shirato, Y., 2004. Wind erosion and airborne dust deposition in farmland during spring in the horqin sandy land of eastern inner mongolia, china. *Soil and Tillage Research* 75, 121–130.
- Li, Y., Xu, Y., Thornton, C., 2005. A comparison of discrete element simulations and experiments for ‘sandpiles’ composed of spherical particles. *Powder Technology* 160, 219–228.
- Liffman, K., Nguyen, M., Metcalfe, G., Cleary, P., 2001. Forces in piles of granular material: an analytic and 3d dem study. *Granular matter* 3, 165–176.
- Liu, C.h., Jaeger, H.M., Nagel, S.R., 1991. Finite-size effects in a sandpile. *Phys. Rev. A* 43, 7091–7092.
- Livingstone, I., Wiggs, G.F., Weaver, C.M., 2007. Geomorphology of desert sand dunes: a review of recent progress. *Earth-Science Reviews* 80, 239–257.
- Lobell, D., Asner, G., 2002. Moisture effects on soil reflectance. *Soil Science Society of America Journal* 66, 722–727.
- Longmore, J.P., Marais, P., Kuttel, M., 2013. Towards realistic and interactive sand simulation: A gpu-based framework. *Powder Technology* 235, 983–1000.
- de Longueville, F., Henry, S., Ozer, P., 2009. Saharan dust pollution: Implications for the sahal? *Epidemiology* 20, 780.
- Luding, S., 1997. Stress distribution in static two-dimensional granular model media in the absence of friction. *Physical Review E* 55, 4720.
- Lynch, K., Delgado-Fernandez, I., Jackson, D., Cooper, J., Baas, A., Beyers, J., 2013. Alongshore variation of aeolian sediment transport on a beach, under offshore winds. *Aeolian Research* 8, 11–18.
- Lynch, K., Jackson, D., Cooper, J., 2006. A remote-sensing technique for the identification of aeolian fetch distance. *Sedimentology* 53, 1381–1390.
- Madsen, A.T., Murray, A.S., 2009. Optically stimulated luminescence dating of young sediments: a review. *Geomorphology* 109, 3–16.
- Malamud, B.D., Baas, A.C.W., 2013. [chapter] nine considerations for constructing and running geomorphological models. *Treatise on Geomorphology* 2, 6–28.
- Mancini, F., Dubbini, M., Gattelli, M., Stecchi, F., Fabbri, S., Gabbianelli, G., 2013. Using unmanned aerial vehicles (uav) for high-resolution reconstruction of topography: The structure from motion approach on coastal environments. *Remote Sensing* 5, 6880–6898.

- Mando, A., Stroosnijder, L., 1999. The biological and physical role of mulch in the rehabilitation of crusted soil in the sahel. *Soil use and management* 15, 123–127.
- Martin, R.L., Barchyn, T.E., Hugenholtz, C.H., Jerolmack, D.J., 2013. Timescale dependence of aeolian sand flux observations under atmospheric turbulence. *Journal of Geophysical Research: Atmospheres* 118, 9078–9092.
- Matuttis, H., Luding, S., Herrmann, H., 2000. Discrete element simulations of dense packings and heaps made of spherical and non-spherical particles. *Powder technology* 109, 278–292.
- McCullough, B., Heiser, D.A., 2008. On the accuracy of statistical procedures in microsoft excel 2007. *Computational Statistics & Data Analysis* 52, 4570 – 4578.
- Mckenna Neuman, C., Langston, G., 2003. Spatial analysis of surface moisture content on beaches subject to aeolian transport, in: *Proceedings of the Canadian Coastal Conference 2003*, pp. 15–17.
- McKenna Neuman, C., Langston, G., 2006. Measurement of water content as a control of particle entrainment by wind. *Earth Surface Processes and Landforms* 31, 303–317.
- McKenna Neuman, C., Maljaars Scott, M., 1998. A wind tunnel study of the influence of pore water on aeolian sediment transport. *Journal of Arid Environments* 39, 403–419.
- McKenna-Neuman, C., Nickling, W., 1989. A theoretical and wind tunnel investigation of the effect of capillary water on the entrainment of sediment by wind. *Canadian Journal of Soil Science* 69, 79–96. Cited By (since 1996)112.
- McLean, R., Shen, J.S., 2006. From foreshore to foredune: Foredune development over the last 30 years at moruya beach, new south wales, australia. *Journal of Coastal Research* 22, pp. 28–36.
- Mctainsh, G., Strong, C., 2007. The role of aeolian dust in ecosystems. *Geomorphology* 89, 39–54.
- Mehta, A., 2007. *Granular physics*. Cambridge University Press.
- Mei, F., Rajot, J., Alfaro, S., Gomes, L., Zhang, X., Wang, T., 2006. Validating a dust production model by field experiment in mu us desert, china. *Chinese Science Bulletin* 51, 878–884.
- Mendez, M., Funk, R., Buschiazzo, D., 2011. Field wind erosion measurements with big spring number eight (bsne) and modified wilson and cook (mwac) samplers. *Geomorphology* 129, 43–48.
- Mikami, M., Yamada, Y., Ishizuka, M., Ishimaru, T., Gao, W., Zeng, F., 2005. Measurement of saltation process over gobi and sand dunes in the taklimakan desert, china, with newly developed sand particle counter. *Journal of Geophysical Research: Atmospheres* (1984–2012) 110.
- Mitha, S., Tran, M., Werner, B., Haff, P., 1986. The grain-bed impact process in aeolian saltation. *Acta Mechanica* 63, 267–278.
- Mollon, G., Richefeu, V., Villard, P., Daudon, D., 2012. Numerical simulation of rock avalanches: influence of a local dissipative contact model on the collective behavior of granular flows. *Journal of Geophysical Research: Earth Surface* 117.
- Mulder, J., Tonnon, P., 2010. "sand engine": Background and design of a mega-nourishment pilot in the netherlands.

- Murray, A., Clemmensen, L.B., 2001. Luminescence dating of holocene aeolian sand movement, thy, denmark. *Quaternary Science Reviews* 20, 751–754.
- Murray, B., Fonstad, M.A., 2007. Preface: Complexity (and simplicity) in landscapes. *Geomorphology* 91, 173–177.
- Namikas, S., Bauer, B., Edwards, B., Hesp, P., Zhu, Y., 2009. Measurements of aeolian mass flux distributions on a fine-grained beach: implications for grain-bed collision mechanics. *Journal of Coastal Research* , 337–341.
- Namikas, S., Edwards, B., Bitton, M., Booth, J., Zhu, Y., 2010. Temporal and spatial variabilities in the surface moisture content of a fine-grained beach. *Geomorphology* 114, 303 – 310.
- Namikas, S.L., 2003. Field measurement and numerical modelling of aeolian mass flux distributions on a sandy beach. *Sedimentology* 50, 303–326.
- Namikas, S.L., 2006. A conceptual model of energy partitioning in the collision of saltating grains with an unconsolidated sediment bed. *Journal of coastal research* , 1250–1259.
- Namikas, S.L., Sherman, D.J., 1996. A review of the effects of surface moisture content on aeolian sand transport, in: *Desert Aeolian Processes*. Springer, pp. 269–293.
- Nanney, R., Fryrear, D., Zobeck, T., 1993. Wind erosion prediction and control. *Water Science & Technology* 28, 519–527.
- Navier, C., 1823. Mémoire sur les lois du mouvement des fluides. *Mémoires de l'Académie Royale des Sciences de l'Institut de France* 6, 389–440.
- Neuman, C.M., 2003. Effects of temperature and humidity upon the entrainment of sedimentary particles by wind. *Boundary-Layer Meteorology* 108, 61–89.
- Newton, I., Bernoulli, D., MacLaurin, C., Euler, L., 1833. *Philosophiae naturalis principia mathematica*. volume 1. excudit G. Brookman; impensis TT et J. Tegg, Londini.
- Ni, J.R., Li, Z.S., Mendoza, C., 2003. Vertical profiles of aeolian sand mass flux. *Geomorphology* 49, 205–218.
- Nicholas, A., 2010. Reduced-complexity modeling of free bar morphodynamics in alluvial channels. *Journal of Geophysical Research: Earth Surface* 115.
- Nickling, W., Ecclestone, M., 1981. The effects of soluble salts on the threshold shear velocity of fine sand. *Sedimentology* 28, 505–510.
- Nickling, W., McKenna Neuman, C., 1997. Wind tunnel evaluation of a wedge-shaped aeolian sediment trap. *Geomorphology* 18, 333–345.
- Nickling, W.G., Neuman, C.M., 2009. Aeolian sediment transport, in: *Geomorphology of Desert Environments*. Springer, pp. 517–555.
- Nield, J.M., Baas, A.C., 2008. Investigating parabolic and nebkha dune formation using a cellular automaton modelling approach. *Earth Surface Processes and Landforms* 33, 724–740.

- Nield, J.M., King, J., Jacobs, B., 2014. Detecting surface moisture in aeolian environments using terrestrial laser scanning. *Aeolian Research* 12, 9 – 17.
- Nield, J.M., Wiggs, G.F., 2011. The application of terrestrial laser scanning to aeolian saltation cloud measurement and its response to changing surface moisture. *Earth Surface Processes and Landforms* 36, 273–278.
- Nield, J.M., Wiggs, G.F., Squirrell, R.S., 2011. Aeolian sand strip mobility and protodune development on a drying beach: examining surface moisture and surface roughness patterns measured by terrestrial laser scanning. *Earth Surface Processes and Landforms* 36, 513–522.
- Nolet, C., Poortinga, A., Roosjen, P., Bartholomeus, H., Ruessink, G., In Press. Measuring and modeling the effect of surface moisture on the spectral reflectance of coastal beach sand. *PloS ONE* .
- Nordstrom, K.F., Jackson, N.L., Korotky, K.H., Puleo, J.A., 2011. Aeolian transport rates across raked and unraked beaches on a developed coast. *Earth Surface Processes and Landforms* 36, 779–789.
- Ogawa, A., Ugai, T., 2000. Collection efficiency of cylindrical and elliptic cyclone dust collectors with vortex breaker. *Journal of Thermal Science* 9, 257–264.
- Oosterwijk, H., Eetema, M., 1987. Aansluiting hoogte-en dieptemetingen JARKUS mbt de waterpassing. Dienst Getijdewateren, Rijkswaterstaat.
- Owen, P.R., 1964. Saltation of uniform grains in air. *Journal of Fluid Mechanics* 20, 225–242.
- Pächtz, T., Kok, J.F., Parteli, E.J., Herrmann, H.J., 2013. Flux saturation length of sediment transport. *Physical review letters* 111, 218002.
- Panbianco, J., Buschiazzo, D., Zobeck, T., 2010. Comparison of different mass transport calculation methods for wind erosion quantification purposes. *Earth Surface Processes and Landforms* 35, 1548–1555.
- Pelt, R.S.V., Peters, P., Visser, S., 2009. Laboratory wind tunnel testing of three commonly used saltation impact sensors. *Aeolian Research* 1, 55 – 62.
- Philpot, W., 2010. Spectral reflectance of wetted soils. *Proceedings of ASD and IEEE GRS; Art, Science and Applications of Reflectance Spectroscopy Symposium Vol II*, 11pp.
- Pimentel, D., 2006. Soil erosion: a food and environmental threat. *Environment, development and sustainability* 8, 119–137.
- Pimentel, D., Kounang, N., 1998. Ecology of soil erosion in ecosystems. *Ecosystems* 1, 416–426.
- Poortinga, A., Keijsers, J., Visser, S., Riksen, M., Baas, A., 2015. Temporal and spatial variability in event scale aeolian transport on ameland, the netherlands. *GeoResJ* 5, 23–35.
- Poortinga, A., Keijsers, J.G., Maroulis, J., Visser, S.M., 2014. Measurement uncertainties in quantifying aeolian mass flux: evidence from wind tunnel and field site data. *PeerJ* 2, e454.
- Poortinga, A., Van Minnen, J., Keijsers, J., Riksen, M., Goossens, D., Seeger, M., 2013a. Measuring fast-temporal sediment fluxes with an analogue acoustic sensor: a wind tunnel study. *PloS one* 8, e74007.

- Poortinga, A., Van Minnen, J., Riksen, M., Seeger, M., 2013b. Measuring fast-temporal sediment fluxes with an analogue acoustic sensor: a wind tunnel study. [Http://dx.doi.org/10.4121/uuid:7f4c6e00-4e51-4dc3-a304-57fc2f7f3b19](http://dx.doi.org/10.4121/uuid:7f4c6e00-4e51-4dc3-a304-57fc2f7f3b19).
- Poortinga, A., Visser, S., Riksen, M., Stroosnijder, L., 2011. Beneficial effects of wind erosion: Concepts, measurements and modeling. *Aeolian Research* 3, 81–86.
- Pope, R., Fry, E., 1997. Absorption spectrum (380-700 nm) of pure water. ii. integrating cavity measurements. *Applied Optics* 36, 8710–8723.
- Prandtl, L., 1932. Zur turbulenten strömung in rohren und längs platten. *Ergebn. Aerodyn. Versuchsanst* 4, 18–29.
- Prospero, J.M., 1999. Long-range transport of mineral dust in the global atmosphere: Impact of african dust on the environment of the southeastern united states. *Proceedings of the National Academy of Sciences* 96, 3396–3403.
- Pöschel, T., Buchholtz, V., 1993. Static friction phenomena in granular materials: Coulomb law versus particle geometry. *Physical Review Letters* 71, 3963–3966.
- R Core Team, 2012. R: A Language and Environment for Statistical Computing. R Foundation for Statistical Computing. Vienna, Austria. ISBN 3-900051-07-0.
- Rajot, J.L., 2001. Wind blown sediment mass budget of sahelian village land units in niger [bilan de masse de l'érosion et des dépôts éoliens à l'échelle de terroirs villageois au niger]. *Bulletin de la Societe Geologique de France* 172, 523–531.
- Rasmussen, K.R., Mikkelsen, H.E., 1998. On the efficiency of vertical array aeolian field traps. *Sedimentology* 45, 789–800.
- Rasmussen, K.R., Sørensen, M., 1999. Aeolian mass transport near the saltation threshold. *Earth Surface Processes and Landforms* 24, 413–422.
- Raubenheimer, B., Guza, R., Elgar, S., 1998. Watertable fluctuations in a sandy ocean beach, pp. 3588–3600.
- Ravi, S., Breshears, D.D., Huxman, T.E., D'Odorico, P., 2010. Land degradation in drylands: Interactions among hydrologic–aeolian erosion and vegetation dynamics. *Geomorphology* 116, 236–245.
- Reynolds, O., 1883. An experimental investigation of the circumstances which determine whether the motion of water shall be direct or sinuous, and of the law of resistance in parallel channels. *Proceedings of the royal society of London* 35, 84–99.
- Ridge, J.T., Rodriguez, A.B., Fegley, S.R., Browne, R., Hood, D., 2011. A new 'pressure sensitive' method of measuring aeolian sediment transport using a gauged sediment trap (gast). *Geomorphology* 134, 426–430.
- Rijkswaterstaat, 2014a. Dataset documentation jarkus.
- Rijkswaterstaat, 2014b. Historic data on water quantity and quality.

- Riksen, M., De Graaff, J., 2001. On-site and off-site effects of wind erosion on european light soils. *Land degradation & development* 12, 1–11.
- Riksen, M., Goossens, D., 2005. Tillage techniques to reactivate aeolian erosion on inland drift-sand. *Soil and Tillage Research* 83, 218–236.
- Riksen, M., Jungerius, P., 2010. Development of aeolian activity in inland drift sands in the netherlands after 1900 In: Siepel, H., Fanta, F. (Eds.), *Inland drift-sand landscapes*. Knnv Publishing, Zeist.
- Riksen, M., Ketner-Oostra, R., Turnhout, C., Nijssen, M., Goossens, D., Jungerius, P., Spaan, W., 2006. Will we lose the last active inland drift sands of western europe? the origin and development of the inland drift-sand ecotype in the netherlands. *Landscape Ecology* 21, 431–447.
- Riksen, M., Spaan, W., Stroosnijder, L., 2008. How to use wind erosion to restore and maintain the inland drift-sand ecotype in the netherlands? *Journal for Nature Conservation* 16, 26–43.
- Riksen, M.J., Goossens, D., 2007. The role of wind and splash erosion in inland drift-sand areas in the netherlands. *Geomorphology* 88, 179–192.
- Riksen, M.J., Visser, S.M., 2008. Predicting the effect of tilling practices on wind erosion activity: application of the wind erosion prediction system in a sand drift area in the netherlands. *Earth Surface Processes and Landforms* 33, 1864–1874.
- Ritchie, J.C., McHenry, J.R., 1990. Application of radioactive fallout cesium-137 for measuring soil erosion and sediment accumulation rates and patterns: a review. *Journal of environmental quality* 19, 215–233.
- Roosjen, P.P., Clevers, J.G., Bartholomeus, H.M., Schaepman, M.E., Schaepman-Strub, G., Jalink, H., Van Der Schoor, R., De Jong, A., 2012. A laboratory goniometer system for measuring reflectance and emittance anisotropy. *Sensors* 12, 17358–17371.
- Rosen, P., 1978. An efficient, low cost, aeolian sampling system. *Geological Survey of Canada, Current Research, Part A* , 531–532.
- Rotnicka, J., 2013. Aeolian vertical mass flux profiles above dry and moist sandy beach surfaces. *Geomorphology* 187, 27–37.
- Ruessink, G., Brakenhoff, L., Van Maarseveen, M., 2014. Measurement of surface moisture using infrared terrestrial laser scanning, in: *Geophysical Research Abstracts*, Vol. 16, EGU2014-2797.
- Sallenger Jr, A., Krabill, W., Swift, R., Brock, J., List, J., Hansen, M., Holman, R., Manizade, S., Sontag, J., Meredith, A., et al., 2003. Evaluation of airborne topographic lidar for quantifying beach changes. *Journal of Coastal Research* , 125–133.
- Sauermann, G., Kroy, K., Herrmann, H.J., 2001. Continuum saltation model for sand dunes. *Physical Review E* 64, 031305.
- Schonfeldt, H.J., von Lowis, S., 2003. Turbulence-driven saltation in the atmospheric surface layer. *Meteorologische Zeitschrift* 12, 257–268.

- Schubauer, G., Adams, G., 1954. Lag of anemometers. National Bureau of Standards, NBS Report 3245, 16.
- Schwämmle, V., Herrmann, H., 2005. A model of barchan dunes including lateral shear stress. *The European Physical Journal E: Soft Matter and Biological Physics* 16, 57–65.
- Schönfeldt, H.J., 2012. High resolution sensors in space and time for determination saltation and creep intensity. *Earth Surface Processes and Landforms* 37, 1065–1073.
- Scoones, I., 1999. New ecology and the social sciences: what prospects for a fruitful engagement? *Annual Review of Anthropology* 28, 479–507.
- Segelstein, D., 1981. The complex refractive index of water. Master's thesis. University of Missouri. Kansas City.
- Sensit, C., 2013. MOVEMENT DETECTOR, Technical Manual - Model FP5-RevC.
- Shao, Y., Raupach, M.R., Leys, J.F., 1996. A model for predicting aeolian sand drift and dust entrainment on scales from paddock to region. *Soil Research* 34, 309–342.
- Sherman, D., Houser, C., Baas, A., 2013a. 14.17 electronic measurement techniques for field experiments in process geomorphology, in: Shroder, J.F. (Ed.), *Treatise on Geomorphology*. Academic Press, San Diego, pp. 195 – 221.
- Sherman, D., Swann, C., Barron, J., 2014. A high-efficiency, low-cost aeolian sand trap. *Aeolian Research* 13, 31–34.
- Sherman, D.J., 1995. Problems of scale in the modeling and interpretation of coastal dunes. *Marine Geology* 124, 339 – 349.
- Sherman, D.J., Houser, C., Ellis, J.T., Farrell, E.J., Li, B., Davidson-Arnott, R.G., Baas, A.C., Maia, L.P., 2013b. Characterization of aeolian streamers using time-average videography. *Journal of Coastal Research*, Special Issue , 1331–1336.
- Sherman, D.J., Jackson, D.W., Namikas, S.L., Wang, J., 1998. Wind-blown sand on beaches: an evaluation of models. *Geomorphology* 22, 113–133.
- Sherman, D.J., Li, B., 2012. Predicting aeolian sand transport rates: A reevaluation of models. *Aeolian Research* 3, 371–378.
- Sherman, D.J., Li, B., Farrell, E.J., Ellis, J.T., Cox, W.D., Maia, L.P., Sousa, P.H., 2011. Measuring aeolian saltation: a comparison of sensors. *Journal of Coastal Research* , 280–290.
- Shimokawabe, T., Aoki, T., Muroi, C., Ishida, J., Kawano, K., Endo, T., Nukada, A., Maruyama, N., Matsuoka, S., 2010. An 80-fold speedup, 15.0 tflops full gpu acceleration of non-hydrostatic weather model asuca production code, in: *High Performance Computing, Networking, Storage and Analysis (SC)*, 2010 International Conference for, IEEE. pp. 1–11.
- Shuchman, R.A., Rea, D.K., 1981. Determination of beach sand parameters using remotely sensed aircraft reflectance data. *Remote Sensing of Environment* 11, 295–310.

- Silbert, L.E., Grest, G.S., Landry, J.W., 2002. Statistics of the contact network in frictional and frictionless granular packings. *Physical Review E* 66, 061303.
- Skidmore, E., Dickerson, J., Schimmelpennig, H., 1975. Evaluating surface-soil water content by measuring reflectance. *Soil Science Society of America Journal* 39, 238–242.
- Smith, L., Tüzün, U., 2002. Life after computer simulations: towards establishing bulk evolution rules based on discrete granular dynamics. *Chemical Engineering Science* 57, 253–264.
- Solomon, S., 2007. *Climate change 2007-the physical science basis: Working group I contribution to the fourth assessment report of the IPCC. volume 4.* Cambridge University Press.
- Sørensen, M., 2004. On the rate of aeolian sand transport. *Geomorphology* 59, 53–62.
- Spaan, W., van den Abeele, G., 1991. Wind borne particle measurements with acoustic sensors. *Soil Technology* 4, 51–63.
- Stahl, M., Konietzky, H., 2011. Discrete element simulation of ballast and gravel under special consideration of grain-shape, grain-size and relative density. *Granular Matter* 13, 417–428.
- Sterk, G., Herrmann, L., Bationo, A., 1996. Wind-blown nutrient transport and soil productivity changes in southwest niger. *Land Degradation and Development* 7, 325–335.
- Sterk, G., Jacobs, A., Van Boxel, J., 1998. The effect of turbulent flow structures on saltation sand transport in the atmospheric boundary layer. *Wind Erosion in the Sahelian Zone of Niger: Processes, Models, and Control Techniques* , 11.
- Sterk, G., Parigiani, J., Cittadini, E., Peters, P., Scholberg, J., Peri, P., 2012. Aeolian sediment mass fluxes on a sandy soil in central patagonia. *Catena* 95, 112–123.
- Sterk, G., Raats, P., 1996. Comparison of models describing the vertical distribution of wind-eroded sediment. *Soil Science Society of America Journal* 60, 1914–1919.
- Sterk, G., Spaan, W., 1997. Wind erosion control with crop residues in the sahel. *Soil Science Society of America Journal* 61, 911–917.
- Sterk, G., Stein, A., Stroosnijder, L., 2004. Wind effects on spatial variability in pearl millet yields in the sahel. *Soil and Tillage Research* 76, 25–37.
- Stive, M.J., 2004. How important is global warming for coastal erosion? *Climatic Change* 64, 27–39.
- Stive, M.J., de Schipper, M.A., Luijendijk, A.P., Aarninkhof, S.G., van Gelder-Maas, C., van Thiel de Vries, J.S., de Vries, S., Henriquez, M., Marx, S., Ranasinghe, R., 2013. A new alternative to saving our beaches from sea-level rise: The sand engine. *Journal of Coastal Research* 29, 1001–1008.
- Stockdon, H.F., Holman, R.A., Howd, P.A., Sallenger Jr, A.H., 2006. Empirical parameterization of setup, swash, and runup. *Coastal engineering* 53, 573–588.
- Stockton, P.H., Gillette, D.A., 1990. Field measurement of the sheltering effect of vegetation on erodible land surfaces. *Land Degradation and Development* 2, 77–85.
- Stokes, G.G., 1851. *On the effect of the internal friction of fluids on the motion of pendulums.* volume 9. Pitt Press.

- Stoorvogel, J., Smaling, E., et al., 1990. Assessment of soil nutrient depletion in Sub-Saharan Africa: 1983-2000. volume 1. Winand Staring Centre Wageningen.
- Stoorvogel, J., Smaling, E.A., Janssen, B., 1993. Calculating soil nutrient balances in africa at different scales. *Fertilizer research* 35, 227–235.
- Stout, J., Zobeck, T., 1997. Intermittent saltation. *Sedimentology* 44, 959–970.
- Stout, J.E., 1998. Effect of averaging time on the apparent threshold for aeolian transport. *Journal of Arid Environments* 39, 395 – 401.
- Stout, J.E., 2004. A method for establishing the critical threshold for aeolian transport in the field. *Earth Surface Processes and Landforms* 29, 1195–1207.
- Stout, J.E., Zobeck, T.M., 1996. Establishing the threshold condition for soil movement in wind-eroding fields, in: *Proceedings of the International Conference on Air Pollution from Agricultural Operations* (1996), pp. 65–71.
- Stroosnijder, L., 2005. Measurement of erosion: is it possible? *Catena* 64, 162–173.
- Swann, C., Sherman, D., 2013. A bedload trap for aeolian sand transport. *Aeolian Research* 11, 61–66.
- Swap, R., Garstang, M., Greco, S., Talbot, R., Kållberg, P., 1992. Saharan dust in the amazon basin. *Tellus B* 44, 133–149.
- Taboada, A., Estrada, N., 2009. Rock-and-soil avalanches: Theory and simulation. *Journal of Geophysical Research: Earth Surface* 114.
- Tebaldi, C., De Menech, M., Stella, A.L., 1999. Multifractal scaling in the bak-tang-wiesenfeld sandpile and edge events. *Phys. Rev. Lett.* 83, 3952–3955.
- Temur, C., Tiryaki, O., Uzun, O., Basaran, M., 2012. Adaptation and validation of quechers method for the analysis of trifluralin in wind-eroded soil. *Journal of Environmental Science and Health - Part B Pesticides, Food Contaminants, and Agricultural Wastes* 47, 842–850.
- Tesfai, M., Stroosnijder, L., 2001. The eritrean spate irrigation system. *Agricultural water management* 48, 51–60.
- Tester, M., Morris, C., 1987. The penetration of light through soil. *Plant, Cell & Environment* 10, 281–286.
- Teweldebrhan, B., Hsu, L., Dietrich, W., Hill, K., 2011. Boundary stresses due to impacts from dry granular flows, in: *AGU Fall Meeting Abstracts*, p. 04.
- Tidjani, A.D., Biolders, C., Rosillon, D., Ambouta, K.M., 2011. Uncertainties in plot-scale mass balance measurements using aeolian sediment traps. *Soil Science Society of America Journal* 75, 708–718.
- Utili, S., Crosta, G., 2011. Modeling the evolution of natural cliffs subject to weathering: 1. limit analysis approach. *Journal of Geophysical Research: Earth Surface* 116.
- Valentin, C., Bresson, L.M., 1992. Morphology, genesis and classification of surface crusts in loamy and sandy soils. *Geoderma* 55, 225–245.

- Van Boxel, J., Arens, S., Van Dijk, P., 1999. Aeolian processes across transverse dunes. i: Modelling the air flow. *Earth Surface Processes and Landforms* 24, 255–270.
- Van Boxel, J., Sterk, G., Arens, S., 2004. Sonic anemometers in aeolian sediment transport research. *Geomorphology* 59, 131–147.
- Van Dijk, P., Arens, S., Van Boxel, J., 1999. Aeolian processes across transverse dunes. ii: Modelling the sediment transport and profile development. *Earth Surface Processes and Landforms* 24, 319–333.
- Van Dijk, P., Stroosnijder, L., De Lima, J., 1996. The influence of rainfall on transport of beach sand by wind. *Earth Surface Processes and Landforms* 21, 341–352.
- Van Donk, S.J., Skidmore, E.L., 2003. Measurement and simulation of wind erosion, roughness degradation and residue decomposition on an agricultural field. *Earth surface processes and landforms* 28, 1243–1258.
- Van Genuchten, M.T., 1980. A closed-form equation for predicting the hydraulic conductivity of unsaturated soils. *Soil Science Society of America Journal* 44, 892–898.
- Van Koningsveld, M., Mulder, J.P.M., 2004. Sustainable coastal policy developments in the netherlands. a systematic approach revealed. *Journal of Coastal Research* , 375–385.
- Van Pelt, R.S., Peters, P., Visser, S., 2009. Laboratory wind tunnel testing of three commonly used saltation impact sensors. *Aeolian Research* 1, 55–62.
- Van Slobbe, E., De Vriend, H., Aarninkhof, S., Lulofs, K., De Vries, M., Dircke, P., 2013. Building with nature: in search of resilient storm surge protection strategies. *Natural hazards* 66, 1461–1480.
- VanKoningsveld, M., Mulder, J.P., Stive, M.J., VanDerValk, L., VanDerWeck, A., 2008. Living with sea-level rise and climate change: a case study of the netherlands. *Journal of Coastal Research* , 367–379.
- Visser, S., Leenders, J., Leeuwis, M., 2003. Farmers' perceptions of erosion by wind and water in northern burkina faso. *Land Degradation & Development* 14, 123–132.
- Visser, S., Sterk, G., 2007. Nutrient dynamics—wind and water erosion at the village scale in the sahel. *Land Degradation & Development* 18, 578–588.
- Visser, S., Sterk, G., Ribolzi, O., 2004a. Techniques for simultaneous quantification of wind and water erosion in semi-arid regions. *Journal of Arid Environments* 59, 699–717.
- Visser, S., Stroosnijder, L., Chardon, W., 2005a. Nutrient losses by wind and water, measurements and modelling. *Catena* 63, 1–22.
- Visser, S., Wijers, M., Leenders, J., 2010. Larger sowing pit, larger profit. Luis (Ed.), VII International Symposium Agroenviron 2010, Cancún, Mexico.
- Visser, S.M., Sterk, G., Karssenber, D., 2005b. Wind erosion modelling in a sahelian environment. *Environmental Modelling & Software* 20, 69–84.
- Visser, S.M., Sterk, G., Snepvangers, J.J., 2004b. Spatial variation in wind-blown sediment transport in geomorphic units in northern burkina faso using geostatistical mapping. *Geoderma* 120, 95–107.

- de Vries, S., Southgate, H., Kanning, W., Ranasinghe, R., 2012. Dune behavior and aeolian transport on decadal timescales. *Coastal Engineering* 67, 41–53.
- van der Wal, D., 1998. Effects of fetch and surface texture on aeolian sand transport on two nourished beaches. *Journal of Arid Environments* 39, 533 – 547.
- van der Wal, D., 2000a. Grain-size-selective aeolian sand transport on a nourished beach. *Journal of coastal research* 16, 896–908.
- van der Wal, D., 2000b. Modelling aeolian sand transport and morphological development in two beach nourishment areas. *Earth Surface Processes and Landforms* 25, 77–92.
- van der Wal, D., 2004. Beach-dune interactions in nourishment areas along the dutch coast. *Journal of Coastal Research* , 317–325.
- Walker, I.J., 1999. Secondary airflow and sediment transport in the lee of a reversing dune. *Earth Surface Processes and Landforms* 24, 437–448.
- Walker, I.J., 2005. Physical and logistical considerations of using ultrasonic anemometers in aeolian sediment transport research. *Geomorphology* 68, 57–76.
- Walker, I.J., Hesp, P.A., Davidson-Arnott, R.G., Bauer, B.O., Namikas, S.L., Ollerhead, J., 2009. Responses of three-dimensional flow to variations in the angle of incident wind and profile form of dunes: Greenwich dunes, prince edward island, canada. *Geomorphology* 105, 127–138.
- Walker, I.J., Nickling, W.G., 2002. Dynamics of secondary airflow and sediment transport over and in the lee of transverse dunes. *Progress in Physical Geography* 26, 47–75.
- Warren, A., 2002. Land degradation is contextual. *Land Degradation & Development* 13, 449–459.
- Warren, A., French, J.R., et al., 2001. *Habitat conservation: managing the physical environment*. John Wiley & Sons.
- Weaver, C.M., Wiggs, G.F., 2011. Field measurements of mean and turbulent airflow over a barchan sand dune. *Geomorphology* 128, 32 – 41.
- Webb, N.P., McGowan, H.A., 2009. Approaches to modelling land erodibility by wind. *Progress in Physical Geography* 33, 587–613.
- Weidong, L., Baret, F., Xingfa, G., Qingxi, T., Lanfen, Z., Bing, Z., 2002. Relating soil surface moisture to reflectance. *Remote sensing of environment* 81, 238–246.
- Werner, B., 1995. Eolian dunes: Computer simulations and attractor interpretation. *Geology* 23, 1107–1110.
- Werner, B., 2003. Modeling landforms as self-organized, hierarchical dynamical systems. *Geophysical Monograph Series* 135, 133–150.
- Wesseling, J.G., Ritsema, C.J., Stolte, J., Oostindie, K., Dekker, L.W., 2008. Describing the soil physical characteristics of soil samples with cubical splines. *Transport in Porous Media* 71, 289–309.
- Wiggs, G., 2001. Desert dune processes and dynamics. *Progress in Physical Geography* 25, 53–79.

- Wiggs, G., Atherton, R., Baird, A., 2004a. Thresholds of aeolian sand transport: establishing suitable values. *Sedimentology* 51, 95–108.
- Wiggs, G., Baird, A., Atherton, R., 2004b. The dynamic effects of moisture on the entrainment and transport of sand by wind. *Geomorphology* 59, 13 – 30. *æolian Research: processes, instrumentation, landforms and palaeoenvironments*.
- Willetts, B., Rice, M., 1986. Collisions in aeolian saltation. *Acta Mechanica* 63, 255–265.
- Williams, J.R., Mustoe, G.G., 1987. Modal methods for the analysis of discrete systems. *Computers and Geotechnics* 4, 1–19.
- Wilson, S., Cooke, R., 1980a. Wind erosion.
- Wilson, S., Cooke, R., 1980b. Wind erosion. *Soil erosion* , 217–251.
- Winter, R., Sterl, A., Ruessink, B., 2013. Wind extremes in the north sea basin under climate change: an ensemble study of 12 cmip5 gcms. *Journal of Geophysical Research: Atmospheres* .
- Wolf, D.E., 1996. Modelling and computer simulation of granular media, in: *Computational Physics*. Springer, pp. 64–95.
- Wolfe, S.A., Nickling, W.G., 1993. The protective role of sparse vegetation in wind erosion. *Progress in physical geography* 17, 50–68.
- Wosten, J., Van Genuchten, M.T., 1988. Using texture and other soil properties to predict the unsaturated soil hydraulic functions. *Soil Science Society of America Journal* 52, 1762–1770.
- Wösten, J., Veerman, G., De Groot, W., Stolte, J., 2001. Water retention and permeability characteristics of top and sub soils in the netherlands: the staring series. renewed edition 2001. Alterra, research instituut voor de groene ruimte (Wageningen) .
- Wright, L., Short, A.D., 1984. Morphodynamic variability of surf zones and beaches: a synthesis. *Marine geology* 56, 93–118.
- Yang, P., Dong, Z., Qian, G., Luo, W., Wang, H., 2007. Height profile of the mean velocity of an aeolian saltating cloud: Wind tunnel measurements by particle image velocimetry. *Geomorphology* 89, 320 – 334.
- Yang, X., Preusser, F., Radtke, U., 2006. Late quaternary environmental changes in the taklamakan desert, western china, inferred from osl-dated lacustrine and aeolian deposits. *Quaternary Science Reviews* 25, 923–932.
- Yang, Y., Davidson-Arnott, R., 2005. Rapid measurement of surface moisture content on a beach. *Journal of Coastal Research* 21, 447–452.
- Youssef, F., Erpul, G., Bogman, P., Cornelis, W., Gabriels, D., 2008. Determination of efficiency of vaseline slide and wilson and cooke sediment traps by wind tunnel experiments. *Environmental Geology* 55, 741–750.
- Youssef, F., Visser, S., Karssenbergh, D., Bruggeman, A., Erpul, G., 2012a. Calibration of rweq in a patchy landscape; a first step towards a regional scale wind erosion model. *æolian Research* 3,

- 467–476.
- Youssef, F., Visser, S.M., Karssenbergh, D., Erpul, G., Cornelis, W.M., Gabriels, D., Poortinga, A., 2012b. The effect of vegetation patterns on wind-blown mass transport at the regional scale: A wind tunnel experiment. *Geomorphology* 159–160, 178 – 188.
- Yurk, B.P., Hansen, E.C., Hazle, D., 2013. A deadtime model for the calibration of impact sensors with an application to a modified miniphone sensor. *Aeolian Research* 11, 43–54.
- Zhang, K., Douglas, B.C., Leatherman, S.P., 2004. Global warming and coastal erosion. *Climatic Change* 64, 41–58.
- Zhou, Y., Wright, B., Yang, R., Xu, B., Yu, A., 1999. Rolling friction in the dynamic simulation of sandpile formation. *Physica A: Statistical Mechanics and its Applications* 269, 536–553.
- Zhou, Y., Xu, B., Yu, A., Zulli, P., 2002. An experimental and numerical study of the angle of repose of coarse spheres. *Powder technology* 125, 45–54.
- Zhou, Y., Xu, B., Zou, R., Yu, A., Zulli, P., 2003. Stress distribution in a sandpile formed on a deflected base. *Advanced Powder Technology* 14, 401–410.
- Zingg, A., 1953. Wind tunnel studies of the movement of sedimentary material, in: *Proceedings of the 5th Hydraulic Conference Bulletin*, pp. 111–135.
- Zobeck, T., Pelt, S.v., Stout, J., Popham, T., Flanagan, D., et al., 2001. Validation of the revised wind erosion equation (rweq) for single events and discrete periods., in: *Soil erosion research for the 21st century. Proceedings of the International Symposium, Honolulu, Hawaii, USA, 3-5 January, 2001.*, American Society of Agricultural Engineers. pp. 471–474.
- Zobeck, T., Sterk, G., Funk, R., Rajot, J., Stout, J., Van Pelt, R., 2003. Measurement and data analysis methods for field-scale wind erosion studies and model validation. *Earth Surface Processes and Landforms* 28, 1163–1188.
- Zou, X.Y., Wang, Z.L., Hao, Q.Z., Zhang, C.L., Liu, Y.Z., Dong, G.R., 2001. The distribution of velocity and energy of saltating sand grains in a wind tunnel. *Geomorphology* 36, 155 – 165.

Summary

Since the book of Ralph Alger Bagnold on the physics of blown sand and desert dunes was published in 1947, a wide variety of theories, techniques and models have been developed to the physics and effects of aeolian sediment transport. While many other disciplines have undergone fast improvements in terms of measurement techniques and (standardized) proven theories last decades, the field of aeolian research remains still in its infancy. Data on the process is scarce and measurement techniques to measure air borne sediment have remained disproportionally unsophisticated. The aim of this thesis is to explore, challenge and enhance current concepts, measurements and modelling techniques of wind blown sand. The following research questions were posed (1) What are the current measurement techniques to measure aeolian saltation, how reliable are they and can they be improved? (2) Is it possible to measure aeolian sediment transport in a coastal environment on a field scale? (3) What are the regulating factors and processes on aeolian transport fluxes in coastal environments at different scales? (4) How can recent advances in computational techniques be used to model sediment transport processes? This thesis contains eight chapters. Chapters 2 discusses current concepts in aeolian research, chapter 2 describes a new modelling approach, chapters 4 - 8 present the results of laboratory, field and wind tunnel experiments on aeolian transport processes.

The second chapter gives an overview of current measurement techniques, models and conceptualizations of aeolian research. It is shown that aeolian research is still dominated by a technocentric worldview. With a focus on the negatives, it is believed that all separate components should studied as detailed and possible, and combined,

they explain the complete system dynamics. The chapter presents a new conceptualization of the benefits of wind erosion and argues to work towards a more holocentric approach. Three examples show how aeolian process can be beneficial for biodiversity, recreation, coastal defense and even for harvesting soil fertility. Current measurement techniques and modeling approaches are contested. As data from lacking measurement techniques are used for extrapolation and modeling purposes. Larger system dynamics are studied by simulating the small scale (reductionist) processes, leading to a complex model structure based on weak empirical and physical considerations. A more holistic approach suggest to monitor the greater systems dynamics, in technocentric studies. An integration between stochastic and physical based models is proposed, in order to simulate the non linear complex interactions with a minimum of physical parameters. By choosing a more holocentric approach, wind erosion becomes an essential part in the natural system dynamics.

A new modelling approach was applied in chapter 3. In this chapter we use a state-of-the-art parallel implementation of the discrete element method on a graphical processing unit to simulate non-linear self-emergent behaviour in complex systems. In this chapter, we use the example of sand-pile formation, as it is often used to describe scale-invariant power law fluctuations in a system, whereas cellular automata are often used to model this behaviour. In the model, interactions between individual grains were simulated using a contact model in an Euler integration scheme. Computational results show non-linear self-emergent power-law and scale-invariant behaviour, which is in good agreement with experimental results, theoretical work and self organized criticality (SOC) approaches. The chapter shows that a fully deterministic model approach, where the position and forces on every individual particle can be determined every iteration has great potential to study non-linear and self-emergent behaviour in aeolian research.

There have been many devices developed, tested, and applied to investigate a range of aeolian-based phenomena. However, determining the most effective application and data analysis techniques is widely debated in the literature. In chapter 4, we investigate

the effectiveness of two different sediment traps (the BEST trap and the MWAC catcher) in measuring vertical sediment flux. The study was performed in a wind tunnel with sediment fluxes being measured using saltiphones. Contrary to most studies, we used the analogue output of five saltiphones mounted on top of each other to determine the total kinetic energy, which was then used to calculate aeolian sediment budgets. Absolute sediment losses during the experiments were determined using a balance located beneath the test tray. Test runs were conducted with different sand sizes and at different wind speeds. The efficiency of the two traps did not vary with the wind speed or sediment size but was affected by both the experimental setup (position of the lowest trap above the surface and number of traps in the saltation layer) and the technique used to calculate the sediment flux. Despite this, good agreement was found between sediment losses calculated from the saltiphone and those measured using the balance. The results of this study provide a framework for measuring sediment fluxes at small time resolution (seconds to milliseconds) in the field.

Acoustic sensors are frequently used to measure aeolian saltation. Different approaches are used to process the signals from these instruments. Chapter 5 describes and discusses a method to measure aeolian saltation with acoustic sensors. In a laboratory experiment, the output from an advanced signal processing scheme on the circuit board of the Saltiphone was measured. Furthermore a software implementation of the saltiphone signal processing scheme was used to re-analyse data from four miniphones obtained during a field experiment. It is shown that a set of filters remove background noise outside the frequency spectrum of aeolian saltation (at 8 kHz), whereas signals within this frequency spectrum are amplified. The resulting analogue signal is a proxy of the energy. with a pulse convertor, the signal is be converted into a digital and analogue count signal or an analogue energy signal, using a rectifier and integrator. Spatio-temporal correlation between field deployed miniphones increased by using longer integration times for signal processing. To quantify aeolian grain impact, it is suggested to use the analogue energy output, as this mode is able to detect changes in frequency and amplitude. The analogue and digital count signals are able detect an increase in

frequency, but are not able to detect an increase in signal amplitude. A two-stage calibration scheme was proposed consisting of (1) a factory calibration, to set the frequency spectrum of the sensor and (2) a standardized drop-test conducted before and after the experiment to evaluate the response of the sensor.

In chapter 6, wind tunnel and field site data are compared to identify uncertainties in aeolian mass flux quantification using the Modified Wilson And Cook (MWAC) aeolian sediment traps. These traps are widely used to estimate the total volume of wind-driven sediment transport, but also to study the vertical mass distribution of a saltating sand cloud. The reliability of sediment flux estimations from this data are dependent upon the specific configuration of the measurement compartments and the analysis approach used. In this study, we analyse the uncertainty of these measurements by investigating the vertical cumulative distribution and relative sediment flux derived from both wind tunnel and field studies. Vertical flux data were examined using existing data in combination with a newly acquired dataset; comprising meteorological data and sediment fluxes from six different events, using three customized catchers at Ameland beaches in northern Netherlands. Fast-temporal data collected in a wind tunnel shows that the median transport height has a scattered pattern between impact and fluid threshold, that increases linearly with shear velocities above the fluid threshold. For finer sediment, a larger proportion was transported closer to the surface compared to coarser sediment fractions. It was also shown that errors originating from the distribution of sampling compartments, specifically the location of the lowest sediment trap relative to the surface, can be identified using the relative sediment flux. In the field, surface conditions such as surface moisture, surface crusts or frozen surfaces have a more pronounced but localized effect than shear velocity. Uncertainty in aeolian mass flux estimates can be reduced by placing multiple compartments in closer proximity to the surface.

In chapter 7, the horizontal and vertical variability of event scale aeolian sand transport on a wide beach on the island of Ameland, The Netherlands was analysed. A meteorological station, 37 customized MWAC catchers, groundwater monitoring wells and a camera were installed on the beach. Fifteen different aeolian transport events

were measured over a three month period. The highest sand transport rates and largest variability was found for alongshore events. Surface moisture, governed by groundwater, was found to be an important controlling parameter for aeolian transport rates and vertical flux profiles. Groundwater levels were largely dominated by beach inundation, influencing the groundwater table for a two week period. Variations in vertical flux profiles between traps were larger for wet sand transport events than dry ones. In general, sand transport rates were highest at the foreshore and lowest at the dune toe. Sand transport dynamics are dependent on local conditions such as beach dimensions, beach orientation and also meteorological and surface characteristics. Moderate (high frequency, low magnitude) events are also capable of transporting large amounts of sand. Future studies should include spatially explicit measurements of elevation and surface moisture to obtain a more complete understanding of the complex sand transport dynamics.

An optical remote sensing approach to quantify surface moisture levels was investigated in Chapter 8. As an important supply limiting factor for aeolian sediment transport, it is critical to account for the control of surface moisture on available sand for dune building. With optical remote sensing surface moisture can be measured at a high spatio-temporal resolution. The goals of this study were to measure and model reflectance under controlled laboratory conditions as function of wavelength and surface moisture over the optical domain of 350-2500 nm, and to explore the implications of our laboratory findings for mapping the distribution of surface moisture under natural conditions. A laboratory spectroscopy experiment was devised to measure spectral reflectance under different surface moisture conditions using beach sand. We observed a non-linear increase of reflectance upon drying over the full range of wavelengths. We developed and tested two models. The first model describes the proportional contribution of scattering and absorption of light by pore water in an unsaturated sand matrix. The second model is related to soil physics and links the hydraulic behaviour of pore water in an unsaturated sand matrix to its optical properties. It was found that the optical model performed well for volumetric moisture content $< 24\%$ ($R^2 > 0.97$), but

underestimated reflectance for moisture levels between 24-30% ($R^2 > 0.92$), most notable around the 1940 nm water absorption peak. The soil-physical model performed very well ($R^2 > 0.99$) but is limited to moisture levels $> 4\%$ and $< 24\%$. Results from the field experiment show that a short-wave infrared terrestrial laser scanner ($\lambda=1550$ nm) can accurately relate surface moisture levels to reflectance (standard error 2.6%). This demonstrates the potential of optical remote sensing in SWIR to derive spatially extensive surface moisture maps of a natural coastal beach.

Finally, chapter 9 present the synthesis of the results and conclusion of the previous chapters. It was shown that this thesis makes an important contribution to current themes in aeolian research, by identifying and quantifying the inherent uncertainties of passive sediment traps, while improving current methods to measure aeolian saltation using acoustic sensors. It was also shown that, while quantification of aeolian processes on a field scale was difficult in the past using conventional equipment, recent technological developments allow for a detailed assessment of aeolian processes on a field scale. Technologies developed and discussed in this thesis to measure saltation and surface moisture can be used for field scale assessments. A qualitative assessment shows that, on the event scale variability in sediment transport quantities are mainly determined by local conditions, such as surface moisture, groundwater, meteorology, topology and vegetation. Recent advances in computational technologies allow to simulate geophysical processes on a grain scale. While the computational complexity and computation time remains a constraint, they offer great potential for future studies. The findings presented in the various chapters offer exciting new opportunities to measure and model aeolian transport at a variety of scales in the future.

Samenvatting

Sinds het boek van Ralph Alger Bagnold genaamd "the physics of blown sand and desert dunes" werd gepubliceerd in 1947, hebben een breed scala van theorieën, technieken en modellen de revue gepasseerd om de fysica en de effecten van eolisch sediment transport te beschrijven. Terwijl veel andere disciplines snel verbeteringen hebben ondergaan op het gebied van meettechnieken en de (gestandaardiseerde) bewezen theorieën in de laatste decennia is het vakgebied van eolisch onderzoek in zijn kinderschoenen gebleven. Data over het proces is schaars en meettechnieken zijn nog steeds onderontwikkeld. Het doel van dit proefschrift is om hedendaagse concepten, meet en modelleer methodes te verkennen, te verbeteren en te betwisten. Daartoe zijn de volgende vier onderzoeksvragen geformuleerd: (1) Wat zijn de huidige meettechnieken om eolische saltatie te meten, hoe betrouwbaar zijn deze technieken en kunnen ze worden verbeterd? (2) Is het mogelijk om eolisch sediment transport te meten op het strand op een veld schaal? (3) Wat zijn de regulerende factoren en processen op eolische zand transport in kustgebieden op verschillende schalen? (4) Hoe kunnen recente ontwikkelingen in rekentechnieken worden gebruikt voor het modelleren van sediment transport processen? Dit proefschrift bestaat uit acht hoofdstukken. Hoofdstuk 2 bespreekt de huidige concepten in eolische onderzoek, hoofdstuk 2 beschrijft een nieuwe modelmatige benadering, hoofdstukken 4-8 presenteren de resultaten van het laboratorium, veld en windtunnel experimenten op eolisch transport processen.

Het tweede hoofdstuk geeft een overzicht van de huidige meettechnieken, modellen en conceptualisering in eolische onderzoek. Er wordt aangetoond dat eolisch onderzoek nog steeds wordt gedomineerd door een technocentrische wereldbeeld. Met een

focus op de negatieven, wordt aangenomen dat alle afzonderlijke componenten zo gedetailleerd mogelijk moeten worden onderzocht en gecombineerd, totdat zij alle dynamiek in het systeem verklaren. Het hoofdstuk presenteert een nieuwe conceptualisering van de voordelen van winderosie en stelt voor meer naar het algemene systeem te kijken. Drie voorbeelden laten zien hoe eolisch processen gunstig zijn voor de biodiversiteit, recreatie, kustverdediging en zelfs voor bodemvruchtbaarheid. Huidige meet en model technieken worden betwist. De gegevens van gebrekkige meettechnieken worden gebruikt voor extrapolatie en modellen. De grotere systeem dynamiek wordt bestudeerd door de kleine schaal (reductionistische) processen te simuleren, waardoor een complexe modelstructuur gebaseerd op zwakke empirische en fysische overwegingen. Door meer naar de systeem dynamiek te kijken wordt winderosie een essentieel onderdeel in natuurlijke systemen.

Een nieuwe modelmatige benadering is toegepast in hoofdstuk 3. In dit hoofdstuk gebruiken we een parallelle implementatie van de discrete elementen methode op de grafische verwerkingseenheid van een computer om niet-lineair zelf-organiserend gedrag in complexe systemen te simuleren. In dit hoofdstuk gebruiken we het voorbeeld van de ontwikkeling van een hoop zand, omdat het vaak wordt gebruikt in zelf-organiserende modellen om schaal onafhankelijke fluctuaties gerelateerd aan een machtsfunctie te beschrijven. In het model werden interacties tussen individuele korrels gesimuleerd met behulp van een contact-model in een Euler integratie methode. De berekeningen tonen niet-lineaire schaal-invariant zelf organiserend gedrag, dat in goede overeenstemming met de experimentele resultaten, theoretisch werk en modellen die werken op basis van zelf organisatie. Het hoofdstuk laat zien dat een volledig deterministische model aanpak, waarbij de positie en de krachten op elk individueel deeltje kan worden bepaald elke tijdschap, groot potentieel heeft om niet-lineaire en zelf-organiserend gedrag in eolische onderzoek te bestuderen.

Er is veel apparatuur ontwikkeld, getest en toegepast om eolisch onderzoek te bestuderen. Echter, het bepalen van de beste meet methode en data-analyse techniek wordt veel besproken in de literatuur. In hoofdstuk 4 onderzoeken we de effectiviteit van

twee verschillende sedimentvangers (De BEST en de MWAC) in het meten van verticale sediment flux. De studie werd uitgevoerd in een windtunnel, waar sediment transport gemeten werd middels saltiphones. In tegenstelling tot de meeste studies gebruikten we de analoge uitgang van vijf boven elkaar geplaatste saltiphones om de totale hoeveelheid kinetische energie te bepalen, die vervolgens werd gebruikt om eolische sediment budgetten te bepalen. Het absolute sediment verlies tijdens de experimenten werden bepaald met een weegschaal die zich onder de meetplank bevond. Experimenten werden uitgevoerd met verschillende zand fracties en met verschillende windsnelheden. De efficiëntie van de twee sedimentvangers bleek niet afhankelijk van de windsnelheid of sediment grootte, maar werd beïnvloed door zowel de experimentele opstelling (positie van de laagste trap boven het oppervlak en het aantal vallen in de saltatie laag) en de techniek voor het berekenen sediment flux. Ondanks dit, werd een goede overeenkomst gevonden tussen sediment verliezen berekend op basis van de Saltifoon en die gemeten met behulp van de balans. De resultaten van deze studie bieden een belangrijk kader voor het meten van eolische zand verplaatsing op kleine tijds schaal (seconden milliseconden) in het veld.

Akoestische sensoren worden vaak gebruikt om eolische saltatie te meten. Verschillende benaderingen worden gebruikt om de signalen van deze instrumenten verwerken. Hoofdstuk 5 beschrijft en bediscuseert een methode om eolische saltation met akoestische sensoren meten. In een laboratorium experiment, werden de uitgangen van een geavanceerde signaalverwerking schakeling op de printplaat van de Saltifoon gemeten. Daarnaast werd een software-implementatie van dit schema gebruikt om de data van vier miniphones, gemeten tijdens een veldexperiment opnieuw te analyseren. Het is aangetoond dat een aantal filters achtergrond ruis verwijderen buiten het frequentiespectrum van eolische saltatie (8 kHz). Maar ook dat signalen op deze frequentie spectrum versterkt werden. Het resulterende analoge signaal een proxy van de energie. met een puls converteerder, wordt het signaal omgezet in een digitaal en analogo tel signaal of een analogo energie signaal, met een gelijkrichter en integrator. De ruimtelijke en temporele

correlatie wordt hoger door de signalen over een langere tijd te integreren. Om eolische sediment transport te kwantificeren, wordt voorgesteld de analoge energie-uitvoer te gebruiken, omdat deze modus veranderingen in frequentie en amplitude detecteert. De analoge en digitale telsignalen kunnen een frequentieverhoging detecteren, maar zijn niet geschikt een toename in signaal amplitude te detecteren. Een tweetrapse kalibratie methode is voorgesteld bestaande uit (1) een fabriekskalibratie, waar het frequentiespectrum van de sensor wordt afgesteld en (2) een gestandaardiseerde valtest, die voor en na het experiment uitgevoerd dient te worden om de de respons van de sensor te evalueren

In hoofdstuk 6 worden de windtunnel en veld data vergeleken om de onzekerheden om de onzekerheden van de Modified Wilson And Cook (MWAC) zandvangervangert te identificeren. Deze vangervangert worden veel gebruikt om het totale volume zand transport in te schatten, maar ook de verticale massaverdeling van een saltatie te bestuderen. De betrouwbaarheid van sediment flux metingen en berekeningen zijn afhankelijk van de specifieke configuratie van de verschillende compartimenten en analyse methode. In deze studie analyseren we de onzekerheden van deze metingen met behulp van de verticale cumulatieve verdeling en relatieve sediment flux afkomstig van zowel windtunnel als veldonderzoek. Verticale flux gegevens zijn onderzocht met behulp van bestaande gegevens, in combinatie met een nieuwe metingen; bestaande meteorologische gegevens en sediment fluxen uit zes verschillende metingen, vergaard met behulp van drie aangepaste catchers op het strand van Ameland in het noorden van Nederland. Uit de windtunnel metingen blijkt dat de mediane transport hoogte een verspreid patroon heeft tussen de impact- en bewegingsgrens, die lineair toeneemt met schuifspanningen boven de bewegingsgrens. Voor fijner sediment werd een groter deel dichter bij het oppervlak getransporteerd vergeleken met grovere sediment fracties. Ook werd aangetoond dat fouten veroorzaakt door de verdeling van de compartimenten, in het bijzonder de locatie van het laagste compartiment ten opzichte van het oppervlak, kan worden geïdentificeerd met de relatieve sediment flux. Oppervlakte condities zoals vocht, korsten or bevrozing hebben een meer uitgesproken maar lokaal effect dan schuifspanning. Onzekerheden kunnen worden gereduceerd by het plaatsen van meerdere compartimenten dicht bij het

oppervlak.

In hoofdstuk 7, is de horizontale en verticale variabiliteit van eolische zand transport metingen op Ameland geanalyseerd. Een meteorologisch station, 37 aangepaste MWAC zand vangers, peilbuizen en een camera werden op het strand geïnstalleerd. Vijftien verschillende eolisch transport metingen vonden plaats over een periode van drie maanden. De hoogste zand transport hoeveelheden en de meeste variabiliteit was gevonden voor transport langs de kust. Het bleek dat de vochtigheid van het strand, gereguleerd door het grondwater een belangrijke sturende parameter voor transport hoeveelheid maar ook het flux profiel. De hoogte van het grondwater was voornamelijk bepaald door overstroming van de zee, wat twee weken lang effect kon hebben. Variatie in de vertical flux profielen tussen de verschillende zand vangers waren groter voor nat zand transport dan droog zand. De dynamiek in transport patronen is voornamelijk afhankelijk van lokale omstandigheden, zoals de afmetingen en oriëntatie van het strand, maar ook de meteorologische en oppervlakte eigenschappen. Metingen met een hoge frequentie maar lage magnitude zijn in staat grote hoeveelheden zand te transporteren. Toekomstige studies moeten ruimtelijk expliciete metingen van de hoogte en het oppervlak en vocht gehalte om een beter begrip van de complexe vervoer zand dynamiek te verkrijgen.

Een optische remote sensing benadering om vochtgehalte van het strand te kwantificeren werd onderzocht in hoofdstuk 8. Omdat bodemvocht een belangrijke beperkende factor voor eolisch sediment transport is, is het belangrijk om rekening te houden het vochtgehalte op beschikbare zand voor duinopbouw. Met optische remote sensing kan vochtgehalte gemeten worden met een hoge ruimtelijke resolutie. De doelstellingen van dit onderzoek waren voor het meten en modelleren van reflectiewaarden onder de gecontroleerde laboratorium omstandigheden als functie van de golflengte vochtgehalte in optische domein van 350-2500 nm, en de implicaties van onze laboratorium resultaten te onderzoeken voor het in kaart brengen van de verdeling van de vochtgehalte onder natuurlijke omstandigheden. Een laboratorium spectroscopie experiment werd bedacht om spectrale reflectie onder verschillende vochtgehaltes met strand zand te meten. We observeerden een niet-lineaire toename van reflectie bij drogen over het gehele bereik

van golflengten. We ontwikkelden en testten twee modellen. Het eerste model beschrijft het proportionele aandeel van verstrooiing en absorptie van licht door poriewater in een onverzadigd zandmatrix. Het tweede model is gerelateerd aan de bodem fysica en verbindt het hydraulische gedrag van poriewater in een onverzadigde zand matrix om de optische eigenschappen. Het bleek dat het optische model goed presteerde voor volumetrisch vochtgehalte $< 24\%$ ($R^2 > 0,97$), maar vonden een onderschatting in de reflectie voor het vochtgehalte tussen 24-30% ($R^2 < 0,92$), het meest rond de 1940 nm wateropname piek. Het bodemfysische model presteerde zeer goed ($R^2 > 0,99$), maar is beperkt tot het vochtgehalte $> 4\%$ en $< 24\%$. Uit de resultaten van het veldexperiment blijkt dat een korte-golf infrarood laserscanner ($\lambda = 1550$ nm) het vochtgehalte nauwkeurig kan bepalen op basis van de reflectie (standaardfout 2,6%). Dit toont de potentie van optische remote sensing om ruimtelijke vochtkaarten van een natuurlijk strand langs de kust te maken.

Tot slot wordt in hoofdstuk 9 de synthese van de resultaten en de conclusie de voorgaande hoofdstukken gepresenteerd. Er is aangetoond dat dit proefschrift een belangrijke bijdrage aan de actuele thema's in eolische onderzoek, door het identificeren en kwantificeren van de inherente onzekerheden van passieve sedimentvallen en het verbeteren van de huidige methoden om eolische saltation meten met behulp van akoestische sensoren. De technieken en methodes die gepresenteerd worden in dit proefschrift bieden een duidelijk handvat hoe eolische processen aan het strand gekwantificeerd kunnen worden. Uit een kwalitatieve analyse blijkt dat variatie in sediment transport voornamelijk bepaald wordt door lokale omstandigheden zoals oppervlakte vocht, grondwater, meteorologie, topologie en vegetatie. De nieuwste technieken waren gebruikt om sediment transport op een korrelschaal te simuleren. Ondanks dat de rekenschema's nog behoorlijk complex zijn, en reketijden erg lang, biedt deze methode veel potentie voor het onderzoeken van geofysische processen. De verschillende hoofdstukken in dit proefschrift bieden interessante nieuwe mogelijkheden voor het meten en modelleren van eolisch transport op verschillende schalen in de toekomst.

PE&RC Training and Education Statement

With the training and education activities listed below the PhD candidate has complied with the requirements set by the C.T. de Wit Graduate School for Production Ecology and Resource Conservation (PE&RC) which comprises of a minimum total of 32 ECTS (= 22 weeks of activities)



Review of literature (6 ECTS)

- Beneficial effects of wind erosion

Writing of project proposal (3 ECTS)

- Beneficial effects of wind erosion

Post-graduate courses (6 ECTS)

- Getting to the bottom of Mount Kenya: analysis of land dynamics and sustainable development in an inter disciplinary perspective; PE&RC, Kenya (2009)
- Climate KIC summer school J4; Climate KIC (2014)

Laboratory training and working visits (4.5 ECTS)

- Aeolian sand transport at the beach; Kings College London, Wageningen University (2010)
- Measuring fast-temporal sediment fluxes with an analogue acoustic sensor: a wind tunnel study; International Centre for Eremology (ICE), Ghent University, Belgium (2011)

Invited review of (unpublished) journal manuscript (2 ECTS)

- Geoderma: wind erosion (2014)
- Aeolian Research: wind erosion (2014)

Competence strengthening / skills courses (1.5 ECTS)

- Getting to the bottom of Mount Kenya: analysis of land dynamics and sustainable development in an interdisciplinary perspective; PE&RC, Kenya (2009)
- Workshop OpenEarth; Deltares (2011)
- How to write a world-class paper; WUR Library (2013)

PE&RC Annual meetings, seminars and the PE&RC weekend (1.2 ECTS)

- PE&RC PhD Weekend (2010)
- PE&RC Meeting (2014)

Discussion groups / local seminars / other scientific meetings (4.5 ECTS)

- SPAM Discussion group (2010)
- Workshop modelling concepts in biogemorphological (2011)
- Participating in WUR Open Data Pilot (2013)

International symposia, workshops and conferences (9 ECTS)

- ICARVII; Santa Rosa, Argentina (2010)
- EGU; Vienna, Austria (2011)
- Agro Environ; Wageningen, the Netherlands (2012)
- ICARVII; Lanzhou, China (2014)

Supervision of MSc students (6 ECTS)

- Measuring and modelling the effect of surface moisture on the spectral reflectance of coastal beach sand
- Using spectrometry and a 2D CCD camera to inquire water quality parameters

Ate Poortinga

Curriculum Vitae

About the author

Ate Poortinga was born on 11 february 1985 in Kollumerzwaag, the Netherlands. Het obtained his secondary education from the Bornego College in 2004 and then moved to Wageningen to start his studies of International land- and water management. He finished his Msc. Program (cum laude) in 2009, after which he started his PhD research. Besides his PhD research, he worked part-time at Water Insight.

Education

- 2009–2015 **PhD**, *Soil Physics and Land Management Department*, Beach sand dynamics: measurements, models and scales, Wageningen University.
- 2007–2009 **MSc**, *International Land and Water Management*, Land Degradation and Development Group, Wageningen University.
Cum Laude.
- 2004–2007 **BSc**, *International Land and Water Management*, Wageningen University.

Employment

- 2015–Now **Winrock International**, *Water accounting expert in Vietnam Forest and Delta program.*, Hanoi, Vietnam.
- 2009–2015 **Water Insight**, *Research and development, Embedded software development, Data processing, Data integration, Hydrological modelling, System administration*, Wageningen, The Netherlands.

Professional experience

- 06-2014 **FAO**, *Providing training and technical assistance in hydrological modelling Food and Agricultural Organization*, Lima, Peru.
- 05-2013 **FAO**, *Providing training and technical assistance in hydrological modelling Food and Agricultural Organization*, Rabat, Morocco.
- 09-2012 **FAO**, *Providing training and technical assistance in hydrological modelling Food and Agricultural Organization*, Manila, Philippines.
- 05-2012 **AgroEnviron**, *Member of the organizing committee AgroEnviron 2012 International Conference*, Wageningen, The Netherlands.
- 02-2011 **Workshop on Modelling concepts in biogeomorphology**, *Participant and member of the organizing committee*, Wageningen, The Netherlands.

12-2010 **Postgraduate Course**, *Getting to the bottom of Mount Kenya. Analysis of land dynamics and sustainable development in an interdisciplinary perspective*, Kenya.

12-2009–02-2010 **SFRI - IRD, MSc.** *Thesis on a lumped surface and sub-surface runoff for erosion modeling within a small hilly watershed in northern Vietnam*, Hanoi, Vietnam.

Languages

Dutch **Mothertongue**

English **Fluent**

Computer skills

Programming Expert knowledge on R and Python, advanced knowledge on c (++) and basic knowledge on GLSL, OpenCL.

Software Experienced user of Microsoft Windows and expert in Linux based operating systems. Familiar with software packages such as Microsoft office, LaTeX, ArcGIS, PCRaster ILWIS, GRASS, Qgis, GDAL, ERDAS IMAGINE.

Teaching experience

2009–present **Practical, MSc.** *practical on GIS Applications for Land Management.*

2009–present **Lecturer, MSc.** *course on soil erosion processes and modelling.*

Conferences attended

07-2014 **ICAR**, *International Conference on Aeolian Research*, Lanzhou, China.

05-2012 **AgroEnviron**, *Impacts of Agro systems on the Environment: challenges and opportunities*, Wageningen, The Netherlands.

02-2012 **FOSDEM**, *Free and Open Source Software Developers' European Meeting*, Brussels, Belgium.

04-2011 **EGU**, *European Geosciences Union*, Vienna, Austria.

02-2011 **FOSDEM**, *Free and Open Source Software Developers' European Meeting*, Brussels, Belgium.

02-2011 **ICAR**, *International Conference on Aeolian Research*, Santa Rosa, Argentina.

Scientific publications (peer reviewed)

Poortinga, A., van Rheenen H., Sherman D. J., 2014, Measuring aeolian sand transport using acoustic sensors, *Aeolian Research* 16 (2015): 143-151..

Poortinga A., Keijsers, J.G.S., Riksen, M.J.P.M, Visser, S.M., Baas, A, 2014, Temporal and spatial variability in event scale aeolian transport on Ameland, The Netherlands, *GeoResJ*, Volume 5, March 2015, Pages 23-35.

Nolet, C., Poortinga, A., Roosjen, P., Bartholomeus, H., Ruessink, G., 2014, Measuring and Modeling the Effect of Surface Moisture on the Spectral Reflectance of Coastal Beach Sand. *PloS one*, 9(11), e112151.

Poortinga A, Keijsers J.G.S., Maroulis J, Visser S.M., 2014, Measurement uncertainties in quantifying aeolian mass flux: evidence from wind tunnel and field site data. *PeerJ* 2:e454.

Keijsers, J.G.S., Giardino, A., Poortinga, A., Mulder, J. P., Riksen, M.J.P.M., & Santinelli, G., 2014, Adaptation strategies to maintain dunes as flexible coastal flood defense in The Netherlands. *Mitigation and Adaptation Strategies for Global Change*, 1-16.

Keijsers J.G.S., Poortinga A., Riksen M.J.P.M., Maroulis J., 2014, Spatio-Temporal Variability in Accretion and Erosion of Coastal Foredunes in the Netherlands: Regional Climate and Local Topography, *PLoS ONE* 9(3): e91115.

Stürck, J., Poortinga, A., Verburg, P. H., 2014, Mapping ecosystem services: The supply and demand of flood regulation services in Europe, *Ecological Indicators*, 38, 198-211.

Bui, Y. T., Orange, D., Visser, S. M., Hoanh, C. T., Laissus, M., Poortinga, A., Tran, D. T., Stroosnijder, L., 2014, Lumped surface and sub-surface runoff for erosion modeling within a small hilly watershed in northern Vietnam, *Hydrological Processes*, 28(6): 2961-2974.

Jones, N., Graaff, J., Duarte, F., Rodrigo, I., Poortinga, A., 2013, Farming systems in two less favoured areas in Portugal: their development from 1989 to 2009 and the implications for sustainable land management, *Land Degradation & Development*, 25: 29-44.

Poortinga, A., Van Minnen, J., Keijsers, J., Riksen, M., Goossens, D., Seeger, M., 2013, Measuring fast-temporal sediment fluxes with an analogue acoustic sensor: a wind tunnel study, *PloS one*, 8(9), e74007.

Youssef, F., Visser, S. M., Karssenbergh, D., Erpul, G., Cornelis, W. M., Gabriels, D., Poortinga, A., 2012, The effect of vegetation patterns on wind-blown mass transport at the regional scale: A wind tunnel experiment, *Geomorphology*, 159, 178-188.

Poortinga, A., Visser, S. M., Riksen, M. J., Stroosnijder, L., 2011, Beneficial effects of wind erosion: Concepts, measurements and modeling, *Aeolian Research*, 3(2), 81-86.

Scientific publications (preprint)

Poortinga, A., Wesseling, J. G., Ritsema, C. J., 2014, Stratified chaos in a sand pile formation, *arXiv preprint arXiv:1403.0741*.

Publications (conference)

Poortinga, A., Delobel, F., Rojas, O., 2012, MOSAICC: An inter-disciplinary system of models to evaluate the impact of climate change on agriculture, *Agro Environ* 2012.

Groot, A.V. de Vries, S., Keijsers, J.G.S., Riksen, M.J.P.M., Ye, Q., Poortinga, A., Arens, S.M., Bochev-Van der Burgh, L.M., Wijnberg, K.M., Schretlen, J.L., van Thiel de Vries, J.S.M., 2012, Measuring and modeling coastal dune development in the Netherlands. In: NCK-days 2012 : Crossing borders in coastal research, 13 March 2012 - 16 March 2012, Enschede, the Netherlands.

Keijsers, J. G. S., Poortinga, A., Riksen, M. J. P. M., Groot, A. D., 2012, Connecting aeolian sediment transport with foredune development.

Data sources

Ate Poortinga; Geert Sterk; Saskia Visser, 2014, Measurement uncertainties in quantifying aeolian mass flux: evidence from wind tunnel and field site data. Wageningen University, Dataset.

<http://dx.doi.org/10.4121/uuid:e1c16aac-02e2-4ec9-b2aa-b171cb034293>

Joep Keijsers; Ate Poortinga; Michel Riksen, 2014, Spatio-temporal variability in accretion and erosion of coastal foredunes in The Netherlands: regional climate and local topography. Wageningen University, Dataset.

<http://dx.doi.org/10.4121/uuid:54ed4c8f-e7b6-4139-bc20-dc8168c2f890>

Ate Poortinga; Jan Van Minnen; Michel Riksen; Manuel Seeger, 2013, Measuring fast-temporal sediment fluxes with an analogue acoustic sensor: a wind tunnel study. Wageningen University, Dataset.

<http://dx.doi.org/10.4121/uuid:7f4c6e00-4e51-4dc3-a304-57fc2f7f3b19>